Human head neck response in frontal, lateral and rear end impact loading : modelling and validation

Human Head Neck Response in Frontal, Lateral and Rear End Impact Loading

- modelling and validation -

Human Head Neck Response in Frontal, Lateral and Rear End Impact Loading

- modelling and validation -

PROEFSCHRIFT

ter verkrijging van de graad van doctor aan de Technische Universiteit Eindhoven,
op gezag van de Rector Magnificus, prof.dr. R.A. van Santen,
voor een commissie aangewezen door het College voor Promoties,
in het openbaar te verdedigen op donderdag 25 april 2002 om 16.00 uur

door

Marike Joanne van der Horst

geboren te Sneek

Dit proefschrift is goedgekeurd door de promotoren:

prof. dr. ir. J.S.H.M. Wismans
en
prof. dr. H. Kingma

Copromotor:

dr. ir. R. Happee
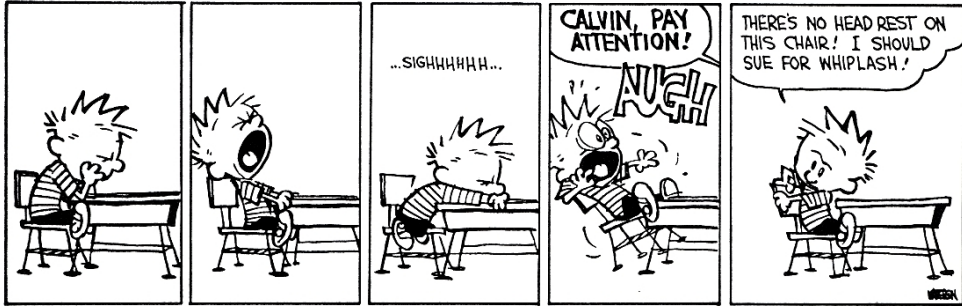
voor Simone

en mijn ouders en zus

Summary

Whiplash associated disorders are among the most common injuries reported for automotive rear end impacts. Although these injuries are typically considered minor, their high incidence rate and often long-term consequences lead to significant societal costs. The rationale of this research is that a mathematical model of the human head and neck can contribute to a better understanding of neck injury mechanisms and can be used in injury prevention research. The first objective is to develop and validate a detailed three dimensional mathematical model, that describes both the global dynamic behaviour of the human head and neck and the local loading of the neck tissues in accident situations. The second objective is to apply the model to provide insight in factors that might influence the risk of neck injury, such as the amount of activation of the neck muscles, the initial seating posture and the head restraint position.

A detailed multibody neck model has been developed. The model consists of a rigid head, rigid vertebrae, (non)linear viscoelastic discs, frictionless facet joints, nonlinear viscoelastic ligaments and segmented contractile muscles. These muscles follow the curvature of the neck, resulting in realistic muscle force lines of action. Stiffness properties of the tissues are based on literature data. The neck model can be applied separately or integrated into a model of an entire human body. The global kinematics like head, translational and angular, movements and accelerations as well as local kinematics such as vertebral rotations and tissue loads can be predicted with this neck model.

The neck model is validated quasi-statically as well as dynamically. Published quasi-static experimental data were used to test the segment models for 6 degrees of freedom and to test the entire ligamentous cervical spine model for flexion and extension. Frontal, lateral and rear end sled experiments using volunteers as well as post mortem human subjects (PMHSs) were simulated to validate the model dynamically. Neck model simulations of 15 g frontal and 7 g lateral volunteer experiments were performed. The rear end validations were performed with the neck model included in a total human body model. The rear end impact validation ranged from high severity (12 g) for PMHS experiments to mid (4-5 g) and low severity (0.7 g) for volunteer experiments. Accurate muscle activation properties were missing for the volunteer validations. Therefore, simulations were performed with several settings of the reflex delay and activation levels in the muscle model. These settings were based on muscle activation scenarios presented in the literature and

derived from low severity rear end experiments performed at Maastricht University. Additionally, simulations with varying head restraint position and initial seating posture were performed for the rear end impacts.

The main conclusions of this study are:

- The quasi-static passive mechanical behaviour of the model agreed reasonably with the experimental data.

- The combined findings of existing experimental data presented in the literature and the modelling results presented in this thesis indicate that neck muscles can alter the head and neck kinematics during rear end impacts, as well as during frontal and side impacts.

- The model with muscle activation predicted reasonably to well, the head and neck kinematics for the frontal, lateral and rear end impact simulations without head contact. Without muscle activation, the model showed larger head motions compared to the experimentally defined volunteer corridors. In case of simulations with head impact with a head restraint less accurate results were obtained.

- For varying conditions of muscle properties (muscle reflex time, activation level, co-contraction and initial activation), head restraint position and initial posture different trends were observed for several global and local loads and for the head-neck kinematics. Varying muscle activation showed larger influences on the internal loads for the discs, facet joints and ligaments than varying head restraint position or initial seating posture. This indicates that defining accurate model input for the muscle activation is not only necessary to predict the global response, but is also necessary to predict the local response correctly.

- The correlation found between numerically predicted global injury criteria and local tissue loads with the simulations performed within this research is not strong. Therefore, it is questionable whether global injury criteria may be used to predict local injuries.

- The model presented in this thesis is suitable for studying further the neck injury mechanisms and neck injury criteria, since it reveals the loads and deformations of individual tissues of the neck.

Samenvatting

Whiplash trauma is een van de meest bekende letsels bij achteraanrijdingen. Hoewel deze letsels behoren tot de categorie lichte letsels, kunnen de sociale en financiële gevolgen aanzienlijk zijn. De achterliggende gedachte van dit onderzoek is dat wiskundige modellen van de menselijke nek bij kunnen dragen aan het inzicht in het letselmechanisme en gebruikt kunnen worden in letselpreventie onderzoek. Het eerste doel van dit onderzoek is het ontwikkelen en valideren van een gedetailleerd drie dimensionaal wiskundig model dat zowel het globale dynamische gedrag maar ook de lokale belastingen van het nekweefsel kan beschrijven tijdens ongevallen. Het tweede doel is het model toe te passen om inzicht te krijgen in factoren die het letselrisico kunnen beïnvloeden, zoals de mate van spieractivatie, de initiële zithouding en de hoofdsteunpositie.

Er is een gedetailleerd nekmodel ontwikkeld dat uit de volgende elementen bestaat: een onvervormbaar hoofd en onvervormbare wervellichamen, niet lineair visco-elastische tussenwervelschijven, wrijvingsloze facetgewrichten, niet lineair visco-elastische ligamenten en contractiele spierelementen. Deze spieren volgen de kromming van de nek wat resulteert in realistische werklijnen van de spierkrachten. De stijfheidseigenschappen van de weefsels zijn gebaseerd op literatuurgegevens. Het nekmodel kan als losse module gebruikt worden, maar kan ook geïntegreerd worden in een model van de gehele mens. De globale kinematica, zoals hoofd verplaatsingen en rotaties kunnen worden voorspeld met dit nekmodel.

Het nek model is gevalideerd voor zowel quasi-statische als dynamische condities. Gepubliceerde quasi-statische experimentele gegevens zijn gebruikt om modellen van neksegmenten te valideren voor 6 vrijheidsgraden. Daarnaast zijn ook quasi-statische flexie-extensie testen van de gehele nek gebruikt voor validatie. Slede testen met vrijwilligers als ook met menselijke kadavers zijn gebruikt voor de validatie van het dynamische gedrag van de nek. Simulaties van 15 g frontale en 7 g zijdelingse botsingen zijn uitgevoerd met het nekmodel. De achteraanrijdingen zijn gesimuleerd met het mensmodel met gedetailleerde nek. Deze validatiereeks beslaat achteraanrijdingen in de range van 12 g voor de kadaver experimenten, 4-5 g en 0.7 g voor de experimenten met vrijwilligers. Nauwkeurige gegevens over de spieractivatie van de vrijwilligers waren niet beschikbaar. Daarom zijn er modelparameter variaties van de reflextijd en het spieractivatieniveau uitgevoerd. De gebruikte invoer voor het spiermodel was voornamelijk gebaseerd op experimentele gegevens uit de literatuur alsmede op gegevens uit testen van achterwaartse belastingen bij lage snelheden met

vrijwilligers uitgevoerd in Maastricht. Bovendien zijn er voor de achteraanrijdingen ook simulaties uitgevoerd met verschillende zithoudingen en hoofdsteunposities.

De hoofdconclusies van deze studie zijn:

- Het quasi-statische passieve gedrag van de nek komt redelijk tot goed overeen met de experimentele gegevens.

- De simulatieresultaten gecombineerd met gepubliceerde experimentele resultaten geven aan dat nekspieren de hoofd- en nekbeweging kunnen beïnvloeden tijdens achterwaartse, frontale en zijdelingse botsingen.

- Het model met actief spiergedrag voorspelt een redelijke tot goede hoofd- en nekbeweging voor frontale, zijdelingse en achteraanrijdingen waarbij geen hoofdcontact optreedt. Zonder spieractivaties voorspelt het model grotere hoofd- en nekbewegingen dan de experimentele resultaten. Voor de simulaties waarbij contact tussen hoofd en hoofdsteun optreedt is de voorspellende waarde minder goed.

- Voor variaties in de condities van de spieren (reflextijd, activatieniveau, co-contractie van de verschillende spiergroepen), de hoofdsteunposities en de zithoudingen zijn verschillende trends zichtbaar voor de globale en lokale krachten en hoofd- en nekbewegingen. De spiervariaties hebben een grotere invloed op de interne krachten voor de tussenwervelschijven, facetgewrichten en ligamenten dan de variaties in zithouding en hoofdsteunposities. Dit impliceert dat nauwkeurige modelinvoer voor spieractivatie niet alleen noodzakelijk is voor het voorspellen van een goede globale response, maar ook voor de lokale response van het model.

- Een correlatie studie uitgevoerd met het nekmodel laat geen sterke relatie zien tussen de globale nekletsel criteria en lokale weefselbelastingen. Op basis hiervan kan het gebruik van globale criteria voor het voorspellen van lokale letsels worden betwijfeld.

- Aangezien het model de krachten en kinematica van het nekweefsel kan berekenen, is het model dat in dit proefschrift gepresenteerd wordt, geschikt voor verdere studie naar nekletselmechanismen en nekletselcriteria.

Contents

Chapter 1

Introduction

Neck injury in car collisions, often referred to as whiplash injury, is one of the most aggravating traffic related safety problems, resulting in serious implications for the western society [176]. The precise definition of whiplash injury remains controversial [25, 44, 137]. A widely accepted definition is that formulated by the Quebec Task Force in 1995 based on an extensive literature review [137].

> *Whiplash is an acceleration-deceleration mechanism of energy transfer to the neck. It may result from rear end or other motor vehicle collisions, but can also occur during diving or other mishaps. The impact may result in bony or soft tissue (whiplash) injuries, which may lead to a variety of clinical manifestations (Whiplash-Associated Disorders, WADs).*

The research described in this thesis is concerned with the prevention of neck injuries due to automotive accidents. In the literature, the term whiplash has been used both for the injury and its symptoms as well as for its assumed injury mechanism. Many different terms commonly are found in the literature to describe the whiplash trauma. In this thesis the term whiplash-associated disorder (WAD) [137] will be used. The next section provides background information on WADs. The rationale and objective for this research are presented in Section 1.2. Section 1.3 presents the research strategy and states the outline of this thesis.

1.1 Background information on Whiplash Associated Disorders

In the following paragraphs a short overview is given of the injury statistics and the clinical observations of WADs. Also a brief overview of the biomechanical approach of WAD research is presented.

1

Injury statistics   Historically, WADs referred to the motion of the head and neck during rear end collisions [25]. However, research over the last decades has shown that WADs can also occur from other vehicle collisions or even other mishaps [137]. At the end of the 1970s WADs represented nearly 30% of all disabling injuries in motor vehicile collisions in Sweden [98]. According to Ono and Kanno [106], 50% of all car to car collisions in Japan resulted in WADs, with the number of WADs still increasing over time. In England, the incidence of WADs has doubled over a ten year period [91]. WADs occur in all impact directions even though rear impacts are most often mentioned. Hell *et al.* [59] identified risk factors and the population at risk of WADs, using a large database of retrospective insurance data material covering 15000 car to car collisions in Germany in 1990 involving injured occupants. In about 54% of these cases the pattern was a rear end collision, in correspondence with the Japanese findings by Ono and Kanno [106]. In order to obtain an overview of the real scenarios 517 rear end collisions were analyzed medically and technically. Females were generally at higher risk, and older people showed higher risk for high-grade cervical spine distorsion injuries. Indepth collision analysis by Boström *et al.* also indicated higher risk for females [41]. The fact that women generally have smaller values of neck circumference suggests that this may relate to the actual risk factor, although more research in this area should be performed [59].

The incidence of new WAD patients due to automotive accidents in the Netherlands is estimated to be more than 15,000 per year with total costs to the Dutch society of more than 300 MEuro based on insurance data from 1994 [168] . The socio-economic losses for rear end collisions are increasing [59]. The costs to the society of WADs in the early nineties have been estimated to be 700 MEuro in Germany [153] and 210 MEuro in Sweden [148]. Based on these data a cost estimate for the European society for neck injuries in rear end impacts is in the order of 5-10 billion Euro per year. Similar dramatic figures have been reported outside Europe [101, 106].

Clinical observations   WADs are diagnostically difficult to establish. Often no clear sign of structural injuries of the tissues within the neck is found with medical imaging, neurological, or orthopaedic investigations [6]. A clinical classification of WAD published by the Quebec Task Force is presented in Table 1.1.

The onset of the symptoms mentioned in Table 1.1 occurs for 45.9% within 1 hour after the accident, for 28.6 % it occurs later but within 24 hours, while for a smaller group (25.5 %) the symptoms occur after 24 hours [138]. The public health problems concerning WADs are those leading to long term disability. However, not all occupants who suffer a WAD develop chronic symptoms, and some researchers even question the existence of WADs. For example, based on the results of a retrospective questionnaire-based cohort study among 202 individuals in Lithuania, Schrader *et al.* [42] suggested that chronic symptoms were not usually caused by the car accident [42]. In contrast with these results, Nygren [98] found that 1 out of 10 occupants remained disabled at least one year after a collision. A recent study from the UK showed a progressive reduction in the proportion of patients with WADs during a 48-month period [49]. A Canadian study showed that 2.9 % of people with WADs were still absent from their usual activities or work, one year after the collision [137]. In 1994 Barnsley et al. [6]

Table 1.1: *The Quebec classification of Whiplash-Associated Disorders (WADs) [137] compared with AIS classification [4].*

WAD Grade	AIS	Clinical Presentation
0	0	No complaint about the neck
		No physical sign(s)
1	I	Neck complaint of pain, stiffnes, or tenderness only
		No physical sign(s)
2	I	Neck complaint and musculoskeletal sign(s) *
3	I	Neck complaint and neurological sign(s) ᵒ
4	II	Neck complaint and fracture or dislocation

* Musculoskeletal signs include decreased range of motion and point tenderness
ᵒ Neurological signs include decreased or absent deep tendon reflexes, weakness and sensory deficits.
Symptoms and disorders that can be manifest in all grades include deafness, dizziness, tinnitus, headache, memory loss, dysphagia, and temporomandibular joint pain.

published a clinical review on WADs. This review indicates that between 14 and 42 % of patients with whiplash injuries develop chronic neck pain and that approximately 10 % will have constant, severe pain indefinitely [6].

In the clinical literature, the leading contenders for explaining chronic neck pain following WADs are injuries to the facet joints, the intervertebral discs and the upper cervical ligaments [6]. The facet joint has been reported as the most common source of neck pain based on clinical research, accounting for 25 to 62 % of neck pain sufferers [160]. Damage to other cervical structures can occur, however results from the review by Barnsley *et al.* [6] suggest that tears and sprains of muscles and ligaments are likely to heal within several weeks with loss of pain, and consequently do not result in a chronic WAD.

Despite the ongoing discussion on the existence of (chronic) WADs it is not a subject of this thesis. The focus is on the biomechanical response resulting from a rear end impact, assuming that this will be of help in understanding WADs.

Biomechanical approach Physical injury will take place if the biomechanical response is of such a nature that the biological system deforms beyond a tolerable limit resulting in damage to anatomical structures and/or alteration in normal function [169]. The mechanism involved is called an injury mechanism. In rear end collisions the head and neck are exposed to inertia and contact forces, which may load or deform the (soft)tissues in the neck beyond tolerable limits, resulting in injury.

The typical loading scenario in a rear end collision can be described as follows (see Figure 1.1 and [176]): the car is subjected to a forward acceleration during which the body of a subject is pushed forward by the seatback. During the first phase the head is translating rearward relative to the seat. The upper cervical spine is undergoing a flexion motion and the lower part is undergoing an extension motion relative to the torso (S-shape). During this phase also a vertical displacement of T1 is seen. This T1 displacement is caused by the vertical displacement of the pelvis (i.e. ramping up) together with the straightening of the spine. Subsequently a C-shaped curvature with extension of the entire cervical spine is seen. In the first phase an anterior shear force

together with a compression force and an extension moment can be recognized for the neck loads. It should be noted that the head-neck system is seen as a pivot mechanism when calculating the neck loads. The net force and moment on the neck is taken, including the loads caused by the ligaments and the muscles, this is not the load on the real anatomical OC joint, but the load on a virtual single hinge joint between head and neck. During the second phase posterior shear, tension and a flexion moment can be found. Naturally, the presence of a head restraint will influence the C-shape and the neck loads. The extension will be followed by a rebound of the body. This thesis deals with the relative head-neck motion as presented in Figure 1.1 focussing on what may be the first injury event during the neck motion in a rear end impact.

S-shape   C-shape

initial   spine   max.   extension
position   straightening   retraction
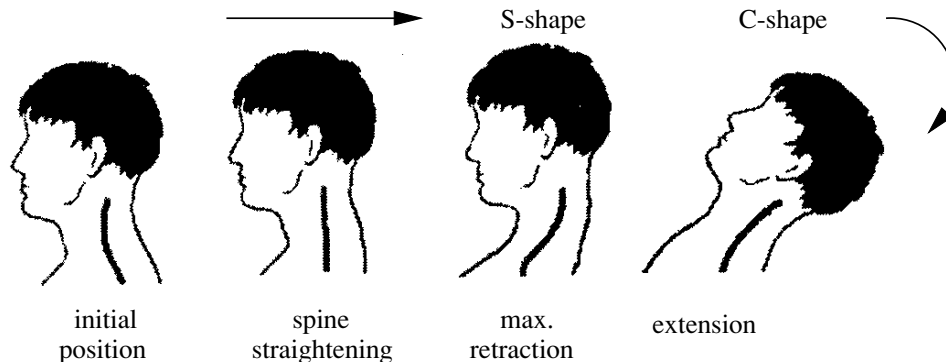
Figure 1.1: *Occupant Kinematics during rear end impact [27].*

Although the biomechanical responses in rear end impact have been investigated for many years using experimental research [7, 8, 29, 50, 68, 71, 82, 84, 85, 88, 102, 133, 135, 141, 142, 144, 145] as well as biomechanical models [66, 70, 72, 75, 174] the injury mechanisms of WADs are still unknown. Different hypotheses, offering explanations for the source of WADs are reviewed briefly. A list of injury types and mechanisms relevant for a rear end impact are presented in Table 1.2.

Table 1.2: *List of injury types and mechanisms relevant to this thesis (as regarded by the author).*

Injury	Mechanism	Criterium	Reference
-	hyperextension	-	[78]
soft tissue upper neck	hypertranslation	-	[118]
soft tissue lower neck	hypermotion lower neck	-	[51]
-	unphysiological intervertrebral motion	IV-NIC	[115]
neural damage	violent pressure transients	NIC	[40]
facet joint	pinching	-	[105, 177]
soft tissue	compression-shear	-	[173]

The first and most simple hypothesis was based on primate studies in which head and neck extensions (bending backward) exceeded 90 degrees during a rear end impact without head restraint. Neck hyperextension was suggested as the injury

cause [78]. Additionally, based on resemblance between experiments and literature, Penning [117, 118] hypothesized that during a rear end impact the injury of the head-neck system is caused by posterior hypertranslation of the head, almost immediately resulting in damaging hyperflexion (bending forward) of the upper neck joint ("hypertranslation theory"). Grauer *et al.* [51] assumed that intervertebral motions beyond the physiological limits have the potential to cause soft tissue injury. In correspondance with Penning's study [118], the S-shape (see Figure 1.1) was identified as the injury stage. However, injury risk at the lower cervical levels was also expected. This is in contrast with Penning's theory [118], who hypothesized that the upper cervical level, the cranioverteberal junction, is the principle site of cervical trauma in a rear end impact.

Svensson *et al.* [139] verified a hypothesis by Aldman [3] predicting that the volume changes inside the spinal canal during swift extension-flexion motions of the cervical spine (S-shape, see Figure 1.1) would result in transient pressure changes in the Central Nervous System (CNS). Aldman also hypothesized that these pressure effects could induce injurious mechanical loads to the tissues in the intervertebral foramina ("pressure hypothesis"). The extension motion causes a pressure rise and flexion motion causes a corresponding pressure drop. Experimental findings on porcines [139] made it plausible that the transient pressure changes induce injurious mechanical loads to the tissues inside the intervertebral foramina, according to the "pressure hypothesis".

A facet joint impingement injury mechanism has been proposed by Ono *et al.* [105] and Yoganandan *et al.* [177]. This theory is based on the assumption that during the S-shape of the neck, a portion of the facet capsule can be trapped between the facet joint surfaces and pinched, causing pain. Evidence is lacking, to show that the capsule is loose enough to be trapped between the facet joint and even if it was trapped, it is unknown if this could cause pain.

Yang *et al.* [173] hypothesized that axial compression in the neck, together with the shear force (the "compression-shear hypothesis"), is responsible for the higher observed frequency of neck injuries in rear end impacts versus frontal impacts of comparable severity. This axial compression occurs during the first phase of the rear end impact due to ramping up or other mechanical interactions between the seat back and the spine [82]. The axial compression reduces the shear stiffness of the cervical spine (loosening of cervical ligaments) and makes it easier for the shear type soft tissue injuries to occur.

Boström *et al.* [40] performed additional research on the experiments presented by Svensson *et al.* [139]. This resulted in a neck injury criterion (NIC) based on the relative acceleration between the top and the bottom of the cervical spine [40]. A tolerance level of 15 m^2/s^2 for AIS type I cervical injury was proposed based on pig experiments. Although several studies [38, 41] indicate that NIC is a useful indicator for the prediction of neck injuries following rear end impacts, other studies question the value of NIC [157].

Another criterium recently proposed by Panjabi *et al.* [115] is the intervertebral neck injury criterium (IV-NIC). This IV-NIC, which showed correlation with NIC, is based on the hypothesis that a neck injury occurs when an intervertebral rotation exceeds

its physiological limit during a rear end impact. However, until now tolerance levels are not available for IV-NIC.

Different theories about the cause of WADs are presented here. Any one theory does not necessarily preclude the others, as until now no single answer has been found for the mechanism causing WADs in rear end impact car accidents. Further research is needed to validate existing hypotheses and to gain understanding of the relative cervical vertebral motions, the facet joint motions and the pressure changes in the central nervous system occuring during a rear end impact.

1.2   Research Objective

Research designed to understand the mechanisms of injury in the cervical spine has employed clinical observations, experimental laboratory investigations and biomechanical models. However, in clinical observations and experimental research, tissue loads and deformations are often impracticable if not impossible to determine. The rationale of this research is that a mathematical model of the human head and neck can contribute to a better understanding of neck injury mechanisms and can be used in injury prevention research.

The objective of this PhD research is to develop and validate a detailed three dimensional mathematical model that describes the dynamic behaviour of the human head and neck in accident situations. The model has to provide insight into the motion of the head relative to the torso (global behaviour) and into deformations and loads that occur within the cervical spine (local behaviour). Such a model, provided that it is well validated, will contribute to the understanding of injury mechanisms. In addition this study aims to provide insight in the role of initial seating posture and head restraint position, and the role of muscle behaviour on the global and local behaviour of the head neck system.

1.3   Research Strategy and Outline

The strategy in this study is to proceed from an existing human neck model to a more detailed and better validated one, with the focus on rear end impacts. The model needs anatomical details to describe not only the global but also the local response related to the injury mechanisms mentioned in Table 1.2. Active force-generating muscle elements are necessary to simulate reflex based muscle contraction [134]. The model needs to be integrated into a whole body model, since in the case of a rear end impact, the head to head restraint contact, and therefore the head neck response, will be influenced by the interaction of the human back and seat [140]. Finally the model needs to be computationally efficient, which will enhance the practical usefulness of the model for the automotive industry - time is money, in particular with regard to future application for design optimization.

The De Jager model [64,65] is used as a basis of the research. The De Jager multibody neck model is detailed enough to describe the loads and deformations of most tissues

[65]. Also active force-generating muscle elements are included. The model has been validated for quasi-static loading and frontal and lateral impact conditions [65]. Moreover, the model is computationally more efficient than finite element models. Further discussion of the choice to use the De Jager model can be found in Chapter 2.

After more knowledge and insight was gained with the De Jager model (see [61]), the complexity of the model was increased and recent biomechanical data was used to obtain an anatomically more realistic head-neck model. The enhanced model includes separate mathematical representations of the intervertebral discs, ligaments, facet joints and muscles. Chapter 2 gives a detailed description of the human head neck model.

The original quasi-static and dynamic validations are repeated to show the quality of the model. In Chapter 3 quasi-static validation of segments of the model, as well as of the whole neck model, is presented. Dynamic validation for frontal and lateral impacts using published sled acceleration test data with human volunteers is presented in Chapter 4. Additionally, the role of muscle behaviour on frontal impact is studied in Chapter 4. In order to study the interaction of human body and seat in a rear end impact, the detailed neck model is integrated into a published human body model. The model validation is then extended for rear end impacts. At Maastricht University, additional experiments are performed simulating a low speed rear end impact, measuring the EMG activity of the neck muscles. In Appendix E these experiments are described. Chapter 5 presents the model validation for rear end impact using published sled acceleration test data with post mortem human subjects (PMHS) and human volunteers as well as the experimental results as presented in Appendix E. For the volunteer responses, initial seating posture, head restraint positioning and muscle activation are important determinants of the human head-neck response. The role of these parameters is studied in Chapter 5. As a step towards studying injury criteria for WADs, local behaviour such as relative cervical vertebral rotations and tissue loads are quantified by numerical modelling and correlated with existing global injury criteria (see Chapter 6).

Chapter 7 concludes this thesis by summarizing the main finding of this research. Furthermore recommendations to enhance the model and its validation are given.

Chapter 2

Model Description

The objective of this chapter is to present a three dimensional mathematical neck model which describes the dynamic behaviour of the human head and neck in impact conditions. The model should be detailed enough to predict local kinematics, such as vertebral rotations and tissue loads. Firstly a review of existing neck models is presented. In Section 2.2 the general model setup is introduced, followed by subsections with detailed information. Section 2.3 concludes this chapter with a discussion.

2.1 Literature Review on Neck Models

Biomechanical models of the neck as presented in the literature have different degrees of complexity [169]. Two-pivot lumped mass models are the simplest models. The head and torso are modelled as rigid bodies connected by a rigid or extensible neck-link, e.g. [12, 13, 56, 131, 146, 165, 166]. The mechanical behaviour of the neck is lumped into the head-neck and neck-torso pivot, usually as rotational spring-damper elements. These pivot models are often used for analysis and specification of global kinematics in experiments. Multibody (MB) models form an extension of the lumped mass models. In the case of multibody models, links are connected by various joint types. These models can include many anatomic details, e.g. [33, 52, 62, 64, 66, 72, 147]. The head and vertebrae are modelled as rigid bodies, whereas the soft tissues (e.g. intervertebral discs, facet joints, ligaments, muscles) are modelled as massless spring-damper elements. Finally, finite element (FE) models e.g. [7, 19, 28, 96, 159, 174] allow for even more detailed representations of geometry and material behaviour of the cervical spine.

An overview of the most important neck models of the last ten years according to the best knowledge of the author is presented in Table 2.1. It is remarkable that more finite element models than multibody models have been published over the last 10 years. For most models the geometry is based on different sources, but the characteristics both for the finite element models and the multibody models are

9

mostly based on the same literature.

The modelling stategy for the multibody model by De Jager was to proceed from a relatively simple multi-body model to a more detailed one. First, the model of Deng and Goldsmith [33] was modified and validated against frontal and lateral acceleration impacts as described in detail by De Jager [63]. A new model was developed to remove shortcomings of the Deng-model. This model includes the head and vertebrae as rigid bodies, and all the mechanical behaviour of the soft tissues is lumped into the intervertebral joints [64]. The second De Jager model [64] is more detailed and consists of rigid vertebrae and a rigid head, linear viscoelastic intervertebral discs, nonlinear viscoelastic ligaments, contractile muscles and frictionless, nonlinear viscoelastic facet joints.

Although finite element codes are potentially better suited than multibody models for description in detail the cervical spine, the differences in detail of the currently available neck models (FE and MB) are not large (see Table 2.1). For example, Camacho *et al.* [19] lumped the soft tissue properties into the flexion/extension, compression/tension and anteroposterior shear stiffness functions for the intervertebral joints. Others simplified the upper neck joint by including spherical joints with lumped stiffness functions. In the past, a FE model with active muscles [159] was developed, however, the current FE models lack active muscle modelling. Although the multibody model by De Jager contains less detail in vertebral geometry, the upper neck joint was modelled in detail and active muscle behaviour was available. However very detailed finite element segment models of the facet joints [74, 160] and the intervertebral discs [36] are published. These models can be used when one is interested in the local behaviour of specific tissues of the cervical spine.

In the past, biomechanical neck models were developed to study frontal and lateral acceleration impacts. In the last 5 years the focus has been more on rear end impact simulation and WAD injuries and most models have been updated to improve their usefullness for rear end impact simulations. The models by Yang [174] and Bertholon [7] are already validated for rear end acceleration impacts. Additionally, both models are also validated for axial compression together with flexion and extension. Although the finite element models are the most detailed models in geometry, the multibody model by De Jager has much detail in modelling of the tissue characteristics. One advantage of the De Jager model is the ability to model of active muscle behaviour. Additionally, the model shows reasonable response to both frontal and lateral impact, is detailed enough to describe the loads and deformations of the tissues, and can be used to evaluate injury mechanisms [65]. As deformation of the vertebrae is relevant only for high severity loading and prediction of fracture, the use of a rigid head and rigid vertebrae as in the De Jager model is accurate enough. Deformation of the discs is essential, but a very fine mesh is required to realistically simulate the behaviour of the disc. Moreover, dynamic characteristics of the discs are hardly available in literature. In most FE neck models simple disc models with about 8 to 12 elements are applied to minimize computational demands. Although the disc model by De Jager is represented by spring damper elements (6 degrees of freedom) the disc model can compete with the simple discs of the FE models. Finally,

the multibody model is computationally more efficient than finite element models. Therefore, the De Jager model [64, 65] has the potential to be further developed for rear end impact and is chosen as a basis for this research.
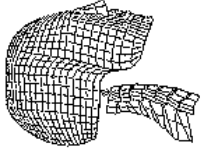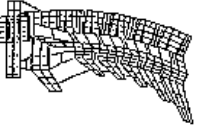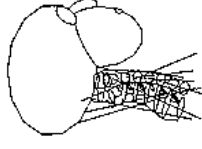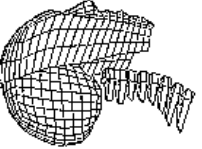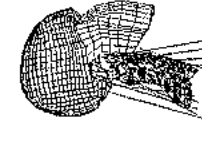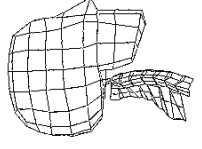
2.2   Model Setup

The human cervical spine comprises seven vertebrae, usually referred to in the existing literature as C1 through C7. The upper cervical spine comprises occiput (C0), atlas (C1) and axis (C2), and is also called the occipito-atlanto-axial region (see Figure 2.1). The occiput (C0) is the base of the skull and articulates with the atlas (C1) through the occipital condyles (OC) which are convex in shape. The atlas (C1) has no vertebral body, but consists of a bony ring with anterior and posterior arches on which the articular facets and transverse processes are situated. The upper facets are large, concave and oval. The axis (C2) comprises a body and an arch, but has an additional element, the odontoid process or dens. The dens points out upwards from the body of C2 and is the missing body of the atlas fused to the axis. The muscles and ligaments are attached to the vertebrae. The upper cervical spine (C0-C2) is distinct from the lower cervical spine (C3-C7). The lower five vertebrae are all similar, in contrast to the differing vertebrae of the upper cervical spine. A vertebra of the lower cervical spine consists of a cylindrically shaped body of an arch (see Figure 2.2). The lower end of the body is concave from front to back, whereas its upper end is concave from side to side and has an uncinate process on each side. The upper and lower ends of the body are covered by thin layers of hyaline cartilage, the endplates. The intervertebral disc is a fibrocartilaginous joint between these endplates. The arch includes two pairs of articular facets, a spinous process and two transverse processes. The articular facets are almost flat and covered with cartilage, and have a backward inclination of about 45 degrees in the horizontal plane. The transverse and spinous processes constitute attachment points for muscles and ligaments. The arch and body enclose the vertebral foramen to form the spinal canal through which the spinal cord and associated structures run.

In this study the De Jager model [65] is choosen as the basis of the model development. A main limitation of the existing De Jager model is that , as a result of the muscles being modelled by straight line segments, the muscles can not follow the curvature of the neck [65]. Also only the large superficial muscles are represented and moreover, the contact of the spinous processes is not modelled, and the contact of the facet surfaces is modelled using hyperellipsoids, which can only represent convex or almost flat surfaces with an elliptic or rectangular shape [65]. This simple modelling was deemed insufficient for the facets of the upper cervical spine, which are concave and have a complex shape [65]. The orientation of the facets in the De Jager model was based on an experimental study on 12 cervical spines [113]. The orientations of the facets were averaged over subjects, not representing correct interaction of these joints when subjected to extension [65].

In the current study, the complexity of the De Jager model has been increased. In the first year of this project an intermediate model was developed, solving the problems

Table 2.1: *Overview of relevant neck models in the last 10 years.*

	Dauvilliers [28]	Nitsche [96]	De Jager [64,65]	Camacho [20]	Yang [174]	Bertholon [7]
Reference						
Model	FE [+]	FE	MB *	FE	FE	FE
Code	Radioss	PamCrash	MADYMO	LS-DYNA	PamCrash	Radioss
Head	rigid	-	rigid	rigid	rigid or viscoelastic	rigid or viscoelastic
Vertebra	rigid	elastic	rigid	rigid	elastic	rigid
Intervertebral Joints	free@	free	free	2D #	free	free @
Intervertebral Disc	elastic	elastic	linear viscoelastic [r]		elastic and viscoelastic	linear viscoelastic
Ligaments [k]	linear anisotrope	linear anisotrope	nonlinear viscoelastic	-	linear anisotrope	nonlinear viscoelastic
Facet joint contact	frictionless	frictionless	frictionless	-	frictionless	frictionless
OC and dens contact	-[s]	frictionless	frictionless	-	frictionless	-[s]
Muscles	-	-	active and passive	-	passive	passive
Illustration						
Detail	150 solids 104 shells 415 springs	1852 solids 86 membranes	13 pairs of muscles 11 ligaments divided in many springs	639 rigid shells 448 deformable shells 25 springs 108 springs	7351 solids for head 11498 solid for neck 3071 membranes	
Application	frontal and lateral acc.	frontal and lateral acc. axial impact	frontal and lateral acc.	axial impact	frontal and rear acc. axial impact	omnidirectional acc.
Validation	15g frontal acc. [146] 7g lateral acc. [45]	15g frontal acc. [146] 7g lateral acc. [45] axial compression [121, 122]	15g frontal acc. [146] 7g lateral acc. [45] 7g lateral acc. [45]	axial impact at 3.2 m/s [95]	8g rear acc. axial impact at 3.2 m/s [95]	15g frontal acc. [146] 7g lateral acc. [45] 12g rear acc. [7] axial impact at 3.2 m/s [95]

[+] FE = finite element model
[o] DOF = degrees of freedom
[k] including facet joint capsules
[#] all soft tissue characteristics lumped into kelvin solid with flexion/extension, compression/tension and anteroposterior shear
[s] all soft tissue characteristics of upper neck lumped in stiffness of spherical joints

* MB = multibody model
@ upper neck joints spherical
[r] rotational and translational springs and dampers

on muscle curvature [61]. Since the new model must also be suitable for rear end impact (see Chapter 1), correct contact interactions of the upper neck joints are needed. Therefore, a new geometry of the cervical spine, with new locations of ligaments and muscles, to obtain an anatomically more realistic head-neck model will be presented. Furthermore, recent biomechanical data will be used. Since the new model will be validated for rear end impact, contact of the spinous process will be included. Details of the components of the new model are given in the following sections (see also Table 2.8).

The model has been implemented using the multibody part of the integrated multibody finite-element package MADYMO, version 5.4.1, of the TNO Crash Safety Centre [150]. The multibody algorithm in MADYMO yields the second time derivatives of the degrees of freedom in explicit form. Theoretical background information on multibody dynamics are provided, among others, by Roberson and Schwertassek [128] and Wittenburg [170].

(a) Atlas (C1)   (b) Axis (C2)
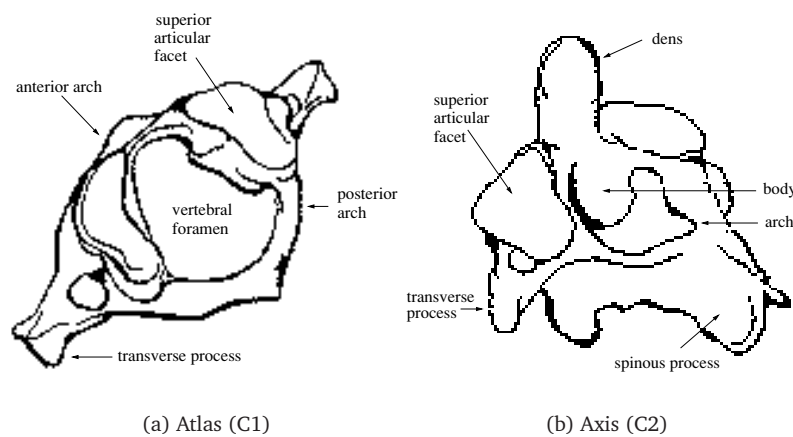
Figure 2.1: *Vertebrae of the upper cervical spine.*

2.2.1   Head and vertebrae

In the model, the head, the seven cervical vertebrae and the first thoracic vertebra (T1) are represented by nine rigid bodies. T1 serves as the base of the model. Views of motion segments (two adjacent vertebrae with the surrounding soft tissues: intervertebral disc, facet joints and ligaments) are presented in Figures 2.3 and 2.4. The model of the skull is shown in Figure 2.5.

The outer surface of the vertebrae and skull have been implemented as "arbitrary surfaces". These surfaces consist of triangular or quadrangular facets which are supported by nodes (vertices) on rigid bodies [150]. Contact can be simulated with other rigid bodies (surfaces described in MADYMO as arbitrary surfaces, ellipsoids,
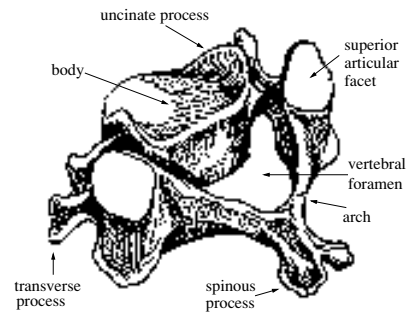
Figure 2.2: *A typical vertebra of the lower cervical spine.*

Table 2.2: *Definition of loads and displacements [65].*
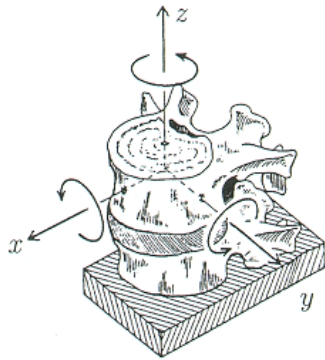
load	displ	name	abbr
$+F_x$	$+t_x$	anterior shear	AS
$-F_x$	$-t_x$	posterior shear	PS
$\pm F_y$	$\pm t_y$	lateral shear	LS
$+F_z$	$+t_z$	tension	TNS
$-F_z$	$-t_z$	compression	CMP
$\pm M_x$	$\pm\phi_x$	lateral bending	LB
$+M_y$	$+\phi_y$	flexion	FLX
$-M_y$	$-\phi_y$	extension	EXT
$\pm M_z$	$\pm\phi_z$	axial rotation	AR

oblique view

top view

frontal view

left lateral view
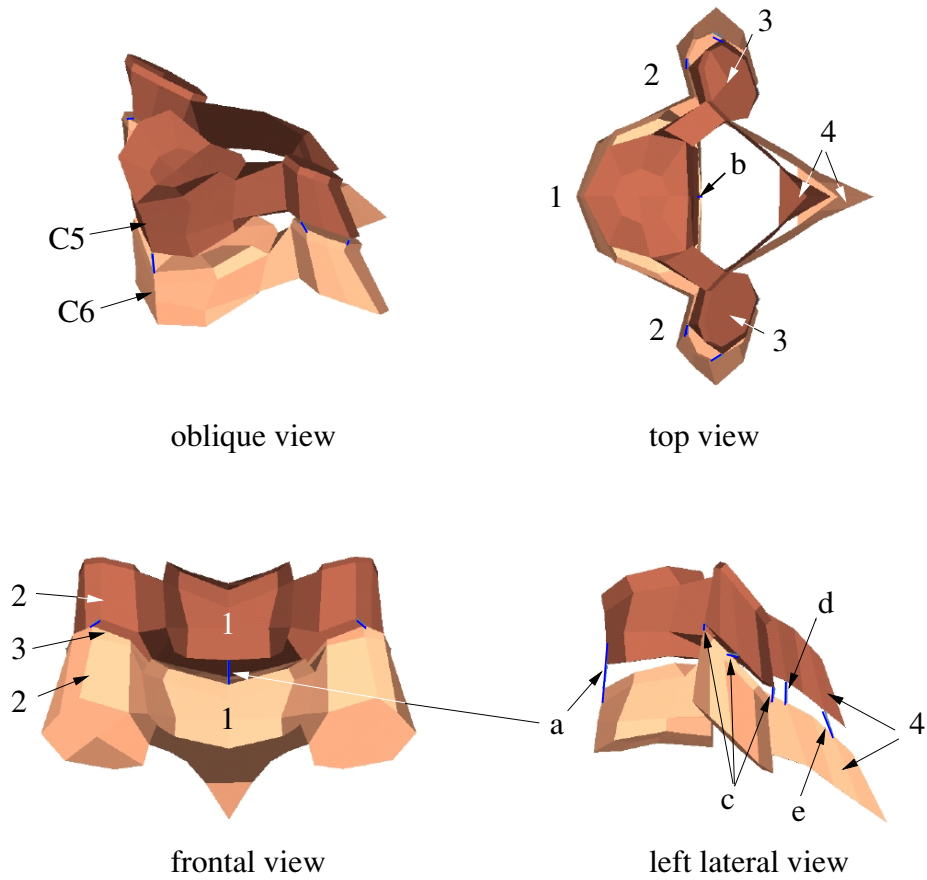
Figure 2.3: *Model of motion segment C5-C6. Legend: 1. vertebral body, 2. transverse process, 3. articular facets, 4. spinous process; a. anterior longitudinal ligament, b. posterior longitudinal ligament, c. facet joint capsule, d. flaval ligament, e. interspinous ligament, the intervertebral disc is not shown.*
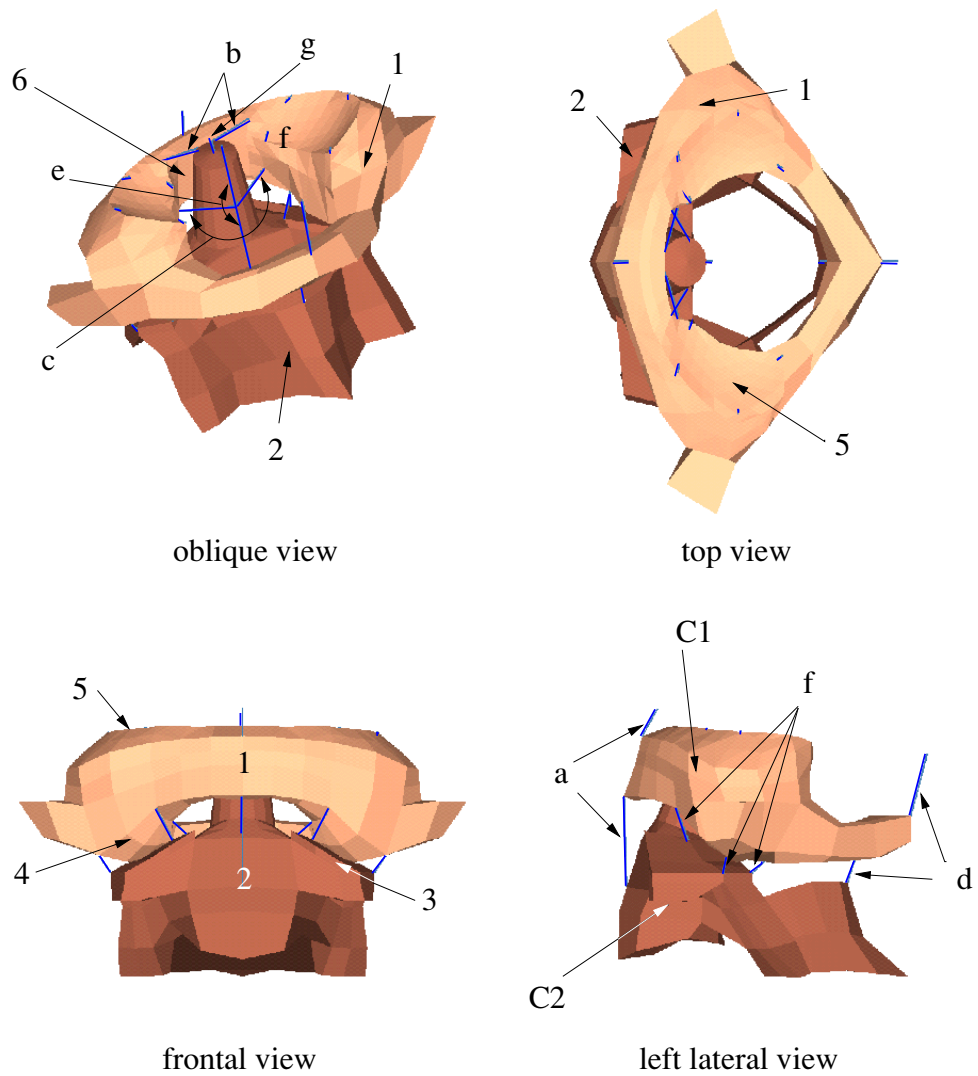
Figure 2.4: *Model of segment C2-C1. Shown are the ligaments and the facet surfaces representing axis with dens, atlas, and articular facet surfaces. For clarity, the skull with the occipital condyles is shown in Figure 2.5. Legend: 1. atlas (C1), 2. axis with dens (C2), 3. upper facets of C2, 4. lower facets of C1, 5. upper facets of C1, 6. facets for the atlas-dens contact; a. anterior membrane, b. alar ligament, c. transverse ligament , d. posterior membrane, e. tectorial membrane, f. joint capsule, g. apical ligament.*
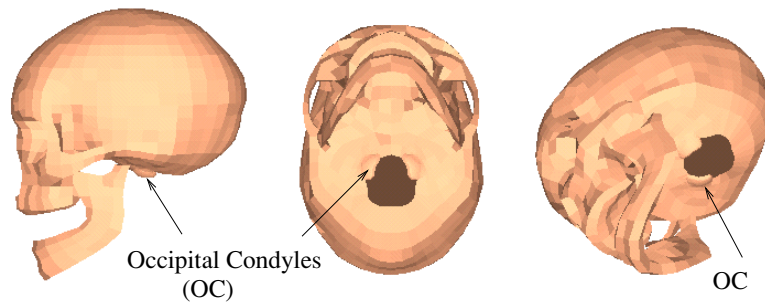
Figure 2.5: Lateral, bottom and oblique view of skull with occipital condyles (OC).
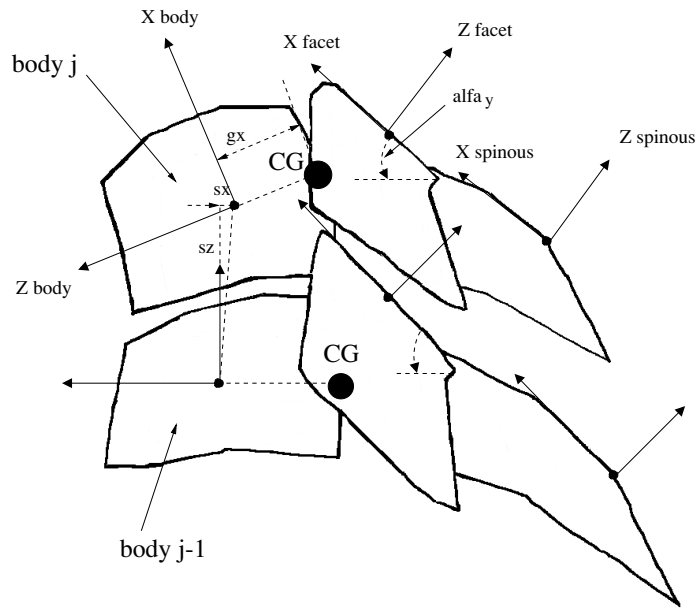
Figure 2.6: Lateral schematic view of two vertebrae showing the position of the local coordinate systems. See Section 2.2.1, 2.2.3 and 2.2.5 for definitions.

Table 2.3: *Inertial and geometric data with respect to lower body used for the rigid bodies in initial position. Due to midsagittal symmetry, $s_y = g_y = 0$. Adapted from [65].*

body no.	name	mass	moments of inertia				origin of coordinate system		position of centre of gravity	
			I_{xx}	I_{yy}	I_{zz}	I_{xz}	s_x	s_z	g_x	g_z
		kg		kg·cm^2			mm		mm	
1	T1	-	-	-	-	-	0.0	0.0	-	-
2	C7	0.22	2.2	2.2	4.3	-	0.0	18.0	−8.2	0.0
3	C6	0.24	2.4	2.4	4.7	-	0.0	17.5	−8.3	0.0
4	C5	0.23	2.3	2.3	4.5	-	0.0	17.0	−8.1	0.0
5	C4	0.23	2.3	2.3	4.4	-	−3.0	16.5	−7.9	0.0
6	C3	0.24	2.4	2.4	4.6	-	−3.0	16.5	−7.8	0.0
7	C2	0.25	2.5	2.5	4.8	-	−3.0	18.0	−7.7	0.0
8	C1	0.22	2.2	2.2	4.2	-	−2.0	18.5	−7.7	0.0
9	C0	4.69	181.0	236.0	173.0	71.0	−0.0	17.0	27.0	43.0

Table 2.4: *Orientation of facet joints (see Figure 2.6).*

body no.	name	orientation of upper facet joint w.r.t. to horizontal plane α_x	α_y
		deg	deg
1	T1	2.3	-24.0
2	C7	4.0	-28.8
3	C6	3.6	-28.3
4	C5	4.0	-30.6
5	C4	4.0	-40.5
6	C3	45.8	-47.7
7	C2	-28.6	0.0
8	C1	– *	– *

* concave facets of the atlas

planes or cylinders) or with finite elements.

The human anatomical data needed to define the geometry and inertial properties of the rigid bodies in the model are scarce. Data obtained within an European project are used, since these data were to the best knowledge of the author the best data accessible at that time. The 3D shape of the vertebrae and skull of the model is based on a 78 year old male post mortem human subject (PMHS) with a weight of 80 kg and standing and sitting height of 1.73 m and 0.92 m, respectively. The PMHS was seated in an automotive seat and frozen before it was sliced into pieces of 5 mm thick. The observed anatomy was used to define the geometry of the complete PMHS. The geometry of the vertebrae and skull was used to define a mesh for the model. Since however the neck of the 78 year old PMHS was too much slouched forward to represent a head-neck system of an average young human, the initial relative orientation of the vertebrae in the model is modified using a study of the curvature of the neck [65].

The inertial properties of the system are lumped into the rigid bodies, and represent the inertia of segments of the neck including the vertebrae and surrounding soft tissues. These properties are adapted from the De Jager model [65] (see Table 2.3). The position and the orientation of a body are described relative to its adjacent lower body in thoracic direction, by the coordinates s_x, s_y, s_z. Therefore, a local right-handed coordinate system was assigned to each body ($X_{body}, Y_{body}, Z_{body}$, see Figure 2.6 and Table 2.2). The position of the centre of gravity (CG) of body j is given relative to the local coordinate system of body j by the coordinates g_x, g_y, g_z (see Figure 2.6 and Table 2.3). The principal moments of inertia are defined with respect to a coordinate system with its origin at the CG and parallel to the body local coordinate system.

2.2.2 Discs

The intervertebral disc is a fibrocartilaginous joint between the endplates of two adjacent vertebral bodies. There are no discs between axis, atlas and occiput. The disc is modelled as a parallel connection of a spring and a damper for each of its six degrees of freedom (translational and rotational). The loads exerted by the disc on the vertebrae are given by:

$$F_{di} = k_{ti} \cdot t_i + b_{ti} \cdot v_i \tag{2.1}$$

$$M_{di} = k_{\phi i} \cdot \phi_i + b_{\phi i} \cdot \omega_i \tag{2.2}$$

with $i = x, y, z$ in which F_{di} and M_{di} are the components of the forces and moment relative to the i-axis of the lower body, t_i and ϕ_i the relative translations and rotations of the geometric centre of the disc, and v_i and ω_i the relative translational and rotational velocities of the disc centre. Note that the coupling between different degrees of freedom is neglected. The disc centre lies in the middle of the intervertebral disc space between the endplates of the disc [65]. A local coordinate system is used with its origin in the middle of the disc. The z-axis is defined perpendicular to the disc, and the x-axis is pointing posterior-anterior (see

Figure 2.6). The translations of the disc centre are measured relative to the lower body coordinate system and the rotations are measured as Bryant angles (in the order x, y, z) describing the orientation of the upper body relative to the lower one.

The stiffness data, used in the neck model, were based on literature (see Table 2.5). The stiffness for the disc segments in axial rotation, lateral bending and shear is based on Moroney *et al.* [90] and completed with the average disc stiffness in tension from Pintar *et al.* [120]. Both experimental studies were focussed on the low load responses. For compression it is expected that the force will increase non-linearly, based on the incompressible nucleus and the non-linear behaviour of the fibres of the intervertebral disc. The compression stiffness is based on a numerical study of a lumbar disc [36]. The response in compression of this finite element lumbar disc [36] lies well within the range of experimental data [18, 80] for low loads. The axial force-displacement relation for the lumbar disc was converted to an axial stress-strain relation using disc area and height. Assuming identical material properties of the lumbar and cervical disc, this stress-strain relation was converted to an axial force-displacement relation for the cervical disc. Earlier studies [65] with linear disc behaviour in flexion and extension showed non realistic model responses for flexion and extension loads. This could indicate that the disc bending stiffness should be nonlinear, such that the disc can more effectively constrain large displacements. Camacho *et al.* [20] published a non linear flexion and extension relationship of motion segments (two adjacent vertebrae with the surrounding soft tissues: intervertebral disc, facet joints and ligaments) for low loads. Because of the lack of data, experiments on these complete segments are used to define a nonlinear disc stiffness for flexion and extension. It is assumed that half of the flexibility of the segments is caused by the ligaments and half by the disc. Therefore the flexion/extension stiffness functions at each cervical level defined by Camacho *et al.* [20] are divided by 2 and used for the current intervertebral disc models. In summary, for compression, flexion and extension of the disc a non linear stiffness behaviour is modelled, while for the other directions a linear stiffness model is used. The disc stiffness is identical for each cervical level, however, the stiffness is dependent on the loading direction. Since the stiffness behaviour in flexion and extension is known for each cervical level separately [20], these stiffness functions are modelled unique per cervical level.

Soft tissues, such as the intervertebral discs, exhibit dynamic stiffening behaviour: the stiffness of the tissue increases with increasing deformation rate. From experimental studies [22, 48, 86, 175] it is known that the stiffness increases two to five times when the deformation rate increases by a factor 100 to 1000 relative to quasi-static loading rate of about 10 mm/s or 10 deg/s. The damping coefficients (see Table 2.5) used in the model are adapted from De Jager [65]. Since these damping coefficients were not sufficient however to account for the dynamic stiffening [65] the damping is used to attenuate the maximum linear and angular vibration accelerations of the head [65]. Additionally, the stiffening of the disc is explicitly included in the model as an on-off effect. The static elastic force F_{stat} transforms to the dynamic elastic force by:

$$F_{dyn} = F_{stat} \cdot M \tag{2.3}$$

As discussed above, deformation rates vary considerably in impacts. Based on experimental studies mentioned above [22, 48, 86, 175] the dynamic stiffness is assumed to be twice the static stiffness (static analysis $M = 1$; dynamic analysis $M = 2$).

Table 2.5: *Stiffness and damping values for intervertebral discs.*

Direction of Load		Stiffness [N/mm]		Damping [Ns/m]
Anterior shear [b]	k_{tx}	62	b_{tx}	1000
Posterior shear [b]	k_{t-x}	50	b_{t-x}	1000
Lateral shear [b]	k_{ty}	73	b_{ty}	1000
Tension [c]	k_{tz}	53	b_{tz}	1000
Compression [a,d]	k_{t-z}	822–2931	b_{t-z}	1000
		[Nm/rad]		**[Nms/rad]**
Flexion [a]	$k_{\phi y}$	0.022–5.4 [e]	$b_{\phi y}$	1.5
Extension [a]	$k_{\phi -y}$	0.022–8.2 [e]	$b_{\phi -y}$	1.5
Lateral bending [b]	$k_{\phi x}$	0.33	$b_{\phi x}$	1.5
Axial rotation [b]	$k_{\phi z}$	0.42	$b_{\phi z}$	1.5

[a] non linear; see text
[b] based on Moroney *et al.* [90]
[c] based on Pintar *et al.* [120]
[d] based on Eberlein *et al.* [36]
[e] for C3-C4; each cervical level has its own stiffness function
(functions by Camacho *et al.* [20] divided by 2)

2.2.3 Facet Joints

Facet joints are synovial joints formed by the corresponding articular facets of adjacent vertebrae and enclosed by joint capsules. The articular surfaces of the facet joints are rigidly attached to the vertebrae (see Figure 2.3). The articular facet joints are covered with a thin layer of hyaline cartilage allowing for sliding motion with almost no friction, due to the lubrication with synovial fluid [48]. Little deformation of the thin cartilage layer and stiff vertebra is expected.

Contact in the facet joints is modelled by three dimensional nonlinear translational springs, because the detailed geometrical information needed to define a smooth mesh of the facet joints was not available. A schematic view of the facet surfaces together with the local coordinate systems X_{facet}, Y_{facet}, Z_{facet} is shown in Figure 2.6. This facet joint coordinate system has its origin in the middle of the upper facet surface of the lower vertebra. The z-axis is defined perpendicular to the facet surface, and the x-axis is pointing posterior-anterior. The orientation of the upper facet joint of the lower vertebra with respect to a horizontal plane α_x, α_y is presented in Table 2.4 and Figure 2.6.

To approximate the synovial joint behaviour of the facet joints (i.e. no friction) the spring resistance in the shear directions, x and y is zero. The compression facet joint
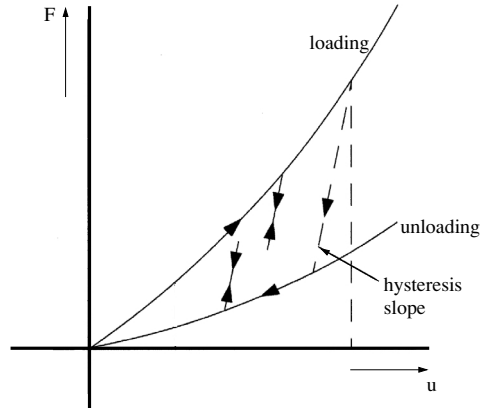
Figure 2.7: *Hysteresis model used for facet joint and spinous process [150].*

force F_{fz} is given by:

$$F_{fz} = \begin{cases} k_{fz} \cdot u_z & \text{for loading ;} \\ 0.5 \cdot k_{fz} \cdot u_z & \text{for unloading ;} \\ 10^{-7} & \text{hysteresis slope (see Figure 2.7).} \end{cases} \tag{2.4}$$

with u_z the compression of the spring, representing the relative penetration of the bodies of the facet joint surfaces, and k_{fz} the compression stiffness. The reader is referred to [150] for a more detailed description of the hysteresis model. Although not visualized in the model (see Figure 2.3 and 2.6) the neighbouring facet joints are initially in contact with each other. Since no experimental date on the contact between the facet joints are known, the compression stiffness k_{fz} representing contact between the facet joints, is based on the nonlinear static compression stiffness of the disc. It is expected that the facet joint contact will be stiffer than static disc compression allowing minimal deformation of the facet joints. The facet joint compression stiffness is assumed, based on engineering judgement, to be twice the static compression stiffness of the intervertebral discs ($k_{fz} = 2 \cdot k_{tz}$). The loss of energy during unloading is defined to be 50 %, using a hysteresis slope of 10^{-7} (see Figure 2.7). Additional resistance is offered through joint capsules in tension and shear. These capsules are modelled as ligaments and described in Section 2.2.6.

2.2.4   Occipital Condyles and Dens

It is assumed that the contact between the occipital condyles is important during motions of the occipito-atlanto-axial region. Therefore, the occipital condyles (OC) of C1-skull and the dens-contact area of C1-C2 are meshed in detail to define a convex-concave smooth contact area (see Figures 2.4 and 2.5). In these contacts the compliance of the materials is taken into account by allowing penetrations in

the contacting surfaces. For each node of the surface the contact force is obtained by multiplying the area around the node by the contact stress, which is based on a stress-strain function. This contact force is transferred from the surface model to the applicable rigid body.

It is assumed that little deformation will occur in the contact areas of the occipital condyles and the dens. Therefore a stiff contact is modelled. The contact stiffness of OC and dens was choosen such that the force-displacement relation of the complete contact was similar to that of the facet joints. Ligaments surrounding the dens and joint capsules offer resistance in tension and shear and are described in Section 2.2.6.

2.2.5   Spinous Processes

Spinous processes are protrusions of the vertebrae pointing to the back (see Figure 2.3). They constitute attachment points for muscles and ligaments. In extension, contact could occur between these protrusions. Since the mesh is too coarse to model realistic contact, this spinous process contact is modelled instead by a nonlinear spring model, as was done for the facet joints. A schematic view of the spinous processes together with the local coordinate systems $X_{spinous}, Y_{spinous}, Z_{spinous}$ is shown in Figure 2.6. The spinous process coordinate system has its origin at the back site of the spinous process of the lower vertebra. The z-axis is defined perpendicular to the spinous process surface, and the x-axis is pointing posterior-anterior (see Figure 2.6).

Since no experimental data are available on spinous process contact, stiffness functions as defined for the facet joint contact are used ($F_{spi} = F_{fi}$ see section 2.2.3 equation 2.4). The relative compression u_z is, in this case, the z displacement of the upper spinous process with respect to the lower vertebra in the local coordinate system of the spinous process. Initially there is no contact between the spinous processes. The contact force is initiated only once interpenetration of neighbouring spinous processes begins.

2.2.6   Ligaments

Ligaments in the spine allow motion within physiologic limits and prevent excessive motion. They may connect adjacent vertebrae, or extend over several vertebrae. Ligaments resist tension and become slack in compression. A load deformation curve of a ligament shows a sigmoidal shape: small loads produce large displacements (toe region) and when the ligaments are stretched their resistance to deformation increases (linear part) until failure occurs, which can be seen as a drop of force while the displacement is still increasing.

For simplicity, the broad ligaments are modelled as single line elements. The joint capsules are modelled as four single line elements around each facet joint (see Figures 2.3 and 2.4 and Table 2.7).

The origins and insertions of the ligaments are based on anatomical landmarks of the vertebral geometry. Ligament behaviour is modelled with elements producing force

only in tension. Ligament force F_l is given by

$$F_l = \begin{cases} F_{el}(\epsilon) & \text{for } \epsilon \geq 0 \text{ and } d\epsilon/dt \leq 0 \text{ (unloading)}; \\ F_{el}(\epsilon) \cdot (1 + C \cdot d\epsilon/dt) & \text{for } \epsilon > 0 \text{ and } d\epsilon/dt > 0 \text{ (loading)}; \\ 0 & \text{for } \epsilon < 0 \text{ (slack)}. \end{cases} \quad (2.5)$$

Elastic behaviour is prescribed by the nonlinear force-strain curve $F_{el}(\epsilon)$ with strain defined as ϵ, the elongation divided by its rest length. The rest length is defined as the length of the ligament in the initial position (i.e. an erect position of the cervical spine), assuming that the ligaments are neither slack nor taut initially. The dynamic behaviour of the ligaments is represented by the coefficient C.

The elastic properties of a ligament are determined both by the ratio of collagen and elastin fibres in the ligament and by their arrangement [35], therefore each ligament has its own material properties. The elastic properties are based on experimental studies by Pintar [119] and Yoganandan *et al.* [178] (see Table 2.7). Since unrealistic large motions of the upper neck occured during flexion and extension (see previous studies [65] and Chaper 3) the stiffness of the upper neck ligaments of the model is increased compared to experimental data. The toe region is defined per ligament and based on engineering judgement (see Figure 2.8). The end of the toe region is defined where the linear part starts, at 20% of the initial length of the ligament.
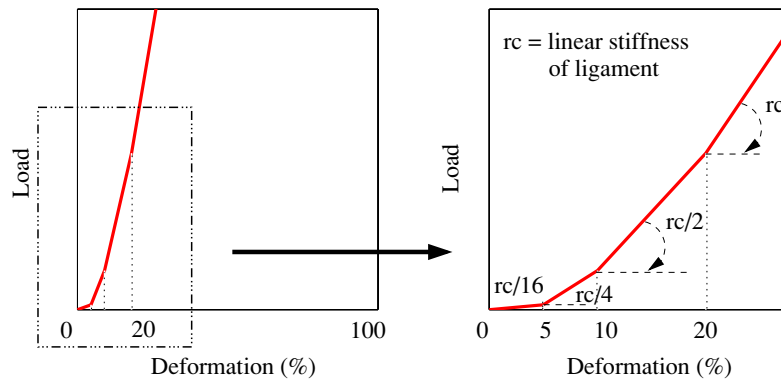
Figure 2.8: *Load deformation curve for ligaments (see also Table 2.7).*

Comparison of the literature describing tensile tests performed on ligaments shows that there is little agreement about the effect of loading velocities. Four different statements can be found in the literature for the effect of increasing strain rate: 1) failure stress and failure strain increase [26, 97, 171], 2) no change in the failure stress or failure strain occurs [34, 77], 3) failure stress increases and failure strain remains constant [39, 175], and 4) failure stress remains constant and the failure strain decreases [5, 76, 110, 154]. The different conclusions could be explained by the differences in the elastic properties of the ligaments used. Also, an exact measurement of mechanical properties of biomaterials in tensile tests at high

velocities is still very difficult. Therefore, results of these tests have to be used with caution. In contrast with the elastic properties in dynamic conditions, most authors agree about the failure mechanisms. In this study the results of Panjabi [110] are used for the Alar (ALAR) and transverse (TL) ligament, while the other ligaments have the dynamic behaviour as reported by Yoganandan [175]. This assumption results in a rate dependency coefficient $C = 0.4$ for all ligaments [175], except for ALAR and TL, which have a coefficient 100 times higher resulting in $C = 40$ [110].

2.2.7 Muscles

Muscles perform three tasks in the human neck. Firstly, muscle reflexes provide stability of the neck and head in a given posture. Secondly, they enable movements of the head during physiological activity. The third task is to assist in the protection of the cervical spine. In the model the neck muscles are included to study the effect of passive and active muscle behaviour on the head-neck response to impacts.

The muscles in the neck model are shown in Appendix A, in Figures A.1, A.2 and A.3. The coordinates of the origins and insertions of the muscles represent an average position, since most cervical muscles have several origins and insertions. The positions are based on detailed anatomy textbooks [69, 123, 124], data on bony geometry [111, 114] and choices made by other researchers in this field [33, 132, 163]. T1 serves as the base of the neck model. Muscles which have their anatomical origin on T2 or lower are mathematically connected to body 1 representing T1. The origins of these muscles are based on assumed anatomical locations of the thoracic vertebrae (i.e. below and outside the T1 vertebra, see Figures in Appendix A). This results in realistic anatomical lenghts and location of the muscles (i.e. realistic muscle force lines of action).

Most muscles are represented by more than one muscle element to account for different points of attachment of the muscle group [132]. This methodology resulted in 68 mid-sagittal symmetrical pairs of muscle elements. Each element is divided into segments which are supported on the applicable vertebrae by intermediate sliding points enabling muscles to curve around the vertebrae. These sliding points are located on the points of intersection of the muscle line of action in initial position and the xy-plane of the intermediate vertebrae. The origins and insertions of the muscle elements are presented in Appendix A, in Tables A.1, A.2 and A.3.

Hill-type Muscle Elements

A Hill-type muscle model is available in MADYMO. The muscle elements comprise a contractile element (CE) describing the active force F_{CE} generated by the muscle through contraction, and a parallel elastic element (PE) describing the passive elastic force F_{PE} due to elongation of the muscle tissues. Muscle force F_{mus} is the sum of both forces, thus

$$F_{mus} = F_{CE} + F_{PE} \tag{2.6}$$

Passive muscle behaviour

Passive muscle behaviour is modelled similar to the model of Deng and Goldsmith [33] by the nonlinear stress-strain relation (see Figure 2.9):

$$\sigma = \frac{k \cdot \epsilon}{1 - \epsilon/a} \tag{2.7}$$

with strain ϵ defined as the elongation relative to the rest length of the muscle, k the passive muscle stiffness, a the strain asymptote. The strain is defined as [17]:

$$\epsilon = \frac{l - l_{free}}{l_{free}} \tag{2.8}$$

The free length, l_{free} [17] is defined as the length of a muscle at rest when it is removed from the body, the "removed" length. The free length of a muscle is however unknown. A passive muscle (a muscle without neural input) *in situ*, at rest experiences an initial stress, therefore, the muscle at rest will shorten when it is removed from the body. This results in a smaller free length than the muscle length in initial position (i.e. an erect position of the cervical spine) which is defined as l_{rest}. Assuming a linear relationship between sarcomere length s (known from literature, see Table 2.6) and muscle length, the free length can be calculated as:

$$l_{free} = l_{rest} \cdot \frac{s_{free}}{s_{rest}} \tag{2.9}$$

The muscle optimum or reference length l_{ref} is based on [17]:

$$l_{ref} = l_{rest} \cdot \frac{s_{ref}}{s_{rest}} \tag{2.10}$$

Knowing the passive muscle stress for any length of muscle, the force F_{PE} due to the passive component can be computed from:

$$F_{PE} = \sigma \cdot PCSA \tag{2.11}$$

with $PCSA$ the physiologic cross-sectional area of the muscle. See Tables 2.6, A.1, A.2 and A.3 for the values of above mentioned parameters.

Active muscle behaviour

The active muscle force functions are based on standard functions presented in the MADYMO manual [151]. The active force is given by

$$F_{CE} = A \cdot F_{max} \cdot f_H(v_r) \cdot f_L(l_r) \tag{2.12}$$

The factor A, the activation state, describes the normalized activation level of the muscle and varies between 0 (rest state) and 1 (maximum activation). The parameter

F_{max} is the muscle force at maximum activation in isometric conditions ($v = 0$) and at the reference length. F_{max} is calculated as follows:

$$F_{max} = \sigma_{max} \cdot PCSA \tag{2.13}$$

with σ_{max} the maximum isometric muscle stress and $PCSA$ the physiological cross-sectional area of a muscle. The dimensionless lenghtening velocity is defined as $v_r = v/V_{max}$ with v the momentaneous lenghtening velocity and V_{max} the maximum shortening velocity of the muscles. It is assumed that V_{max} is independent of the activation state. Function f_H is the normalized active force-velocity relation (Hill-curve). Separate functions are defined for lenghtening and shortening of the CE-element:

$$f_H(v_r) = \begin{cases} 0 & v_r \leq -1 \\ \dfrac{1 + v_r}{1 - v_r/CE_{sh}} & -1 < v_r \leq 0 \\ \dfrac{1 + v_r CE_{ml}/CE_{shl}}{1 + v_r/CE_{shl}} & v_r > 0 \end{cases} \tag{2.14}$$

The shape is determined by the parameters CE_{sh} and CE_{shl}, whereas CE_{ml} defines the maximum force the muscle can generate during lengthening relative to the maximum isometric force F_{max} (see Figure 2.9).
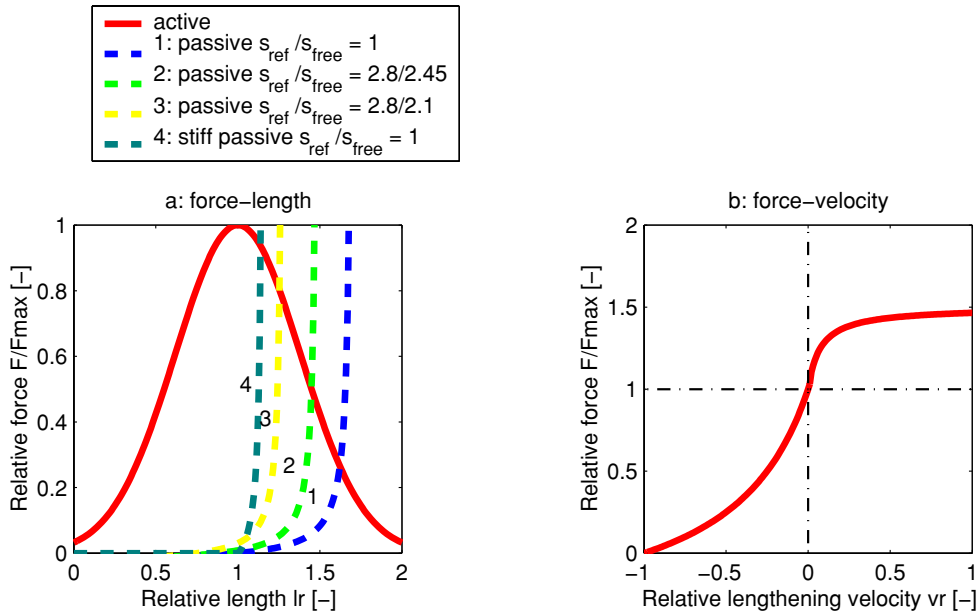
Figure 2.9: *Muscle functions. (a) Normalized passive force-length curve F_{PE} (dashed) and standard active force-length curve f_L for $S_k = 0.54$. (b) Standard force-velocity curve f_H (Hill-curve) for $CE_{sh} = 0.5$, $CE_{shl} = 0.075$ and $CE_{ml} = 1.5$.*

Function f_L is the normalized active force-length relation with function

$$f_L(l_r) = e^{-\left(\frac{l_r - 1}{S_k}\right)^2}$$
(2.15)

in which parameter S_k determines the shape (width) of the curve (see Figure 2.9) and l_r is the dimensionless muscle length

$$l_r = \frac{l}{l_{ref}}$$
(2.16)

with l the momentaneous muscle length and l_{ref} the optimum or reference length at which the active force is generated most efficiently (see also equation 2.10).

The mechanical parameters used in the model are presented in Table 2.6. The maximum isometric muscle stress at the fibre rest length, σ_{max} has been estimated between 20 and 100 N/cm^2 in the human model literature [164]. Maximum muscular forces are easily underrated, because subjects can hardly be expected to fully activate muscles over some time without co-contraction of antagonist muscles. Our research aim is to determine to what extent muscle forces can be relevant in impact conditions. Therefore, we adopted the rather high value of 70 N/cm^2, which can be assumed to represent well trained subjects. The $PCSA$ of the muscles is based on a study by Meyers [93] and on isometric volunteer experiments (see next section). The sum of the $PCSAs$ of the muscle elements is equal to the human muscle $PCSA$ according to literature [93], see Appendix A Table A.1, A.2 and A.3.

The relative maximum shortening velocity V_{maxr} depends on the ratio of slow and fast twitch muscle fibres. Winters and Stark [161] proposed ranges V_{maxr} = 2-10 and CE_{sh} = 0.1-5 for slow to fast twitch muscle fibres. Winters [162] proposed ranges V_{maxr} = 2-8 and CE_{sh} = 0.1-1 for slow to fast twitch muscle fibres. Zajac [181] proposed using V_{maxr} = 10 for all mixed fibre-type muscles. Intermediate values, representing an average fibre composition (see Table 2.6), are used in this study. The parameter CE_{ml}, representing lengthening muscle force, is reported to range from 1.1-1.8 [181]. Winters and Stark [164] have used CE_{ml} = 1.3. Krylow and Sandercock [73] report eccentric forces more than twice the isometric force. Cole *et al.* [23] were able to accurately reproduce eccentric loading data from Joyce et al. [67] and Walmsley and Proske [156] with a Hill type model. They estimated eccentric forces increasing asymptotically to 2.3 times the isometric force. In the new neck model CE_{ml} is defined to be 1.5. The shape parameter CE_{shl} has been given a value of 0.075 to obtain a smooth force-velocity curve (see Figure 2.9). The resulting Hill curve describing the relation between elongation velocity and active force is given in Figure 2.9.

Muscle activation is described by two dynamical processes: neural excitation and active state dynamics. The normalized neural excitation E ($0 \leq E \leq 1$) is described by the first-order system

$$\frac{dE}{dt} = \frac{u - E}{T_e}$$
(2.17)

Table 2.6: *Model parameters for passive and active muscle behaviour.*

Muscle parameter	Symbol	Value	Reference
average sarcomere length of "free" muscle	s_{free}	2.1 μm	[79]
length of sarcomere at rest	s_{rest}	see Table A.1, A.2, A.3	[93]
sarcomere length at muscle optimal length	s_{ref}	2.8 μm	[125]
length of "free" muscle	l_{free}	$l_{rest} \cdot \frac{s_{free}}{s_{rest}}$ *	[17]
length of muscle at rest	l_{rest}	based on initial position of model	
optimum length of muscle	l_{ref}	$l_{rest} \cdot \frac{s_{ref}}{s_{rest}}$	[17]
maximal isometric stress	σ_{max}	70 N/cm^2	[164]
relative maximum shortening velocity	V_{maxr}	6/s	[162, 164]
maximum shortening velocity	V_{max}	$V_{maxr} \cdot l_{ref}$	[162, 164]
shape force-velocity curve (shortening)	CE_{sh}	0.25	[162, 164]
shape force-velocity curve (lengthening)	CE_{shl}	0.075	[151]
maximum relative force (lengthening)	CE_{ml}	1.5	[23]
shape active force-length curve	S_k	0.54	[151]
passive force-length stiffness	k	3.34 N/cm^2	[32]
passive force-length asymptote	a	0.7	[32]

* for $\frac{s_{ref}}{s_{free}}$ < 1 slack initially; = 1 neither slack nor taut initially; > 1 initial muscle stress

with dE/dt the derivative of E towards time t, T_e the time-constant and u the normalized neural input ($0 \leq u \leq 1$) [161]. Here, it is assumed that the activation of a muscle is determined by a single neural input: the muscle is not activated for $u = 0$ and maximally activated for $u = 1$. The normalized activation state A ($0 \leq A \leq 1$) is described by the first-order system

$$\frac{dA}{dt} = \frac{E - A}{T_a} \text{ with time-constant } T_a = \begin{cases} T_{ac} & \text{if } E > A \text{ activation} \\ T_{da} & \text{else deactivation.} \end{cases} \tag{2.18}$$

Deactivation is not considered here.

Muscle dynamics are described by time-constants T_e, T_{ac} and T_{da}, and the neural input u. The time-constants lie in the range $25 \leq T_e \leq 50$ ms and $5 \leq T_{ac} \leq 15$ ms according to Winters and Stark [161]. A step response is assumed for input u: it changes instantaneously from 0 to 1 at a certain time t_{act} defined as the time it takes to start activation of a neck muscle in reaction to an external disturbance such as an impact. Figure 2.10 shows the change of u, E, and A with time for $t_{act} = 74$ ms, $T_e = 45$ ms and $T_{ac} = 10$ ms. Signal A is used in the model simulation to describe muscle contraction.

Isometric Voluntary Muscle Contraction

To describe the 68 muscle pairs in the model, many experimental data, often from different sources, were used. As a first test for the biofidelity of the model, especially with respect to muscle behaviour, the torque distribution in the neck during isometric voluntary muscle contraction has been studied. It is generally assumed that in the human body the dorsal muscles generate the largest torque at T1-level and that this torque decreases in the direction of the head, cranially. This behaviour is verified for the neck model using experimental studies published in literature. The muscle stress
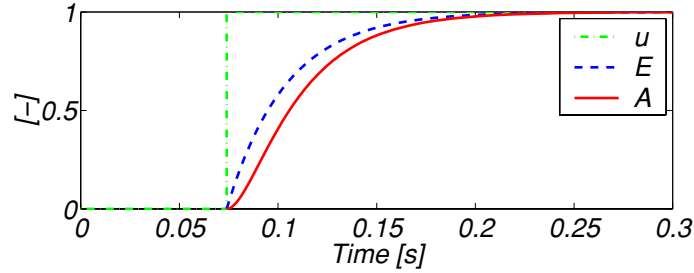
Figure 2.10: *Time signals of neural input u, neural excitation E and activation state A for t_{act} = 74 ms, T_e = 45 ms and T_{ac} = 10 ms.*

σ, muscle $PCSA$ and muscle line of action will influence the torque distribution. When necessary muscle $PCSA$ is adapted to meet the torque distribution as described above.

Snyder *et al.* [136] have determined the maximal isometric force exerted by the head in forward and backward direction in a neutral head position. Only the back of the subjects was supported. For 18-24 year old, 40-60 percentile males (N=9), Snyder *et al.* [136] found a maximal force of 149 N (33.4 lbf) flexion and 163 N (36.6 lbf) extension. Mayoux-Benhamou *et al.* [83] found a maximum isometric extension force of 200 N averaged over 9 young females and 7 young males. In these experiments the torso was stabilized in a sitting position. Marotzki [81] found similar forces in a comparable experiment, but found strongly increased head forces when the torso was supported by hand bracing. For young males bracing yielded 176 N (39.6 lbf) flexion and 356 N (80.1 lbf) extension. The moment arm of the applied head forces with respect to C7 was about 0.2 m for the referred young male population of Snyder *et al.* [136]. In combination with the maximum forces of Marotzki [81] this yields 35 Nm flexion and 71 Nm extension torques at C7.

The isometric voluntary contraction is simulated by activating the flexor or extensor muscles maximally, maintaining the neck in initial position. The sternocleidomastoid is an extensor for the upper neck whereas it is a flexor for the lower neck, therefore the torque depends on the activation of this muscle. To reach an acceptable torque distribution the $PCSA$ of a few muscles have been changed compared to the data presented by Myers [93] see Table A.1, A.2 and A.3. The final torque distribution is shown in Figure 2.11. Acceptable maximum isometric torques for the model are reached at T1 level given the above estimated torques from the volunteer head loading experiments.

Table 2.7: *Overview static stiffness in the ligamentous cervical spine.*

tissue			data source	value in model [+]
discs [o]	*direction of load*			
	anterior shear		[90]	average [d]
	posterior shear		[90]	average [d]
	compression		[36]	average
	tension		[120]	average [d]
	flexion		[20]	0.5 * average [c]
	extension		[20]	0.5 * average [c]
	lateral bending		[90]	average [d]
	axial rotation		[90]	average [d]
facet joint [o]				
	compression		-	2 * disc
	others		-	no stiffness
occipital condyles [o]				
	compression		-	2 * disc
	others		-	no stiffness
spinous process [*]				
	compression		-	2 * disc
	others		-	no stiffness
ligaments [,o]*	*full name*			
ALL	Anterior longitudinal ligament		[178]	average
PLL	Posterior longitudinal ligament		[178]	average
FL	Flaval ligament		[178]	average
ISL	Interspinous ligament		[178]	average
JC lower neck [a]	Joint capsules		[178]	average
LN lower neck [b,*]	Nuchal ligament		as ISL [119]	average
JC upper neck [a]	Joint capsules		[119]	3 * (average+SD)
LN upper neck [b,*]	Nuchal ligament		as PM [119]	3 * (average+SD)
AM	Anterior membrane		[119]	3 * (average+SD)
PM	Posterior membrane		[119]	3 * (average+SD)
ALAR	Alar ligament		[119]	average+SD
AP [*]	Apical ligament		[119]	3 * (average+SD)
TL [b]	Transverse ligament		as APICAL [119]	average
TM [b]	Tectorial membrane		[119]	average
CF [b,*]	Cruciform ligament		[119]	average

[*] new compared to De Jager model
[o] modified compared to De Jager model
[+] average of experiments
[a] symmetrically modelled as 4 line elements on left (JCl) and right side (JCr). The 3 ventrolateral segments are twice as stiff as the dorsal segment (JC3) [152]
[b] modelled as segmented line elements with slip rings
[c] each cervical level has its own stiffness function, 0.5 * segment stiffness
[d] linear stiffness function

Table 2.8: *Overview of detailed multibody and finite element neck models.*

Model	Multibody		Finite Element		Multibody	
Reference	De Jager [64, 65]		Bertholon [7]		this thesis	
	mechanical behaviour	element	mechanical behaviour	element	mechanical behaviour	element
Head	rigid	ellipsoids	rigid or viscoelastic	solids	rigid	arbitrary surfaces
Vertebra	rigid	ellipoids	rigid	solids	rigid	arbitrary surfaces
C0-C1 joint			3D nonlinear viscoelastic	lumped joint rotational spring-damper (3 DOF)		
C1-C2 joint			3D nonlinear viscoelastic	lumped joint rotational spring-damper (3 DOF)		
Disc	3D linear viscoelastic	spring-damper (6 DOF)	3D linear viscoelastic	solids (6 DOF)	3D (non)linear viscoelastic	spring-damper (6 DOF)
Ligaments	2D nonlinear viscoelastic	spring-damper (1 DOF)	2D nonlinear viscoelastic	spring-damper (1 DOF)	2D nonlinear viscoelastic	spring-damper (1 DOF)
Facet joints contact	frictionless	ellipsoids	frictionless	rigid FE surface	3D nonlinear viscoelastic	spring-damper (3 DOF)
OC and dens contact	frictionless	ellipsoids	-		frictionless	arbitrary surfaces
Spinous process contact	-		frictionless	rigid FE surface	3D nonlinear viscoelastic	spring-damper (3 DOF)
Muscles	force-generating Hill type	straight lines (1 DOF)	anisotropic nonlinear with unloading	solids (passive only)	force-generating Hill type	curved lines (1 DOF)
Skin	-		nonlinear elastic	membranes	-	
Soft tissue	-		linear	solids	-	

DOF = degrees of freedom
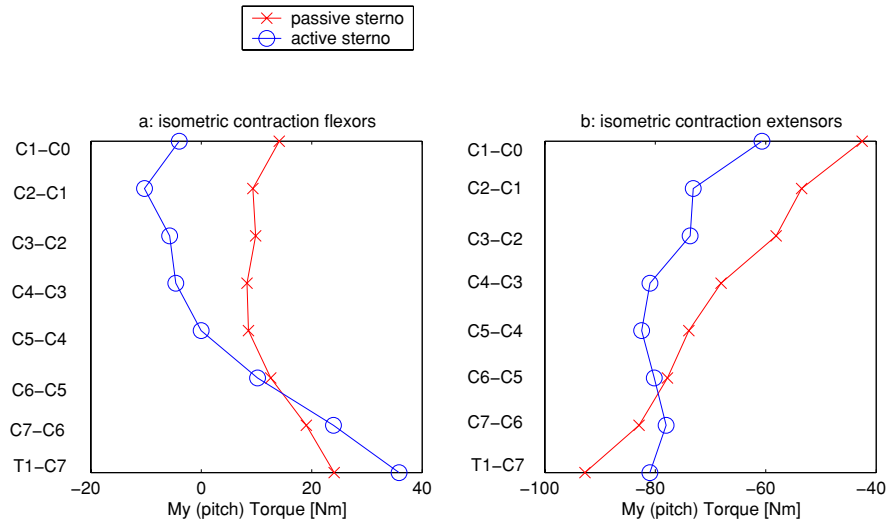
Figure 2.11: *Flexion and extension torques in initial position due to maximum isometric muscle forces. For flexion all flexor muscles (with and without activation of the sternocleidomastoid) are maximally activated, while for extension torques the extensor muscles (with and without activation of the sternocleidomastoid) are maximally activated.*
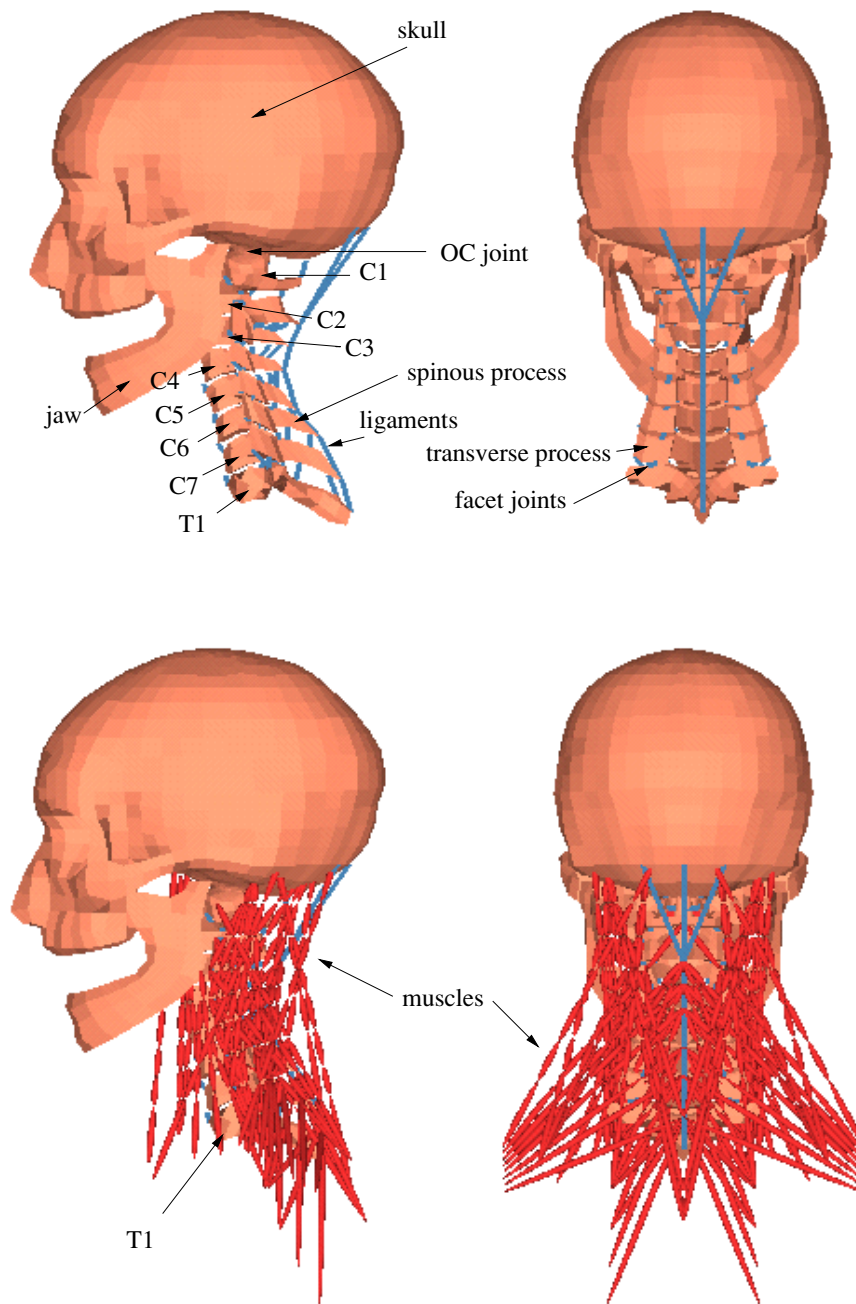
Figure 2.12: *General lateral and rearward view of the detailed neck model without (upper) and with muscles (lower).*

2.3   Discussion

In this chapter a detailed multibody neck model has been presented. The model consists of a rigid head, rigid vertebrae, (non)linear viscoelastic discs, frictionless facet joints, nonlinear ligaments and segmented contractile muscles. Earlier versions of the neck model have been published in [64, 65]. An intermediate model in which the muscles line of actions are updated is presented elsewhere [61]. The model can be applied separately or integrated into a model of an entire human body (see Chapter 5).

The neck model has been extended with a surface description of the vertebrae based on a human cadaver, which is more realistic and detailed compared to the ellipsoid model used by De Jager. The occipital condyles and the dens contact area are meshed in detail to define smooth contact areas. This new geometry resulted in better defined locations of the intervertebral disc, spinous processes, facet joints, ligaments and muscles. The mesh used is however too coarse for modelling contact between the facet joints in the lower neck. Therefore, these joints are modelled using a spring damper system, allowing resistance in compression only. The same modelling technique was used to model contact between the spinous processes. As a result of using compression contact the force is always applied to the back end of the spinous process, and in the middle of the facet joint surface respectively (the begin and end positions of the spring models). This situation will be unrealistic for large extension rotations with contact of the vertebrae, where the end point of the spinous process of the upper vertebra could impact halfway the spinous process of the lower vertebra.

Static data in the model are based on experimental studies on cervical spine components (see Table 2.7). However, no data were found which could be used for modelling the contact stiffness of the facet joints and the spinous processes. Therefore, these stiffness functions are based on engineering judgement representing stiffer contact than the compression of the disc. Linear stiffness functions for the intervertebral disc are based on static experiments at low loads on cervical spine discs [90]. The disc stiffness for compression, flexion and extension was improved by adding nonlinear stiffness for these loading directions. Non-linear stiffening is defined for compression based on a model of a lumbar segment [36]. For flexion and extension the non linear stiffness is based on experiments on cervical spine segments performed by Camacho *et. al* [20]. Dynamic tests were not available for the intervertebral disc, therefore the dynamic behaviour is based on dynamic experiments on other spinal tissues [22, 48, 86, 175]. The disc in the new model has non linear stiffness in contrast with the De Jager model, but the dynamic behaviour of the disc was modelled in a similar way to the De Jager model [65].

More ligaments have been added, and the ligament stiffness of the De Jager model has been updated using recent literature data. It should be noted that for both models (the De Jager model and the new model) the ligament stiffness is nonlinear. Parameters for ligaments are based mostly on static [119, 178] and together with a few dynamic tests [110, 175]. The stiffness of the upper neck ligaments was increased compared to literature data to limit the large motions of the C0-C2 complex. For most ligaments failure forces are given in the literature. Thus ligament injury risk can be

monitored with the model (see Chapter 6) but actual failure modelling has not been implemented.

Finally, the muscle physiological cross sectional areas and the maximum isometric stress have been updated. Muscle parameters were based on general properties [161, 162, 164] combined with recent data for PCSA [93]. Both muscle models (De Jager and current model) use the Hill type muscle model available in MADYMO, however, different values for the parameters are used. Additionally, muscles in the De Jager model are modelled as straight line elements, while muscles in the current model can follow the curvature of the neck, resulting in more realistic muscle force line of action.

In reality, the neck muscles are slightly activated to maintain an initial position of the head. To incorporate this into the model would require neural excitation of the muscles utilizing a complex feedback mechanism. Since this is beyond the primary interest of this study a simpler approach has been used for muscle activation during impact (see Section 4.1.2). It should be noted that the disadvantage of this simpler method is that the model does not predict a stable upright initial position of the head when subjected to gravity only. This limitation was also present however in the De Jager model.

The new model is a major update of the De Jager model [65]. Comparable multibody techniques to the De Jager model were applied, but the geometrical description of the vertebrae is considerably improved, and ligaments and muscles are implemented in more detail. Stiffness properties of the tissues, when available are based on literature data (see Table 2.7). In Table 2.8 the current neck model is compared to the De Jager model [65] and the finite element model by Bertholon [7].

A major advantage of the new model compared to other multibody models and finite element models is the realistic and detailed modelling of active force generating muscle elements. Another advantage of the new multibody model is the detailed geometry especially of the upper neck joints. The most important simplifications in the model are the rigid head and vertebrae, and the use of spring damper models for the discs and the facet joints in the lower cervical spine. Finally, the time efficiency is much greater for multibody models compared to finite element models.

A disadvantage of all models is the lack of published tissue properties. Therefore, it is recommended that experiments are performed to quantify the characteristics of cervical intervertebral discs, cervical spinal ligaments, facet joints and contact of spinous processes in static and dynamic conditions, in order to verify, and when necessary improve, these tissue properties in the new model. The new model has the potential to study local kinematics, such as vertebral rotations, tissue forces and elongations. Since some model inputs are based on assumptions, model validation is needed to show the reliability of the model response. Therefore, in the following chapters quasi-static and dynamic validation of the new model using published experiments will be presented.

Chapter 3

Response to Quasi-Static Loading

A new detailed multibody neck model has been presented in Chapter 2. The objective of this chapter is to demonstrate the biofidelity of this new neck model for quasi-static loading. The response under such loading conditions is important when using the model for studying injury mechanics at small impact severity levels, as well as when using the model for vibration analysis [58]. Published quasi-static experiments of upper and lower cervical spine segments, as well as experiments of the whole cervical spine, are used to study the biomechanical response of the new neck model.

3.1   Material and Methods

The lower and upper cervical spine models are validated for 6 degrees of freedom (DOF) by comparing the responses of the modelled motion segments with published experimental data of quasi-static tests (see Section 3.1.1). Additionaly, large loads are applied on the same segments to study the response of the model under more severe static loads (see Section 3.1.2). Finally, quasi-static flexion and extension experiments of the entire ligamentous spine are simulated to validate the entire model (see Section 3.1.3).

The experiments used for model validation were performed to define the *in vitro* physiologic range of motion (ROM). The physiologic range starts with the neutral zone in which little load is needed to deform the structure. The transition for the neutral to the elastic zone is characterized by a substantial increase in load. Throughout the elastic zone, the relation between deformation and load is fairly linear and when the load is released the specimen will return to the state it had before being loaded. The ROM is defined as the sum of the neutral zone and the elastic zone, and represents the total amount of displacement that a motion segment can sustain without being damaged [65]. However, identifying precisely when damage (microtrauma) starts and the ROM ends is difficult, causing differences between

37

studies. Specifying the ROM together with the load that caused it enables a better comparison of ROMs reported in different studies.

All model simulations were carried out without inclusion of the effects of muscular tissue, allowing a direct comparison with the available experimental data. The dynamic stiffening factor for the intervertebral discs was set to one ($M = 1$), which represents static stiffness (see equation 2.3). An acceleration field of 9.81 m/s^2 was included to simulate the effect of gravity. Loads were applied slowly to minimize viscous effects, such that the load displacement curves represent the elastic response. Translations were measured at the centre of the local body coordinate systems and rotations were measured using Bryant angles in the order x, y, z. See Table 2.2 for the definition of directions for the loads (forces F and moments M) and the corresponding displacements (translations t and rotations ϕ).

3.1.1   Small Loads on Motion Segments

Moroney *et al.* [90] subjected disc segments and motion segments of the cervical spine to static loads (20 N, 1.8 Nm). These disc experiments are used to define the disc stiffness of the model (see Chapter 2), while the experiments on motion segments are used here for validation of whole segments (including disc, ligaments and facet joints). Loads were applied to the upper vertrebra. The resulting three-dimensional displacements and rotations at the geometric centre of the upper vertebra were measured.

Although the experimental data is available for all segment levels, for simplicity only two representative segments are validated. Segments C3-C4 and C5-C6 were chosen as the facet surface orientations of these segments differ significantly: the upper facets of C4 are more backward facing than those of C6. In accordance with the experiments not only the muscles, but also the nuchal ligament is excluded in the segment models. In the simulations the loads were applied to the upper vertebra at the centre of the disc, such that the direction of the load did not change relative to the lower vertebra. Moroney applied an axial preload of 49 N to the segments for all experiments, but this preload is not applied in the simulations because its effect is already incorporated in the disc characteristics. The model response is compared with the average ($\pm$ SD) of all segment experiments in the cervical spine [90].

The upper cervical spine (C2-C1-C0) is validated by simulating the experiments by Panjabi and co-workers [99, 107, 108, 112]. These researchers subjected upper cervical spine specimens to static rotational loads (1.5 Nm) at the occiput (C0) while the axis (C2) was fixed. The main and coupled rotations were measured. Coupled translations measured at the anterior edge of the foramen magnum of the occiput and at the anterior ring of the atlas were presented by Oda *et al.* [100]. Experimental data for translational loading on C2-C1-C0 are not available for model validation, and therefore these simulations are not performed.

In the model simulations 1.5 Nm moments are applied at the occiput such that the direction of the applied moment does not change relative to C0 in the simulations,

similar as in the experiments [108]. The coupled translations are measured at the foramen magnum of the occiput and at the anterior ring of the atlas [100]. These points are positioned at coordinates (9,0,-10) and (10,0,-4) mm in the local coordinate system of C0 and C1, respectively.

3.1.2 Large Loads on Motion Segments

The vertebral rotations of the motion segments of the model are compared to the *in vivo* ROM published by White and Panjabi [158] (see Table 3.1). Their data is based on various studies. In most of these studies, measurements were derived from radiographic examination of volunteers.

The segment models (C5-C6, C3-C4, C0-C1-C2) are subjected to large loads (500 N and 20 Nm) to determine their load-displacement curves. To determine C0-C1 behaviour, C0 is loaded at the origin of its body local coordinate system whilst C1-C2 is locked (behaving as one fixed segment). Similarly, whilst C0-C1 is locked, when C1 is loaded to determine the C1-C2 response.

Table 3.1: *Representative ranges of motion for* in vivo *rotation of the cervical joints [158] adapted from [65]. Values in bold are used for qualitative validation.*

motion	C0-C1	C1-C2	C2-C3	C3-C4	C4-C5	C5-C6	C6-C7	C7-T1
				degrees				
one side lateral bending	**5**	**5**	10	**11**	11	**8**	7	4
combined flexion/extension	**25**	**20**	10	**15**	20	**20**	17	9
one side axial rotation	**5**	**40**	3	**7**	7	**7**	6	2

3.1.3 Flexion/Extension Loads on Entire Cervical Spine

Camacho *et al.* [20] published static flexibility experiments on ten unembalmed male human head and cervical spine preparations. The sagittal plane bending responses were measured in a load frame designed to apply pure moments. Pure moments up to 1.5 Nm (flexion) and up to -1.5 Nm (extension) were applied in 0.1 Nm increments. For each motion segment the data points were fitted using the function:

$$\theta = \frac{1}{B} \ln \left(\frac{Mom}{A} + 1 \right) \tag{3.1}$$

where A and B are constant coefficients, Mom is the applied moment and θ is the measured angular displacement.

In the model simulation pure moments are applied to T1 (0 ± 1.5 Nm with increments of 0.1 Nm). To study the behaviour of the model under higher loads, the simulations are extended to larger moments (2.0 ± 10 Nm with increments of 2 Nm).

3.2   Simulation Results

The static load simulations are presented for the three different cases as described above.   The terms *good*, *reasonable* and *poor* are introduced to compare the model response with the experimental results.   *Good* means close to the average of experimental results, *reasonable* means within the standard deviation (SD) of experimental results and *poor* means outside the SD of experimental results.
Simulations performed on a SG-O2 R10000 workstation using a fifth order Runge Kutta-Merson (RK5) integration with variable time step ($\geq 10^{-6}$ s) showed virtually identical results as using a fourth order Runge-Kutta (RK4) integration with a fixed time step of $2.5x10^{-5}$ s.   Therefore, in the simulations RK4 is used in order to save time, without losing accuracy.   For the different simulations reported in this chapter the run times varied between a few minutes to more than one hour.

3.2.1   Small Loads

The main and coupled displacements of model C3-C4 and C5-C6 are shown in Figure 3.1, together with the experimental results of Moroney *et al.* [90], shown by vertical lines (average $\pm$ SD). The applied loads are given along the horizontal axis.   The left-hand figures show the translational loads while the figures on the right side (column 6-10) give the rotational loads.   The resulting displacements and rotations are presented along the vertical axis.   The top row shows anterior translation t_x response followed by the other degrees of freedom finishing with rotation ϕ_z.   The main displacements are printed in bold.   It should be noted that experimental data for tension was not available.   In Table 3.2 a qualitative comparison is presented. The main displacements and rotations of the models are reasonable to good, except for anterior shear, which shows poor agreement.   The coupled displacements for the applied moments are good, while ϕ_y exceeds the SD when instead forces are applied. The differences in response between C3-C4 and C5-C6 are small, except for the coupled displacement t_x and ϕ_y.

In Figure 3.2 the main and coupled model displacements of C0-C1-C2 subject to rotational loading are shown together with the experimental results by Panjabi and co-workers [99,107,108,112] by vertical lines (average $\pm$ SD) are shown. It should be noted that simulation and experimental data for rotational loads only are presented. The applied loads are given along the horizontal axis.   In the left-hand figures the rotational loads are presented for C0-C1.   Whilst on the right side (column 5-8) the rotational loads for C1-C2 are shown.   The resulting displacements and rotations are presented along the vertical axis.   The top row shows the anterior translation t_x response followed by the other degrees of freedom finishing with rotation ϕ_z.   The main displacements are printed in bold.   In Table 3.3 a qualitative comparison is presented. The main motions for C0-C1 are reasonable, although the model is too stiff in extension. The coupled motions are reasonable to good. For the C1-C2 model the main extension motion is good.   The C1-C2 model is reasonable for lateral bending,

but too stiff for flexion and axial rotation. The coupled displacements are reasonable except for lateral bending and axial rotation.

Table 3.2: *Qualitative comparison of model response of segment C3-C4 and C5-C6 with experimental results [90] as presented in Figure 3.1.*

load		main displacement[a]	comment
AS	Anterior Shear	poor	too flexible
PS	Posterior Shear	reasonable	
LS	Lateral Shear	reasonable	
CMP	Compression	good	
LB	Lateral Bending	reasonable	
FLX	Flexion	good	
EXT	Extension	reasonable	
AR	Axial Rotation	reasonable	

[a] good: close to average of experimental response
   reasonable: within SD of experimental response
   poor: outside SD of experimental response

Table 3.3: *Qualitative comparison of model response of segment C0-C1 and C1-C2 with experimental results [99, 107, 108, 112] as presented in Figure 3.2.*

load		main displacement[a]	comment
C0-C1			
LB	Lateral Bending	reasonable	
FLX	Flexion	reasonable	
EXT	Extension	poor	too stiff
AR	Axial Rotation	reasonable	
C1-C2			
LB	Lateral Bending	reasonable	
FLX	Flexion	poor	too stiff
EXT	Extension	good	
AR	Axial Rotation	poor	too stiff

[a] good: close to average of experimental response
   reasonable: within SD of experimental response
   poor: outside SD of experimental response

3.2.2 Large Loads

The responses of the model motion segments subjected to large rotational loads are shown in Figure 3.3 together with the experimental data from the literature on the ranges of motion of the segments (see Table 3.1). The upper row shows the responses of the upper neck segments (C0-C1 and C1-C2), while the lower row shows the response of the lower neck segments (C3-C4 and C5-C6). In the three columns (from left to right) the reponse to lateral bending, flexion/extension and axial rotation, respectively are shown. In Figure 3.4 the segment model responses of large translational loads are presented. Experimental data for the ranges of motion
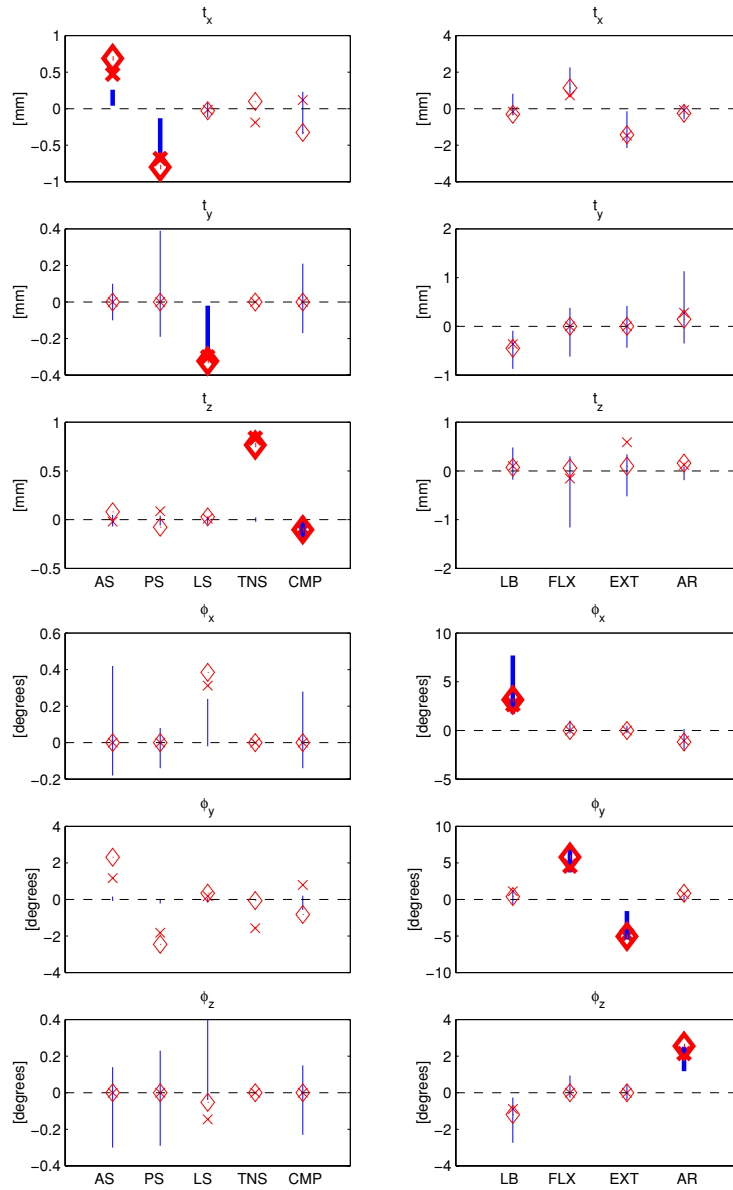
Figure 3.1: *Main (bold) and coupled displacement of models C3-C4 (◇) and C5-C6 (×) with experimental results of Moroney* et al. *[90] shown by vertical lines (average ± SD); for tension, no experimental data are given. See Table 3.2 for qualitative description. The applied loads are given along the horizontal axis and the resulting displacements and rotations along the vertical axis: anterior shear (AS, $+t_x$), posterior shear (PS, $-t_x$), lateral shear (LS, t_y), tension (TNS, $+t_z$), compression (CMP, $-t_z$), lateral bending (LB, ϕ_x), flexion (FLX, $+\phi_y$), extension (EXT, $-\phi_y$), axial rotation (AR, ϕ_z). $+$x is forward, $+$z is upward.*
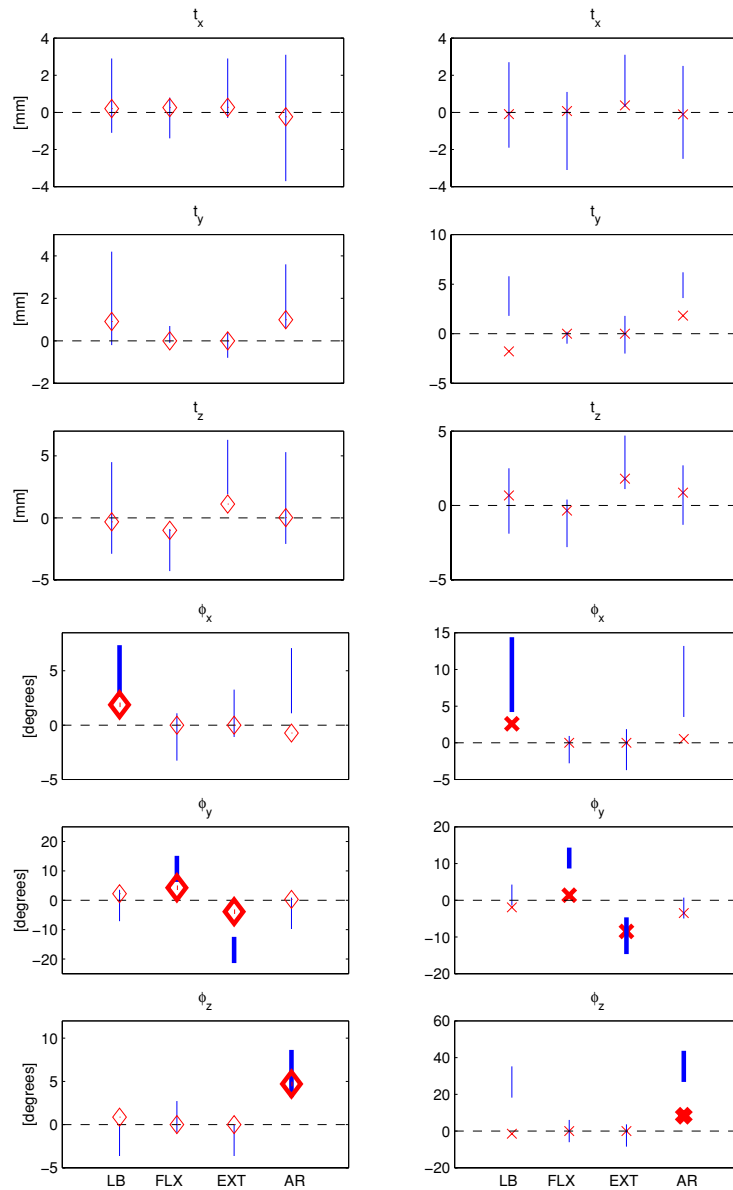
Figure 3.2: *Main (bold) and coupled displacement of models C0-C1 (◇ left) and C1-C2 (× right) with experimental results of Panjabi and co-workers [99, 100, 107, 108, 112] shown by vertical lines (average ± SD); for rotational loading only. See Table 3.3 for qualitative description. The applied loads are given along the horizontal axis and the resulting displacements and rotations along the vertical axis: lateral bending (LB, ϕ_x), flexion (FLX, $+\phi_y$), extension (EXT, $-\phi_y$), axial rotation (AR, ϕ_z). $+$x is forward, $+$z is upward.*
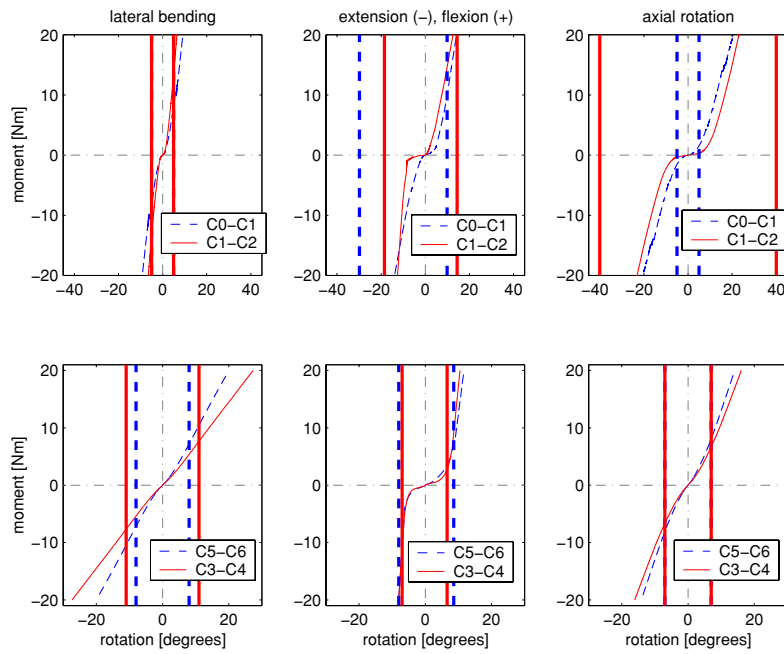
Figure 3.3: *Elastic response of segment models when subjected to large rotational loads. The vertical lines in bold represent the experimental ROM of the motion segments (see Table 3.1).*
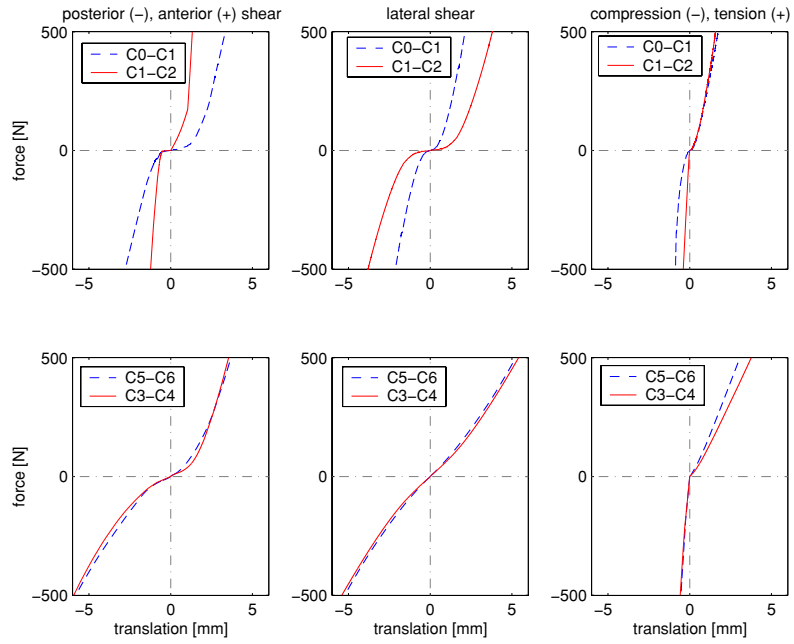
Figure 3.4: *Elastic response of segment models when subjected to large translational loads.*

Table 3.4: *Loads in the disc, ligaments and facet joints of C3-C4, for a C3 loading of 500 N or 20 Nm. The 3D forces are expressed in the body coordinate system of the lower vertebra. Ligament forces are one-dimensional and are expressed in the direction of their orientation. Values in bold represent the load in the disc in the loading direction (see Figure 3.3 and 3.4).*

|	AS	PS	LS	TNS	CMP	LB	FLX	EXT	AR
disc forces [N]									
Fx disc	**-149.66**	**265.12**	12.76	-89.03	165.81	133.15	-26.71	42.56	86.56
Fy disc	0.00	0.00	**349.12**	0.00	0.00	19.88	0.00	0.00	-88.48
Fz disc	-68.73	11.61	13.68	**-233.61**	**430.38**	24.67	134.02	-45.26	-118.49
Fres disc	164.69	265.37	349.55	250.00	461.20	136.80	136.65	62.13	171.32
disc moments [Nm]									
Mx disc	0.00	0.00	1.62	0.00	0.00	**9.05**	0.00	0.00	-2.71
My disc	3.91	-4.32	0.03	-0.21	-0.33	0.55	**17.48**	**-18.71**	-1.63
Mz disc	0.00	0.00	-1.06	0.00	0.00	-3.46	0.00	0.00	**6.78**
Mres disc	3.91	4.32	1.92	0.21	0.33	9.40	17.48	18.71	7.71
facet forces left [N]									
Fx left facet	-154.59	-0.65	0.00	0.00	-23.87	0.00	0.00	-27.56	0.00
Fy left facet	-9.11	-0.05	0.00	0.00	-1.77	0.00	0.00	-2.26	0.00
Fz left facet	137.24	0.83	0.00	0.00	32.20	0.00	0.00	43.24	0.00
Fres left facet	206.92	1.06	0.00	0.00	40.12	0.00	0.00	51.33	0.00
facet forces right [N]									
Fx right facet	-154.59	-0.65	-63.78	0.00	-23.87	-291.92	0.00	-27.56	-237.48
Fy right facet	9.11	0.05	6.00	0.00	1.77	79.16	0.00	2.26	65.13
Fz right facet	137.24	0.83	70.65	0.00	32.20	234.73	0.00	43.24	344.37
Fres right facet	206.92	1.06	95.36	0.00	40.12	382.86	0.00	51.33	423.35
spinous process forces [N]									
Fx spinous process	0.00	0.00	0.00	0.00	0.00	0.00	0.00	0.00	0.00
Fy spinous process	0.00	0.00	0.00	0.00	0.00	0.00	0.00	0.00	0.00
Fz spinous process	0.00	0.00	0.00	0.00	0.00	0.00	0.00	0.00	0.00
Fres spinous process	0.00	0.00	0.00	0.00	0.00	0.00	0.00	0.00	0.00
ligament forces [N]									
ALL *	0.00	79.22	56.72	76.91	10.31	19.92	0.00	39.09	80.13
PLL	21.30	32.29	16.80	44.35	0.00	28.68	8.45	0.00	23.89
FL	30.05	22.02	7.18	5.05	0.00	64.95	40.97	0.00	36.36
ISL	10.29	8.13	2.04	0.16	0.00	27.80	16.61	0.00	15.59
JCl1	23.02	6.94	27.08	21.85	0.00	76.46	9.66	0.00	27.23
JCl2	15.95	30.44	24.19	17.78	1.63	89.14	8.64	3.04	66.38
JCl3	10.81	6.89	8.09	7.23	0.00	36.94	9.64	0.00	19.67
JCl4	19.62	20.42	13.76	18.50	0.00	52.59	12.33	0.00	29.46
JCr1	23.02	6.94	5.16	21.85	0.00	15.57	9.66	0.00	36.50
JCr2	15.95	30.44	22.87	17.78	1.63	64.45	8.64	3.04	35.62
JCr3	10.81	6.89	3.40	7.23	0.00	13.66	9.64	0.00	13.93
JCr4	19.62	20.42	18.42	18.50	0.00	14.94	12.33	0.00	22.31

* see Table 2.7 for abbreviatons of ligaments

are not available for these loading conditions. Again, the upper row presents the responses of the upper neck segments (C0-C1 and C1-C2), while the lower row presents the response of the lower neck segments (C3-C4 and C5-C6). The reponse to posterior/anterior shear, lateral shear and compression/tension are presented from left to right.

As is expected, it is seen that for larger displacements stiffness tends to increase due to additional resistive forces exerted by the ligaments (with nonlinear stiffness characteristics) which become more and more restrained, and due to compression of the disc (non linearity for compression, flexion and extension). It should be noted that the disc is absent in the upper neck (C0-C1-C2). Neutral zones, in which only small load is needed to deform the structure, reflecting the fact that the tissues offer little resistance initially, are observed for flexion and extension of the upper and lower neck segments and for shear and axial rotation of the upper neck segments.

The responses of models C3-C4 and C5-C6 are almost identical for extension (Figure 3.3) and compression (Figure 3.4). They differ slightly for flexion and shear. For tension, lateral bending and axial rotation C5-C6 is clearly stiffer than C3-C4. For flexion and extension the segment models C5-C6 and C3-C4 increase asumptotically with increasing moments, resulting in a combined flexion/extension of about 15 degrees for both segments. This is in correspondence with the reported ROM for C3-C4 and roughly 25 % too small for C5-C6. The model response for axial rotation and lateral bending at 20 Nm is about 50 % larger compared to the ROM.

For tension, the responses of C0-C1 are similar to the responses of C1-C2. The stiffening of the upper neck segments at larger loads is due to the ligaments, as there are no discs in the upper cervical spine. The small translation range for C1-C2 in posterior shear is a result of contact between the anterior ring of the atlas and the dens. The anterior shear is limited by the ligaments. The combined flexion/extension is about 25 degrees for the segment model C1-C2 and about 30 degrees for C0-C1. Experimentally, it was also seen that C0-C1 is more flexible during flexion and extension compared to C1-C2. Lateral bending at 20 Nm of both segment models results in larger values than the ROM. It is calculated that C1-C2 is stiffer than C0-C1 during lateral bending. This is in contrast with the experimental ROM, where both segments showed the same flexibility. The axial rotation of the C0-C1 model is smaller than the rotation for C1-C2, as was observed in the ROM experiments. However, when loaded with 20 Nm, the axial flexiblity of C0-C1 is larger compared to the ROM, while the model C1-C2 has not reached the experimental ROM at this load.

A knowledge of load distribution for segment models contributes to the insight into the biomechanics of the human neck. Therefore, Table 3.4 shows the loads exerted by the disc, ligaments, facet joints and spinous process of segment model C3-C4 required to counterbalance the load applied at C3. The 3D forces are expressed in the body coordinate system of the lower vertebra. Ligament forces are one-dimensional and are expressed in the direction of their orientation. Note the symmetric loads in the left and right facet joints for flexion, extension, anterior shear, posterior shear, compression and tension. The C3-C4 spinous processes are not loaded, however contact of the protrusions of the vertebrae was observed for large extension loads on

C5-C6, and C1-C2. In the case of anterior shear both disc and facet joints are loaded together with all ligaments, except for the anterior longitudinal ligament (ALL). For posterior shear the facet joints are hardly loaded and most forces are generated by the disc and all ligaments, including ALL. In tension all ligaments are loaded, together with the disc. For compression the load is mainly distributed over the facet joints and the disc. Small loads are observed for ALL and joint capsule part 2 (JC2) left and right.

The disc and all ligaments except ALL are loaded when the segment is subjected to flexion. For extension facet joints, disc and ALL and JC2 left and right are loaded. For flexion and extension in both cases the moment (M_y) excerted by the disc is about 90 % of the applied load. In axial rotation, lateral bending and lateral shear, the facets are loaded only on one side. Additionally, disc forces and moments together with forces in all ligaments are observed. In all loading cases a moment in the saggital plane (M_y) on the disc has been observed. For compression, flexion and extension the disc dominates in sustaining the applied loads. The disc takes 86%, 88% and 93%, respectively, of the applied load.

3.2.3   Flexion/Extension Loads

The results of simulation of the experiments of Camacho *et. al* [20] are shown in Figure 3.5. Due to difficulties in visualizing C1 during testing, the C0-C2 complex was treated as a single motion segment. The simulation results are presented together with the torque-rotation functions for the motion segments defined by Camacho [20] and with the ROM data published by Moroney [90] (average $\pm$ SD). It is seen that the data by Moroney is in agreement with Camacho, but for C3-C2, Moroney reports less flexible extension of the segment than that observed by Camacho.

A good correlation for extension of the model with the ROM by Camacho and Moroney is seen in Figure 3.5. For flexion all segments show good agreement with the ROM at 1.5 Nm according to the data of Moroney. However, the initial flexion stiffness of all segments, except C3-C2 is larger than the experimental data presented by Camacho.

Experimental results were only available for moments up to 1.5 Nm. However, assuming that equation 3.1 could be used for larger moments as well, it could be seen that the model will be more flexible compared to the new Camacho curve (not shown in Figure 3.5), except that is for the C0-C2 complex. The upper neck model still shows higher flexion stiffness.
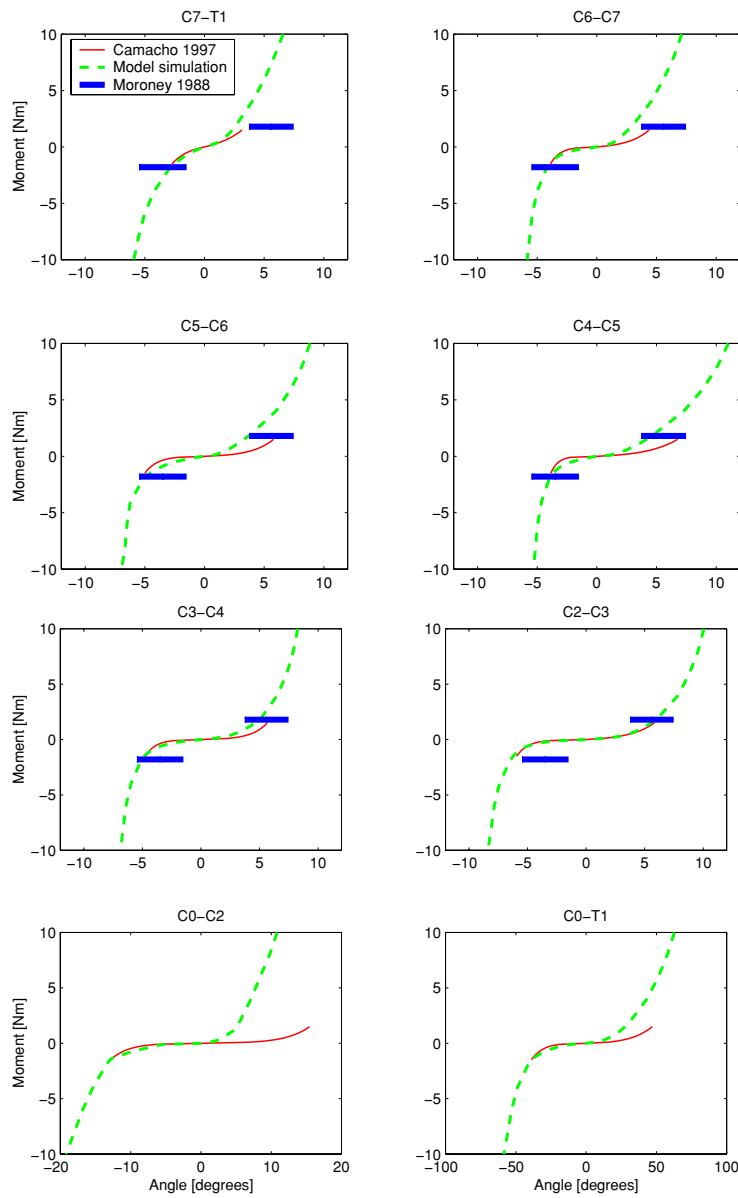
Figure 3.5: *Flexibility curves for all segments in flexion (positive moment) and extension (negative moment) for model simulation together with the experimental data (average ± SD) by Moroney et al. [90] and the torque-rotation functions defined by Camacho et al. [20].*

3.3   Discussion

Before the neck model can be used for studying injury mechanisms, the model must be validated. In this chapter a quasi-static validation has been presented, using experiments on ligamentous segment models [90, 99, 100, 107, 108, 112] as well as the entire ligamentous cervical spine [20].

In the small load quasi-static simulations, loads were applied up to 20 N or 1.5 Nm. The responses of the segment models C5-C6 and C3-C4 are within one standard deviation (SD) of the experimental response as reported in the literature [90], except for anterior shear which shows too much flexibility for both the lower cervical spinal segments. The upper cervical spinal segment model C0-C1 shows a reasonable response compared to the experimental data, but the segment is too stiff in extension [99, 100, 107, 108, 112]. Model segment C1-C2 shows a good to reasonable response for extension and lateral bending, but the model predicts too high a stiffness for flexion and axial rotation [99, 100, 107, 108, 112].

Simulations of large loads have also been performed and the results compared with the range of motion (ROM) for *in vivo* rotation. It should be noted that the loads accompanying the experimental motions are not known, therefore, the comparison is of qualitative value only. For flexion and extension, stiffening of the segment models is observed. In general the segment models show a realistic response for large flexion/extension loads. The lower neck segments are too flexible though for lateral bending and axial rotation, while C1-C2 is too stiff and C1-C0 too flexible for axial loading. However, the segment model C1-C2 still shows more axial rotational flexibility than the C0-C1 segment model, as is reported for human upper cervical spinal segments (see Table 3.1). Whether the translational motions exceed ROM for large loads is not known, since experimental data is not available for these cases.

By simulating pure flexion and extension experiments [20] the entire ligamentous spine can be studied, without damaging the tissues running over the entire column. The response of the model shows good agreement with data from the flexion and extension experiments performed by Camacho *et al.* [20]. Only the C0-C1-C2 complex shows an initial lower flexibility than in the experiments. This difference is caused by the increased stiffness of the upper neck ligaments, as desribed in Chapter 2. However, for larger loads, these stiff ligaments reduce large motions of the head-neck system.

Coupled displacements show the 3D characteristics of cervical segments when loaded in one direction. In the literature, two characteristic couplings in the lower cervical spine have been discussed, occurring due to the spatial orientation of the facet joints [89]. Firstly, it has been observed experimentally that flexion is coupled with anterior translation, and extension with posterior translation. This coupling is also observed in the model simulations. However, the model displacements for anterior and posterior shear are above the SD for the small load experiments and, the coupled motions are also large compared to the experimental data. The other characteristic coupling experimentally observed occurs during lateral bending, which is associated with axial rotation, such that the spinous processes move to the left ($-\phi_z$) when the head and neck are bent to the right ($+\phi_x$). This phenomenon is also seen in the

model simulations. In the upper cervical spine, axial rotation of the atlas is coupled with vertical translation of the atlas due to the shape of the C1-C2 facet joints [158]. This is also observed in the model simulations.

The load distribution for segment C3-C4 subjected to large loads also shows these 3D coupling effects (see Table 3.4). For flexion it is seen that the disc is in compression and anterior shear, and the ligaments are in tension (all except for the anterior longitudinal ligament (ALL) which is located on the anterior side). For extension the disc is in tension together with posterior shear and the facet joints are in compression. Most ligaments are not loaded except the anterior longitudinal ligament and the joint capsule 2 (ALL and JC2), which are located on the anterior side of the segment. The dominating behaviour of the disc in compression, flexion and extension emphasizes the influence of the nonlinear stiffness functions defined for these directions.

The initial position, and orientation of the vertebrae are critical in determining the calculated main displacement, as well as the coupled displacements which occur during loading. The initial strain in the ligaments will also affect the response of the models [65]. No experimental data exist however for the initial ligament strain. In the model, the ligaments are neither slack nor taut initially. It is recommended that experimental studies are carried out to determine the magnitude of pretensioning in the ligaments.

In conclusion, published quasi-static experimental data were used to test segment models for 6 degrees of freedom and to test the entire ligamentous cervical spine model for flexion and extension. The mechanical behaviour of the models agreed reasonably with the experimental data, i.e. the simulated global force-displacement and global moment-rotation relations were generally within 1 standard deviation of the experimental data. The model segments showed realistic 3D coupling effects and was able to predict local tissue forces and torques.

Chapter 4

Response to Frontal and Lateral Impact

In the previous chapters a new multibody neck model has been presented and validated for quasi-static loading conditions. Earlier versions of the neck model (the De Jager model [64, 65] and an intermediate model [61]) have also been validated for frontal and lateral impact, using experiments performed with volunteers. The main objective of this chapter is to validate the new neck model also for frontal and lateral impact. A second objective is to investigate the influence of muscle activity on the head neck response. As a first step in the dynamic validation of the new neck model, simulations of the same frontal and lateral volunteer experiments, used for validation of the earlier neck models [61, 64, 65], are performed (Section 4.1). As the experiments were performed with human volunteers muscle activation must potentially also be taken into account. Recent research indicates that muscles are activated early in impact events and are capable of generating forces which can alter head and neck kinematics (see review by Siegmund and Brault [134]). Therefore, simulations are performed first with passive muscles and secondly, with active muscles (i.e. with muscle activation). The results of the simulations are presented in Section 4.2. A parametric study on muscle parameters of the simulations is also performed for the frontal impact simulation in order to investigate further the influence of muscle activation on the kinematic response (Section 4.3). A discussion is presented in Section 4.4.

4.1 Material and Methods

Data for validation of the neck model for frontal and lateral impact are taken from studies on human volunteers subjected to 15g and 7g sled tests (1g = 9.81 m/s^2), respectively, performed at the Naval Biodynamics Laboratory (NBDL) [45, 146].

4.1.1   Experimental Data

In the tests the volunteers (young and well trained marines) were seated in an upright position on a rigid seat mounted on a HYGE accelerator and exposed to short duration accelerations simulating frontal or lateral impacts. Clusters of accelerometers and photographic targets were mounted to the subject and used to monitor the resulting three-dimensional motions of the head and T1 (see Figure 4.1). A detailed description of the instrumentation and test methods is provided in [1, 46]. The subjects are restrained by shoulder straps, a lap belt and an inverted V-pelvic strap tied to the lap belt. Upper arm and wrist restraints are used to prevent flailing [1]. In the lateral tests a chest strap is used to minimize the load on the right shoulder. In addition a lightly padded wooden board is placed against the right shoulder of the subject to limit the upper torso motion. The volunteers were asked to take a normal automotive posture. The initial head angle was 0 degrees, where the head angle was defined as the angle between the Frankfort plane and the horizontal plane. The Frankfort plane is defined as the imaginary plane passing through the external ear canals and across the top of the lower bone of the eye sockets. The test conditions are summarized in Table 4.1. Mean values of the sled acceleration-time histories for frontal and lateral impact are shown in Figure 4.2.
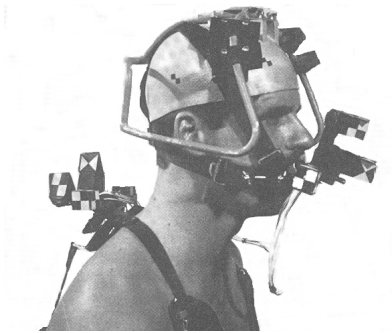
Figure 4.1: *Test setup of NBDL volunteer experiments [146].*

Table 4.1: *Test conditions of the frontal and lateral NBDL experiments.*

Parameter	Unit	Frontal	Lateral
Reference		[146]	[45]
Subject		volunteer	volunteer
Total number of subjects		5	9
Total number of tests		9	9
Average mass	kg	68.6	76
Average height	m	1.69	1.77
Seat type		rigid	rigid
Max sled pulse	g	15	7
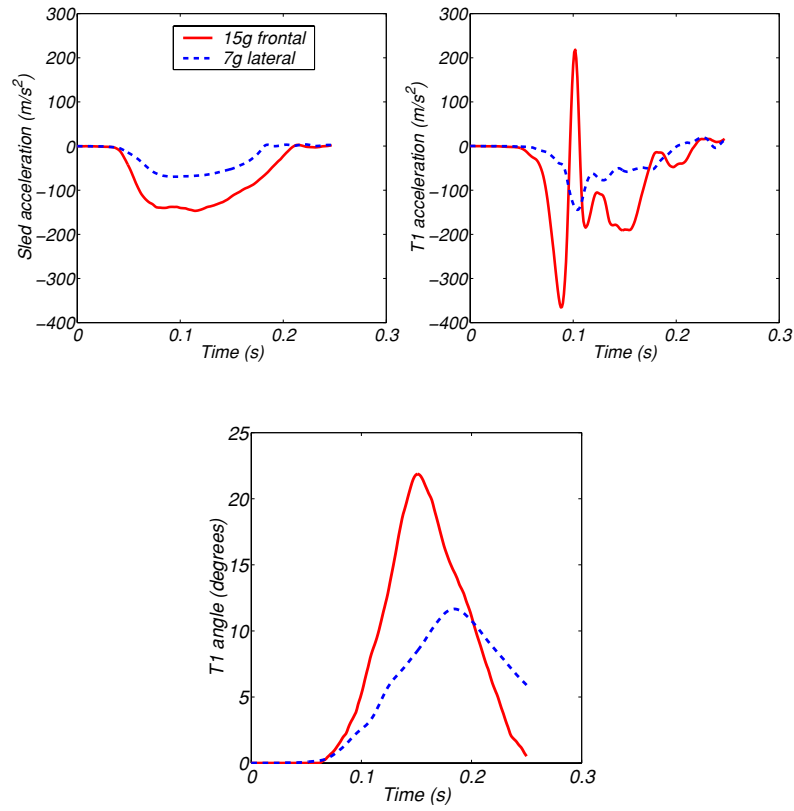
Figure 4.2: *NBDL experiments: Mean sled acceleration, T1 acceleration in impact direction, and T1 rotation angle in the plane of impact for frontal and lateral impact [146].*

4.1.2   Setup of the Simulation

In the impact simulations, only the head and neck were modelled. In the experiments it was observed that the measured horizontal T1-acceleration differed from the acceleration applied to the sled due to the flexibility of straps and thorax: the peak T1-accelerations being about twice the peak sled accelerations (see Figure 4.2). Additionally the T1 motion was dominated by horizontal translation and rotation about the y-axis, whereas the movements of the other directions were negligible [65]. To simulate the impact, the horizontal T1-acceleration in the impact direction (using an average of frontal and lateral experiments respectively) is used as input to the model, since this circumvents the modelling of the straps and thorax flexibility. In addition the average rotation of T1 in the plane of impact is prescribed (see Figure 4.2).

Gravity is neglected to create a stable upright initial position of the head. Simulations with gravity showed about 5% larger head rotation and displacement for the frontal and lateral impact with active muscle behaviour compared to simulations without gravity. These differences were even smaller for the calculated acceleration.

Firstly, simulations with passive muscles (i.e. without muscle activation) were performed. Recent research has indicated that muscles are active early in injury events and are capable of generating forces which can alter head and neck kinematics (see review by Siegmund and Brault [134]). It is possible that the volunteers, who were exposed to impacts of increasing severity, were tensed during the high severity impacts, as they had become trained to counter the effect of the impact. Therefore, secondly, for frontal and lateral impacts simulations with active muscles (i.e. with muscle activation) were performed. For the simulations with muscle activation, it is assumed that the muscles are not immediately activated at the time of impact. Instead, the activation starts at

$$t_{act} = t_{trigger} + t_{reflex} \qquad (4.1)$$

where $t_{trigger}$ is defined as the time a certain sensory threshold level has been exceeded, and t_{reflex} is a neural reflex time as a pure delay (see Figure 4.3). Activation dynamics have been implemented as the step-response to two linear first-order systems in series, describing the excitation and activation dynamics with time constants respectively of 45 ms and 10 ms (see equation 2.18 and Figure 2.10).

Several possiblities have been suggested for the trigger mechanism for muscle activation including stimulation of the somato-sensory, the auditory, the vestibular and the visual system. It was suggested that the trigger could be caused by acceleration of the spine [141]. In this study a sensory threshold for T1 acceleration is arbitrarily chosen at 0.5 g, resulting in $t_{trigger}$ of 49 ms and 62 ms for frontal and lateral impact, respectively. Reported motor reflex delays range from 10 to 120 ms [24, 47, 127, 130, 143] (see also Appendix E). For the simulations, a motor reflex delay of 25 ms (t_{reflex}) was chosen. For simplicity, in the simulations all muscles are activated when t_{act} is reached.
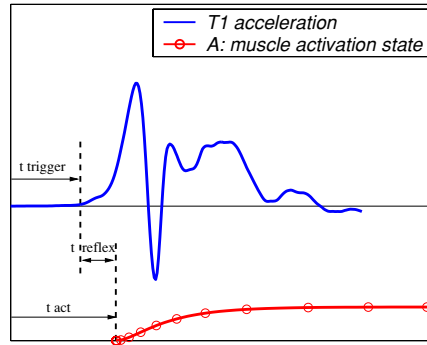
Figure 4.3: *Activation state of the muscles together with frontal T1 impact pulse for the head-neck. Muscle activation starts at $t_{act} = t_{trigger} + t_{reflex}$.*

4.1.3   Criteria for Model Quality Assessment

For validation of the model kinematics during impact, the set of responses given in Table 4.2 were used. The corridors used to validate the model are defined as the average volunteer response plus or minus the standard deviation [146].

The following terms are introduced helping to describe the results: *good* means within the corridor of the experimental data, *reasonable* means close to this corridor, and 25% deviation allowed, while a *poor* correlation stands for more than 25% deviation from the corridor.

Table 4.2: *Set of responses used for model validation.*

Response parameter	with respect to
linear acceleration of the centre of gravity of the head (CG)	laboratory coordinate system
angular acceleration of the head	laboratory coordinate system
trajectory of the occipital condyles (OC)	T1 +
trajectory of the centre of gravity (CG) of the head	T1 +
head rotation ϕ ^{o}	T1 +
neck rotation θ *	T1 +
head rotation versus neck rotation	T1 +

$^+$ a coordinate system fixed to T1, note that T1 rotates, see [146]
^{o} head rotation is the angle between the Frankfort plane and an xy plane through T1
* neck rotation is the neck link rotation; neck link is defined as the straight line
connecting T1 to OC

4.2   Simulation Results

The response of the model with passive (0% activation) and active muscle behaviour (t_{reflex} = 25 ms and 100% activation of all muscles) for frontal and lateral impact is presented in the following sections.

A simulation of a frontal impact of 300 ms required 1448 CPU-seconds using MADYMO 5.4.1 with a fifth order Runga-Kutta-Merson (RK5) integration with variable time step ($\geq 10^{-6}$ s) on a SG-O2 R1000 workstation. Virtually identical results were obtained using a fourth order Runge-Kutta (RK4) integration with a fixed time step of $2.5 \cdot 10^{-5}$ s, taking 539 CPU-seconds. Similar results were found for lateral impact simulations. For the simulations presented in this thesis integration method RK4 was used in order to save time without losing accuracy.

4.2.1   Frontal Impact

The overall response of the active model for frontal impact is shown in Figure 4.4. For clarity, the muscles are not shown in the lower figure, while the upper figure shows the model with all internal structure. During the first 100 ms the head only translates, without any rotation with respect to inertial space (this is called head lag [165]). After this the head starts to rotate forward, resulting in maximum head flexion at about 170 ms.

| 0 ms | 80 ms | 100 ms | 120 ms | 140 ms | 160 ms | 180 ms | 200 ms |
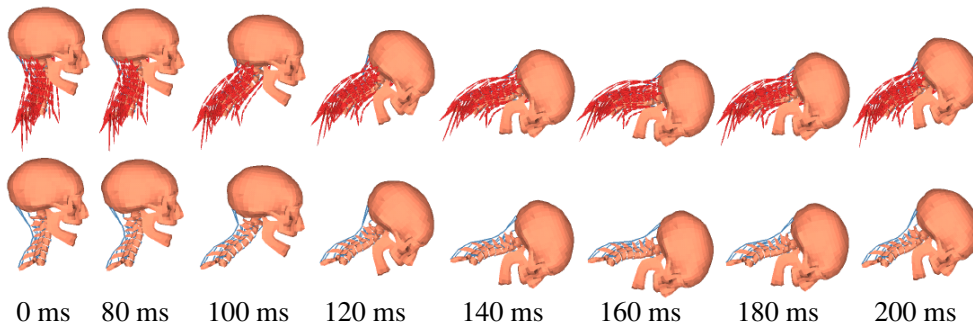
Figure 4.4: *Kinematics of the active neck model (100% muscle activation and 25 ms reflex, t_{act} = 74 ms) for a 15g frontal simulation at successive times. In the upper figure all internal structure is visible, while in the lower figure ligaments are shown and muscles are made invisible.*

Figure 4.5 shows the neck link angle and the head angle versus time, as well as the neck link angle versus the head angle. The neck link is defined as the straight line connecting T1 and OC. The passive and active model show a similar response for the neck link angle until 150 ms, and both show good agreement with the experimental response corridor. Beyond this time, while the neck angle of the passive model still increases, the neck angle of the active model is reduced by reactant muscle forces, resulting in a smaller neck link angle for the active model compared to the volunteer response. Overall, both active and passive model response show reasonable agreement for the neck link angle. The head angle of the passive and active model show a similar response until 110 ms. Beyond this time the passive model shows a large head rotation, exceeding the volunteer response by up to more than 25 %. The head angle of the active model shows a good response until 200 ms. After this time a

stronger reduction of the head angle is seen in the model compared to the volunteer response. In the beginning of the response, the neck rotates while the head angle remains constant (see Figure 4.5(c)). This results in head translation referred to as head lag. The extent and magnitude of the predicted head lag is similar for both the passive and active models. In both cases , after a neck rotation of about 35 degrees the head starts to rotate as well.
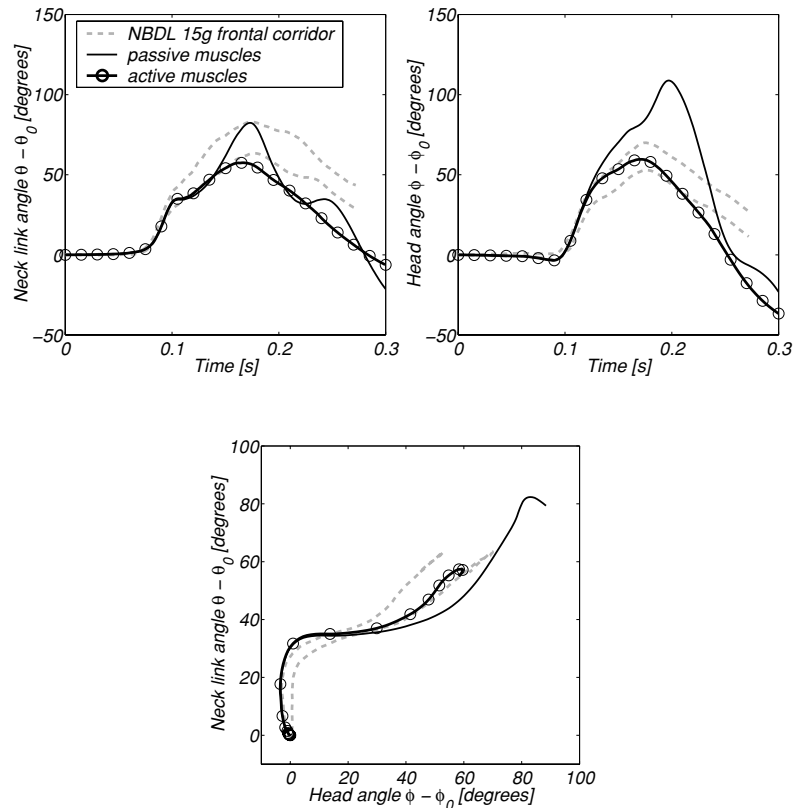
Figure 4.5: *Head and neck angles versus time together with the variation of the neck angle versus the head angle. Simulated response to 15g frontal impact with passive and maximum active (t_{act} = 74 ms) muscle behaviour. The model data is compared with human volunteer response corridors.*

Figure 4.6 shows both the displacement with respect to T1 of the occipital condyles (OC) and the centre of gravity of the head (CG), together with the experimental defined response corridors. The head displacements with respect to T1 in the x and z directions are reduced as a result of the muscle activation. For the first 110 ms the passive and active model OC x and CG x response are identical and

close to the response corridor. After this time the passive model predicts larger displacement followed by a strong oscillatory decrease, while the active model follows the trend of the response corridor. Nevertheless, the active model displacement is too small compared to the corridor. Compared to the experimental corridor the vertical displacement (OC z and CG z) begins too late for the passive model, while the active model prediction lies completely within the corridor for the first 110 ms. The active model underestimates the displacement, but overall the shape is much better than for the passive curves.

Figure 4.6: *Displacement of Occipital Condyles (OC) and Centre of Gravity of Head (CG) with respect to T1 versus time. Simulatie response to 15g frontal impact of the neck model with passive and maximum active (t_{act} = 74 ms) muscle behaviour compared with human volunteer response corridors. +x is forward, +z is upward.*

The acceleration response of the model is presented in Figure 4.7. Head linear and angular accelerations oscillate less for the active model response compared to the passive model response. The model with active muscle behaviour shows reasonable to good agreement for the accelerations compared to the response corridors.
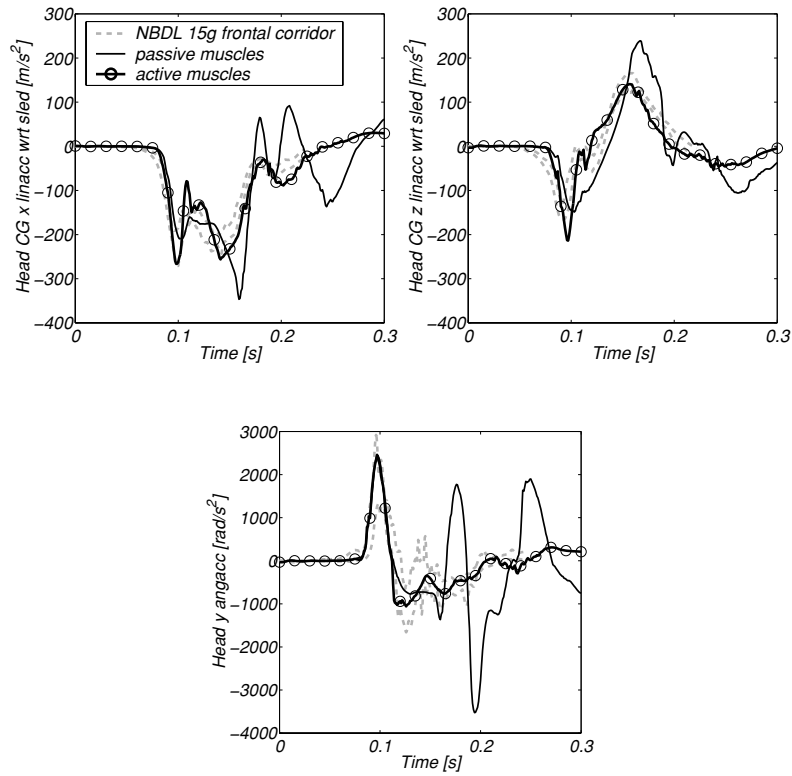
Figure 4.7: *Head acceleration versus time. Simulated response to 15g frontal impact of the neck model with passive and maximum active (t_{act} = 74 ms) muscle behaviour compared with human volunteer response corridors.*

4.2.2 Lateral Impact

In Figure 4.8 the overall response of the active model for a lateral impact is shown. For clarity, the muscles are not shown in the lower figure, while the upper figure shows the model with all internal structures. During the first 100 ms the head only translates, without any rotation with respect to inertial space. Following this the head bends to the right, followed by a rotation around the z axis (twist).

0 ms   80 ms 100 ms 120 ms   140 ms   160 ms   180 ms   200 ms
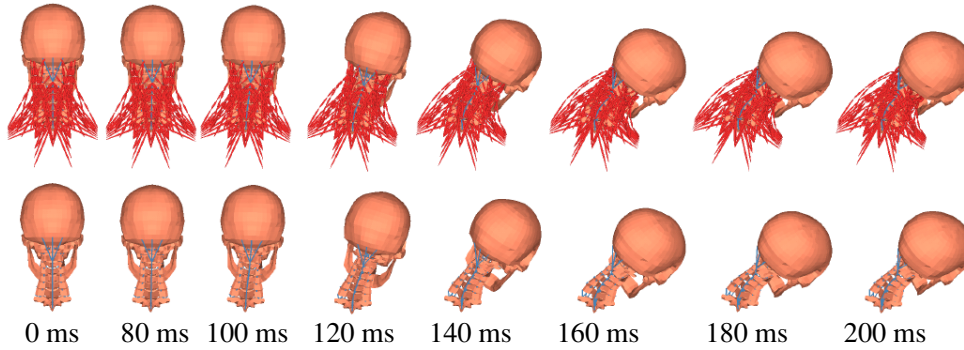
Figure 4.8: *Kinematics of the active neck model (100% muscle activation and 25 ms reflex, t_{act} = 87 ms) for a simulation of 7g lateral impact at successive times. In the upper figure all internal structure is visible, while in the lower figure ligaments are shown and muscles are made invisible.*

Figure 4.9 shows the head angle and the head OC and CG displacements versus time. During the first 110 ms both active and passive responses are similar and within the response corridor. After 110 ms the passive model shows poor agreement with the volunteer response. For the active model the head x angle shows reasonable correlation with the volunteer data, although the maximum head angle is about 20% larger than the experimentally reported head angle. The head z angle as well as the OC and CG displacements of the active model show a good correspondence with the response corridors.

The acceleration response of the model is presented in Figure 4.10. The passive model acceleration response shows considerable oscillation resulting in poor correlation with the experimentally defined corridors. The model with active muscle behaviour shows reasonable to good agreement for both linear and angular accelerations, as compared to the measured volunteer data.
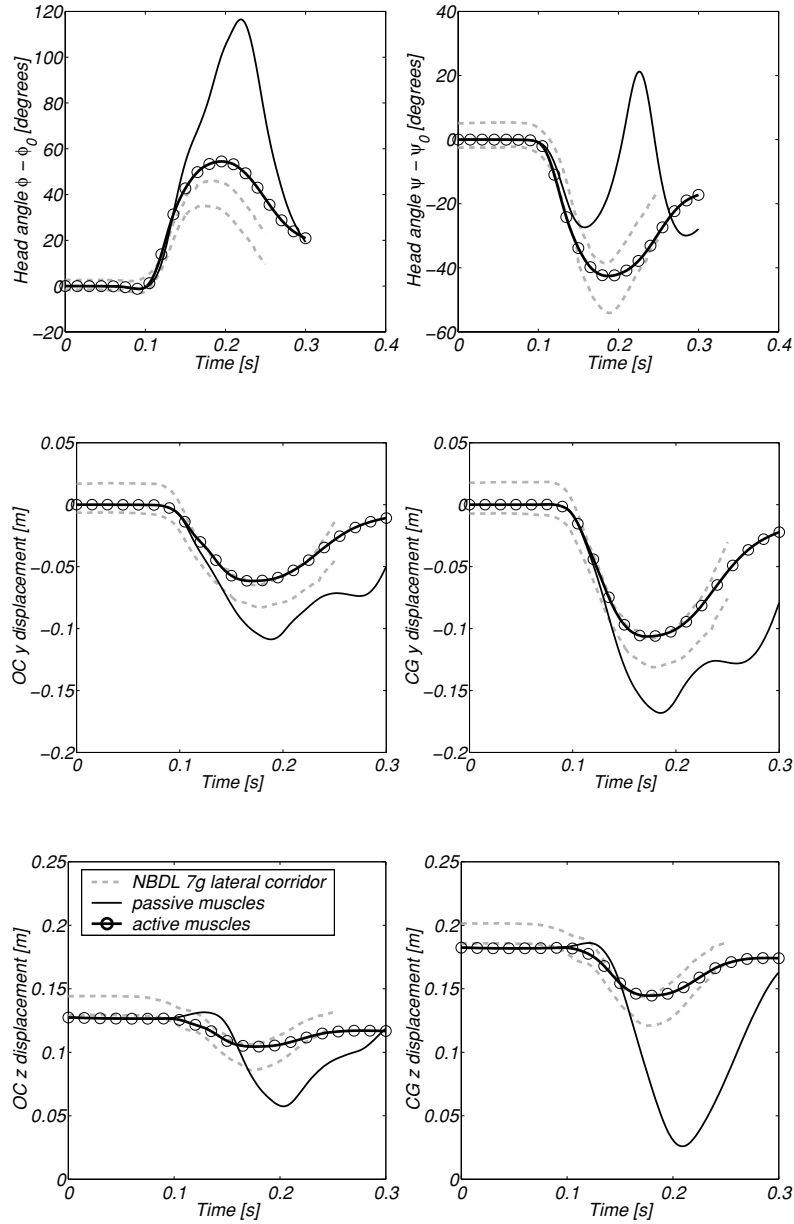
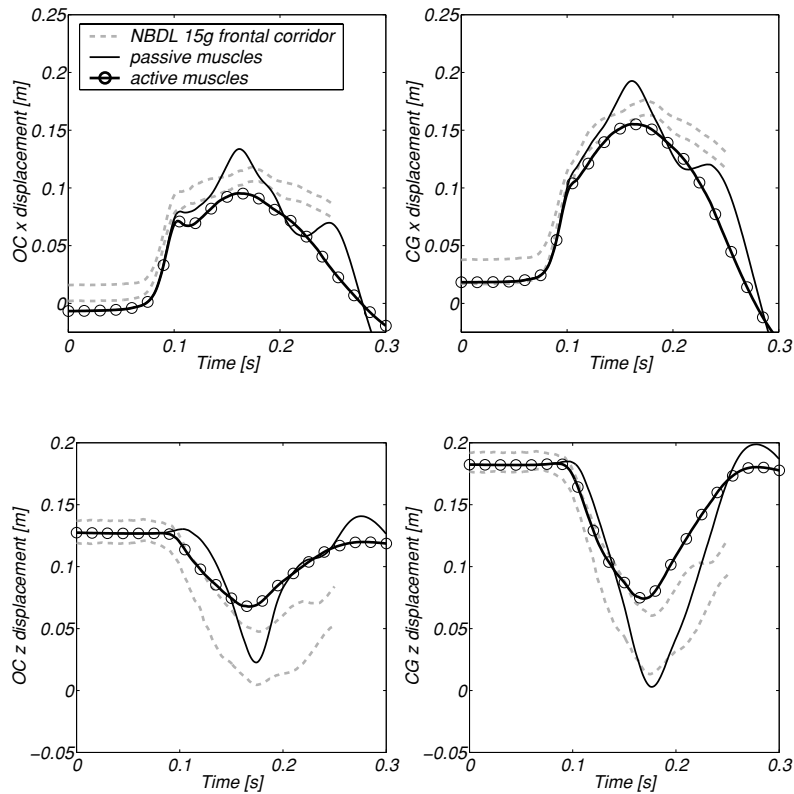**Figure 4.9:** *Head angles and displacement of the Occipital Condyles (OC) and Centre of Gravity of Head (CG) with respect to T1 versus time. Simulated response to 7g lateral impact of the neck model with passive and maximum active (t_{act} = 87 ms) muscle behaviour compared with human volunteer response corridors. +x is forward, +z is upward.*
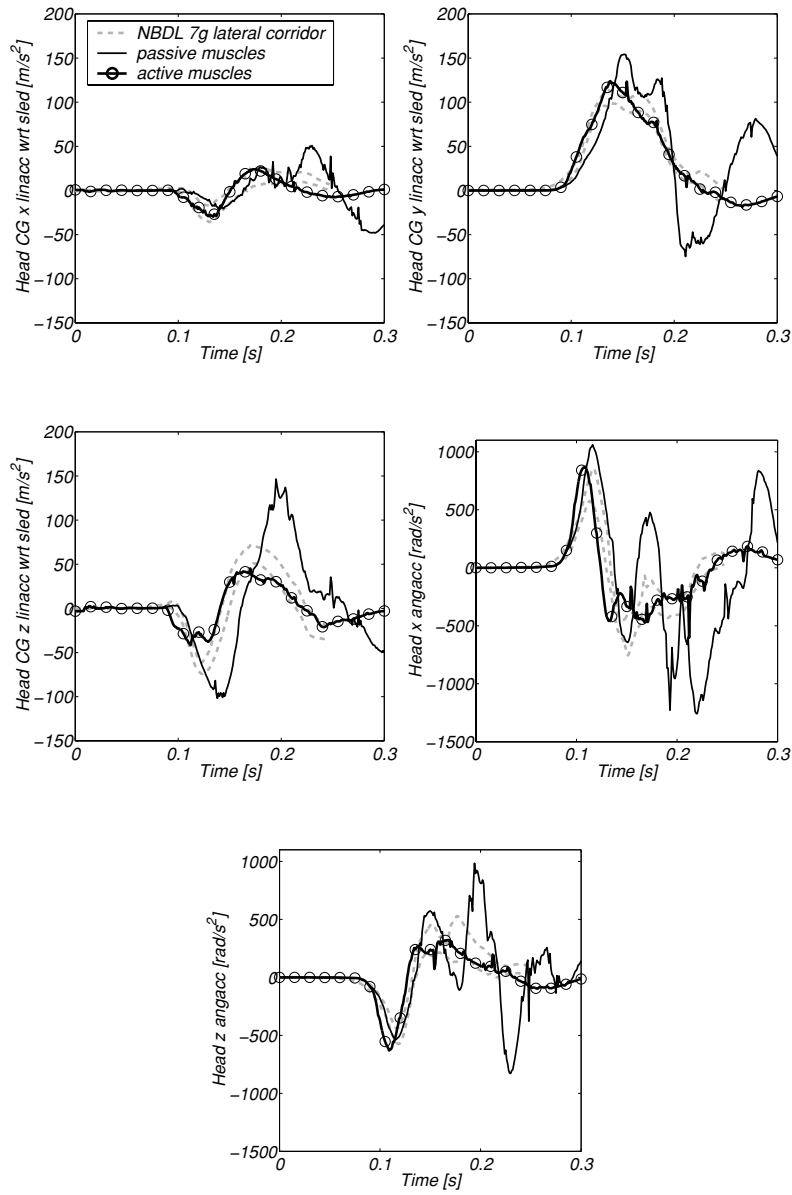
Figure 4.10: *Head acceleration versus time. Simulated response to 7g lateral impact of the neck model with passive and maximum active (t_{act} = 87 ms) muscle behaviour compared with human volunteer response corridors.*

4.3 Parameter Study on Muscle Behaviour

The effect of muscle activation on the head and neck response depends, among other things, on both the onset time of muscle activation and on the level of muscle activation. In this section, the influence of muscle activity on the head neck response is investigated for frontal impacts. Three different parameters are studied in the following cases (see also Table 4.3):

Case A: Role of passive pre-stress of muscles, without muscle activation.

Case B: Role of passive pre-stress of muscles, with muscle activation.

Case C: Role of maximum activation level, all muscles activated.

Case D: Role of reflex delay, all muscles activated.

A passive muscle (a muscle without neural activation) *in situ*, at rest has some initial stress, therefore the muscle at rest will shorten when it is removed from the body. This pre-stress results also in stiffening of the passive muscles (see Figure 2.9). Since little is known about the initial passive muscle stress (pre-stress), this influence has been studied in a frontal impact both without muscle activation (case A) and with muscle activation (case B) (see Table 4.3). The passive muscle properties are studied by varying the value of s_{free} (see Section 2.2.7 and Table 2.6). The pre-stress results in small initial passive muscle forces disturbing the equilibrium. However, this disturbance is small compared to the 15g impact severity.

The influence of the level of muscle activity has been studied in case C. Four cases with increasing maximum activation level (0-100%) are simulated. In each case, all muscles are activated in the simulations.

In case D the muscle reflex delay has been varied, using in each case a maximum activation level of 100%. The reflex delay variation was varied from 0 to 50 ms.

Results The results of the variation of the head angle with time are shown in Figure 4.11, and the maximum head angles (together with the time following impact, at which the maximum head angle is reached) are summarized in Table 4.3. Values in bold exceed the volunteer response corridor. Increasing pre-stress, proceeding from simulation A1 to A3, resulted in a decreasing maximum head angle for simulations with passive muscle behaviour. However, the pre-stress had almost no influence on simulations with active muscle behaviour. The maximum head angle decreases with increasing muscle activation level, or decreasing motor reflex delay. The time at which the maximum head angle occurs decreases with increasing pre-stress and increasing activation level. This trend is not seen for the motor reflex delay.

Table 4.3: *Maximum head angle at varying muscle conditions for a 15g frontal impact simulation (see Figure 4.11). Values in bold exceed the volunteer response corridor. Case A: role passive pre-stress muscles, without muscle activation, Case B: role passive pre-stress muscles, with muscle activation, Case C: role of maximum activation level, all muscles activated, Case D: role of reflex delay, all muscles activated.*

case	pre-stress	reflex delay	muscle activation level				results	
			initial	maximum			max head angle	time at max head
	$\frac{s_{ref}}{s_{free}}$	t_{reflex}	all muscles	flex*	ext+	sterno^o	$\phi - \phi_0$	angle
	[μm]	[ms]	[%]	[%]	[%]	[%]	[deg]	[ms]
A1	1 [65]	-	0	0	0	0	**117**	202
A2^a	2.8/2.45	-	0	0	0	0	**109**	197
A3	2.8/2.1 [17]	-	0	0	0	0	71	174
B1	1 [65]	25	0	100	100	100	60	171
B2^b	2.8/2.45	25	0	100	100	100	60	171
B3	2.8/2.1 [17]	25	0	100	100	100	58	168
C1^a	2.8/2.45	-	0	0	0	0	**109**	197
C2	2.8/2.45	25	0	25	25	25	**101**	194
C3	2.8/2.45	25	0	50	50	50	**83**	185
C4^b	2.8/2.45	25	0	100	100	100	60	171
D1	2.8/2.45	0	0	100	100	100	42	176
D2	2.8/2.45	15	0	100	100	100	51	174
D3^b	2.8/2.45	25	0	100	100	100	60	171
D4	2.8/2.45	50	0	100	100	100	**82**	176

* all flexor muscles (see Section 2.2.7)
+ all extensor muscles (see Section 2.2.7)
^{o} sternocleidomastoid
^{a} standard (std) passive, case A2 and C1 are the same
^{b} standard (std) active, case B2, C4 and D3 are the same

(a) passive muscles

(b) active muscles

(c) Varying muscle activation level
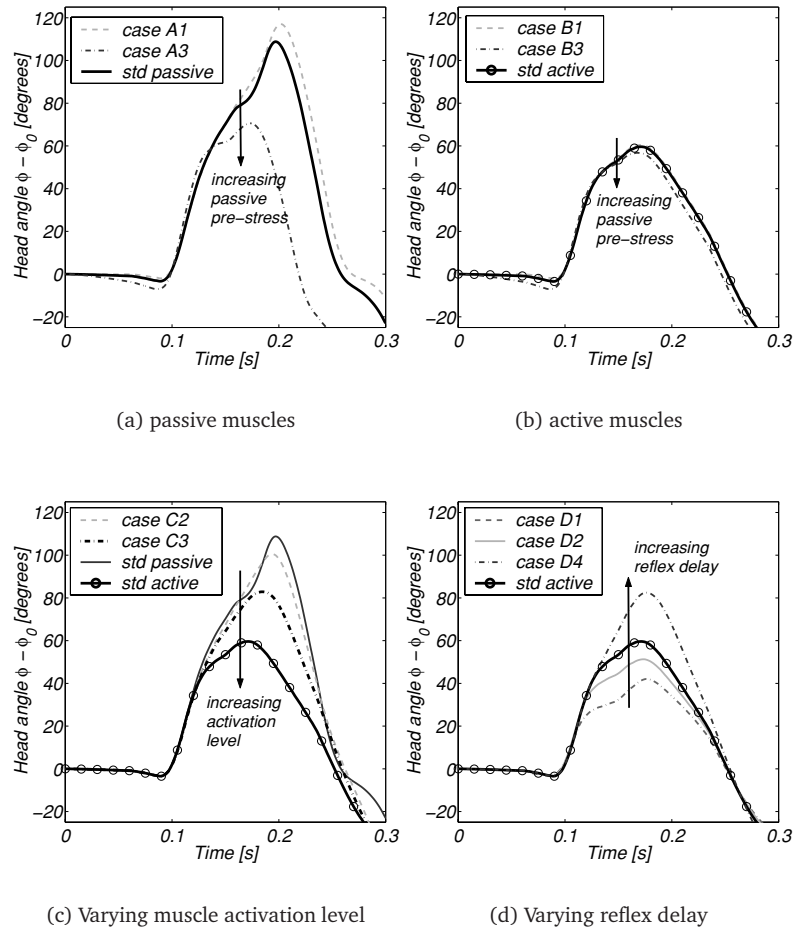
(d) Varying reflex delay

Figure 4.11: *Variation of the head angle with time for a 15g frontal impact simulation under varying muscle conditions (see Table 4.3, std passive = case A2 and C1; std active = case B2, C4 and D3).*

4.4   Discussion

The objective of this chapter was to validate the neck model for 15g frontal and 7g lateral volunteer experiments performed at Naval Biodynamics Laboratory (NBDL) [45,146]. For this purpose simulations were carried out both with and without muscle activation.

The neck model does not have a stable upright position when subjected to gravity only. Including complex feedback mechanisms for the neural excitation of the neck muscles to create an equilibrium is beyond the primary task of this study. It is assumed however that gravity can be neglected for the high severity 15g frontal and 7g lateral impacts used in this study. Simulations with and without gravity showed that differences in response are smaller than 5 %. Therefore, the assumption to neglect gravity is justified for the simulations performed in this Chapter.

Overall, the model response without muscle activation shows poor agreement with both the frontal and lateral sled experiments. The passive model is too flexible for frontal impact and even more so for lateral impact, showing larger head rotations compared to the experimentally defined response corridor. The head accelerations of the passive model show oscillations for frontal and lateral impact simulations. This oscillatory behaviour is probably caused by bottoming out of the stiffness behaviour of the model, when reaching large rotations. Muscle contraction clearly influences the response, as was already indicated by other simulation studies [61, 64, 159]. The response of the model with maximally activated muscles lies within or near the frontal and lateral response corridors for both head rotation and displacement. Also for the active model the linear and angular accelerations of the head are close to the response corridors Interestingly, the head lag for the active and passive response are nearly identical. This observation is in contrast with observations made by Wismans *et. al* [165], who concluded from volunteer and post mortem human subject (PMHS) experiments that muscle activation is responsible for the head lag. It is more likely that the differences in head lag are caused by the different initial positions in volunteer and PMHS tests studied by Wismans *et. al* [165].

In the active model head rotations are reduced somewhat below experimental values. This difference is due to the selected maximal activation and the 25 ms reflex delay. Experimental values for muscle activation during impact conditions are scarce [105, 141]. Several combinations of the reflex delay and activation level, or even activation of different sets of muscles at successive time phases are possible [134]. To study the influence of these parameters, as well as the influence of the passive muscle initial stress, a parameter study has been performed. The initial passive muscle stress influences the response of the head-neck system when simulating with passive muscles only. The influence of passive muscle properties is negligible when simulating active muscle behaviour, indicating that the forces generated by the active muscles are much larger, and therefore dominate the passive muscle forces. The influence of muscle activation has been studied by varying the muscle activation level and the reflex delay (see Table 4.3). A muscle activation level of 100% and a reflex delay of 25 ms shows the best correspondence with the reponse of the volunteers. A smaller activation level results in larger head angle compared to the corridor, while

a smaller reflex delay results in a head angle response below the volunteer corridor. A reflex delay of more than 25 ms results in larger head angles compared to the volunteer corridor. Although the extent of muscle activation of the volunteers is not known, according to the new neck model, active muscle behaviour should have been present in the volunteers.

It is most reasonable to assume that the passive model should best describe the response of a post mortem human subject (PMHS). Wismans *et. al* compared the NBDL volunteer 15g frontal impact tests to identical PMHS experiments [165]. Larger head rotations were observed for PMHS compared to the volunteers [165] (see Figure 4.12(a)). The model responses are in agreement with these observations, showing also larger head angles of the passive model compared to the active model (see Figure 4.12(b)). The maximum head angle for the passive model is 11 % larger than observed in the PMHS data. Also, the maximum head angle for the PMHS is reached at 160 ms , while the passive model shows a maximum head angle later, at 200 ms. Based on above findings it seems that the passive model is somewhat weak compared to cadaveric response. Note that the rotations in Figure 4.12 are with respect to the sled, a fixed coordinate system, while in the previous figures in this chapter the head rotations are presented with respect to T1. It should be noted also that the muscles of the PMHS in the experiments were injected with 100 ml 10% solution of formaldehyde, to simulate muscle tone of living people [165], resulting in stiffer passive muscles. In Chapter 5 more attention is paid to the modelling of the properties of the passive muscles of a PMHS.
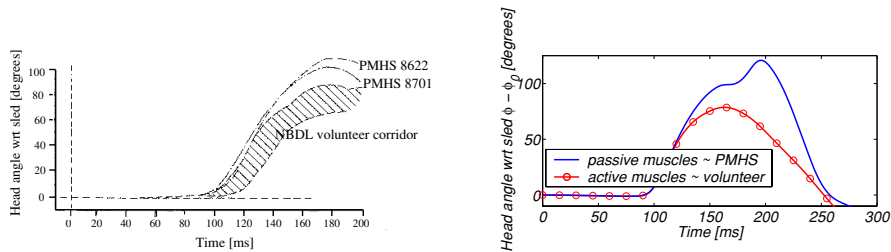
(a) Response of PMHS and NBDL volunteers adapted from [165]

(b) Response of standard passive and standard active model (see Table 4.3)

Figure 4.12: *Head angle with respect to sled for 15g frontal impact.*

The new model response has been compared to the model by De Jager [65] and an intermediate model (an update of the De Jager model by adaptation of muscle geometry, including more muscles and division of the muscles into segments to enable muscle curvature [61]). The new model showed similar response compared to the intermediate model. Figures showing a comparison of the response of the De Jager model and the new model for a frontal and lateral impact simulation are presented in Appendix B. In comparison with the earlier model of De Jager both the predicted

head and neck rotations and the displacement of the head OC and CG are reduced. It is concluded that the reduction of head motion is a result of the more realistic muscle lines of action due to the segmented muscles used in the new model. This reduction was also seen for the intermediate neck model [61]. Compared to the NBDL 15g frontal and 7g lateral impact data, the new model with active muscles shows reasonable to good agreement for head displacement, rotation and acceleration. In contrast, the De Jager model with muscle activation shows poor agreement with the NBDL volunteer response for the head displacement and head rotation (see Appendix B). The main advantage of the new model compared to the intermediate model is the improved biomechanical basis of the tissue properties and the detailed contact surface description of the cranio-vertebral joint. These factors are also important when simulating rear end impact (see Chapter 5). All three models (De Jager [65], intermediate [61] and new multibody neck model) provide comparable conclusions on the role of muscle activation, showing that inclusion of muscle activity seems necessary for reasonable simulations of impact conditions with human volunteers. This conclusion is in agreement with a statement made by Siegmund and Brault [134] based on experimental impact studies on human volunteers.

In this chapter it is assumed that the extreme flexibility of the passive model was caused by the absence of active muscle behaviour. However, it should be noted that an incorrect dynamic response of the ligamentous spinal model could also be a cause of the poor passive model behaviour in comparison with the volunteer experiments. In Chapter 3 the ligamentous segment models as well as the entire ligamentous model showed reasonable to good correspondence with quasi-static experiments. However, validation for large loads was only qualitative. Since dynamic experimental data on the ligamentous spine are not available, the model could not be validated for those conditions. Although dynamical tissue stiffening has been introduced into the model (see Chapter 2), this is also of limited value since dynamic experiments on cervical spine tissues are scarce. From previous research [65] it has been shown that an increase of 25 % of the dynamic rotational stiffening factor of the disc (see equation 2.3) resulted in a decrease of the head rotation of more than 5%. Therefore, it should be noted that despite the statement made in this chapter that modelling active muscle behaviour is necessary, stronger dynamic ligamentous tissue stiffening could also be necessary. Experiments on the ligamentous spine are recommended to verify these assumptions. Additional experimental research on muscle behaviour is presented in Appendix E), while numerical research on muscle behaviour in rear end impact is presented in Chapter 5.

Chapter 5

Response to Rear End Impact

In order to study the mechanics of the neck during rear end impact an existing global human body model [52–55, 72] and the detailed submodel of the neck as presented in Chapter 2 are combined into a new model. The **first and main objective** of this chapter is to validate this new model using rear end sled experiments performed on post mortem human subjects (PMHSs) and volunteers sitting on rigid seats and standard car seats. In Section 5.1 the material and methods used are discussed, and the results are presented in Section 5.2.

Experimental impact studies on PMHSs to study the human response are useful when the risk of injury is too high, and volunteers can not be used anymore. The usefulness of the PMHS response in representing the human response is governed by the anthropometric similarity of the PMHS and the human and the degree to which the constitutive properties of PMHS tissues match those of human tissue. Although the tissues of bone, ligament, tendon and skin undergo only small changes in mechanical properties postmortem, skeletal muscle stiffness is a source of uncertainty [37]. Results by van Ee *et al.* [37] demonstrated that postmortem post-rigor handling of cadaveric tissue prior to testing greatly affects muscle properties. The immediate postmortem response was found not to be different from the live passive response. The post-rigor muscle response was unrepeatable and stiffer than the immediate postmortem or live passive response. After "preconditioning" (repeating elongation tests on muscle tissue until the peak force varied by less than 2 percent), the response was repeatable but was significantly less stiff than perimortem and live passive muscle. Subsequently, the **second objective** of this chapter is to study the effect of the postmortem change of passive muscle properties on neck response in rear end impact by mathematical modelling (also presented in Section 5.1 and 5.2).

From literature (see review by Szabo [140]) it is known that initial seating posture and head restraint position are important parameters influencing the human head neck response. Therefore, the **third objective** is formulated: to study the influence of the initial seating posture and the position of the head restraint for simulations in a standard car seat. The results are presented in Section 5.3.

Volunteer experiments (see review by Siegmund and Brault [134]) indicate that

71

the muscles are active early in the impact event and capable of generating forces which can alter head and neck kinematics. Simulations of frontal and lateral impact (see Chapter 4) showed that inclusion of active muscle behaviour seems essential to describe accurately the human head neck response of live human subjects. Therefore, the **fourth objective** of this chapter is to study the role of muscle behaviour (passive and active) in rear end impact (see Section 5.4).

5.1 Material and Methods

The neck model as presented in Chapter 2 is included in a full human body model. In this way the interaction of the human with the seatback and the head with the head restraint can be studied. The human body model used is described below, followed by a description of the simulation of the experiments used for validation.

Human Body Model   A mathematical multibody human model representing a 50th percentile male has been developed by TNO Automotive, Crash Safety Centre (see Figure 5.1). The human geometry was obtained from RAMSIS anthropometric data, which provided a realistic surface description, in particular for seated automotive posture. A 50th percentile male model from RAMSIS with 1.74 m standing height and 75.7 kg weight has been chosen [55]. Detailed descriptions of the model and frontal lateral and rear end impact validation can be found in [52–55, 72].
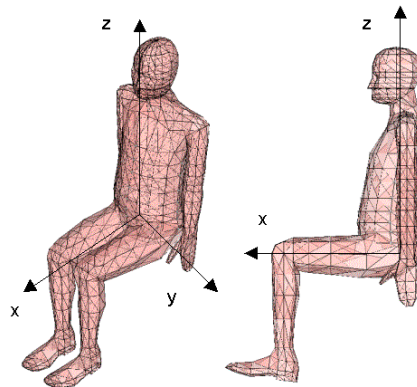

Figure 5.1: *MADYMO human body model representing a 50th percentile male, erect seating position.*

5.1.1 Experimental Data

The human body model with detailed neck is validated with four test series:

- PMHS experiments performed at $\Delta V = 10$ km/h by the Laboratory of Accidentology and Biomechanics (LAB), France [7, 8].

- Volunteer tests performed at $\Delta V = 9.3$ km/h by the Japanese Automobile Research Institute (JARI), Japan [30, 102].

- Volunteer tests performed at $\Delta V = 9.5$ km/h by the Allianz Zentrum für Technik (AZT), Germany [71].

- Volunteer tests performed at $\Delta V = 9.8$ km/h by the Maastricht University (UM), the Netherlands (Appendix E).

ΔV is the change in velocity of the sled. The test conditions are summarized in Table 5.1. It should be noted that although the Δ Vs of the test series are comparable, the sled acceleration ranges from 0.7g to 12g. Model validation using these experiments could indicate the applicability of the model over a large range of impact severities.

Table 5.1: *Test conditions of the rear end sled experiments.*

Parameter	Unit	LAB	JARI	AZT	UM
Reference		[7, 8]	[30, 102]	[71]	Appendix E
Subject		PMHS	volunteer	volunteer	volunteer
Total number of subjects		3	7	7	8
Total number of tests		6	9	7	16
Average mass	kg	50	71	75	76
Average height	m	1.64	1.76	1.80	1.89
Seat type		rigid	rigid	standard car seat	standard car seat
Head restraint		no	no	yes	yes
Belt system		single belts over limbs, pelvis and thorax	no	3-point belt with retractor	4-point belt with retractor
Δ V	km/h	10	9.3	9.5	9.8
Max sled pulse	g	12	4	5	0.7

LAB Test Setup [7, 8]

The experiments were designed to be both simple and reproducible, using a rigid seat without head restraint. The seat back and seat panel had an inclination of 25 and 10 degrees respectively. The subjects were restrained by three belts, which held the thighs, pelvis and thorax tightly to the seat. Since the head-neck position of the PMHSs was not stable, an electromagnet was used to keep the head in the initial position before impact (i.e. Frankfort plane horizontal, see Figure 5.2(a)).

Head accelerometers were screwed on to the skull. The T1 instrumentation was screwed onto the anterior part of the vertebral body. Also instrumentation was mounted onto C2 and C5. Two film targets attached to the subjects head were used for defining head translation and rotation. T1 displacements and rotations were calculated using the acceleration data. The conditions in which these tests were performed were highly reproducible, resulting in quite consistent responses of the PMHSs. The reproducibility of the test was demonstrated by performing two tests on each subject. Furthermore substantial similarities were observed in the responses of all three subjects. A post experimental dissection showed the absence of any injury in the PMHSs after impact.

JARI Test Setup [30, 102]

A rigid seat was mounted on the sled at an angle of 10 degrees with the horizontal, and the back of the seat was at 110 degrees with the horizontal. The feet of the volunteers were on a foot-plate at 45 degrees with the sled. No belts were used during the sled tests. In Figure 5.2(c) the sled test apparatus is shown. Head acceleration measurement was performed using a head bracket fitted into the mouth of the volunteer. The upper part of the bracket was attached to the subject's head. Film targets and head accelerometers were attached to this bracket. T1 accelerometers were attached to the skin overlying the thoracic vertebra using surgical tape. Electromyographic activities were measured using surface EMG electrodes which were attached bilaterally onto the skin over the sternocleidomastoid and paravertebral muscles. Cineradiographic techniques were used to analyse vertebral rotations. Each volunteer was asked to hold the handle and relax during the test. The test was repeated several times for all volunteers, so that they got used to it and were able to relax [53]. Personal interviews with the subjects by a clinical doctor revealed no injury symptoms after the experiments.

AZT Test Setup [71]

In the volunteer experiments a standard car seat selected for the European whiplash project [167] was used. The car seat was mounted on a sled. The seat back angle was set to 25 degrees using an H-point manikin in compliance with regulation SAE J826 §4.3. The head restraint was positioned so that the top of the head and the head restraint were aligned. If this was not possible due to the large subject height, the maximum head restraint height was taken. The volunteers were asked to take a normal automotive passenger posture (see Figure 5.2(e)). The Frankfort plane was initially horizontal, implying an initial head angle of 0 degrees. Head accelerations were measured by accelerometers attached to a head strap. The head strap system consisted of several straps which could be tightened around the chin, around the head circumference at the height of the forehead and at the lower posterior side of the neck. T1 instrumentation was mounted to a thin aluminium plate which was formed to match each volunteer's back contour at T1. Adhesive sports tape was used to attach this plate to the skin overlying the spinous process of vertebra T1. Three film targets

(a) LAB PMHS

(b) Model for LAB simulation

(c) JARI Volunteer

(d) Model for JARI simulation

(e) AZT Volunteer
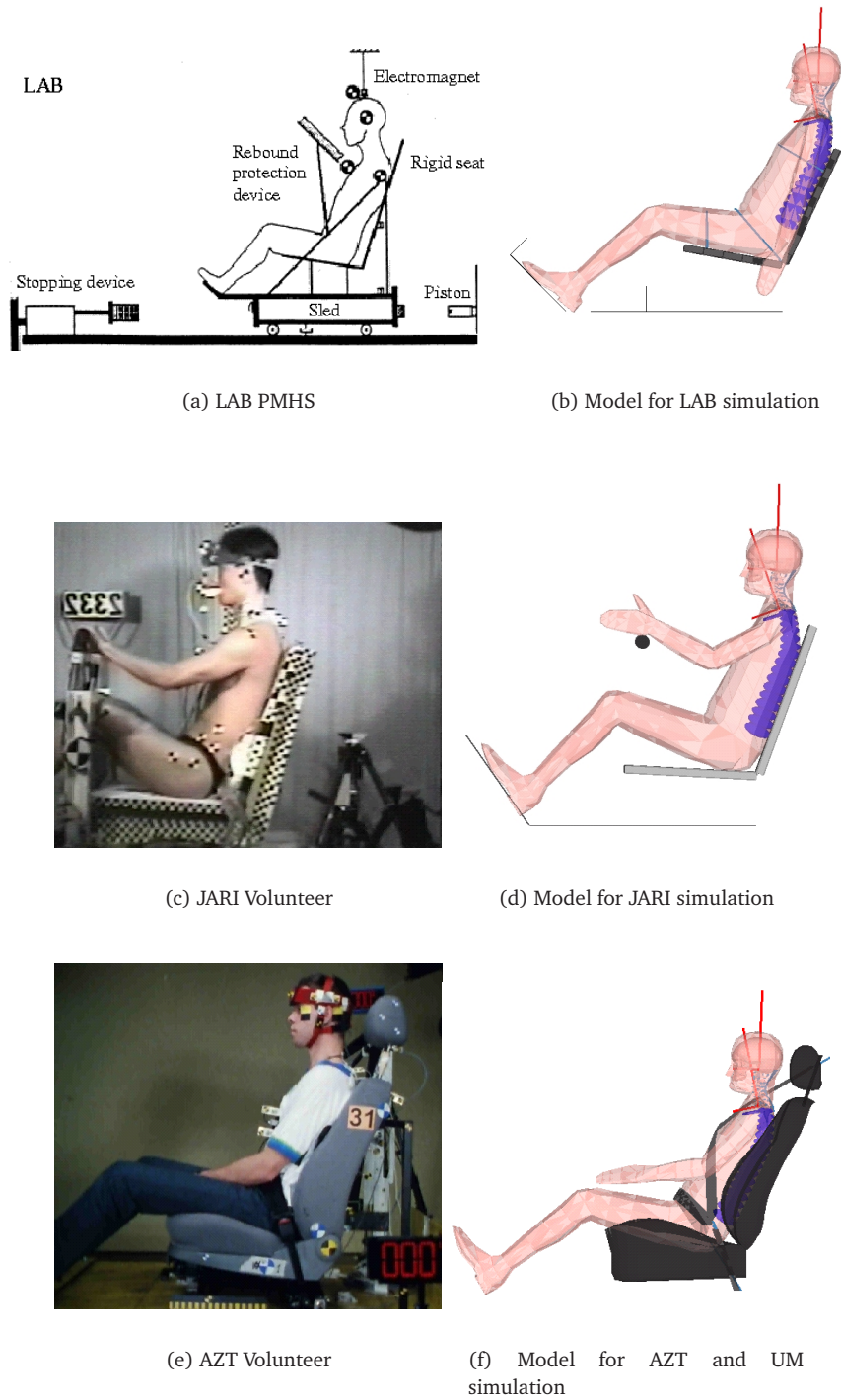
(f) Model for AZT and UM simulation

Figure 5.2: *Test setup of the rear end sled experiments together with model simulation setup. See Appendix E for UM experimental test set up.*

defined on the head and two targets defined on T1 were used for recording head and T1 displacements and rotations. No injuries were reported for these experiments.

UM Test Setup

In these volunteer experiments the same car seat as was used for the AZT experiments was mounted on a sled. The seat back angle was fixed in the same position as for the AZT simulations (i.e. head restraint bar in a 14 degree angle backward relative to the sled). The head restraint was set to the highest position for all subjects. The subjects were asked to adopt a "neutral automotive posture" with the Frankfort plane oriented horizontally. No injuries were reported for these experiments. See Appendix E for a detailed description of the setup and the results of the UM experiments.

5.1.2   Setup of the Simulation

In the simulations of the experiments the outside surfaces of the seats were modelled with so called arbitrary surfaces in MADYMO (see explanation in Chapter 2). The same modelling technique was also used for the floor and foot planes of the LAB, AZT and UM experiments. The floor in the JARI experiments was simply modelled with planes. The standard seat model consists of the following three areas: seat cushion, seat back and head restraint. These sections are connected with joints swivelling around the transverse axis of the seat. The joint connecting the seat cushion and the seat back is the recliner joint. The head restraint is connected to the seat back by tubes, which allow rotation of the total head restraint system with respect to the seat back. The head restraint cushion can rotate as well as translate about these tubes. The rotational joints are modelled in the MADYMO input file as revolute joints, that are constraining the relative motion of the interconnected bodies to a rotation around the corresponding lateral axis. Thus, these joints do have only one rotational degree of freedom. With the used recliner joint it is on the one hand possible to adjust the inclination of the backrest, on the other hand also elastic and plastic deflection of the backrest can be defined over a characteristic of the torsional rigidity. The same goes for the head restraint joint. Additionally, with the translational joint of the head restraint the vertical position of the head restraint can be defined. The load deflection curves and joint characteristics of the standard seat (used in AZT and UM experiments) were based on quasi-static experiments of the seat performed within the European whiplash project [167]. The positions of the head restraint and the belt attachment points were derived from photos of the experimental setups. The belts in the LAB experiment were modelled as single spring elements. The volunteers in the JARI experiments were not belted. In the AZT tests a three point belt was used, which is modelled as a three point finite element belt [149]. In the UM experiments a four point belt was used. The difference between the use of a three or four point belt could be seen only in the rebound phase, however this phase has not been reported for the UM experiments (see Appendix E) and will therefore not be studied here. For simplicity, the test setup of the UM experiments is modelled exactly the same as the AZT simulation, including the same seat and three point finite element belt model.

In the simulations the human body model was positioned based on photos of the experiments. The simulations were organized such that before the beginning of the simulated experiment the human body model was allowed to sink into the seat (rigid or standard soft seat) to find an equilibrium position from a position just above it. The electromagnet used in the LAB experiments to keep the head of the PMHS horizontal was simulated by a stiff translational spring in this pre-simulation stage. In case of volunteer experiments, the muscles are slightly activated to maintain the initial position of the body, while the body settles into the seat. To incorporate this into the model would requires neural excitation of muscles utilizing complex feedback mechanisms, which is beyond the scope of this thesis. The effect of the initial muscle activity was approximated using a translational spring to keep the head horizontal in the pre-simulation stage. In the LAB simulations the arms were modelled along the body and were restricted in motion by the belts. In the JARI experiments the hands were fixed, simulating the holding on to the handle of the volunteers. For the AZT and UM tests the arms were positioned just above the legs of the human model. The final initial positions of the models compared to the experimental set-ups are similar (see Figure 5.2).

Impact simulations were performed using the horizontal sled acceleration (average of all experiments per test series) as input to the model (see Figure 5.3(a)). Furthermore, a vertical acceleration field simulating gravity is added (see Figure 5.3(b)). In case of the JARI experiments, the sled is sliding on a long rail angle at 10 degrees [102]. Due to this orientation of the sled a horizontal and vertical sled acceleration is applied. Gravity is accounted for in the vertical component (see Figure 5.3(b)). The spring used to keep the head horizontal initially in the pre simulation stage was released in the final simulations.

It should be noted that model simulations were performed for 300 ms, but that the data of the LAB, AZT and UM experiments have only been analysed for the first 200 ms.

The main objective of this chapter is to validate the new neck model for rear end impact loading. Therefore, both PMHS and volunteer simulations are performed with passive muscle behaviour based on the tensile properties presented in Section 2.2.7. The results are presented in Section 5.2. An additional simulation is performed for the PMHS experiments to study the effect of the postmortem change of passive muscle properties (second objective). The stiffer passive muscle function (see Figure 2.9) used for this simulation is based on post-rigor PMHS tensile muscle properties [37]. The results of this additional PMHS simulation is also presented in Section 5.2. In section 5.3 the third objective is studied: the influence of initial seating position and the head restraint position for rear end impact loading. In the simulations in Section 5.2 and 5.3 the initial muscle activation as well as the maximum muscle activation are zero. To study the role of muscle behaviour in rear end impacts, i.e. the fourth objective of this chapter, a parametric study varying muscle properties (passive and active) is presented in Section 5.4.
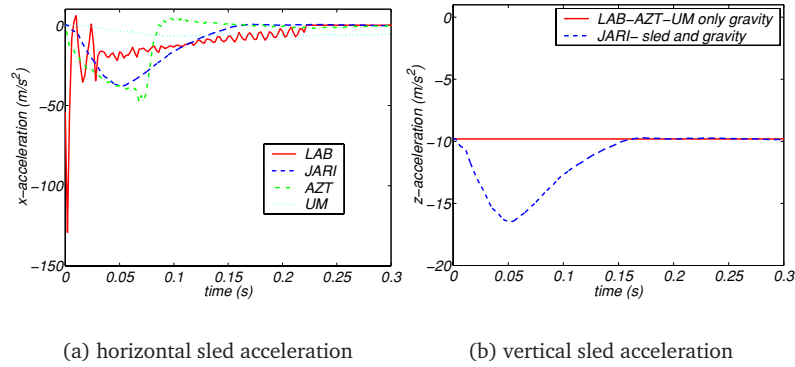
(a) horizontal sled acceleration   (b) vertical sled acceleration

Figure 5.3: *Sled pulses used in the model simulations.*

5.1.3   Criteria for Model Quality Assessment

The model was validated against above mentioned tests (LAB, JARI, AZT, UM). As in Section 4.1.3 the following terms are introduced to describe the results: *good* means within the envelope of the experimental data, *reasonable* means close to this envelope, and 25% deviation allowed, while a *poor* correlation stands for more than 25% deviation from the envelope.

Head and T1 trajectories, linear and angular head accelerations as well as vertebral rotations, neck loads are used for validation (see Table 5.2). The neck loads were derived from head acceleration and transformed to local coordinate systems using rotations derived from film. In the AZT tests head restraint forces were taken into account [71]. It should be noted that the head-neck system is seen as a pivot mechanism when calculating the neck loads (OC loads). The net force on the neck is taken, including the loads caused by the ligaments and the muscles, this is not the load on the real anatomical OC joint, but the load on a virtual single hinge joint between head and neck.

Table 5.2: *Set of responses used for model validation.*

Response parameter	with respect to	LAB	JARI	AZT	UM
T1 trajectory	sled	X	X	X	NA
T1 rotation	sled	X	X	X	NA
head CG trajectory	T1	X	NA	X	X
head OC trajactory	T1	NA	X	-	NA
head rotation	sled	X	X	X	X
	T1	X	X	X	NA
head CG lin. acceleration	local	X	X*	X	NR
head CG ang. acceleration	local	X	X	X	NR
OC loads		X	X	X	NA
vertebral rotations		X$^+$	X^o	NA	NA

X used for validation	- not used
NA not available	NR not reliable
* only available in x direction	$^+$ only C0-C2, C2-C5 and C5-T1
^{o} only available for one experiment	

5.2   Simulation Results

The first and second objective of this chapter are discussed in this section: i.e. 1) to validate the new neck model for rear end impact loading, and 2) to study the effect of the postmortem change of passive muscle properties.

5.2.1   LAB Simulation and Passive Muscle Property Variation

The LAB experiments were simulated with normal and stiffened passive muscle properties. The overall response is shown in Figure 5.4, whereas the T1 and head kinematics versus time are presented in Figures 5.5 to 5.7. In the first 50 ms of the response, the head only translates. The model response of both models, normal and stiffened passive muscles, show similar head-neck response until about 150 ms. But after this time the model with stiffer muscles shows reduced head motion compared to the model with normal passive muscles. The rebound of the model starts 200 ms after the beginning of the input pulse. This is also observed in the PMHS experiments on films. However the kinematics were only analysed until 200 ms.
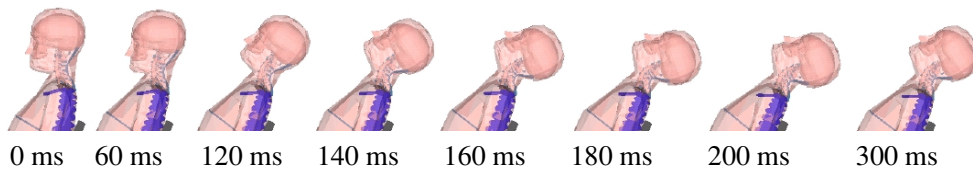

0 ms   60 ms   120 ms   140 ms   160 ms   180 ms   200 ms   300 ms

Figure 5.4: *Kinematics of the human body model with detailed neck with stiff passive muscles at successive times for the LAB simulation.*

Responses of T1 in the experiments and the simulation are shown in Figure 5.5. For each of the three subjects, results of two experiments are shown. The repeatability of the experiment is apparent from the close match between the two tracings for each subject. A consistent rearward motion of T1 of the PMHS is seen. In two subjects, vertical displacement of T1 proceeded linearly in time, but one subject behaved differently and hardly showed any ramping-up with very little z-displacement for T1. Also the T1 rotation is smaller for this subject compared to the other two. The human body model shows reasonable agreement with the experimental T1 responses in rotation and x-displacement, but the T1 z-displacement remains below the experimental results, showing no upward displacement of T1 at all. The model response shows a sudden increase of T1 rotation and displacement at about 160 ms. This increase occurs earlier for the model with stiff muscles.

The head rotation is shown with respect to the sled and T1 in Figure 5.6. Again the consistency of the responses of each subject is clearly visible. The head rotation illustrates that the head starts its backward rotation after T1 does, resulting in a small forward rotation of the head relative to T1. Comparison with the model shows that the timing of the head rotation of both models is good. However the maximum head
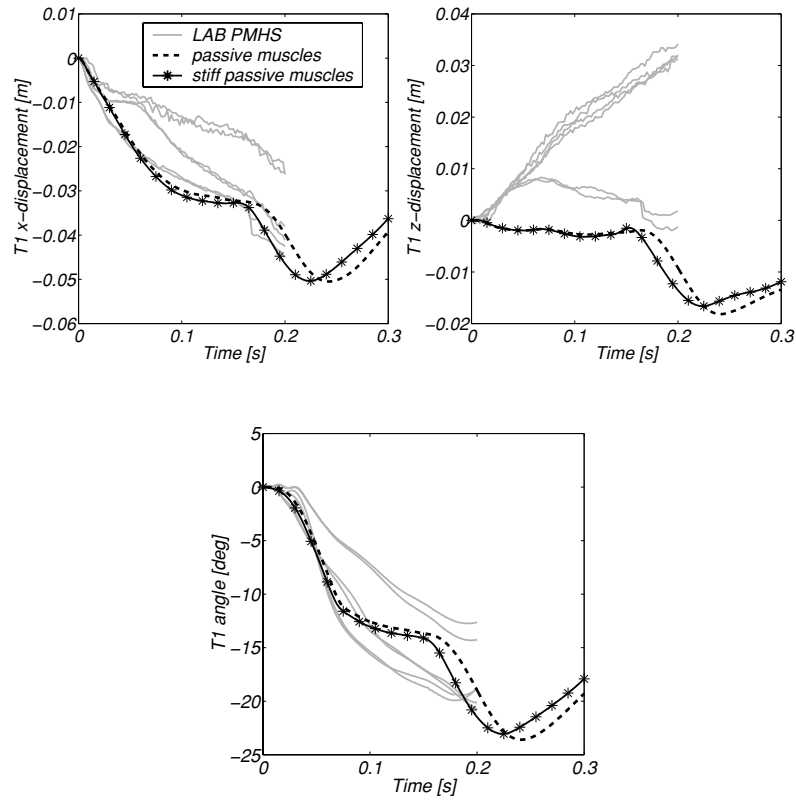
Figure 5.5: *T1 kinematics with respect to sled versus time. Simulated response to 12g rear end impact of the neck model with (stiff) passive muscle behaviour compared to LAB PMHS response.*

rotation is too large for the model with normal passive muscles, but is within the response envelope for the model with stiff muscles.

The position of the head CG with respect to T1 versus time is shown in the lower part of Figure 5.6. The PMHS who showed a rather small T1 z-displacement, showed a positive CG z-displacement with respect to T1, while the CG x-displacement was consistent for all the PMHSs. The model with normal passive muscles falls well within the experimental envelopes of the CG x-displacement. The stiff passive muscle model falls within the envelope during the first 160 ms, but finally shows a smaller CG x-displacement. The CG z-displacements of both models are similar and close to the response of one PMHS until 150 ms. Then, the model with stiff passive muscles almost reached the maximum CG z-displacement while the other model reached a larger maximum at 190 ms.
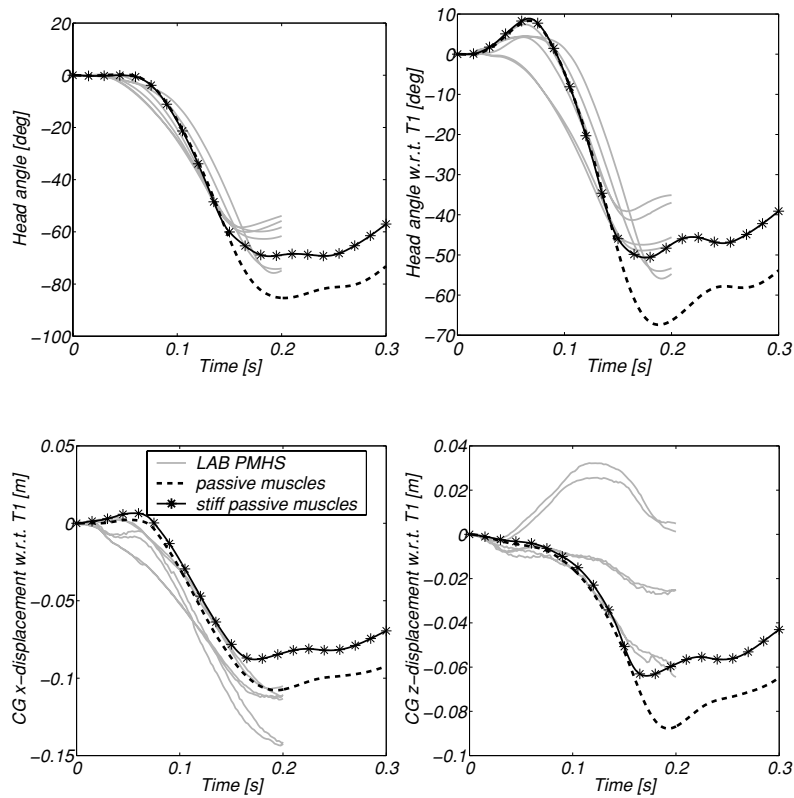

Figure 5.6: *Head kinematics versus time. Simulated response to 12g rear end impact of the neck model with (stiff) passive muscle behaviour compared to LAB PMHS response.*

Figure 5.7: *Head accelerations and OC loads versus time. Simulated response to 12g rear end impact of the neck model with (stiff) passive muscle behaviour compared to LAB PMHS response.*
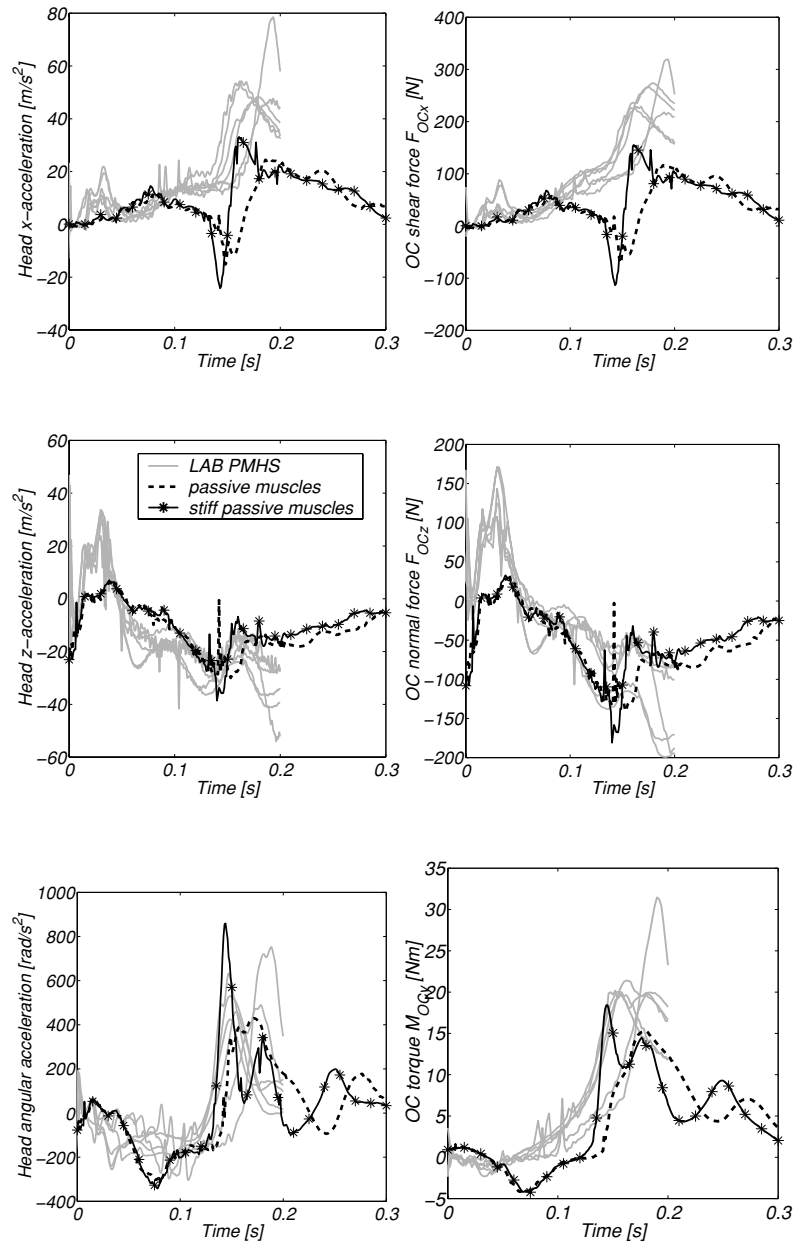
The z-acceleration and angular acceleration of the head CG of both models show reasonable agreement with the PMHS envelope (see Figure 5.7). The head x-acceleration is close to the PMHS response for the first 100 ms, but later the head x-acceleration of both models differs considerably from the PMHS responses.

In the right part of Figure 5.7 the neck loads are presented. The responses of both experiment and model start with increasing anterior shear force. The peak anterior force is about 50 ms later for the model compared to the experimental response. The posterior force is clearly present in the experimental response. For the model response a short posterior peak force is seen. The normal force of the model and the experiments show the same trend. In the experiments the extension moment during the first phase, which generally could be recognized in a rear end impact is not seen. In contrast, the model response shows first an extension followed by a flexion moment. However the peak flexion moments of experiment and model agree well.

The peak vertebral rotations of the model response are compared to the experimental data in Figure 5.8. The model with passive muscles shows reasonable rotation for the lower neck (C5 wrt T1), but the model is too flexible for the mid (C2 wrt C5) and upper neck (C0 wrt C2). The model with stiff passive muscles shows a reduction of the vertebral rotation. However, the model shows too stiff rotational behaviour for the upper and lower neck, while the mid part of the neck model with stiff muscles is too flexible compared to the experimental response.
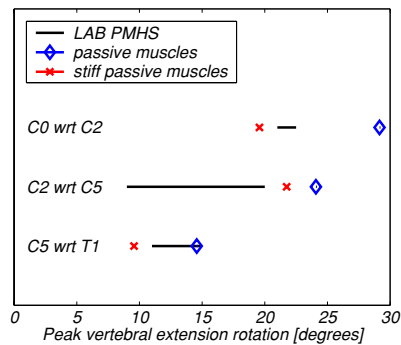

Figure 5.8: *Peak vertebral extension rotations. Simulated response to 12g rear end impact of the neck model with (stiff) passive muscle behaviour compared to LAB PMHS response.*

5.2.2   JARI Simulation

Contrary to the previous section, only the normal passive tensile muscle properties as defined earlier in Section 2.2.7 are used for the volunteer simulations. For the JARI test setup the overall response of one experiment and the model is shown in Figure 5.9. In Figures 5.10, 5.11 and 5.12 the model kinematics together with the experimental results are presented.
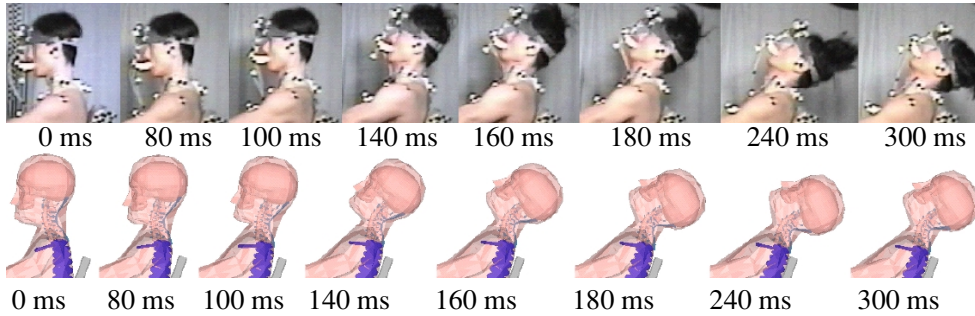

| 0 ms | 80 ms | 100 ms | 140 ms | 160 ms | 180 ms | 240 ms | 300 ms |

| 0 ms | 80 ms | 100 ms | 140 ms | 160 ms | 180 ms | 240 ms | 300 ms |

Figure 5.9: *Kinematics of JARI experiment and the human body model with detailed neck at successive times (see Table 5.3).*

Note the wide range of experimental data of the volunteers, although the same trend is seen for all experiments. In Figure 5.10 T1 responses are shown. A consistent rearward motion of T1 is seen. The model shows good correlation for T1 x-displacement with the experimental data. The T1 z-displacement is a bit too small compared to the volunteers. The T1 rotation lies within the volunteer envelope for the first 200 ms, but then a small increase is seen, resulting in a larger T1 rotation as is seen for the volunteers.

The model shows good agreement with the volunteer response for head rotation for the first 120 ms (see Figure 5.11). The maximum head angle at 200 ms is too large compared to the volunteers, but the head angle with respect to T1 shows a smaller difference between model and experiments. An initial head flexion with respect to T1 is seen for the model as well as for the experiments. The OC x-displacement of the model shows reasonable agreement with the volunteer response. The OC z-displacement shows poor correlation for the first 100 ms, but then the model shows reasonable agreement.

Figure 5.10: *T1 kinematics with respect to sled versus time. Simulated response to 4g rear end impact of the neck model with passive muscle behaviour compared to JARI volunteer response.*

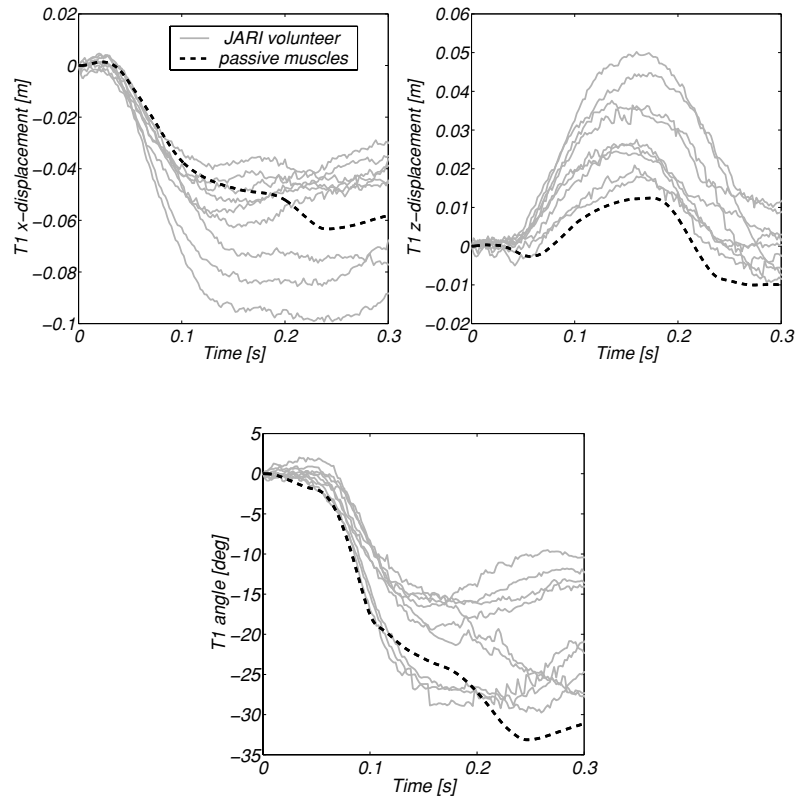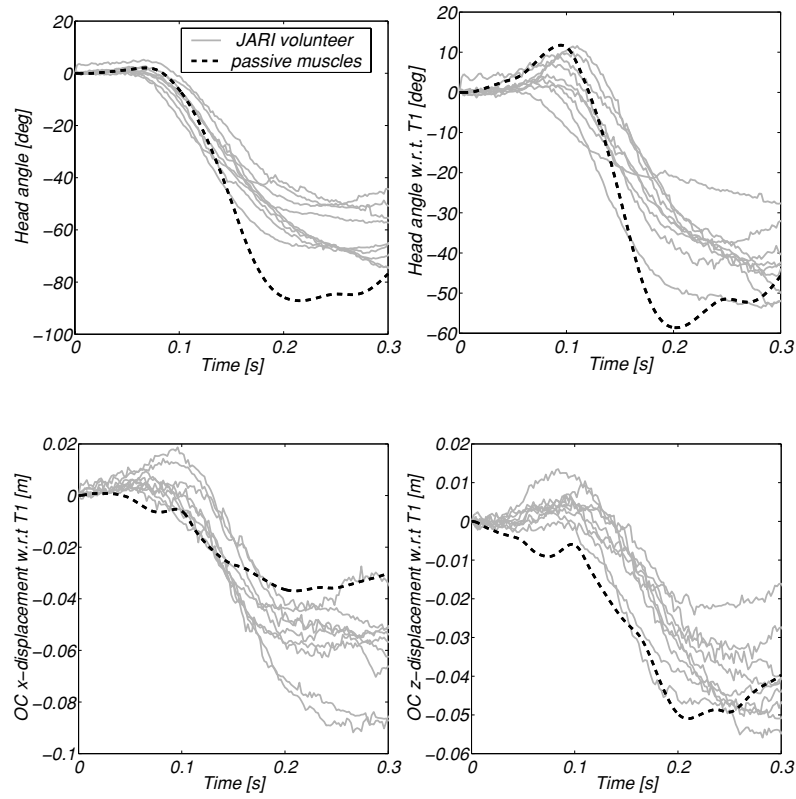**Figure 5.11:** *Head kinematics versus time. Simulated response to 4g rear end impact of the neck model with passive muscle behaviour compared to JARI volunteer response.*
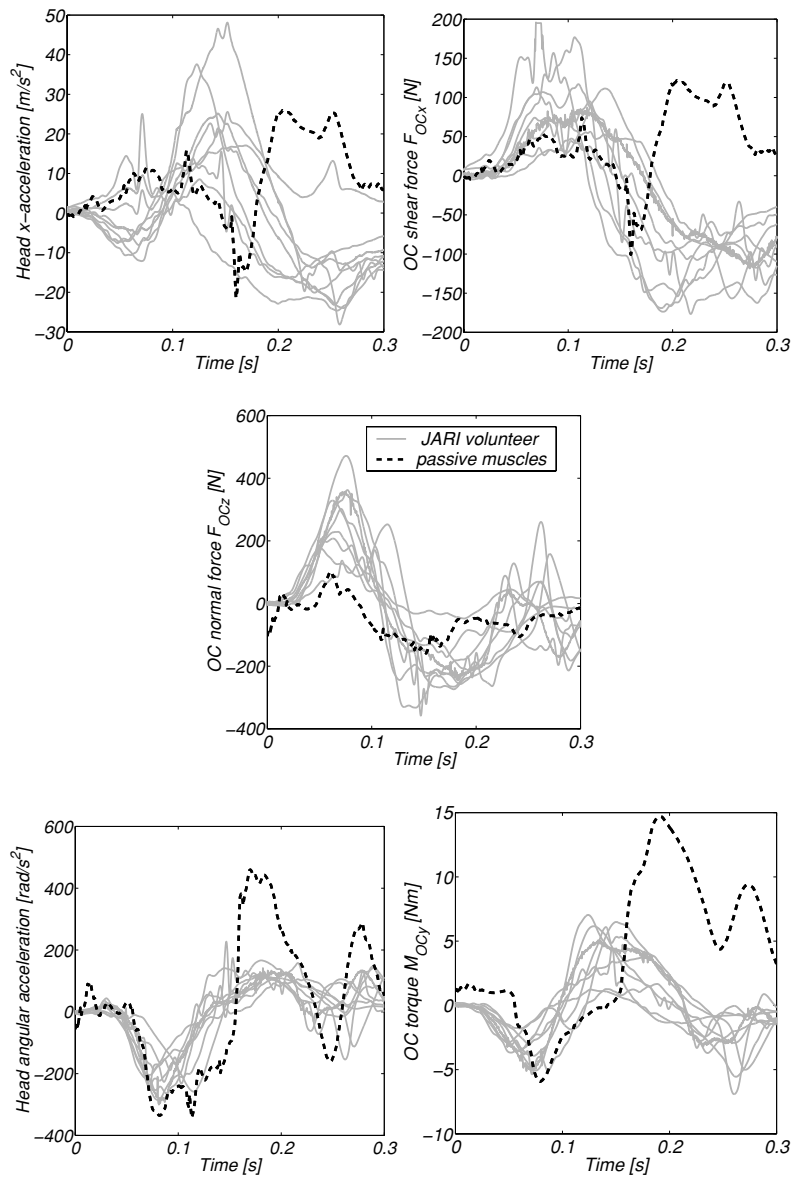
Figure 5.12: *Head accelerations and OC loads versus time (head z-acceleration not available). Simulated response to 4g rear end impact of the neck model with passive muscle behaviour compared to JARI volunteer response.*

The head accelerations are presented in Figure 5.12. Contrary to the head x-acceleration the head angular acceleration shows consistent results for the volunteers. The model response shows reasonable agreement until about 150 ms, however then the model predicts strong forward head rotational acceleration which is not seen for the volunteers (see also the head angle in Figure 5.11).

Also in Figure 5.12 the OC loads of the model and the volunteers are presented. The OC normal force of the model shows reasonable agreement with the experimental data. The OC shear force shows good correspondence compared to the experimental data for the first 150 ms. But afterwards, the experimental response shows an increase of the posterior shear force, whereas, the model predicts a decrease of the posterior shear, even changing in anterior shear after about 180 ms.

The OC torque shows reasonable to good correspondence with the experimental data for the first 150 ms, but the flexion moment occurring in the model starts too late. Additionally, the peak flexion moment of the model is about three times higher compared to the volunteers, and occurs about 50 ms later.

The vertebral rotations of one experiment are published by Ono [104], and used for model comparison. The results are presented in Figure 5.13. The model with passive muscles shows about two times more flexibility for extension than the response of the volunteer.
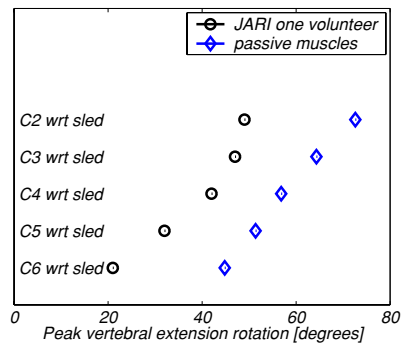

Figure 5.13: *Peak vertebral extension rotations. Response to 4g rear end impact of the neck model with passive muscle behaviour compared to JARI volunteer response.*

5.2.3   AZT Simulation

The overall response of the AZT model simulation is shown in Figure 5.14. The translation phase followed by head extension as well as the head contact and the rebound are clearly seen.
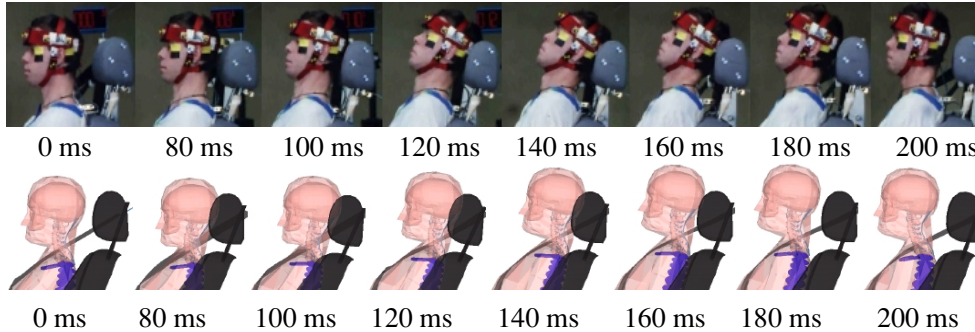

| 0 ms | 80 ms | 100 ms | 120 ms | 140 ms | 160 ms | 180 ms | 200 ms |

Figure 5.14: *Kinematics of AZT experiment 31 and the human body model with detailed neck (passive muscles, head restraint at normal position, seating posture P3) at successive times.*

A good correlation of the T1 response of the model is seen in Figure 5.15. The T1 z-displacement starts a little bit later compared to the volunteers.

In Figure 5.16 the head rotation and the head CG displacement is shown. The head angle with respect to T1 shows initial flexion as is also seen for the volunteers. However the flexion phase of the model takes too much time, resulting in a later start of the extension phase compared to the volunteers. The maximum head angle of the model is too small in the extension phase.

The CG z-displacement of the model agrees well with the volunteer response. The CG x-displacement shows good correspondence for the first 100 ms. After head contact the model response shows forward displacement of CG with respect to T1, while the experimental data shows rearward displacement of CG with respect to T1.

The acceleration of the head is presented in Figure 5.17. The head x-acceleration shows reasonble agreement compared to the volunteer envelope. The head contact of the model occurs slightly earlier than for the volunteers (indicated by the increase of head x-acceleration at about 60 ms). The head z-acceleration shows the same trend as is seen for the volunteers. The model response, however, starts with a negative head z-acceleration and the upward acceleration caused by the T1 vertical displacement is larger compared to the experimental data. The head angular acceleration shows reasonable correlation with the volunteer response for the first 250 ms, however the peak values are much smaller than is seen in the experimental data. The peak value at about 280 ms which is seen in the acceleration and therefore also in the load responses is caused by contact between head and chest.

The corresponding OC loads are presented on the right side in Figure 5.17. The model response for shear force shows poor correlation compared to the experimental
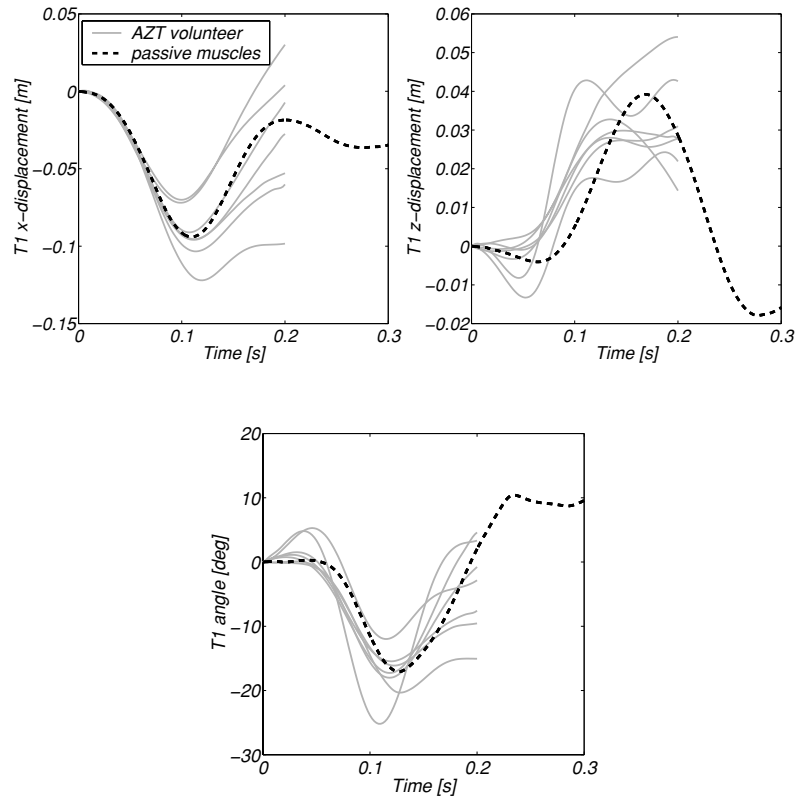
Figure 5.15: *T1 kinematics with respect to sled versus time. Simulated response to 5g rear end impact of the neck model with passive muscle behaviour compared to AZT volunteer response.*
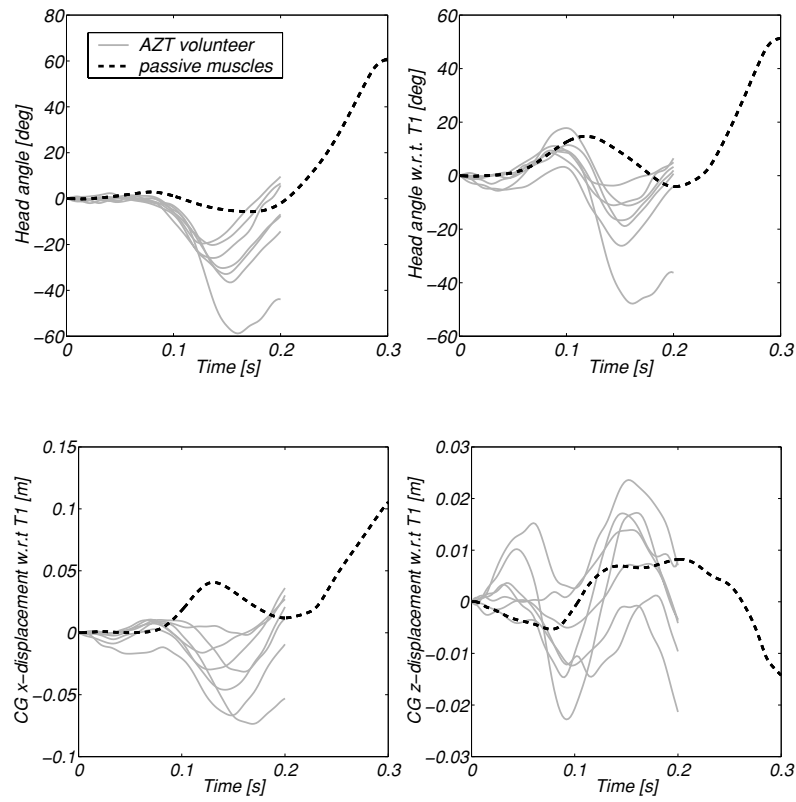
Figure 5.16: Head kinematics versus time. Simulated response to 5g rear end impact of the neck model with passive muscle behaviour compared to AZT volunteer response.

response. The anterior shear force is only limited present for the model and is followed by a long phase of posterior shear. For the OC normal force the model shows poor correlation for the first 100 ms. But the same trend, i.e. compression phase followed by tension, can be seen for both, model and experiments. The OC torque of the model response is smaller than the experimental response. However, the same trend, i.e. first an extension moment followed by a flexion moment is seen for both cases.

5.2.4   UM Simulation

The overall response of the UM experiments is presented in Appendix E. The model response with passive muscles is compared to the experiments in which the volunteers were asked to relax prior to impact (untensed). The head angle and the head CG displacement with respect to the sled are presented in Figure 5.18. The CG x-displacement shows the same trend for the volunteers as for the model, although the rearward displacement of the model starts slightly later than for the volunteers. The maximum value of the model lies in the response envelope of the volunteers. The CG z-displacement of the model shows a downward motion compared to the sled, while the experimental data show an upward motion. The head angle of the model shows initially flexion followed by an extension phase. This initial flexion is not seen for the volunteers. The maximum extension of the model lies within the range of the volunteer data.

Since the head CG z-displacement showed poor correspondence additional simulations are performed for the UM simulations. The impact severity for the UM tests is lower than the gravitational force. When ignoring the gravity of the head (i.e. simplest form of simulating posture maintenance of the head) the vertical head displacement showed better correlation for the UM simulation (see Figure 5.18). Also the initial flexion phase (50-150 ms) disappeared. For the higher severity simulations the influence of neglecting the gravity of the head was very small. This indicated that modelling posture maintenance is necessary when studying low severity impacts or when the model will be used for studying human vibration in driving situations [58].
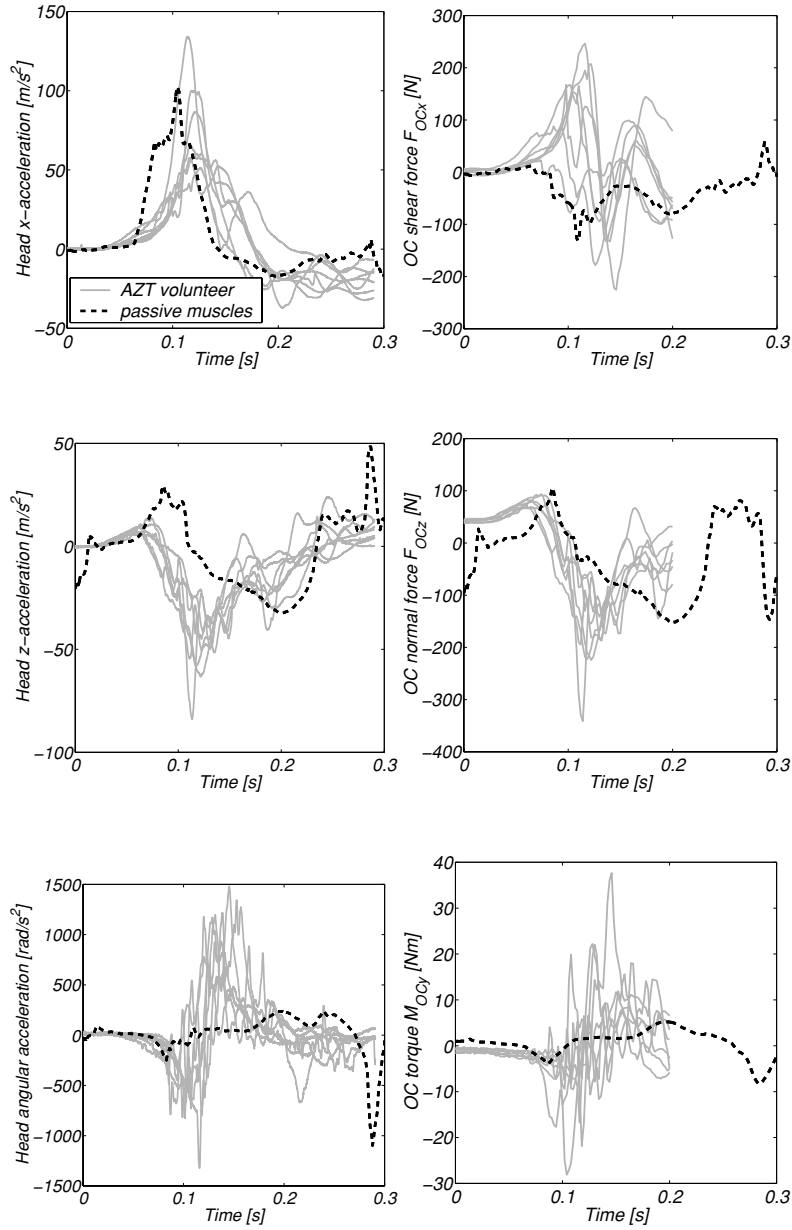
Figure 5.17: *Head accelerations and OC loads versus time. Simulated response to 5g rear end impact of the neck model with passive muscle behaviour compared to AZT volunteer response.*
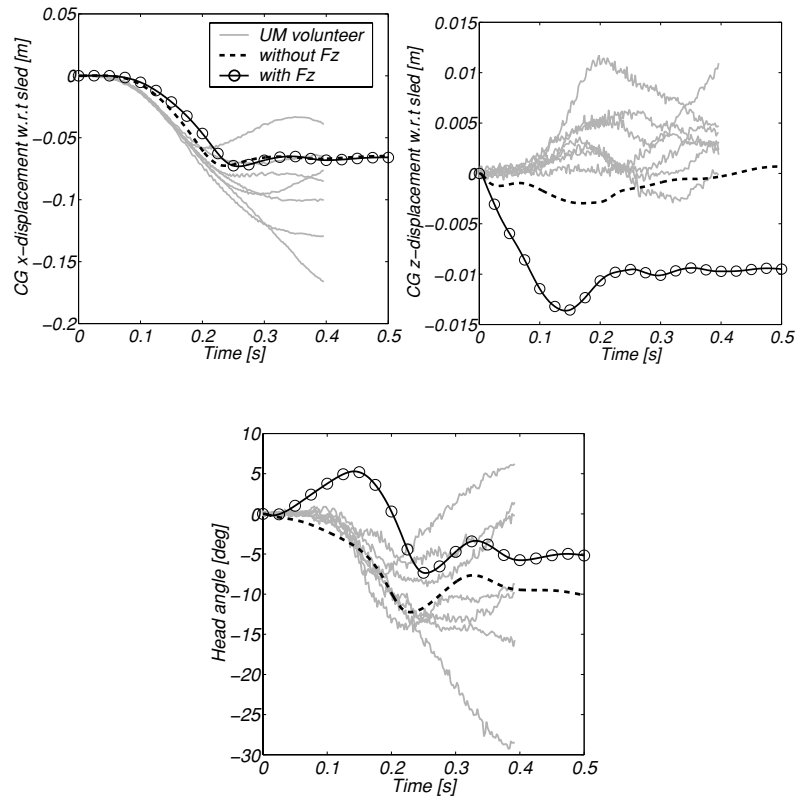
Figure 5.18: *Head kinematics with respect to the sled versus time. Simulated response to 0.7g rear end impact of the neck model with passive muscle behaviour compared to UM volunteer response.*

5.2.5   Discussion Model with Passive Muscles

The neck model was validated for quasi-static loading in Chapter 3 and for frontal and lateral impact in Chapter 4, and showed good performance. The **first objective** of this chapter was to validate the new neck model for rear end impact loading. Therefore, validation simulations of four rear end impact experiment series ranging from 0.7 g to 12 g were performed. Two experiments used a rigid seat (LAB, JARI), while AZT and UM used a similar standard seat with head restraint. Model validation using these experiments could indicate the applicability of the model over a large range of impact severities, e.g. the possibility to use the model in impact studies as well as in vibration studies without severe loads [58].

Contrary to Chapter 4 the model with detailed neck has been validated as a complete unit in a whole body instead of validating the neck model separately. The whole body simulation indicated that the simulated head neck response was influenced not only by the neck model, but also by the spine model as well as by the seat model. Thus validation studies as performed in this chapter, included validation of the seat model as well as of the spine and neck model. The spinal response is represented by the T1 response of the model.

Simulation results of the head kinematics for a deformable standard car seat were less accurate concerning validation than for a rigid seat. It is hard to conclude whether this observation is related to the seat model or the spinal model. The standard seat has been modelled in detail [167] but the load deflection curves and joint characteristics were based on quasi-static experiments instead of dynamic loading conditions. Since the T1 model response showed reduced vertical motion compared to the experimental data (see below) for both deformable and rigid seat simulations, the spinal model could also be the cause of the less accurate response in the standard seat simulations. The T1 x-displacements of LAB, JARI and AZT simulations showed good to reasonable agreement compared to the experiments. The T1 z-displacements of the JARI and AZT simulation were reasonable, whereas the model showed too small T1 z-displacement for the LAB PMHS tests. A sudden increase of the T1 angles at about 180 ms for the LAB and JARI simulations was observed. Although this sudden increase is not seen in the experimental data used, it was observed in other experimental data with volunteers [102] and cadavers [31]. Summarizing, the T1 horizontal response is well predicted but the vertical displacement and rotations are not always realistic. Thus T1 provides only a reasonable input to the neck model.

The model response compared to the 12 g LAB and 4 g JARI experiments, both using rigid seats, showed reasonable to poor agreement with the experimental data (too large head motions). The simulations on the standard seat with head restraint (5 g AZT and 0.7 g UM) showed poor correspondence to the head kinematics of the volunteers. The head extension phase started too late, resulting in smaller backward rotations than was observed for the volunteers.

Validation data for vertebral rotations were only available for the LAB and JARI experiments. Both model simulations, LAB and JARI, showed that the vertebral rotations of the passive model were too large compared to the experimental response. This is in correspondence with the response for the head angle of both models.

Measuring vertebral rotations requires fixations into the vertebrae (only possible for PMHS) or high speed X-ray techniques. These measurements are technically difficult and therefore only few data on vertebral rotations were available.

It should be noted that the head kinematics reduced with reducing impact severity, i.e. head translations and rotations were much smaller for the low severity impacts than in the high severity test series. This trend was also seen for the simulations. These smaller motions make model validation more difficult, since absolute deviations for small head motions result in larger errors in terms of percentage compared to large head motions. The low severity impact tests (UM) indicated that modelling posture maintenance is necessary when studying low severity impacts or when the model would be used for studying human vibration in driving situations [58].

The forces and moments on the head were related to the head accelerations (see Section 5.1.3). Approximately the same deviations between model response and experimental response were seen for the accelerations and the loads on the head (OC loads). It should be noted that the OC loads shown are the net loads on the head joint, including the loads caused by the ligaments and the muscles. They do not reflect the real forces on the anatomical occipital condyles. The local forces will be discussed in Chapter 6.

The **second objective** of this chapter was to study the effect of the postmortem change of passive muscle properties on neck response in rear end impact. Therefore, the LAB simulations were not only performed with normal passive muscle stiffness properties, but also with a stiffer passive muscle function based on post-rigor PMHS tensile muscle properties [37]. The model response with stiffer passive muscles showed a reduction of the head motion, resulting in a closer agreement with the PMHS response, compared to the model with normal passive muscle stiffness. The vertebral rotations showed also a reduction due to the stiffer passive muscles. However, although the head rotation of the model with stiffer passive muscles showed good correspondence with the PMHS, the vertebral rotations of the mid neck were too large and the vertebral rotations of the lower and upper neck were too small. This illustrates that it is possible to obtain a good global model response but with limited accuracy in internal response. The assumption that the muscles of the PMHS were stiffer than for volunteers can be justified from the LAB experiments where the PMHSs were not preconditioned before testing, resulting in unrepeatable but stiffer response than live passive muscle response [37]. Although the PMHSs showed repeatable responses, nothing has been reported about preconditioning. The mechanical properties of the muscles vary significantly over the postmortem period [37]. Therefore, the preparation of the PMHS used in experiments should be documented, making it possible to adjust the model muscle tensile stiffness towards the condition of the PMHS. Substructure testing can provide additional confidence for instance testing without muscles to avoid the effect of tissue property changes.

To summarize, simulation results with a deformable standard car seat with head restraint correlated less than for a rigid seat. Simulation results showed good correspondence for the experimental T1 x-displacement, but the T1 z-displacement of the model was reasonable to poor (too small) compared to the experiments.

The model with stiff passive muscles showed a better response compared to the PMHS experiments than the model with normal passive muscles. For the volunteer simulations, the model with normal passive muscle behaviour showed much more neck extension than was seen in the experiments. In the following sections the influence of the initial seating posture and head restraint position (Section 5.3) as well as the influence of muscle activation (Section 5.4) is studied.

5.3   Parameter Study on Initial Posture and Head Restraint Position

The objective of this section (third objective of this chapter) is to study the influence of the initial seating posture and the head restraint positions for rear end impact simulations in a standard car seat. Postural variability has been studied for the AZT volunteer experiments using modelling techniques. The influence of the initial seating posture as well as of the vertical position of the head restraint is studied. Defining initial positions of the model is done in a similar way as described earlier (see Section 5.1.2). The human model is positioned just above the standard seat in three different positions. One position close to the head-restraint (P3), one with a large distance between head and head restraint (P1) and one in between (P2). In all three situations the model was allowed to sink into the seat to find equilibrium. The final initial positions of the model for the volunteer simulations are shown in Figure 5.19. The horizontal distance between head and head restraint (Δ x) and the T1 angle of the different initial postures are also presented in Figure 5.19. The final seating postures of the model and the AZT experiments were compared to a driver's posture predicted by RAMSIS. Posture P3 showed the best similarity with most experiments and with a posture predicted for this seat using RAMSIS version 3.4.1. RAMSIS predicts a posture of a driver, resulting in arm positioning on the steering wheel. The RAMSIS model showed a larger horizontal head to head restraint distance ($\Delta x = 7$ cm), which could be explained by simulating a driver sitting in a more observant posture than a passenger. However, the spinal posture of the RAMSIS model and the MADYMO P3 model were similar. Varying the initial posture as defined in this thesis results in varying the rearward offset of a head restraint. However, also a rearward offset of the thoracal spine with respect to the seat is created.

To study the influence of the vertical position of the head restraint as well as the absence of the head restraint additional simulations with a low head restraint (P3-lhd) as well as without head restraint (P3-nhd) were performed (see Figure 5.20).

The results of the initial posture variance are presented in Section 5.3.1. In Section 5.3.2 the results of the head restraint position variance are presented. The discussion and conclusions of this study are given in Section 5.3.3.

5.3.1   Results of Initial Posture Variance

The overall responses of two models are shown in Figure 5.21. The head neck kinematics for three different initial positions is presented in Figures 5.22 and 5.23.

(a) case P1: Δ x = 21 cm and T1 angle = 36.7 deg

(b) case P2: Δ x = 13 cm and T1 angle = 27.7 deg

(c) case P3: Δ x = 3 cm and T1 angle = 11.3 deg
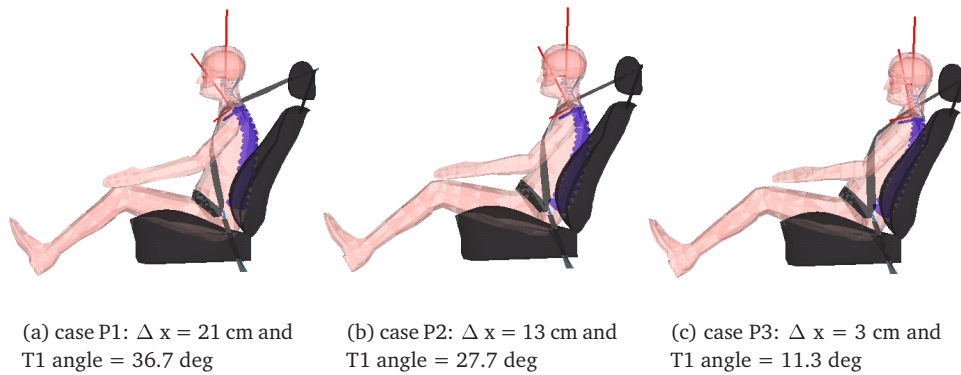
Figure 5.19: *Three different initial positions of the human body model in the standard seat (P1, P2, P3), Δ x = horizontal head to head restraint distance. The head is 2 degrees in extension with respect to the inertial space.*
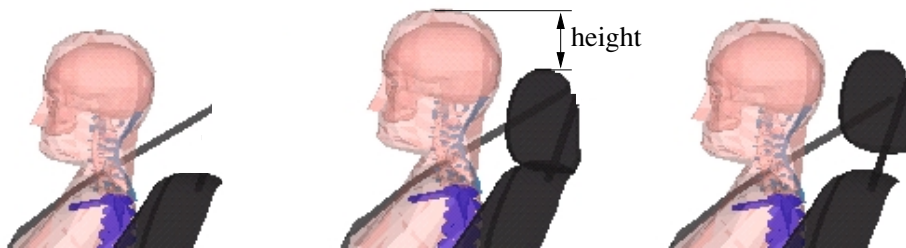

Figure 5.20: *Three different vertical positions of the head restraint for the standard seat. From left to right: no head restraint (P3-nhd), low head restraint (P3-lhd) and normal head restraint (P3-mhd).*

A large influence of posture is seen for all signals. Posture P3 shows the best agreement with the volunteer responses. The T1 motion for P1 and P2 is much larger than for P3, except for the T1 z-displacement, which is smaller. The sudden increase for the T1 angle at about 225 ms (Figure 5.22), becomes smaller for the model with the larger head restraint distance (P1).

For all three models the head translates during the first phase of the impact. Then the head rotates forward with respect to the sled. With respect to T1 the head rotates even more. This forward rotation is decreasing from P1 through P2 to P3 (Figure 5.23). The flexion phase is followed by an extension phase. For model P1 the head never reaches extension.

The head CG displacement with respect to T1 is also presented in Figure 5.23. The data is corrected for the initial position. The model response of P3 is closest to the volunteer response compared to the other initial positions. The CG displacement is the largest for P1, the model in the most forward seating position.

The acceleration of the head is presented in Figure 5.24. The head x-acceleration of model P3 shows reasonable agreement compared to the volunteer envelope. The increase in the CG x-acceleration (showing the head contact with the head restraint) occurs later from model P3 through P2 to P1. The peak of the acceleration for model P3 shows good agreement with the volunteer responses. Model P1 shows a smaller peak, however the peak acceleration of model P2 exceeds twice the experimental results. The head z-acceleration and the head angular acceleration show poor correlation with the volunteer responses.

The resultant external force on the head by the head restraint is also presented in Figure 5.24. It is seen that for P3 the head contact occurs too early, while the head contact for P1 is too late compared to the volunteers response. The time of head contact for posture P2 agrees well with the volunteer response, however the peak force for P2 is too large. The peak forces of model P3 and P1 are closer to the volunteer response, however, still being too large.

| 0 ms | 80 ms | 100 ms | 120 ms | 140 ms | 160 ms | 180 ms | 200 ms |

| 0 ms | 80 ms | 100 ms | 120 ms | 140 ms | 160 ms | 180 ms | 200 ms |
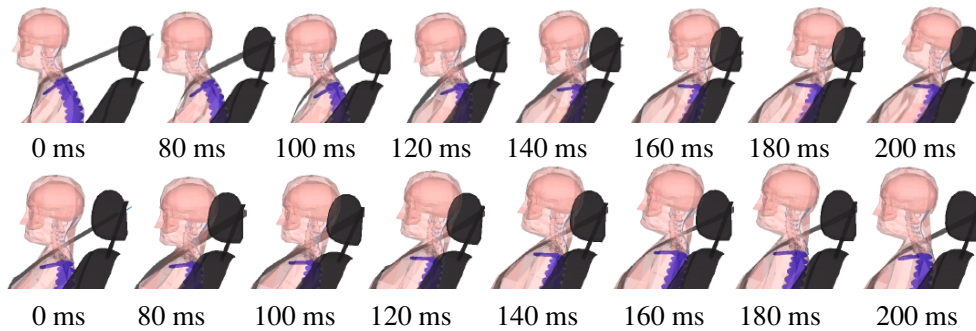
Figure 5.21: *Varying initial posture and head restraint position. Above P1, below P3, both with head restraint in normal position. Kinematics of the human body model at successive times.*

Figure 5.22: *T1 kinematics with respect to sled versus time. Simulated response to 5g rear end impact of the neck model with variance in initial posture (P1, P2, P3), passive muscle behaviour (pas) and head restraint position normal (mhd) compared to AZT volunteer response.*

Figure 5.23: *Head kinematics versus time. Simulated response to 5g rear end impact of the neck model with variance in initial posture (P1, P2, P3), passive muscle behaviour (pas) and head restraint position normal (mhd) compared to AZT volunteer response.*

Figure 5.24: *Head accelerations and external head force versus time. Simulated response to 5g rear end impact of the neck model with variance in initial posture (P1, P2, P3), passive muscle behaviour (pas) and head restraint position normal (mhd) compared to AZT volunteer response.*

5.3.2   Results of Head Restraint Position Variance

The head neck kinematics for varying head restraint position (mhd= normal, lhd= low, nhd= no head restraint) is presented in Figures 5.25 to 5.27. A large difference is seen for the cases with head restraint (P3-mhd and P3-lhd) and the one without head restraint (P3-nhd). Case P3-lhd shows the best correlation compared to the volunteer responses. Although the T1 kinematics is hardly influenced by varying the head restraint height, when simulating an impact without head restraint the T1 x-displacement and T1 angle show larger motions (Figure 5.25). The head motion is strongly reduced by placing a head restraint (mhd and lhd versus nhd). This reduction is stronger for the normal placed head restraint (mhd) compared to the lower head restraint (lhd) (see Figure 5.26). The varying head restraint position hardly influences the head acceleration and head contact force (see Figure 5.27), but the head x-accelerations are much smaller in cases where no head contact occurred (nhd compared to lhd and mhd). On the other hand, the head angular accelerations increase when the head restraint is removed. The highest head restraint position caused the highest resultant external head force (see Figure 5.27). As was mentioned earlier (see Section 5.3.1) the head contact for posture P3 occurs too early compared to the volunteers data.

5.3.3   Discussion Posture and Head Restraint Variance

The third objective of this chapter, and the objective of this section (5.3) was to study the influence of the initial seating posture and the head restraint positions for rear end impact simulations in a standard car seat. Preliminary simulation results on posture and head restraint variance were presented at the ESV conference [60]. The posture prediction model of the software RAMSIS predicted one initial seating posture, which corresponds with posture P3 of the model, however in reality the seating postures of drivers and their passengers show a large variability [116]. The three simulated cases (P1, P2, P3) represent three realistic initial seating postures. The model response showed larger variability due to posture variation than the experimental response, however the range of postures of the simulations was larger compared to the differences in initial seating posture of the volunteers in the AZT experiments (based on photos). It should be noted that visually case P3 corresponds best with most of the volunteer experiments. However, an objective way of measuring human postures and comparing it to simulated postures was not available for these experiments.

The results from the posture variance simulations supported the statement made in literature [2, 116, 126] that posture variation has major effects on T1 and head response. The increasing displacement and rotation of T1 from P3 through P2 to P1 is caused by the fact that the model is sitting more bent forward (P1), having more space between the back and the seat, resulting in larger displacements. The larger T1 z-displacement for P3 can be explained by the interaction of the back and the seat back occurring earlier, resulting in an upward movement of the body. Head contact occurred first for model P3, being closest to the head restraint at the start. This
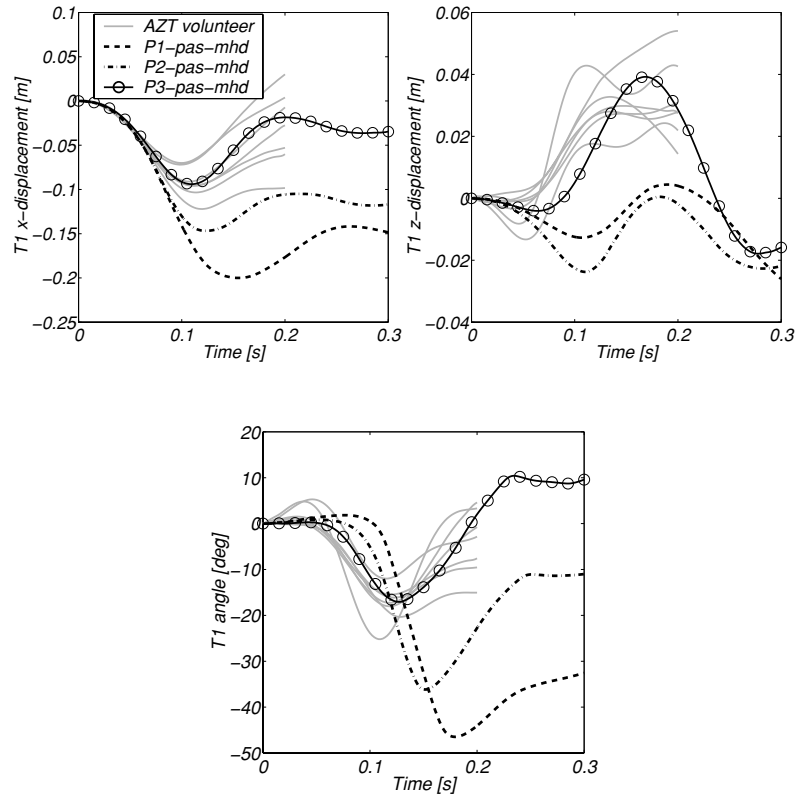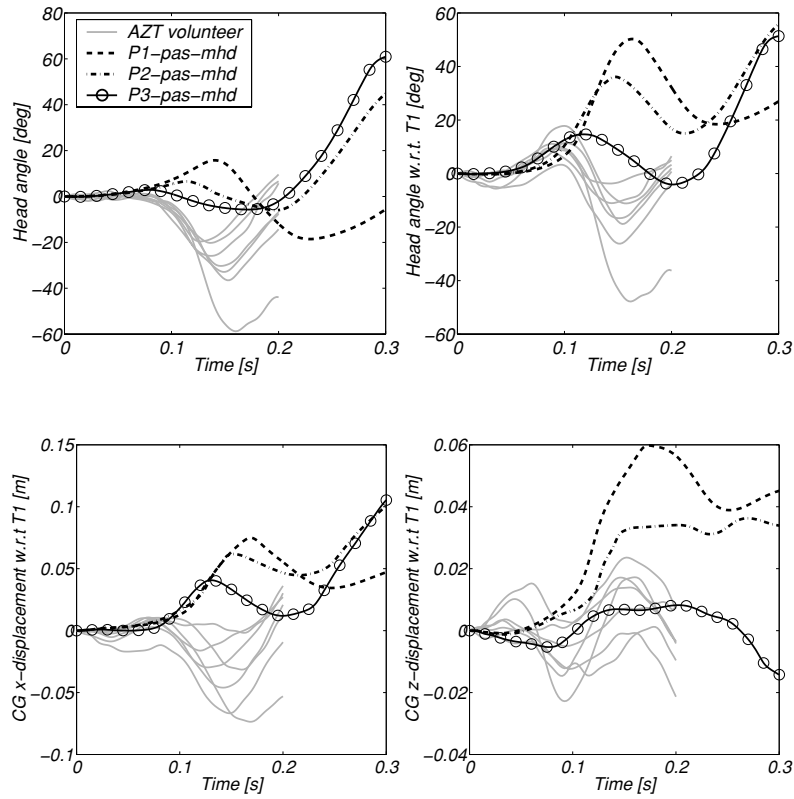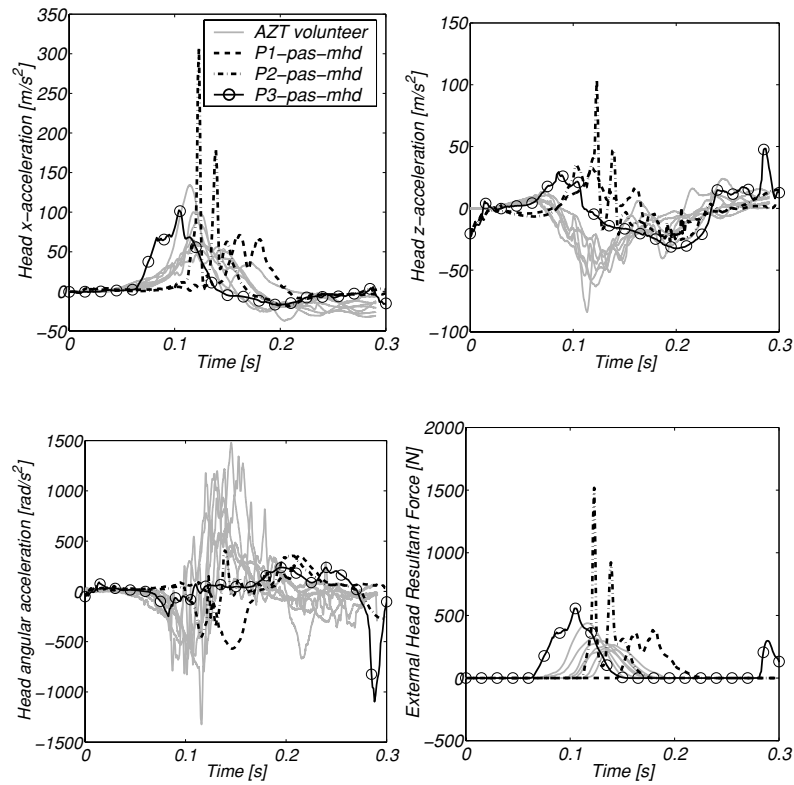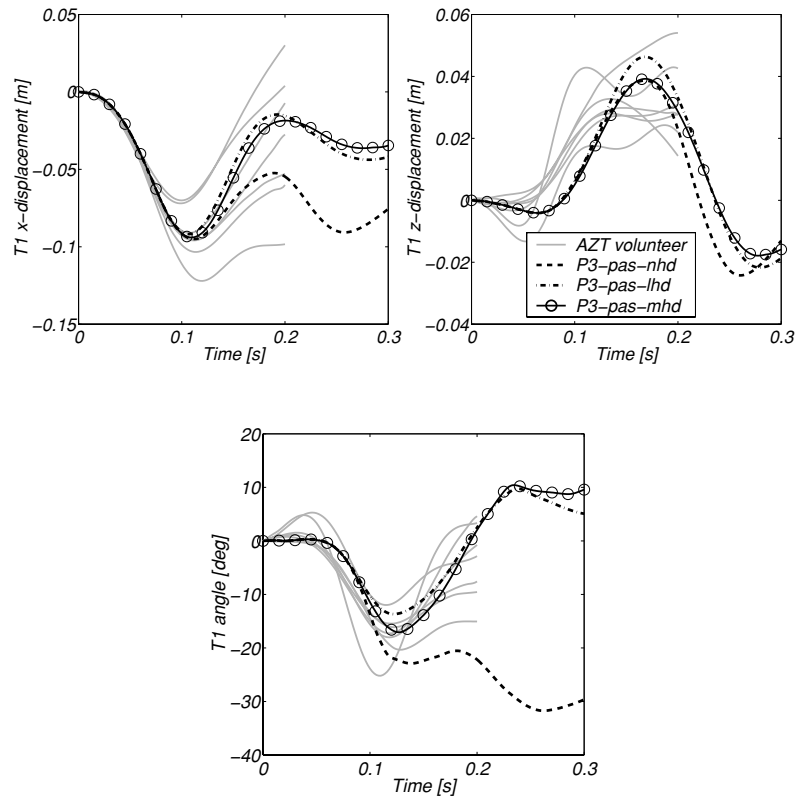
Figure 5.25: *T1 kinematics with respect to sled versus time. Simulated response to 5g rear end impact of the neck model with passive muscle behaviour, position P3, variance in vertical head restraint distance (mhd= normal, lhd= low, nhd= no head restraint) compared to AZT volunteer response.*

Figure 5.26: *Head kinematics versus time. Simulated response to 5g rear end impact of the neck model with passive muscle behaviour, position P3, variance in vertical head restraint distance (mhd= normal, lhd= low, nhd= no head restraint) compared to AZT volunteer response.*

Figure 5.27: *Head accelerations and external head force versus time. Simulated response to 5g rear end impact of the neck model with passive muscle behaviour, position P3, variance in vertical head restraint distance (mhd= normal, lhd= low, nhd= no head restraint) compared to AZT volunteer response.*
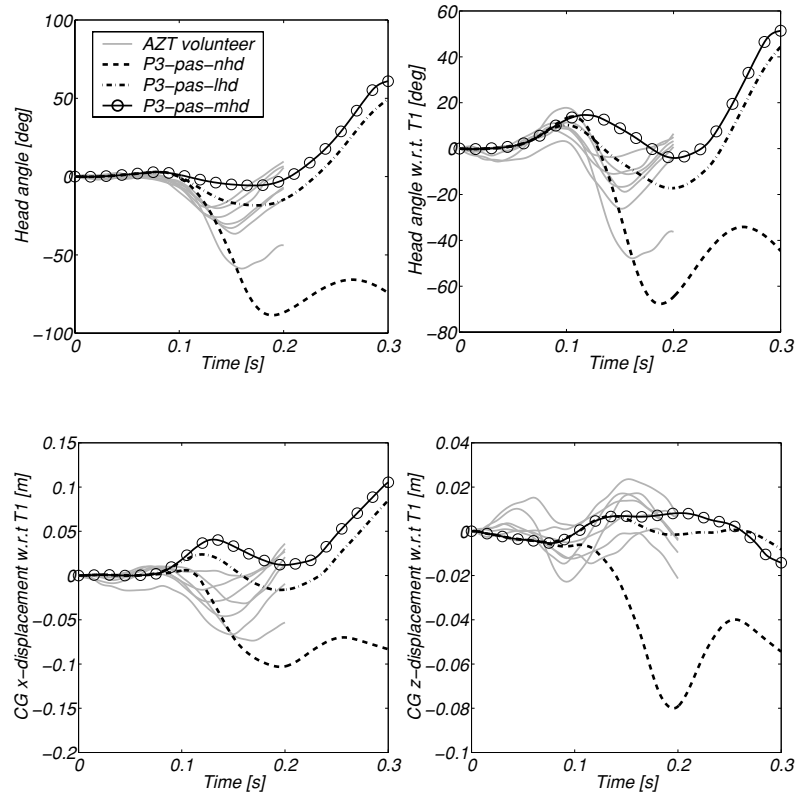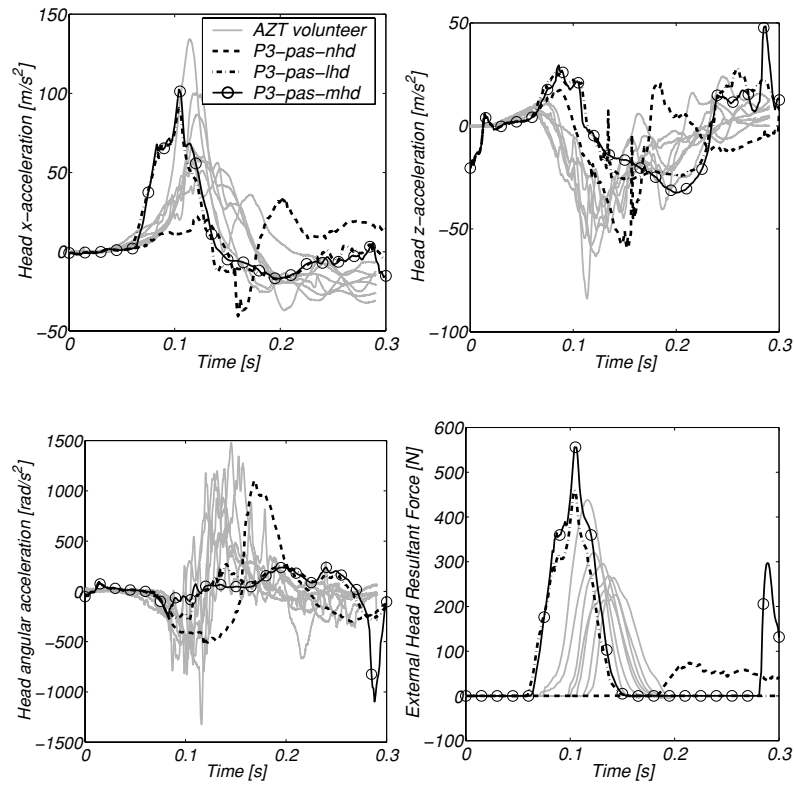
contact resulted in the smallest forward head displacement for P3 in the first phase. Then the head rotated backwards, resulting in backward translation with respect to T1. Since this rotation started late for model P1 the head never reached extension. The model P3 started earlier with rotation, but the rotation was limited by the head restraint, ending in head flexion.

The effect of head restraint height is relatively small for the AZT simulations. However, removing the head restraint showed much larger head and T1 motions compared to the response with head restraint. Lowering the head restraint showed better correspondence with volunteer response for the head rotation, but still the backward rotation was too slow. The difference in head kinematics at varying head restraint positions was caused by the variation of contact point resulting from the variance in vertical height. The lower the contact point with respect to the centre of gravity, the larger the head extension will be.

It has to be remarked that in the test with head restraint, head translations and rotations were much smaller than in the test series without head restraint, this trend was also seen for the simulations. These smaller motions makes model validation more difficult, since absolute deviations for small head motions result in larger errors in terms of percentage compared to large head motions.

The initial position of the subject had more influence on the external force on the head by the head restraint, than the vertical position of the head restraint. It should be noted that the forces occuring after about 200 ms in the simulations were caused by head chest contact, or in case no head restraint was present by contact between seatback and head-neck system. Although the timing of head contact of case P2 showed the best correspondence with the volunteer responses, the head and T1 kinematics of case P3 showed better correlation than P2. The high values in the acceleration signal and the external head force for case P2 were probably caused by the implemented contact definition. Therefore, these results are not further taken into account. Case P3 showed better correlation with the volunteer response than case P2, although the head contact occurred too early compared to the volunteers.

In accordance with other studies (see review by Szabo [140]) it was shown by mathematical modelling that seating in an upright position together with a head restraint adjusted in line with the top of the head reduced the head motion compared to a more forward seating position and a low head restraint. Since initial seating position, and to a lesser degree the head restraint position, do significantly influence the head-neck kinematics, objective measurements of these parameters are needed to generate correct input for model validation.

5.4   Parameter Study on Muscle Behaviour

The objective of this section (fourth objective of this chapter) is to study the role of muscle behaviour (passive and active) in rear end impact. To what extent muscles influence the head and neck response depends, among other things, on:

- the onset of muscle activation (trigger time + reflex delay)

- the level of muscle activation

- the activation scheme (co-contraction of muscles)

In impact conditions, activation of neck muscles can be triggered by sensory information from the movement system for instance from T1 or pelvis acceleration. Also the muscles could be triggered before the impact takes place by an auditive or visual external signal, e.g. hearing the sound of an emergency break, seeing a car approaching in the back mirror. Neck muscle activation due to sensory information from the movement system (reflex) will have a delay in the range from 10-120 ms [24, 47, 127, 130, 143] (see also see review by Siegmund and Brault [134] and Appendix E).

The methods for the parameter study on muscle activation is described below. The results are presented in Section 5.4.1, whereas in Section 5.4.2 the discussion is presented.

To study the influence of the onset and level of muscle activation as well as the activation scheme simulations according to the matrix mentioned in Table 5.3 are performed. In Chapter 4 the influence of muscle activation as well as the role of passive pre-stress of the muscles has been studied for a frontal impact. The same variations are repeated here to study the influence of passive pre-stress and active muscle force on a rear end impact:

Case A: Role of passive pre-stress of muscles, without muscle activation.

Case B: Role of passive pre-stress of muscles, with muscle activation.

Case C: Role of maximum activation level, all muscles activated.

Case D: Role of reflex delay, all muscles activated.

Additional variations are performed to study the role of initial muscle activation and the different activation schemes during the impact (= co-contraction).

Case U,V,W: Role of initial muscle activation, activation level and activation scheme.

Case U-EXP: Role of activation level and activation scheme.

The simulation matrix for the above mentioned cases is presented in Table 5.3. Cases A-D and U-W simulate a 5g rear end impact with a standard car seat without head restraint (same seat characteristics as used for AZT tests). No experimental data is available on these simulations.

For simplicity, the muscles in the model are not activated separately, but as three groups (flexors, extensors and sternocleidomastoid). Initial muscle activation could

be present due to awareness of the impact, leading to stiffening of the neck. Isometric muscle contraction (see Section 2.2.7) has been simulated to estimate the ratio of muscle activities of the three groups mentioned above to obtain a stationary head position in case of initial muscle co-activation.
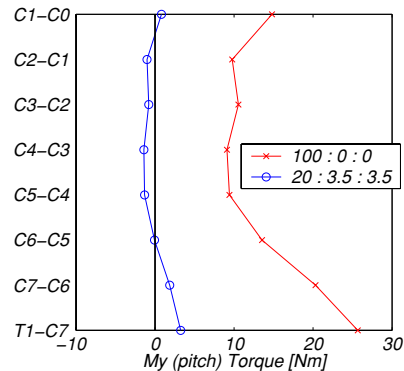
Figure 5.28: *Isometric muscle contraction. Flexor 100% activation and sternocleidomastoid and extensors passive (100 : 0: 0) compared to flexor 20% activation and sternocleidomastoid and extensors 3.5 % activation (20 : 3.5: 3.5).*

Figure 5.28 shows the static neck moment in all joints. Since the muscles are not activated separately, it is not possible to reach zero moment (equilibrium) for the neck system exactly. However, with the ratio 20: 3.5: 3.5 for respectively flexor: extensor: sternocleidomastoid the moments are close to zero and an equilibrium of the head is approximated. Since it is not known how much the muscles will be activated in the initial phase, three conditions are simulated (0%, 20% and 40% initial muscle activation for the flexors, with corresponding initial co-activation for extensors and sternocleidomastoid, case U1, V1, W1). Also simulations are performed in which the muscles are initially activated according to this ratio and where the maximum muscle activation varied between 25% and 100% (U,V,W).

Case U-EXP-JARI is a simulation of the JARI experiments (4g rigid seat without head restraint) and case U-EXP-AZT is a simulation of the AZT experiments (5g standard seat with low head restraint and posture P3), both with varying muscle co-activation.

5.4.1   Results of Parameter Study on Muscle Behaviour

Cases A-D and U-W are not simulating experiments, whereas case U-EXP simulates the JARI and AZT experiments (see Table 5.3). Figure 5.29 shows that varying passive muscle pre-stress hardly influences the passive and active model response. Figure 5.29(a) shows that the initial head flexion is slightly influenced showing a decrease of the head flexion with increasing pre-stress for the passive model. Although no visible influence on the maximum head extension angle is seen, the maximum value is reached slightly earlier when the pre-stress increases. For the active model the head

Table 5.3: *Varying muscle conditions Case A: Role of passive pre-stress muscles, without muscle activation, Case B: Role of passive pre-stress muscles, with muscle activation, Case C: Role of maximum activation level, all muscles activated, Case D: Role of reflex delay, all muscles activated, Case U,V,W: Role of initial muscle activation, activation level and activation scheme, Case U-EXP: Role of maximum activation level and activation scheme.*

case	seat [@]	pre stress [#]	reflex delay t_{reflex}	muscle activation level initial			maximum		
			[ms]	flex* [%]	ext+ [%]	sterno° [%]	flex* [%]	ext+ [%]	sterno° [%]
A1	S	-	-	0	0	0	0	0	0
A2[a]	S	+	-	0	0	0	0	0	0
A3	S	++	-	0	0	0	0	0	0
B1	S	-	25	0	0	0	100	100	100
B2[b]	S	+	25	0	0	0	100	100	100
B3	S	++	25	0	0	0	100	100	100
C1[a]	S	+	-	0	0	0	0	0	0
C2	S	+	25	0	0	0	25	25	25
C3	S	+	25	0	0	0	50	50	50
C4[b]	S	+	25	0	0	0	100	100	100
D1	S	+	0	0	0	0	100	100	100
D2	S	+	15	0	0	0	100	100	100
D3[b]	S	+	25	0	0	0	100	100	100
D4	S	+	50	0	0	0	100	100	100
U1	S	+	-	0	0	0	0	0	0
U2	S	+	25	0	0	0	50	0	25
U3	S	+	25	0	0	0	100	0	50
U4	S	+	25	0	0	0	100	50	50
U5	S	+	25	0	0	0	100	100	100
V1	S	+	25	20	3.5	3.5	20	3.5	3.5
V2	S	+	25	20	3.5	3.5	50	3.5	25
V3	S	+	25	20	3.5	3.5	100	3.5	50
V4	S	+	25	20	3.5	3.5	100	50	50
V5	S	+	25	20	3.5	3.5	100	100	100
W1	S	+	25	40	7	7	40	7	7
W2	S	+	25	40	7	7	50	7	25
W3	S	+	25	40	7	7	100	7	50
W4	S	+	25	40	7	7	100	50	50
W5	S	+	25	40	7	7	100	100	100
U1-EXP-JARI	R	+	-	0	0	0	0	0	0
U2-EXP-JARI	R	+	25	0	0	0	50	0	25
U3-EXP-JARI	R	+	25	0	0	0	100	0	50
U4-EXP-JARI	R	+	25	0	0	0	100	50	50
U5-EXP-JARI	R	+	25	0	0	0	100	100	100
U1-EXP-AZT	Shr	+	-	0	0	0	0	0	0
U2-EXP-AZT	Shr	+	25	0	0	0	50	0	25
U3-EXP-AZT	Shr	+	25	0	0	0	100	0	50
U4-EXP-AZT	Shr	+	25	0	0	0	100	50	50
U5-EXP-AZT	Shr	+	25	0	0	0	100	100	100

[@] R = rigid seat, S = standard seat, Shr = standard seat with low head restraint
[#] - : $\frac{s_{ref}}{s_{free}} = 1$ [65]; + : $\frac{s_{ref}}{s_{free}} = 2.8/2.45$; ++ : $\frac{s_{ref}}{s_{free}} = 2.8/2.1$ [17], see also Section 2.2.7
* all flexor muscles   + all extensor muscles   ° sternocleidomastoid
[a] standard passive: case A2, C1 are the same   [b] standard active: case B2, C4, D3 are the same

flexion initially increases when the pre-stress increases, but again no visible influence on the maximum head extension angle is seen when the passive pre-stress is increased (see Figure 5.29(b)).
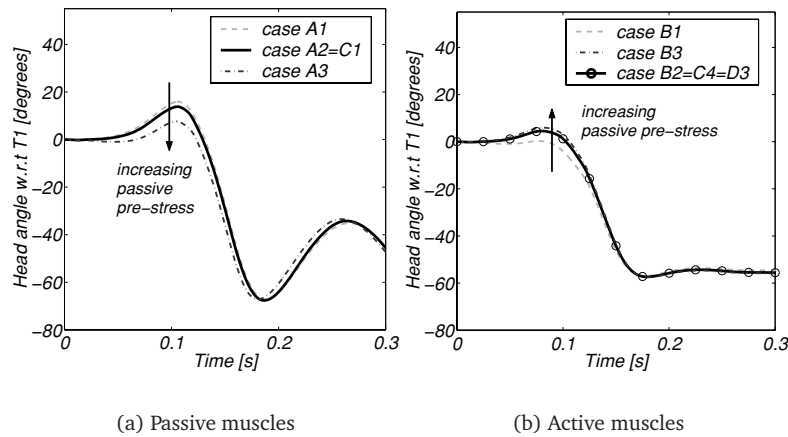

(a) Passive muscles   (b) Active muscles

Figure 5.29: *Head angle at varying passive pre-stress (increasing with A1, A2 to A3 and B1,B2 to B3) for a 5g rear end impact simulation (standard seat without head restraint, see Table 5.3).*

Varying the initial muscle activation shows a larger influence compared to varying the passive pre-stress. Independent of the co-contraction scheme an increase of initial activation shows a decrease in the maximum head angle. This influence is largest when the maximum muscle activation is the same as the initial muscle activation (case 1). For 40 % initial muscle activation about 25 % reduction of the head extension angle is observed (case 1, see Figure 5.30). The reader is referred to Appendix C for the results of the other initial muscle activation variations (UVW 1-5).

The influence of varying the reflex induced muscle activation during impact is presented in Figure 5.31. The initial head flexion and the maximum head extension angle reduces with a higher activation level (see Figure 5.31(a)). Additionally, the shape of the curve changes with varying activation level. Results of varying reflex delay time are presented in Figure 5.31(b). The initial head flexion decreases with decreasing reflex time, but the maximum head extension angle does not change.

The JARI simulations (rigid seat without head restraint, 4g) are performed also with varying level of muscle activation and varying activation scheme (cases U-EXP-JARI, see Figure 5.32). The results are compared to the passive model response (U1-EXP) and the volunteer response. The passive model response (U1-EXP) shows head angle response exceeding the volunteer envelope. With 50% flexor activation (U2-EXP) a realistic reduction of the head rotation is obtained. With 100% flexor activation (U3-EXP) the head rotation is reduced further and an unrealistic response is obtained. After 250 ms the neck is even forced into flexion due to the assumed continued flexor
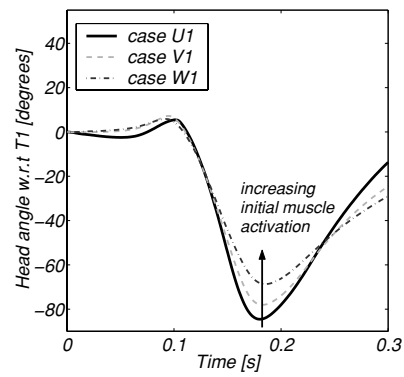
Figure 5.30: *Head angle at varying initial muscle activation conditions (increasing initial muscle activation with U1, V1 to W1) for a 5g rear end impact simulation (standard seat without head restraint, see Table 5.3). Other results are presented in Figure C.4.*

(a) Varying activation level

(b) Varying reflex delay

Figure 5.31: *Head angle at varying muscle conditions (increasing activation level with C1, C2, C3 to C4 and increasing reflex delay with D1, D2, D3 to D4) for a 5g rear end impact simulation (standard seat without head restraint) (see Table 5.3).*

activity. In case all muscles are 100% active the head extension angle becomes too large compared to most volunteers. In this case the extensors, due to their stronger moment generation capability, force the neck into extension. With 100% flexor and 50% extensor co-contraction (U4-EXP) a realistic response is found. This response is presented in Figures 5.33 to 5.36 together with the response for the passive model (U1-EXP) and the volunteer response.

The T1 response is hardly influenced by muscle activation (see Figure 5.33). The head angle and head displacement are reduced by muscle activation (see Figure 5.34. A better correspondence with the volunteer data is seen for the active model (U4) than for the passive model (U1), except for the x-displacement of the head. The reduction caused by muscle activation is too large, resulting in a smaller x-displacement of the head for the active model (U4) compared to the volunteers. In Figure 5.35 the head accelerations are presented. Again, the reduction by the muscle forces is cleary seen for the active model (U4) compared to the passive model (U1), resulting in better agreement with the volunteer data. Also the vertebral rotations show the reduced motion (see Figure 5.36). Although, the active model vertebral rotations are still too large compared to the experimental data of one volunteer.
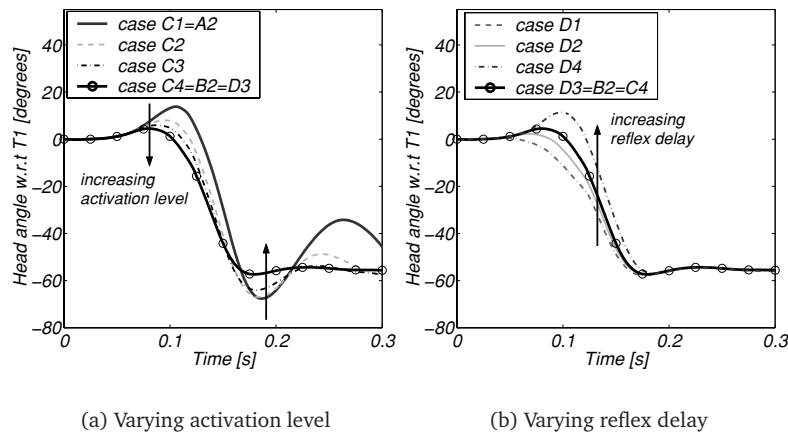

Figure 5.32: *Head angle at varying maximum muscle activation conditions for JARI simulaton (rigid seat without head restraint, 4g rear end impact, see Table 5.3).*

In Figure 5.37 the results are presented for varying muscle activation in a rear end impact using a standard seat with head restraint (AZT). Activating the flexor muscles and the sternocleidomastoid results in head flexion (U2-EXP and U3-EXP), while additional activation of the extensors shows an increase of head extension (U4-EXP and U5-EXP) compared to the passive model (U1-EXP). The best correspondence for the simulations with muscle activation is seen with 100% activation for the flexor muscles and a 50% co-contraction. This trend was also seen for the JARI simulations. In appendix C the kinematics of T1 and the head are presented for the active and passive model simulating the AZT experiments. In general, it is seen that activating the muscles in case of simulating a rear end impact in a standard seat with head restraint has a somewhat smaller effect as compared to the JARI case without head
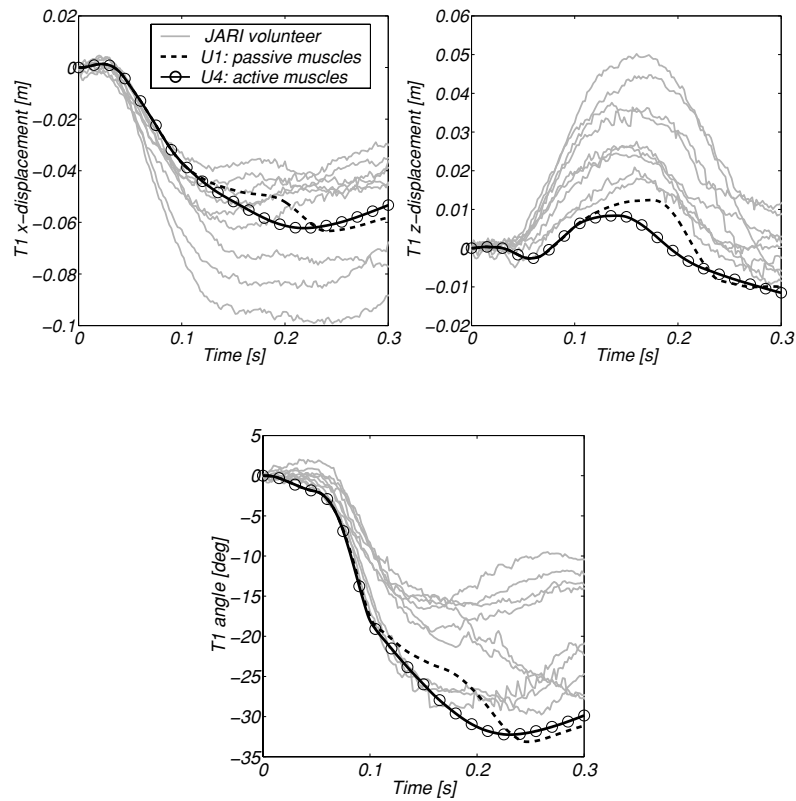
Figure 5.33: *T1 kinematics with respect to sled versus time. Simulated response to 4g rear end impact of the neck model with passive and active muscle behaviour compared to JARI volunteer response.*
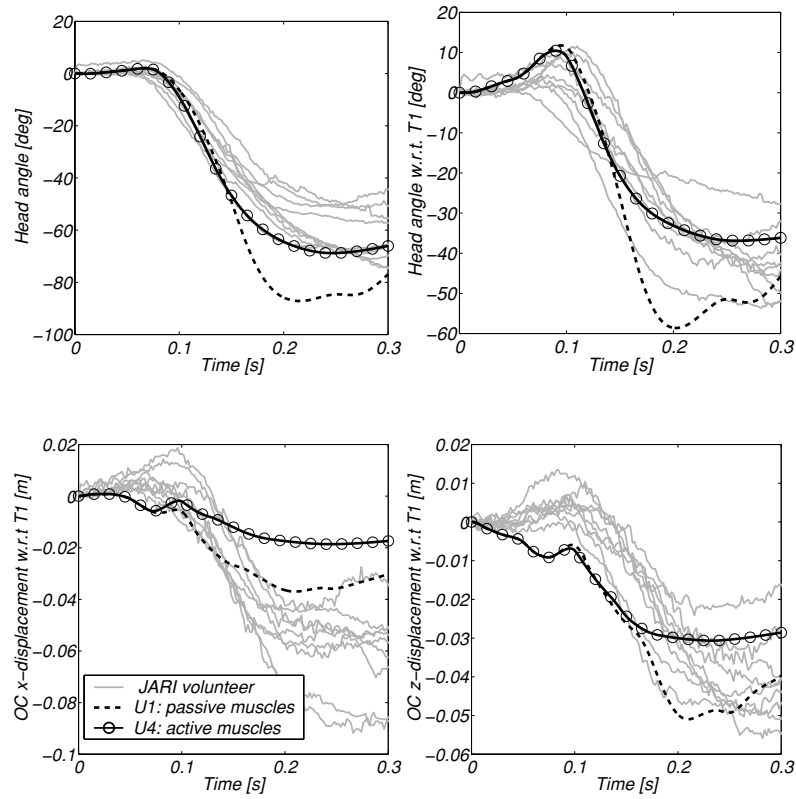
Figure 5.34: *Head kinematics versus time. Simulated response to 4g rear end impact of the neck model with passive and active muscle behaviour compared to JARI volunteer response.*

Figure 5.35: *Head accelerations versus time (head z-acceleration not available). Simulated response to 4g rear end impact of the neck model with passive and active muscle behaviour compared to JARI volunteer response.*

Figure 5.36: *Peak vertebral extension rotations. Simulated response to 4g rear end impact of the neck model with passive and active muscle behaviour compared to JARI volunteer response.*

restraint. However, for the standard seat with head restraint simulations neither the passive model nor the models with varying muscle activation provide a very good correlation with the volunteer experiment.
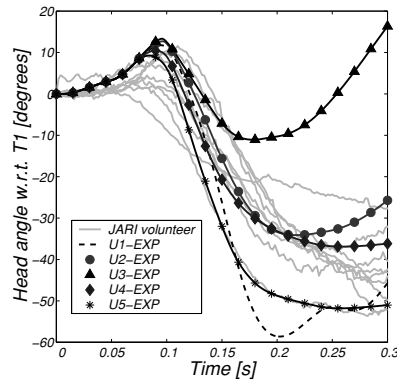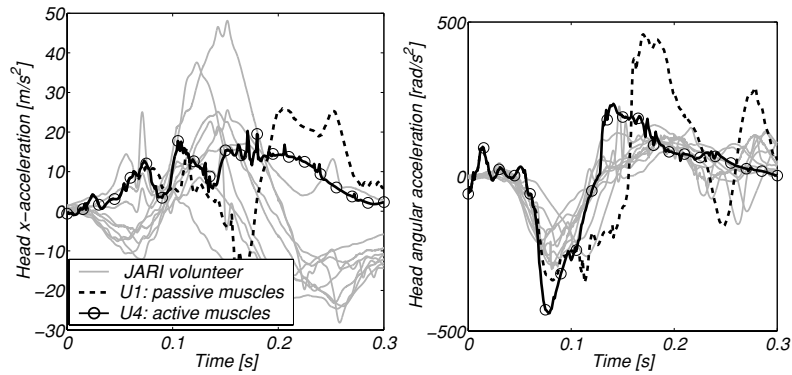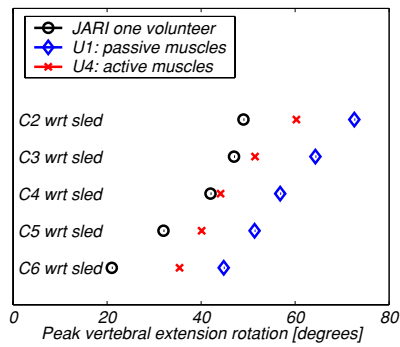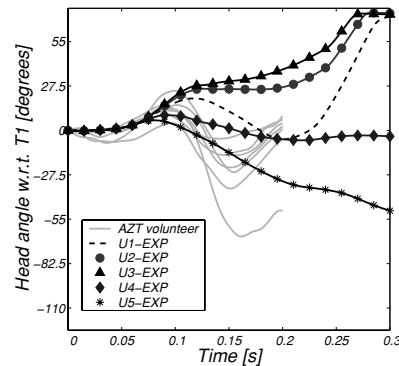

Figure 5.37: *Head angle at varying maximum muscle activation conditions for AZT simulation (standard seat with low head restraint, 5g rear end impact simulation, see Table 5.3).*

5.4.2   Discussion Muscle Parameter Study

The objective of this section (fourth objective of this chapter) was to study the role of muscle behaviour (passive and active) in rear end impact. Simulations with varying muscle parameters (see Section 5.4) showed that in agreement with experimental findings [134] and results from Chapter 4 muscles were capable of generating forces which could alter head-neck kinematics in a rear end impact.

Contrary to the results of Section 4.3 (frontal and lateral loading) the variations of passive pre-stress hardly influence the model response (with passive muscles) for rear end impact. A larger absolute head angle occurred for the high severity frontal impact (see Section 4.3) compared to the rear end impact simulations. Passive pre-stress of the muscles caused an increase of the stiffness of the neck. This resulted in large passive forces for the extensor muscles, which were able to reduce the flexion head angle. The increase in stiffness of the flexor muscles (weaker than the extensor muscles), was too small to reduce the head extension during the rear end impact.

Simulations of the model in a standard seat showed that the head angle could be reduced by varying the activation level, or varying the co-contraction scheme. Varying the reflex delay up to 50 ms hardly influenced the maximum head angle (see Figure 5.31(b)). Varying the activation level, but having the same activation scheme for all muscles, showed only limited effect on the extreme head angle (see Figure 5.31(a)). This is in contrast with the findings for the frontal impact simulations (Chapter 4). Because the extensors dominate the flexors (PCSA and muscle force line of action), the initial flexion of the head with respect to T1 will be reduced by reducing the

activation time or increasing the activation level. Initial muscle activation caused a stiffer neck reducing the head angle. This was seen independent of which muscles were activated. Experimentally (see Appendix E), when the volunteers initially activated their neck muscles also a head angle reduction (about 30 %) was observed, compared to the response of relaxed volunteers.

With the current neck model case U4 (reflex delay of 25 ms, 100% activation of flexor muscles and 50 % activation of extensor muscles and sternocleidomastoid) showed the best correspondence with the JARI experiments. For the AZT simulations both the passive model and U4 active model showed reasonable to poor correspondence with the volunteer response. During the first 200 ms the passive model seemed to show a better fit. However, during the rebound the head motions of the passive model seemed to become too large, while the response of the active model was reduced by muscle activation. Although, the experimental data were not analysed after 200 ms, it was not expected that the head motions should become so large.

In general, it was seen that activating the muscles showed a better result than the passive model for volunteer simulations using a rigid seat without head restraint. Whereas, in case of simulating a rear end impact using a standard seat with head restraint either a better or worse agreement with the volunteer response was seen.

The influence of active muscle forces on head neck kinematics depends on the moment they occur (which phase of the motion), the level of activation, and the muscle group in which these forces occur (co-contraction). Experimental data of these parameters are needed as model input, when simulating human response in impact. A number of studies simulating rear end collisions have been conducted to measure the neck muscle response of human subjects exposed to whiplash loading [14–16, 43, 105, 141]. However, publications on the level of muscle activation and which muscles are active in a rear end impact are rare [134].

Although not shown conclusively by experimental research, the combined findings of numerical modelling and experimental research presented in literature indicate that neck muscles (also when initially relaxed) could alter the head and neck kinematics during a rear end impact. Reflex time, activation level and the co-contraction of the muscles will influence the head and neck motion.

5.5   Discussion Model Response Rear End Impact

The **first objective** of this chapter was to further enhance the model validation towards rear end impacts. To simulate these impacts, the neck model as presented in Chapter 2 is included in a human body model. The validation of the total model ranged from high severe rear end impact (12 g) for Post Mortem Human Subject (PMHS) experiments to mid (4-5 g) and low severe impact (0.7 g) for volunteer experiments. Rigid seats were used for LAB PMHS and JARI volunteer tests, while a standard seat with head restraint was used for the AZT and UM volunteer experiments. It should be noted that the head kinematics reduced with reducing impact severity, i.e. head translations and rotations were much smaller for the low severity impacts than in the high severity test series. This trend was also seen

for the simulations. These smaller motions make model validation more difficult, since absolute deviations for small head motions result in larger errors in terms of percentage compared to large head motions.

The simulated head neck response was influenced not only by the neck model, but also by the spine model as well as by the seat model. Thus validation studies as performed in this chapter, included validation of the seat model as well as of the spine and neck model.

To summarize, the T1 horizontal response is well predicted but the vertical displacements and rotations are not always realistic. Thus T1 provides only reasonable input to the neck model. The passive model response compared to the 12 g LAB and 4 g JARI experiments, both using rigid seats, showed reasonable to poor agreement with the experimental data (too large head motions). The simulations of the passive model on the standard seat with head restraint (5 g AZT and 0.7 g UM) showed poor correspondence to the head kinematics of the volunteers. The head extension phase of the model started too late, resulting in smaller backward rotations than was observed for the volunteers. The low severity (0.7 g) UM tests indicated that modelling posture maintenance is necessary when studying low severity impacts or when the model would be used for studying human vibration in driving situations.

The **second objective** was to study the effect of the postmortem change of passive muscle properties on neck response in rear end impact. Therefore, the LAB simulations were not only performed with normal passive muscle stiffness properties, but also with a stiffer passive muscle function based on post-rigor PMHS tensile muscle properties [37]. The model response with stiffer passive muscles showed a reduction of the head motion, resulting in a closer agreement with the PMHS response, compared to the model with normal passive muscle stiffness.

The study of the influence of the initial posture and the head restraint position was the **third objective**. Simulations of a 5g rear end impact on a standard car seat with and without head restraint were performed. Varying the initial posture showed larger influence on the T1 and head kinematics than varying the vertical height of the head restraint. In accordance with other studies (see review by Szabo [140]) it was shown by modelling that seating in an upright position together with a head restraint adjusted in line with the top of the head reduced the head motion compared to a more forward seating position and a low head restraint. Since initial seating position, and to a lesser degree the head restraint position do significantly influence the head-neck kinematics, objective measurements of these parameters are needed to generate correct input for model validation.

The **fourth objective** of this chapter was to study the role of active and passive muscle behaviour in rear end impact. Muscle activation provides a reduction of the head motion compared to the passive model and seems to be necessary in describing a better model response for the volunteer experiments on a rigid seat without head restraint (JARI). This is in agreement with the conclusions on frontal and lateral impact simulations in Chapter 4. However, for the rear end impact simulations with a standard seat with head restraint, both the passive and active model showed reasonable to poor correlation with the volunteer data. It is unlikely that the AZT volunteers did not show any active muscle behaviour, while the JARI volunteers did.

However, in both cases these activation signals were not measured or not available. Although not shown conclusively by experimental research, the combined findings of numerical modelling and experimental research presented in literature indicate that neck muscles (also when initially relaxed) can alter the head and neck kinematics during a rear and impact. Reflex time, activation level and the co-contraction of the muscles will influence the head and neck motion.

Up till now most models presented in literature focus on one or two impact directions, not including rear end impacts [20, 28, 96]. Although the models by Yang [174] and Bertholon [7] were validated for rear end impact, these models lack the possibility to simulate different initial seating postures. Additionally, all these models did not include active muscle behaviour. In summary, important benefits of the applicability of the new model compared to other models are the extended validation and the possibility to simulate muscle activation. In principle, the model could be used for studying injury mechanisms because deformation and loads of the individual soft tissues can be assessed (see Chapter 6). Recommendations for further model validation are presented in Chapter 7.

Chapter 6

Injury Criteria and Tissue Loads

Injury criteria currently used in automotive test regulations are mostly based on global parameters like the net loads in the neck or the displacement of the chest [150]. These criteria are mostly defined for high severity impacts, and therefore usually for injuries of AIS type III and higher. In contrast, Whiplash Associated Disorders (WADs) are AIS type I injuries. Therefore, recently, several global injury criteria especially for WADs have been proposed in the literature [40, 92, 115, 129]. However, like all neck injuries, WADs are assumed to be caused by local tissue loads, e.g. ligament forces or facet joint contact forces. The relation between the local tissue loads and the global injury criteria, however, is not known. Since local tissue loads are difficult to measure, numerical modelling can be a useful tool to study this relationship.

The detailed neck model presented in Chapter 2 is able to predict global as well as local loads. The model has been validated in Chapters 3 to 5 for quasi-static loads as well as frontal, lateral and rear end impact loading using global performance criteria, i.e. head displacements, rotations, accelerations and neck loads. Also a limited validation of the vertebral rotations for the rear end impact was presented. The model response showed that muscle activation and initial posture and head restraint position did influence the global head neck response. In this Chapter local loads will be analysed with the following objectives:

- to study the peak values of the global neck loads and the peak local tissue loads for rear end impact simulations. The results will be used

    - to further check the validity of the neck model (i.e. do the model results exceed global injury criteria or local tissue criteria?);

    - to study the influence of the muscle activation on the injury risk (i.e. how do muscle forces influence global neck loads and local tissue loads?);

    - to study the influence of the head restraint position and initial posture on the injury risk (i.e. how do head restraint positions and initial posture influence global neck loads and local tissue loads?).

123

- to study the relationship between published global neck injury criteria and the local tissue responses.

In Section 6.1 neck injury criteria available from the literature as well as tissue failure criteria are presented. In Section 6.2 simulation cases from Chapter 5, are selected to study above mentioned objectives. The results are presented in Section 6.3. This chapter concludes with a discussion in Section 6.4.

6.1 Background

6.1.1 Global Injury Criteria

The global neck injury criteria so far used in automotive test regulations are based on the net loads excerted on the head through the neck (Occipital Condyle loads). The neck loads (shear force F_{OCx}, axial force F_{OCz} and torques M_{OCy}) have been derived from head acceleration and transformed to local coordinate systems using rotations derived from film. In the case of head restraint contact the external head contact forces have been taken into account [71].
Mertz [87] proposed tolerance levels for an AIS type III neck injury for frontal impact. The tolerance levels for the neck moments for a 50th percentile male are 190 Nm for flexion and 57 Nm for extension independent of the load duration. For axial compression, tension and shear the proposed tolerances consist of a combination of force magnitude and duration. The most conservative tolerance is for the compression which must not exceed 1.1 kN for a duration longer than 30 ms.
Another biomechanical neck injury predictor (N_{ij}) also used for AIS type III injury risk, is based on the load transferred through the neck. The N_{ij} can be used for frontal and lateral impact. This injury predictor combines the neck axial force (F_z) and the flexion/extension moment about the occipital condyles (M_y) [150].
In a similar way, in 2001 the N_{km} criterion has been proposed, which combines the shear forces and the torques in the neck [92, 129]. This criterion is developed for AIS type I injuries of frontal and rear end impact. However, the N_{km} measure was developed on the basis of crash test dummies and therefore, the critical levels for N_{km} need further validation [92, 129].
In 1996 a new neck injury criterion (NIC) for WADs (AIS type I) caused in rear end impacts was proposed by Boström *et al.* [40]. The criterion is based on the relative acceleration between the top and the bottom of the cervical spine. The NIC criterion is defined by the following equation:

$$NIC(t) = a_{rel}(t) \cdot L + v_{rel}(t)^2 < NIC_{tol} \qquad (6.1)$$

with

$$a_{rel}(t) = a_x^{T1}(t) - a_x^{head}(t) \qquad (6.2)$$

$$v_{rel}(t) = \int a_{rel}(t) \cdot dt \qquad (6.3)$$

and a_x^{T1} the x component of T1 linear acceleration; a_x^{head} the x component of head linear acceleration; and L the neck link length (T1-C1) (= 0.2 m [40]). The accelerations are defined in the global coordinate system, however, NIC is specified for the translation phase, meaning that the rotation of the head with respect to T1 is negligible.

The concept of the NIC criterion is based on pressure measurements in the spinal canal in animal experiments where the head of an anaesthetised animal was retracted with a velocity and acceleration comparable to measurements on human necks during rear end impacts [40]. It was found that the pressure gradient developed in the venous and cerebrospinal fluid in the spinal canal during the retraction could possibly injure nerve root ganglia [3, 40, 41, 139]. A tolerance level $NIC_{tol} = 15m^2/s^2$ during more than 3 ms for AIS type I cervical injury was proposed based on pig experiments. Although several studies [38, 41] indicate that NIC is a useful indicator for the prediction of neck injuries following rear end impacts, other studies question the value of NIC [157].

Another criterium recently proposed for WADs caused in rear end impacts (AIS type I) is the intervertebral neck injury criterion ($IV - NIC$) by Panjabi *et al.* [115]. The $IV - NIC$ criterion, which showed correlation with NIC, is based on the hypothesis that a neck injury occurs when an intervertebral rotation exceeds its physiological limit during a rear end impact. However, Panjabi *et al.* did not define the dynamic physiological ranges of motion which are needed to calculate $IV - NIC$. Also a validation of the criterion is lacking.

Recently, Viano and Davidsson proposed the neck displacement criterion (NDC) to assess WAD risks in rear end impacts [155]. The OC rotation versus OC x-displacement with respect to T1 and the OC x-displacement versus z-displacement with respect to T1 are proposed to evaluate neck injury risks. The time history (i.e. rate dependency) is ignored since, Viano and Davidsson assumed it is probably of secondary order importance in tests with a normally seated occupant. Tolerance values for NDC are not available yet, however, initial working performance guidelines for crash dummies were presented [155].

Summarizing, various criteria for neck injuries are available. The global criteria, the net loads excerted on the head through the neck (F_{OCx}, F_{OCz} and M_{OCy}) and the combination of these loads (N_{ij}) are used in automotive test regulations [150]. However, these criteria represent AIS type III or higher injury risks. The N_{km} criterion is developed for AIS type I injuries, but the tolerance level needs further validation. The NIC and $IV - NIC$ measures are motivated from tissue level, and also represent AIS type I injury risk, however only a tolerance level for NIC is available so far.

6.1.2   Tissue Failure Criteria

It is generally assumed that Whiplash Associated Disorders (WADs) are caused by local tissue loads. In the clinical literature, the leading contenders for explaining chronic neck pain following WADs are injuries to the facet joints, the intervertebral discs and the upper cervical ligaments [6, 9–11]. The clinical relevance of these types

of injuries are discussed also by Yoganandan *et al.* [179]. In the following paragraphs the limited available static or dynamic failure forces are summarized per tissue.

Ligaments   Injuries to the ligament structures could occur when the ligament strain or force exceeds its maximum physiological value. The failure loads for the ligaments are presented in Table 6.3. The static failure loads are based on experimental studies presented in the literature [94, 178], while the dynamic failure forces are assumed to be 2.7 times the quasi-static failure forces. This stiffening factor 2.7 assumes failure strains to be independent of loading rate and is based on quasi-static and dynamic testing results by Yoganandan [175]. The same strategy, defining dynamic properties based on static properties, was used also by De Jager [65] and in Chapter 2.

Discs   Injuries to the intervertebral discs could occur due to local shear, compression or tension forces caused by movement of the vertebral bodies. Moroney et al. [90] found that static failure loads for disc segments averaged 3.5 Nm in flexion, and 3.2 Nm in extension. Cervical discs failed at 580 N in quasi-static tension, according to Pintar [120], and at 3140 N compression, 860 N tension and 5.0 Nm axial torsion, according to Yamada [172]. No data are available for combined or dynamic loading.

Facet Joints   The facet joints are full with pain-sensitive structures and clinical studies have implicated facet joints as a source of pain [179]. Experimental studies showed a pinching mechanism for rear end impact [102, 179], i.e. compression of the posterior region of the facet joint together with distraction of the anterior region. This pinching mechanism could result in pain as proposed in literature [179]. Human volunteer tests have referred to this as facet impingement [102] or collision [103] mechanisms. The pinching action does not refer only to the compression of the facet joint. The resultant motion of the anterior and posterior regions of the joint (axial and sliding motions) describes the stretch of the joint itself. An examination of the local shear and axial components of motion, and resultant stretch motions, could be helpful in explaining WADs. Although several researchers [160, 179] have studied the stress and strain in the facet joints (experimental and numerical) failure forces for the facet joints are not available yet.

6.2   Materials and Methods

The post mortem human subject (PMHS) and volunteer rear end impact simulation studies from Chapter 5 as presented in a simulation matrix in Table 6.1 are used in this chapter. This matrix includes simulations on a rigid seat (LAB, JARI) and a standard seat, with and without head restraint (AZT). The muscle parameter variation simulations (JARI) are used to study the influence of muscle forces. The simulations on the standard seat (AZT) are used to study the variation of head restraint position and initial posture. More information on the simulation set-up can be found in Section 5.1.

The first objective, to study the peak values of the global neck injury criteria and the local tissue loads, is discussed in Section 6.3.1. For the global criteria the net loads excerted on the head through the neck (shear force F_{OCx}, axial force F_{OCz} and torques M_{OCy}) are chosen. Although these criteria represent AIS type III injuries, they do have clear tolerance levels and are well known in automotive test regulations. The Neck Injury Criterion NIC is chosen here as well, since it is assumed to be related to AIS type I injuries. However, the NIC criterion is not yet accepted in test regulations and discussions concerning this criterion are ongoing [157].

The injury criteria and tissue tolerances should not be exceeded since the PMHSs and volunteers used in the experiments were not injured in the sled impact tests. The influence of the muscle activation, the head restraint position and initial posture, is discussed in Section 6.3.2.

In Section 6.3.3 the relationship between global and local criteria is studied, which is the second objective of this Chapter. The same global criteria as used for the first objective are used here (i.e. F_{OCx}, F_{OCz}, M_{OCy}, NIC). The vertebral rotations, the resultant forces in the facet joints as well as the forces in the ligaments are used as tissue level injury parameters. The vertebral rotations represent the motions of the vertebral bodies and will influence to internal loads [115]. The local tissue loads of the facet joints and ligaments are chosen, since they were indicated as leading contenders for WADs injuries [179].

It should be noted that global injury criteria and tolerances are used by the automotive industry [40, 87, 150], whereas, the local tissue tolerances are defined here, and are based on data from experimental tissue studies in the literature (see Table 6.3).

Table 6.1: *Simulation matrix used in this chapter.*

	case	initial [a] seating posture	seat [@]	head [b] restraint	pre stress [#]	reflex delay t_{reflex} [ms]	muscle activation level initial all [%]	flex[*] [%]	maximum ext[+] [%]	sterno[o] [%]
*	LAB	P	R	none	++	-	0	0	0	0
+	AZT-P1-mhd	P1	S	normal	+	-	0	0	0	0
◇	AZT-P2-mhd	P2	S	normal	+	-	0	0	0	0
◯	AZT-P3-mhd	P3	S	normal	+	-	0	0	0	0
X	AZT-P3-lhd	P3	S	low	+	-	0	0	0	0
◁	AZT-P3-nhd	P3	S	none	+	-	0	0	0	0
+	U1-EXP-JARI	P	R	none	+	-	0	0	0	0
◇	U2-EXP-JARI	P	R	none	+	25	0	50	0	25
o	U3-EXP-JARI	P	R	none	+	25	0	100	0	50
x	U4-EXP-JARI	P	R	none	+	25	0	100	50	50
◁	U5-EXP-JARI	P	R	none	+	25	0	100	100	100

[@] R = rigid seat, S = standard seat
[#] - : $\frac{s_{ref}}{s_{free}}$ = 1 [65]; + : $\frac{s_{ref}}{s_{free}}$ = 2.8/2.45; ++ : $\frac{s_{ref}}{s_{free}}$ = 2.8/2.1 [17], see also Section 2.2.7
[*] all flexor muscles
[+] all extensor muscles
[o] sternocleidomastoid
[a] see Figures 5.2 and 5.19
[b] vertical position head restraint: mhd=normal, lhd=low, none= no head restraint (see Figure 5.20)

6.3   Simulation Results

6.3.1   Model Response versus Tolerance Levels

The model results (simulation matrix in Table 6.1) are compared to global neck injury criteria as well as to local tissue tolerance levels as defined earlier. In Table 6.2 the simulation results of the global neck injury criteria are presented in percentages of the tolerance levels. The absolute values are presented together with the experimental results in Appendix D.

The model predictions for the global neck loads and the NIC values do not exceed the critical values. The neck loads range from 0.4 to 25.2 % of the critical values, whereas the simulated NIC values range from 33 to 95 % of the critical value.

The peak ligament forces of all ligaments are compared to dynamic failure forces as defined in Table 6.3. For each ligament the highest value of the 11 simulations used in this Chapter is presented. The absolute values of the forces of the apical ligament and the posterior membrane, showing the highest percentages compared to the dynamic failure forces, are shown in Figures 6.1 and 6.2.

The peak forces of all ligaments are smaller than 50% of the dynamic failure force, except for the apical ligament (AP: 104% of dynamic failure force). When studying the results for the apical ligament in more detail (see Figure 6.1), it was seen that the peak force was smaller than 39% of the dynamic failure force for most simulations. However, for the simulation with passive muscles (JARI-U1) the peak force reached about 69 % of the dynamic failure force. The peak value of 104% of the dynamic failure force was reached for the the simulation with passive muscles on the standard seat without head restraint (AZT-P3-nhd).

The resultant forces for the discs and the facets joints are presented in Figures 6.3 and 6.4. The resultant disc forces and facet joint forces of the passive model (LAB, AZT and U1-EXP JARI) are below 600 N and 400 N, respectively. It should be noted that the forces both for disc and facet joints vary strongly over the segmental levels. Moreover, it was visually observed that the spinous processes of segment C1-C2 made contact for all simulations. For large head motions occuring for the simulations with passive muscles and without head restraint the spinous processes of segment C5-C6 also contacted.

Table 6.2: *Peak percentages of global injury criteria compared to tolerance levels.*

Case[+]	F_{OCx}		F_{OCz}		M_{OCy}		NIC
	neg	**pos**	**neg**	**pos**	**neg**	**pos**	**pos**
	%	%	%	%	%	%	%
LAB	10.3	14.1	16.5	3.0	7.5	9.7	**33.0**
AZT-P1-mhd	6.5	5.9	16.1	13.8	19.3	3.0	**88.5**
AZT-P2-mhd[*]	19.8	6.4	13.4	15.2	19.8	3.7	**95.0**
AZT-P3-mhd	11.9	5.2	13.8	9.6	14.6[o]	2.7	**45.5**
AZT-P3-lhd	7.6	1.9	12.1	11.9	14.6[o]	2.5	**45.5**
AZT-P3-nhd	17.4	9.6	25.2	8.7	14.0	11.8	**64.3**
U1-EXP-JARI	9.2	11.1	14.5	9.3	10.4	7.7	**54.1**
U2-EXP-JARI	0.4	11.1	11.5	9.3	10.2	5.0	**54.1**
U3-EXP-JARI	0.4	12.8	13.3	9.3	9.9	6.8	**54.1**
U4-EXP-JARI	0.4	8.6	11.8	9.3	15.6	5.4	**54.1**
U5-EXP-JARI	1.1	6.3	14.7	9.3	20.1	5.9	**54.1**

F_{OCx} neg = posterior shear force in OC F_{OCx} pos = anterior shear force in OC
F_{OCz} neg = tension force in OC F_{OCz} pos = compression force in OC
M_{OCy} neg = extension moment in OC M_{OCy} pos = flexion moment in OC
tolerance levels: F_{OCx} = 1100 N, F_{OCz} = 1100 N, M_{OCy} pos = 190 Nm,
M_{OCy} neg = 57 Nm and NIC_{tol} = 15 m^2/s^2
results are printed in bold when > 30 % of tolerance level
[+] see Table 6.1 for the simulation matrix
[o] second peak value higher than first peak extension moment
(see Figure 5.17 in Chapter 5)
[*] values are inaccurate, since large horizontal peak accelerations were observed
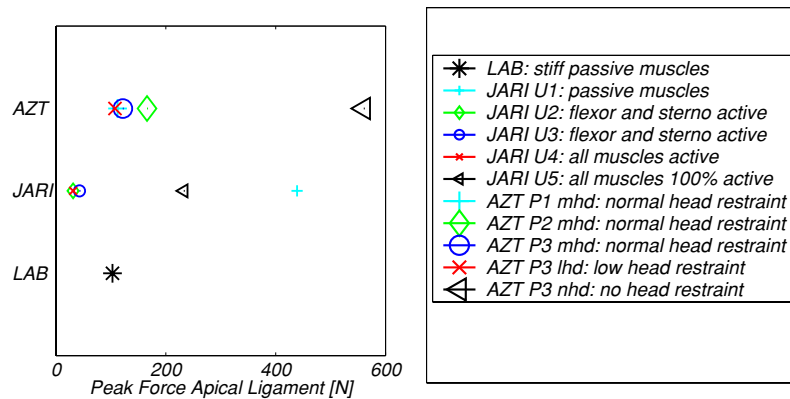(see Figure 5.27 in Chapter 5)

Figure 6.1: *Peak Apical ligament (AP) forces (dynamic failure force 578 N) for LAB, JARI and AZT rear end impact simulations (see Table 6.1).*

Table 6.3: *Ligament forces: failure loads based on literature together with the highest percentage of 11 simulations presented per ligament. (see Table 6.1).*

Ligament name [o]	Failure Force			Simulation result in % of dynamic failure force [c]	
	quasi-static (N)	reference	dynamic[+] (N)	(%)	
ALL-low	155	[178]	418	11	
ALL-mid	90	[178]	243	19	
PLL-low	181	[178]	499	4	
PLL-mid	88	[178]	238	8	
FL-low	126	[178]	340	15	
FL-mid	115	[178]	310	16	
ISL-low	39	[178]	105	28	
ISL-mid	38	[178]	103	19	
JC-low	350	[178]	945	7	
JC-mid	254	[178]	686	10	
AM C0-C1	233	[94]	629	24	
AM C1-C2	281	[94]	759	20	
PM C0-C1	83	[94]	224	36	see Figure 6.2
PM C1-C2	113	[94]	305	46	see Figure 6.2
ALAR	357	[94]	964	13	
TL	354	[94]	956	12	
TM	76	[94]	205	1	
LN	98[a]		265	30	
AP	214[b]		578	**104**	see Figure 6.1
CF	214[b]		578	1	

[o] see Table 2.7 for full names of ligaments
[+] dynamic value = 2.7 times quasi static value (see De Jager [65] and Yoganandan [175])
[a] static failure force of LN is average of PM
[b] static failure force of AP and CF is average of upper neck ligaments (AM,PM,ALAR,TL,TM)
[c] values > 50% dynamic failure force are printed in bold

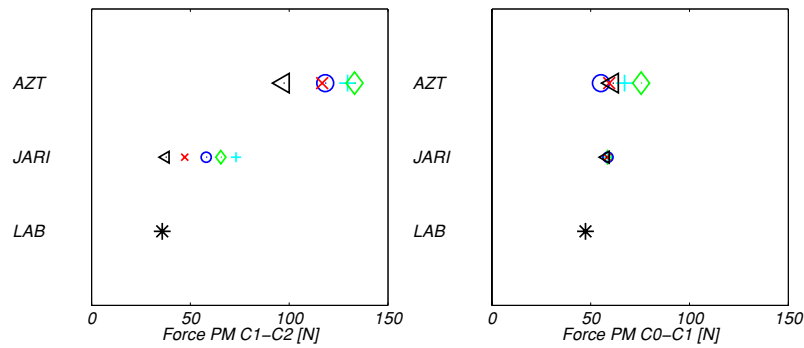
Figure 6.2: *Peak Posterior membrane (PM) forces (dynamic failure forces 305 N and 224 N) for LAB, JARI and AZT rear end impact simulations (see Table 6.1). For explanation of the symbols see the legend in Figure 6.1.*
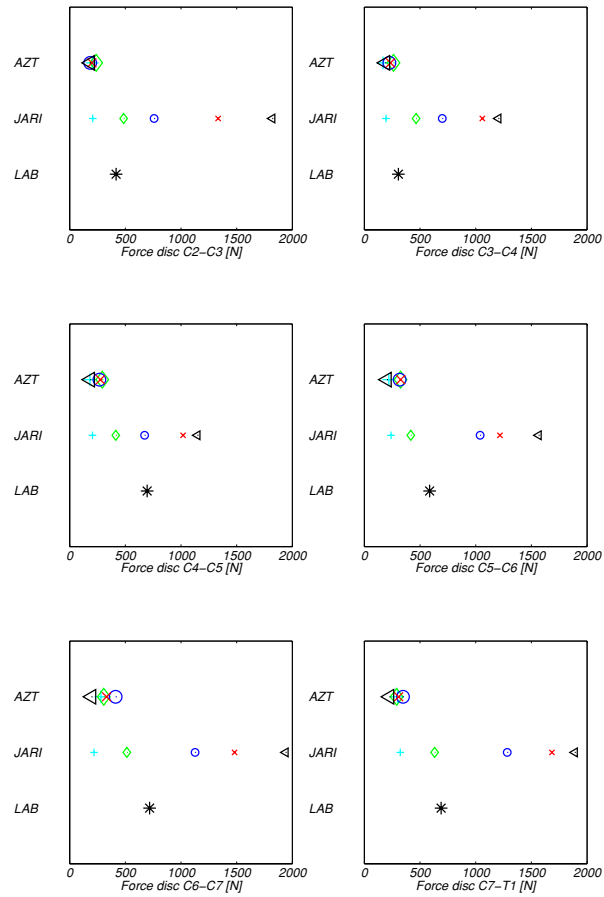
Figure 6.3: *Peak resultant disc forces for LAB, JARI and AZT rear end impact simulations (see Table 6.1). For explanation of the symbols see the legend in Figure 6.1.*
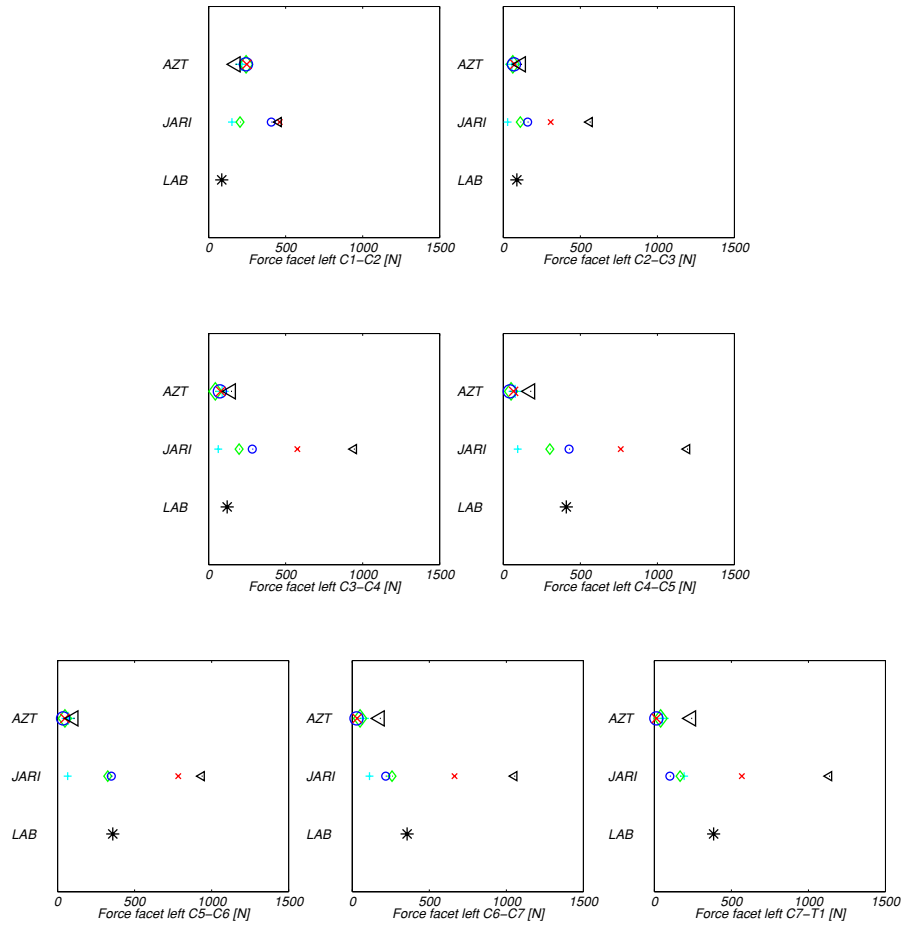
Figure 6.4: *Peak resultant left facet forces for LAB, JARI and AZT rear end impact simulations (see Table 6.1). For explanation of the symbols see the legend in Figure 6.1.*

6.3.2 Relation of Muscle Activation, Head Restraint Position and Initial Posture with Injury Risk

Varying muscle activation The peak values of the JARI simulations are used to study the influence of varying muscle activation on the global injury criteria (see Table 6.2). Absolute values can be found in Appendix D) and the local tissue loads are given in Figures 6.1 to 6.4. The NIC value and the compression force are not influenced by varying muscle activation, since muscle contraction starts after the peak value occurs. The net extension moment decreases slightly by activation of the flexor muscles and the sternocleidomastoid (U2 and U3 compared to U1 (=passive model)), but increases with increasing activity of the extensor muscles (a factor of 1.5 for U4 and 2 for U5). The flexion moments of the models with muscle activation decrease by 25 to 35 % compared to the passive model, however no trend is seen for the varying activation scheme of the muscles. The tension force shows a reduction up to 20 % when the muscles are activated, however, for the simulation with all muscles maximally active (U5), the tension force shows similar values compared to the passive model. The posterior shear force shows a reduction of 90 to 95% when the muscles are activated. For the anterior shear force an increase of about 15 % is seen when the cervical muscles are activated without contracting the extensors. However, when the extensors are activated as well, the anterior shear force decreases up to 55 % compared to the passive model. It should be noted that even with increasing forces or moments due to muscle activation all peak values are below the injury criteria.

The influence of varying muscle activation on the tissue loads was also studied. Examples of the influence on the ligament forces are shown in Figures 6.1 and 6.2. The peak ligament forces are either not changing or reduced when the muscles are activated during the simulations.

The influence of the varying muscle activation on the discs and the facet joints is shown in Figures 6.3 and 6.4. The resultant disc force for the JARI simulation with passive muscles is below 250 N. However, these forces are increasing up to about 2000 N for the simulations with maximum muscle activation. The resultant facet forces for the JARI passive model are below 200 N. Again, the forces are increasing with muscle activation up to 1250 N.

In conclusion, the global forces are decreasing with muscle activation (from 5 to 100 %, depending on the direction of force and activation scheme). The flexion moment decreases by 15 to 35 %, while the extension moment shows a slight reduction when activating the flexors and sternocleidomastoid, but increases by 50 to 80 % when activating the extensor muscles as well. The ligament forces are hardly influenced or show a decrease of the peak loads, while the disc forces and facet joint contact forces are increased by muscle activation (maximally by factors of 8 and 6 respectively).

Varying head restraint position The influence of the head restraint position is studied by comparing the results of the AZT-P3 simulations. The global injury criteria are presented as percentages of the tolerance levels in Table 6.2 (absolute values can be found in Appendix D). Examples of the local tissue loads are presented in Figures 6.1 to 6.4.

Compared to the simulation without a head restraint (AZT-P3-nhd), shear forces are reduced with a head restraint. The simulation with a low head restraint (AZT-P3-lhd) shows a larger reduction (60-80 %) than the simulation with a normal head restraint position (AZT-P3-mhd, 30-45 %). The compression force reduces by a factor of 2 when a head restraint is used, whereas the tension force increases by 10 % for the normal placed head restraint and 40 % for the low placed head restraint. The extension moment increases by about 5% when using a head restraint. However, altering the vertical position of the head restraint did not show differences in the extension moment. The flexion moment decreases by about 80 % for a seat with a head restraint, compared to a simulation without a head restraint. The NIC value shows a 30% reduction when placing a head restraint, however no difference is observed for the low and normal placed head restraint.

Examples of the ligament forces are presented in Figure 6.1 and 6.2. No clear trend is observed between varying the head restraint position and the ligament forces. However, the ligament forces of the anterior part of the lower neck are reduced when a head restraint is added to the seat.

The resultant forces for the disc are hardly influenced by varying the head restraint position (see Figure 6.3). In Figure 6.4 the resultant facet joint forces are presented. The simulation without head restraint (AZT-P3-nhd) predicts by about a factor of 2 to 3 larger facet joint forces than simulations with a head restraint. However, no trend is observed for varying head restraint position.

Varying initial posture The influence of the initial posture is studied by comparing the results of the AZT-P1, P2 and P3 simulations. When comparing the forward seating position (AZT-P1-mhd) with the simulation sitting in a normal upright seating position (AZT-P3-mhd) the global neck forces and moments are increasing varying by 9 to 95 %, except for the posterior shear force, which decreases a factor of 2 for sitting in the forward seating position. The NIC shows the largest value for the simulation with the forward seating position (AZT-P1-mhd), even larger than the NIC predicted for the simulation of an upright seating position without head restraint (AZT-P3-nhd). Examples of the ligament forces are presented in Figure 6.1 and 6.2. No clear trend is observed between varying the head restraint position and the ligament forces. The resultant forces for the disc and the facet joint contacts are hardly influenced by varying the initial seating position (see Figure 6.3 and 6.4).

6.3.3   Correlation between Global Injury Criteria and Local Loads

The relationship between the global injury criteria (shear force F_{OCx}, normal force F_{OCz}, torques M_{OCy} and NIC) and the vertebral rotations, the resultant forces in the facet joints as well as the peak forces in the ligaments has been studied. The Pearson correlation coefficient was calculated using the software package SPSS. Significant linear correlation was assumed when the regression coefficient value was exceeded 0.5 at a 0.01 level (i.e. $r^2 > 0.5$ and $p < 0.01$).
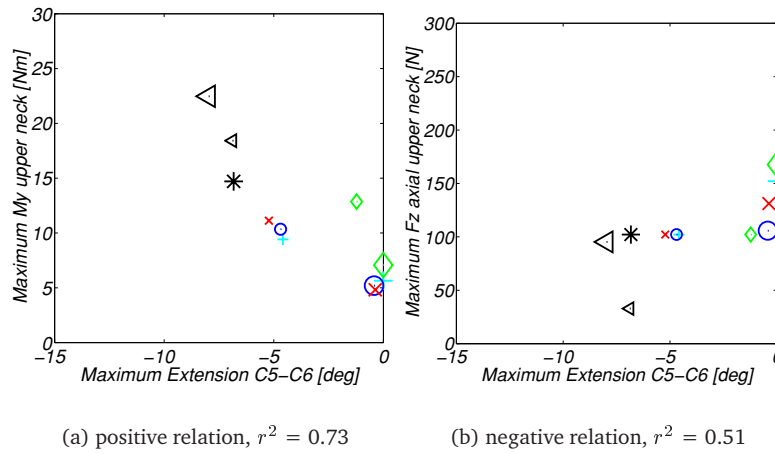
(a) positive relation, $r^2 = 0.73$ (b) negative relation, $r^2 = 0.51$

Figure 6.5: *Example of relationship study for vertebral rotations versus global injury criteria for LAB, JARI and AZT rear end impact simulations (see Table 6.1). For explanation of the symbols see the legend in Figure 6.1.*

Table 6.4: r^2 *for singular correlation between peak vertebral rotation and global injury criteria* ($n=11$, $p < 0.01$).

Peak extension angle	F_{OCx} neg	pos	F_{OCz} neg	pos	M_{OCy} neg	pos	NIC pos
C0-C1	0.24	0.01	**0.5**	0.01	0.04	0.27	0.00
C1-C2	0.17	0.01	0.31	0.26	0.13	0.39	0.27
C2-C3	0.14	0.31	0.06	0.48	0.22	**0.56**	0.03
C3-C4	0.10	**0.54**	0.10	**0.57**$^+$	0.29	**0.69**	0.26
C4-C5	0.03	**0.53**	0.29	**0.64**$^+$	0.36	**0.80**	0.28
C5-C6	0.00	0.36	0.25	**0.51**$^+$	0.19	**0.73**	0.17
C6-C7	0.00	0.30	0.29	0.48	0.12	**0.73**	0.14
C7-T1	0.10	0.18	0.46	0.22	0.10	**0.67**	0.04

F_{OCx} neg = posterior shear force in OC F_{OCx} pos = anterior shear force in OC
F_{OCz} neg = tension force in OC F_{OCz} pos = compression force in OC
M_{OCy} neg = extension moment in OC M_{OCy} pos = flexion moment in OC
$r^2 > 0.5$ are printed in bold
$^+$ negative relationship for $r^2 > 0.5$, i.e. increasing local load
results in decrease of absolute values of global load

Table 6.5: r^2 *for singular correlation between upper neck peak ligament forces and global injury criteria (n=11, $p < 0.01$).*

Peak ligament force	F_{OCx} neg	F_{OCx} pos	F_{OCz} neg	F_{OCz} pos	M_{OCy} neg	M_{OCy} pos	NIC pos
AP	0.29	0.00	**0.59**	0.00	0.00	0.38	0.01
PM C0-C1	0.14	0.18	0.00	**0.83**	0.46	0.15	**0.90**
PM C1-C2	0.38	0.43	0.01	**0.59**	0.22	0.26	0.38
AM C0-C1	0.25	0.00	**0.58**	0.00	0.03	0.32	0.01
AM C1-C2	0.47	0.00	**0.64**	0.00	0.00	0.32	0.02
ALAR left	0.19	0.03	**0.73**	0.04	0.04	0.48	0.00
ALAR right	0.19	0.09	**0.72**	0.04	0.04	**0.61**	0.01

F_{OCx} neg = posterior shear force in OC F_{OCx} pos = anterior shear force in OC
F_{OCz} neg = tension force in OC F_{OCz} pos = compression force in OC
M_{OCy} neg = extension moment in OC M_{OCy} pos = flexion moment in OC
see Table 2.7 for full names of ligaments
$r^2 > 0.5$ are printed in bold

Vertebral rotations   The C0-C1 extension angle showed a positive relationship (r^2 = 0.5) with the tension force in OC (see Table 6.4). The peak extension angle of motion segment C3-C4 and C4-C5 showed a positive relationship (r^2 = 0.53 to 0.54) with the anterior shear force in OC. The mid neck (C3-C4, C4-C5, C5-C6) showed a negative relationship (r^2 = 0.51 to 0.64) of the extension angle with the compression force. A positive relationship was found for the flexion moment in OC (r^2 = 0.56 to 0.8) and the extension angles in the mid and lower neck (C2-C3 to C7-T1). In Figure 6.5 an example of a positive and negative relationship found for the C5-C6 segment is shown.

Facet joint forces   The correlation between the peak resultant facet forces and the global criteria (as mentioned before) was very weak or even absent. For the posterior shear force r^2 ranged from 0.17 to 0.44, showing a small negative relationship, whereas for the other parameters r^2 was even smaller than 0.18 (results not shown).

Ligament forces   The apical ligament, anterior membrane and the alar ligament forces showed a positive relationship with the tension force in the OC (r^2 ranged from 0.58 to 0.73), while the posterior membrane showed positive relationship with the compression force in the OC (r^2 ranged from 0.59 to 0.83)(see Table 6.5).

6.4   Discussion

The **first objective** of this chapter was to study the peak values of the global neck loads and the peak local tissue loads for rear end impact simulations in order to assess the validity of the model as well as to study the influence of muscle activation, head restraint position and initial posture.
The global injury criteria of the simulations were all below the tolerance levels defined in the literature, yielding further confidence in the neck model. The model peak

responses are closer to the tolerance levels of the AIS type I injuries (33 to 95 %) than to the AIS type III injury levels (0.4 to 25 %), which could be expected for these simulated mid severity impacts (4 to 12 g). It should be noted that NIC and its tolerance value used for the AIS type I injury is still questionable [157].

Most ligament forces were below the dynamic failure forces (1 to 46 %), except the apical ligament force (104 %) for the simulation in a standard seat without a head restraint. However, it was not known whether injury would have taken place or not for this simulation, since experimental data for this typical case was not available. It should also be noted that the failure force of the apical ligament was based on the average of the failure force of the upper neck ligaments, since experimental data was not available.

The disc and facet joint contact forces vary strongly over the segmental levels. The resultant peak forces seem realistic for the passive model simulations, however the resulting forces for disc and facet joint contact occuring at maximum muscle activation are increasing up to a factor 8. Since the tissue characteristics of the discs and the facet joint contacts were based on literature data together with engineering judgement (see Chapter 2) the high forces could be caused by a too stiff compression function. It should be noted that the predicted loads could not be compared to the disc failure loads reported in the literature, and that failure forces are missing for the facet joint contacts.

The **first objective** included also a study of the effect of muscle activation, head restraint position and initial posture on the global injury criteria and local tissue loads. Increasing muscle activation showed a reduction of the simulated head and neck motions (see Chapter 5). Smaller extension angles resulted in smaller ligament forces. However, when all muscles were maximally active (including the strong extensor muscles) the head and neck motion increased somewhat in comparison to the passive model response. This resulted in similar ligament forces in comparison to the passive model. In all cases the disc forces and facet joint contact forces increased with increasing muscle activation.

These model observations indicate that simulation of muscle activation results in smaller head motions, which are more in agreement with the experimental response. However, muscle activation could cause higher local tissue loads than for the passive model. This effect of muscles on the internal loads in the cervical spine has also been discussed by others [134].

When removing the head restraint, larger head motions and larger global injury criteria and NIC values were present, compared to simulations with a low and normal positioned head restraint. However, the net compression force decreased, since head contact was absent. Varying the muscle activation showed larger influences on the internal loads for the discs, facet joints and ligaments than varying the head restraint position. This indicates that defining accurate model inputs for muscle activation is not only necessary to predict the global response, as was found in Chapter 4 and 5, but is also necessary to predict the local response.

The **second objective** of this chapter was to study the relationship between global injury criteria and local tissue loads and vertebral rotations. The strongest relationships were found for the peak extension vertebral rotations with the flexion

moment in the occipital condyles (OC), and the ligament forces with the axial force in OC. Although indicated as one of the main contenders in WADs, no significant linear correlation was found between the facet joint contact forces and the global injury criteria. In general, the correlation found between global injury criteria and local tissues loads is not very strong. Therefore, it is questionable whether global criteria, as available in the literature (see Section 6.1.1), may be used to predict local injuries.

Summarizing, further confidence in the neck model was given, since the global injury criteria of the simulations were all below the tolerance levels defined in the literature. For varying conditions of muscle activation, head restraint position and initial posture different trends were observed for several global and local loads. The correlations found between predicted global injury criteria and local tissue loads with the simulations performed within this chapter were not strong. Therefore, the use of global injury criteria to predict local injuries may need further research. The results in this Chapter illustrate how the detailed model can be used to determine the possible occurrence of injuries in simulated impacts.

Chapter 7

Discussion and Conclusions

The rationale of this research was that a mathematical model of the human head and neck can contribute to a better understanding of neck injury mechanisms and can be used in injury prevention research. The objective of this PhD research was to develop and validate a detailed three dimensional mathematical model that describes the dynamic behaviour of the human head and neck in accident situations. The model had to provide insight into the motion of the head relative to the torso (global kinematics) and into deformations and loads that occur within the cervical spine (local kinematics). In addition this study aimed to provide insight in the role of initial seating posture and head restraint position, and the role of muscle behaviour on the global and local kinematics of the head neck system.

This chapter summarizes the main findings of this research. In Section 7.1 the model development is discussed followed by the model validation in Section 7.2. The model applications performed within this research are discussed in Section 7.3, whereas suggestions for future applications are give in Section 7.4. In Section 7.5 limitations and recommendations are given to improve the model and enhance the validation. Finally, some general conclusions are presented in Section 7.6.

7.1 Neck Model Development

In this thesis a detailed multibody neck model has been developed. The model consists of a rigid head, rigid vertebrae, (non)linear viscoelastic discs, frictionless facet joints, nonlinear viscoelastic ligaments and segmented contractile muscles (see Chapter 2). The model is based on a model by De Jager [65]: it uses comparable multibody techniques but is significantly improved with respect to the level of detail of the model components. The geometric description of the vertebrae has been improved and ligaments and muscles are implemented in more detail. Additionally, muscles in the De Jager model are modelled as straight line elements, while muscles in the current model can follow the curvature of the neck, resulting in more realistic muscle force lines of action.

Stiffness properties of the tissues are based on literature data. However, for some model parameters experimental data was lacking. The nonlinear compression behaviour of the cervical disc in the model was based on the stiffness characteristics of the lumbar disc, and the nonlinear flexion and extension stiffness was based on whole segment experiments, instead of using separate disc data. The stiffness functions in the other directions were defined linearly, based on low load experiments. Additionally, the dynamic stiffness of the disc was assumed to be twice the static stiffness, based on dynamic experiments on cervical tissue. The ligament stiffness of some upper neck ligaments was based on the average of other upper neck ligaments. The dynamic stiffness of the ligaments is defined as rate dependent. However, contradictory data were found in the literature, and therefore, the modelled rate dependency could be inaccurate. The compression stiffness for the modelled contact of the facet joints and the spinous processes are assumed to be stiffer than the compression stiffness of the cervical disc. However, this assumption was based on engineering judgment.

The neck model can be applied separately or integrated into a model of an entire human body. Global kinematics, such as head translational and angular movements and accelerations, as well as local kinematics, such as vertebral rotations and local tissue loads, can be predicted with the new model.

A major advantage of the new model compared to other multibody models and finite element models is the realistic and detailed modelling of active force generating muscle elements. Another advantage of this multibody model is the detailed geometry, especially of the upper neck joints. The most important simplifications in the model are the rigid head and vertebrae, and the use of spring damper models for the discs and the facet joints in the lower cervical spine. Finally, the time efficiency is much better for a multibody model compared to a finite element model.

7.2   Validation of the Neck Model

The neck model has been validated quasi-statically as well as dynamically. In Chapter 3 published quasi-static experimental data (up to 20 N or 1.5 Nm) were used to test the segment models for 6 degrees of freedom and to test the entire ligamentous cervical spine model for flexion and extension. The mechanical behaviour of the segment models agreed reasonably with the experimental data, i.e. simulated global force-displacement and global moment-rotation relations generally were within 1 standard deviation of the quasi-static experimental data. The model segments showed realistic 3D coupling effects. Lack of experimental data prevented validation of predicted local mechanics.

Frontal, lateral and rear end sled experiments using volunteers as well as post mortem human subject (PMHS) experiments were simulated to validate the model dynamically. In Chapter 4 neck model simulations of 15 g frontal and 7 g lateral volunteer experiments were performed as was done also by De Jager.

New compared to De Jager's work are the rear end validations, which were performed

with the neck model included in a total human body model (Chapter 5). The rear end impact validation ranged from high severity (12 g) for PMHS experiments to mid (4-5 g) and low severity (0.7 g) for volunteer experiments. Volunteers were tested on a standard car seat with head restraint and on a rigid seat without head restraint, whereas PMHSs were tested only on a rigid seat without head restraint.

Simulation of the rear end impact PMHS study was performed without muscle activation (passive muscle behaviour) (Chapter 5). Too large head motions were observed for the PMHS simulations, when using the normal passive muscle tensile properties as defined for the volunteers. However, adapting the passive muscle tensile properties towards published PMHS tissue properties resulted in reasonable to good model predictions for the 12 g rear end impact.

Accurate muscle activation properties were missing for the volunteer validations. Results from a literature review by Siegmund and Brault [134] and the experiments performed at Maastricht University (Appendix E) provided a range of muscle activation scenarios rather than one probable response. Within this range, several combinations of the reflex delay and activation levels were simulated (Chapter 4 and 5). Simulations for frontal, lateral and rear end impact without head contact provide comparable conclusions on the role of muscle activation, showing that inclusion of muscle activity seems necessary for realistic simulations of impact conditions with human volunteers. The model predicted reasonably to well, the head and neck kinematics for the frontal, lateral and rear end impact simulations without head contact. However, when including only passive muscle behaviour the model showed larger head motions compared to the experimentally defined volunteer corridors. Rear end impact model responses with head restraint showed only reasonable to poor response compared to the experimental results, irrespective of simulating passive muscles only, or including active muscle behaviour for these volunteer simulations.

Dynamic whole human body model simulations for rear end impact included validation of the seat model as well as of the spine and the neck model. Simulation results of the head kinematics for a deformable standard car seat deviated more from experimental data than for a rigid seat. This could be related to both the seat model and the spinal model. Firstly, the standard seat was modelled in detail but the load deflection curves and joint characteristics were based on quasi-static experiments instead of dynamic loading conditions. Secondly, although the T1 horizontal response was well predicted, the vertical displacement and rotations were not always realistic for both deformable and rigid seat simulations. Thus T1 provided only a reasonable input to the neck model for the rear end impact simulations.

Due to lack of available data, local kinematics and kinetics of the cervical spine could not be validated in detail. However, by comparing the ligament loads to failure criteria based on experimental data in the literature, it was shown that the predicted ligament forces were below the level of injury (Chapter 6). This is in agreement with the experiments, showing no injuries.

Most neck models presented in the literature are validated for only one or two impact directions not including rear end impacts [20, 28, 96]. Although the models by Yang [174] and Bertholon [7] were validated for rear end impact, these models lack the possibility for simulation of different initial seating postures. Additionally, all these

models did not include active muscle behaviour. Summarizing, important benefits of the applicability of the new model compared to other models are the extended validation and the possibility for simulation of muscle activation.

7.3   Model Applications

The model was applied to study the role of muscle activation, head restraint position and initial posture. Considering muscle activation, it was already mentioned that inclusion of muscle activity seems necessary for realistic simulation of impact conditions of volunteers. In addition varying muscle activation showed large influences on the internal loads for the discs and facet joints (Chapter 6). This indicates that defining accurate model input for the muscle activation is not only necessary to predict the global response, as was found in Chapter 4 and 5, but is also necessary to predict the local response correctly.

Additionally, simulations were performed to study the influence of the initial seating posture and the position of the head restraint (Chapter 5). In accordance with experimental studies available in the literature it was shown by modelling that seating in an upright position together with a head restraint adjusted in line with the top of the head reduced the head motion and neck loads compared to a more forward seating position and a low head restraint. The reduction of head motion and neck loads is the largest when simulations with a head restraint are compared to simulations without a head restraint. However, the net axial compression force will increase due to contact of the head with the head restraint. Contrary to varying muscle activation, varying head restraint position and initial seating position showed only small influences on the internal loads of the discs and facet joints (Chapter 6).

It is generally accepted that Whiplash Associated Disorders (WADs) are caused by local tissue loads. However, the current neck injury criteria used in automotive test regulations are based on global neck loads in the occipital condyles (OC). Moreover, since they are defined for high severity frontal impacts, these criteria do not satisfy for WADs. Recently, new injury criteria designed especially for WADs have been proposed in the literature. However, these criteria are still based on global loads or global motions, and most of them lack tolerance levels (Chapter 6).

A correlation study (Chapter 6) between predicted global injury criteria and local tissue loads using the model results predicted only strong relations for the OC flexion moment with vertebral extension rotations of the mid and lower neck, and for the OC axial force with forces of a few upper neck ligaments. No relations were found for the global injury criteria and the facet joint contact forces, although the facet joints which were indicated as leading contenders for WAD in the literature. Therefore, the model results indicate that it is questionable whether global injury criteria may be used to predict local injuries (Chapter 6).

7.4   Suggestions for Future Applications

The neck model as a separate model, as well as integrated in a total human body model, can be used to predict the human head-neck response to various impact situations, which makes it useful for the understanding of injury mechanisms and for car safety improvement. As illustrated in Chapter 6 the neck model is, in principle, useful for studying injury mechanisms because deformations and loads of the individual soft tissues can be assessed. Failure tolerances could be established by reproducing experiments or real accidents and correlating real injuries with the predicted tissue loads and deformations. Once appropriate tolerance levels for the tissues are known, these can be used for predicting the probability of the occurrence of injuries in other cases. The neck model integrated in the human body model can be used to study the effect of head restraints, airbags, car interior, muscle activation, and initial seating positions, on the occupant's head-neck response in simulated crashes. It should be noted that the model presented in this thesis represents a 50th percentile male (75.7 kg and 1.74 m), rather close to most subject data used for validation (Chapter 5). However, anthropometric variability between test subjects and the model requires models of different body sizes [57].

Muscle activation   The model presented in this thesis has the capability to simulate passive and active muscle behaviour. The simulation results showed that active muscle behaviour has a substantial influence on the head and neck kinematics for frontal, lateral and rear end impact (Chapter 4 and 5). An even stronger effect was found on the local loads (facet joints and discs) (Chapter 6). The muscles are activated in this research into three groups for simplicity, but it is possible to define the model input per muscle. Variations of initial muscle contraction, reflex times, activation level and co-contraction scheme can be introduced very easily with the current model. Therefore, the model shows the potential to further investigate the importance of muscle activation by numerical research.

Posture and head restraint position   Initial seating posture and head restraint position will influence the head neck response in a rear end impact as was observed experimentally (see review by Szabo [140]) and numerically (see Chapter 5). It is generally assumed that sitting in an extreme position could increase the injury risk. In this thesis, only three rather normal initial seating postures were studied. However, it is possible to define more extreme postures as well; for example, simulating a rear end impact of a subject with the head turned to the left or to the right, or simulating a case in which the occupant is leaning forward to pick up something from the floor.

Injury   For test regulations in the automotive industry, crash test dummies are used to predict injury risk. However, only global injury criteria can be measured with these dummies. Recently, during reconstructions of real accidents in which AIS type I neck injuries were observed, upper neck loads measured in the new RID 2 α dummy have been compared with upper neck loads calculated in human subject tests [21]. The

limited data available so far indicate that a relationship with neck injury risk seems to exist only for the neck axial tensile force. It should be noted that axial force can be compressive, during ramping up and when the head hits the head restraint, and tensile, during large head extension. Both may result in different injury mechanisms. Further research is needed to confirm these possibilities where other potential criteria should also be considered. Local tissue criteria would require a new dummy neck or extensive measurement instrumentation that does not exist today. If there would be experimentally and numerically a strong correlation between local tissue loads and global criteria this would make it possible to use global injury criteria, and therefore, the available dummy models. The model presented in this thesis could be used for further study towards finding such possible correlations.

7.5   Limitations and Recommendations

Limitations   While the experimental basis of the model has been extended as compared to the model of De Jager [65], several areas of uncertainty remain. The need for additional data at the tissue and segment levels were identified in Section 2.3.
An important limitation of the neck model is that the head does not have a stable upright position when subjected to gravity only. Including complex feedback mechanisms for the neural excitation of the neck muscles to create an equilibrium was beyond the primary task of this study. However, for low severity impacts as performed at Maastricht University it seems that posture maintenance has a large influence on the head neck response and needs to be included in the model when studying low severity loading.
The limitations of experimental condition characteristics used for validation studies are: 1) the uncertainty about the amount of muscle activation present in the volunteers; and 2) the range of severities not including experiments with injury.
It was assumed that the extreme flexibility of the passive model for frontal and lateral and rear end impact was caused by the absence of active muscle behaviour (Sections 4.3 and 5.4). However, the dynamic response of the ligamentous spinal model could also be a cause of the poor passive model behaviour for volunteer experiments. The ligamentous segment models as well as the entire ligamentous model show reasonable to good correspondence with quasi-static experiments. However, the segment models were not validated for dynamic conditions.
The experimental data used for validation so far did not represent impacts which resulted in injury (Chapter 5). Therefore, injury predictions by the model should be taken with care. Also model predictions, for differing severities than validated, need extra attention.

Recommendations   To further improve the neck model a parametric study (similar as was done for the De Jager model [65]) is needed to determine the effect of the tissue parameter changes on the model response. Once crucial model parameters have been identified for the new neck model experimental studies quantifying the

mechanical characteristics of the cervical tissues are recommended, to reinforce the experimental basis of the model. Additionally, to further improve the applicability of the model more validation studies are needed. To be more specific:

- Experimental studies quantifying the mechanical characteristics of the cervical tissues are recommended. These experiments should address the following aspects: a) applying low and high loads, both in quasi-static and dynamic testing conditions, b) applying loads and measuring loads in 6 degrees of freedom (coupled motions), c) possible variations in characteristics with vertebral level.

- It is recommended to perform experiments in several impact directions on the ligamentous spine to dynamically validate the kinematics and kinetics of the segment models as well as the whole ligamentous spine without passive or active musculature.

- Experimental studies, focussing on measuring muscle parameters are needed for more accurate model input for the muscle activation. These experiments should address the following aspects: a) the moment of activation with respect to the start of impact. b) the amount of muscle force in impact loading, c) the head and T1 kinematics.

- It is recommended to validate the internal response of the model. Very recent impact studies presenting experimental data on vertebral rotations [31, 102], ligament forces or strains [109], facet joint contact forces and displacements [31, 179] could be used for internal dynamic model validation.

- Model validation for the more severe and injurious impacts is recommended. Since only few rear end impact experiments reproducing injury are available in the literature [180], additional experimental studies with PMHSs are recommended. These experiments should address the following aspects: a) head, T1 and pelvis kinematics, b) vertebral rotations, c) facet joint kinematics, d) ligament kinematics, e) injury monitoring. Additionally, simulations of accident reconstructions could give more insight in the injury biomechanics during a collision.

7.6   Conclusions

In this thesis a detailed multibody neck model has been presented. The model consists of a rigid head, rigid vertebrae, (non)linear viscoelastic discs, frictionless facet joints, nonlinear viscoelastic ligaments and segmented contractile muscles, which follow the curvature of the neck. The model is a major update of the De Jager model [65]. The neck model has been validated quasi-statically as well as dynamically. Quasi-statically, the model agreed reasonably with the experimental data and showed realistic 3D coupling effects. Dynamically, frontal (15 g), lateral (7 g), and rear end (0.7 g to 12 g) impact loadings have been simulated and the model showed reasonable to

good response. Frontal, lateral and rear end impact simulations provide comparable conclusions on the role of muscle activation, showing that inclusion of muscle activity seems necessary for realistic simulations of impact conditions with human volunteers. Although not shown conclusively by experimental research, the combined findings of numerical modelling and experimental research presented in literature indicate that neck muscles can alter the head and neck kinematics during a rear end impact. Reflex time, activation level, co-contraction and the initial activation of the muscles significantly influenced the head and neck motion, but even more so the local loads (forces in disc and contacts of the facets joints). Additionally, initial seating posture and head restraint position influenced the global and local head neck response in a rear end impact as was observed experimentally in the literature. Therefore, for accurate model validation as well as for simulation rear accidents exact information on muscle activation, seating posture and position of seat and head restraint is essential. The correlations found between predicted global injury criteria and local tissue loads with the simulations performed within this research are not strong. Therefore, it is questionable whether global injury criteria may be used to predict local injuries. Several loads, and in particular the facet joint contact forces appeared to be hardly correlated to global neck injury criteria. The model presented in this thesis is suitable for studying the neck injury mechanisms and neck injury criteria, since it reveals the loads and deformations of individual tissues of the neck.

References

[1] Aerospace Medical Panel's Specialistis's meeting, Paris, France. *Multiaxis dynamic response of the human head and neck to impact acceleration*, 1978.

[2] T. Aibe, K. Watanabe, T. Okamoto, and T. Nakamori. Influence of occupant seating posture and size on head and chest injuries in frontal collision. pages 231–238. Society of Automotive Engineers, 1982. SAE Paper No.826032.

[3] B. Aldman. An analytical approach to the impact biomechanics of head and neck injury. In *Proceedings 30th Annual AAAM Conference*, pages 439–454, 1986.

[4] Association for the Advancement of Automotive Medicine. *The Abbreviated Injury Scale - 1990 revision*, Des Plaines, Illinois, USA, 1990.

[5] D.E. Attarian, H.J. McCrackin, D.P. DeVito, J.H. McElhandy, and W.E. Garrett. Biomechanical characteristics of human ankle ligaments. *Foot & Ankle*, 6(2):54–58, 1985.

[6] L. Barnsley, S. Lord, and N. Bogduk. Clinical review: whiplash injury. *Pain*, 58:283–307, 1994.

[7] N. Bertholon. *Modelisation 3D du cou humain en situation de chocs omnidirectionnels analyse cinematique et aspects lesionnels*. PhD thesis, 1999. In French.

[8] N. Bertholon, S. Robin, J.-Y. Le Coz, P. Portier, J.-P. Lassau, and W. Skalli. Human head and cervical spine behaviour during low-speed rear-end impacts. PMHS sled tests with rigid seat. In *International IRCOBI Conference on the Biomechanics of Impacts*. IRCOBI, 2000.

[9] N. Bogduk. Neck pain. *Aust Fam Physician*, 13:26–30, 1984.

[10] N. Bogduk. Anatomy and pathophysiology of whiplash. *Clinical Biomechanics*, 1:92–101, 1986.

[11] N. Bogduk and A. Marsland. The cervical zygapophysical joints as a source of neck pain. *Spine*, 13:610–617, 1988.

[12] A.C. Bosio and B.M. Bowman. Simulation of head-neck dynamic response in -Gx and +Gy. In *Proceedings of the 30th Stapp Car Crash Conference*, pages 345–378. Society of Automotive Engineers, 1986. SAE Paper No. 861895.

[13] B.M. Bowman, L.W. Schneider, L.S. Lustick, W.R. Anderson, and D.J. Thomas. Simulation analysis of head and neck dynamic response. In *Proceedings of the 28th Stapp Car Crash Conference*, pages 173–205. Society of Automotive Engineers, 1984. SAE Paper No. 841668.

[14] J.R. Brault, G.P.Siegmund, and J.B. Wheeler. Whiplash injury biomechanics: cervical electromyographic response and influence on whiplash dynamics. In *Proceedings International Symposium Whiplash (SP-1406)*, page 25, 1998. Phoenix AZ.

[15] J.R. Brault, G.P. Siegmund, and J.B. Wheeler. Cervical muscle response during whiplash: Evidence of a lenghtening muscle contraction. *Clinical Biomechanics*, 15:426–435, 2000.

[16] J.R. Brault, T.A. Smith, J.B. Wheeler, and G.P. Siegmund. Cervical muscle response to rear-end automobile collisions: Implications for injury. In *Proceedings 3rd North American Congress on Biomechanics*, pages 347–348, 1998. Waterloo, Ontario.

[17] J.M. Brelin-Fornari. *A lumped parameter model of the human head and neck with active muscles*. PhD thesis, University of Arizona, USA, 1998.

[18] T. Brown, R.J. Hansen, and A.J. Yorra. Some mechanical tests on the lumbosacral spine with particular reference to intervertebral discs. *Journal of Bone and Joint Surgery*, 39:1135–1164, 1957.

[19] D.L. Camacho, R.W. Nightingale, D.J. Coates, S.K. Vanguri, and B.S. Myers. Dynamic response of a computational head-neck model to near-vertex head impact. In *Proceedings of the 7th Injury Prevention Through Biomechanics Symposium*, pages 149–178, Detroit, May 8,9 1997. Wayne State University.

[20] D.L. Camacho, R.W. Nightingale, J.J. Robinette, S.K. Vanguri, D.J. Coates, and B.S. Myers. Experimental flexibility measurements for the development of a computational head-neck model validated for near-vertex head impact. In *Proceedings of the 41st Stapp Car Crash Conference*, pages 473–486. Society of Automotive Engineers, 1997. SAE paper No. 973345.

[21] H. Cappon, M. Philippens, and J. Wismans. A new test method for the assessment of neck injuries in rear end collisions. In *Proceedings of the 17th ESV Conference, Amsterdam, The Netherlands*. NHTSA, USA, 2001. Paper No. 242.

[22] H. Chang, L.G. Gilbertson, V.K. Goel, J.M. Winterbottom, C.R. Clark, and A. Patwardhan. Dynamic response of the occipito-atlanto-axial (C0-C1-C2) complex in right axial rotation. *Journal of Orthopaedic Research*, 10:446–453, 1992.

[23] G.K. Cole, A.J. van den Bogert, W. Hertzog, and K.G.M. Gerritsen. Modelling of force production in skeletal muscle undergoing stretch. *Journal of Biomechanics*, 29(8):1091–1104, 1996.

[24] J.G. Colebatch, G.M. Halmagyi, and N.F. Skuse. Myogenic potentials generated by a click-evoked vestibulocollic reflex. *Journal of Neurology, Neurosurgery, and Psychiatry*, 57:190–197, 1994.

[25] H.E. Crow. Injuries to the cervical spine. *Presented at meeting of the western Orthopaedic Association, San Francisco*, 1928.

[26] R.D. Crowningshield and M.H. Pope. The strength and failure characteristics of rat medial collateral ligaments. *Journal of Trauma*, 16(2):99–105, 1976.

[27] M. Darok, E.P. Leizinger, A. Eichberger, and H. Steffan. Neck injury criterion validation using humand subjects and dummies. In N. Yoganandan and F.A. Pintar, editors, *Frontiers in Whiplash Trauma, Clinical and Biomechanical*, pages 409–434. IOS Press, Amsterdam, 2000. ISSN 0929-6743, ISBN 1-58603012-4.

[28] F. Dauvilliers, F. Bendjellal, M. Weiss, F. Lavaste, and C. Tarrière. Development of a finite element model of the neck. In *Proceedings of the 38th Stapp Car Crash Conference*, pages 77–91. Society of Automotive Engineers, 1994. SAE Paper No. 942210.

[29] J. Davidsson, C. Deutscher, W. Hell, A. Linder, P. Lövsund, and M.Y. Svensson. Human volunteer kinematics in rear-end sled collisions. In *International IRCOBI Conference on the Biomechanics of Impacts*, pages 289–302. IRCOBI, 1998.

[30] J. Davidsson, P. Lövsund, K. Ono, M.Y. Svensson, and S. Inami. A comparison between volunteer, Biorid P3 and Hybrid III performance in rear impacts. In *International IRCOBI Conference on the Biomechanics of Impacts*, pages 165–178. IRCOBI, 1999.

[31] B. Deng. *Kinematics of human cadaver cervical spine during low speed rear-end impacts*. PhD thesis, Wayne State University, Detroit, Michigan, 1999.

[32] Y.-C. Deng. *Human Head/Neck/Upper-Torso Model Response to Dynamic Loading*. PhD thesis, University of California, 1985.

[33] Y.-C. Deng and W. Goldsmith. Response of a human head/neck/upper-torso replica to dynamic loading - II. analytical/numerical model. *Journal of Biomechanics*, 20:487–497, 1987.

[34] J.M. Dorlot, M. Ait Ba Sidi, G.M. Tremblay, and G. Brouin. Load elongation behavior of the canine anterior crutiate ligament. *Journal of Biomechanical Engineering*, 102:190–193, 1980.

[35] J. Dvorak, E. Schneider, P. Saldinger, and B. Rahn. Biomechanics of the craniocervical region: the alar and transverse ligaments. *Journal of Orthopaedic Research*, 6:452–461, 1988.

[36] R. Eberlein, M. Frohlich, and E.M. Hasler. Finite-element-analyses of intervertebral discs: Structural components and properties. In *ECCM Proceedings of European Conference on Computation Mechanics*. ECCM, 1999.

[37] C.A. van Ee, A.L. Chasse, and B.S. Myers. Quantifiying skeletal muscle properties in cadaveric test speciments: Effects of mechanical loading, postmortem time, and freezer storage. *Journal of Biomechanical Engineering*, 122:9–14, 2000.

[38] A. Eichberger, H. Steffan, B. Geigl, M. Svensson, O. Boström, P.E. Leinzinger, and M. Darok. Evaluation of the applicability of the neck injury criterion (nic) in rear end impacts on the basis of human subject tests. In *International IRCOBI Conference on the Biomechanics of Impacts*, pages 321–333. IRCOBI, 1998.

[39] E.P. France *et al.* Failure characteristics of the medial collateral ligament of the knee: effects of high strain rate. *Aviation, Space, and Environmental Medicine*, 58:488, 1987.

[40] O. Boström *et al.* A new neck injury criterion candidate-based on injury findings in the cervical spinal ganglia after experimental neck extension trauma. In *International IRCOBI Conference on the Biomechanics of Impacts*, pages 123–136. IRCOBI, 1996.

[41] O. Boström *et al.* Prediction of neck injuries in rear impacts based on accident data and simulations. In *International IRCOBI Conference on the Biomechanics of Impacts*, pages 251–264. IRCOBI, 1997.

[42] H. Schrader et al. Natural evolution of late whiplash syndrome outside the medicolegal context. *The Lancet*, 347:1207–1211, 1996.

[43] M.L. Magnusson et al. Cervical electromyographic activity during low-speed rear impact. *European Spine Journal*, 8:118–125, 1999.

[44] R.W. Evans. Some observation on whiplash injuries. *Neurol Clin*, 10(4):975–997, 1992.

[45] C.L. Ewing and D.J. Thomas. Human head and neck response to impact acceleration. Monograph 21 USAARL 73-1, Naval Aerospace and Regional Medical Centre, Pensacola, 1972.

[46] C.L. Ewing, D.J. Thomas, L. Lustik, G.C. Willems, W.H. Muzzy III, E.B. Becker, and M.E. Jessop. Dynamic response of human and primate head and neck to +Gy impact acceleration. Report DOT HS-803-058, Naval Aerospace Medical Research Laboratory, Pensacola, 1978.

[47] D.R. Foust, D.B. Chaffin, R.G. Snyder, and J.K. Baum. Cervical range of motion and dynamic response and strength of cervical muscles. In *Proceedings of the 17th Stapp Car Crash Conference*, pages 285–308. Society of Automotive Engineers, 1973. SAE Paper No. 730975.

[48] Y.C. Fung. *Biomechanics: Mechanical Properties of Living Tissues*. Springer-Verlag, New York, 2nd edition, 1993.

[49] C.S.B. Galasko, P.A. Murray, and M. Pitcher. Whiplash associated disorders. In *Proceedings 15th International Technical Conference on Enhanced Safety of Vehicles*, pages 1504–1513. Melbourne, Australia, 1996.

[50] B.C. Geigl, H. Steffan, P. Leinzinger, P. Roll, M. Mühlbauer, and G. Bauer. The movement of head and cervical spine during rear end impact. In *International IRCOBI Conference on the Biomechanics of Impacts*, pages 127–137. IRCOBI, 1994.

[51] J.N. Grauer, M.M. Panjabi, J. Cholewicki, K. Nibu, and J. Dvorak. Whiplash produces an S-shaped curvature of the neck with hyperextension in lower levels. *Spine*, 22(21):2489–2494, 1997.

[52] R. Happee, M. Hoofman, A.J. van den Kroonenberg, P. Morsink, and J. Wismans. A mathematical human body model for frontal and rearward seated automotive impact loading. In *Proceedings of the 42nd Stapp Car Crash Conference*, pages 75–88. Society of Automotive Engineers, 1998. SAE Paper No. 983150.

[53] R. Happee, R. Meijer, K. Ono, M.J. van der Horst, and K. Yamazaki. Analysis of rear-end impact using mathematical human modelling. In *JSAE Spring Convention Proceedings No.37-00*, pages 9–12. JSAE, 2000. PaperNo. 20005335.

[54] R. Happee, P. Morsink, and J. Wismans. Mathematical human body modelling for impact loading. In *Digital Human Modelling for Design and Engineering, international conference The Hague*, pages 1–9. Society of Automotive Engineers, 1998. SAE Paper No. 1999-01-1909.

[55] R. Happee, S. Ridella, A. Nayef, P. Morsink, R. de Lange, R. Bours, and J. van Hoof. Mathematical human body models representing a mid size male and a small female for frontal, lateral and rearward impact loading. In *International IRCOBI Conference on the Biomechanics of Impacts*. IRCOBI, 2000.

[56] R. Happee and J. Thunnissen. Advances in human body modelling using MADYMO. In *Proceedings of the 5th International MADYMO User's Meeting*. TNO Crash Safety Centre, Delft, The Netherlands, 1994.

[57] R. Happee, R. van Haaster, L. Michaelsen, and R. Hoffmann. Optimisation of vehicle passive safety for occupants with varying antrhopometry. In *Proceedings of the 15th ESV Conference*. NHTSA, USA, 1998. Paper No. 98-S9-O-03.

[58] R. Happee, M. M. Verver, and R. de Lange. Mathematical human body modelling for impact loading and comfort. In *Ergonomie und Verkehrssicherheit*, pages 47–63. Technische Universität München, Konferenzbeiträge der Herbstkonferenz, 2000.

[59] W. Hell, S. Schick, and K. Langwieder. Epidemiology of cervical spine injuries in rear-end collisions and influence of different anthropometric parameters in human volunteer tests. In N. Yoganandan and F.A. Pintar, editors, *Frontiers in Whiplash Trauma, Clinical and Biomechanical*, pages 146–169. IOS Press, Amsterdam, 2000. ISSN 0929-6743, ISBN 1-58603012-4.

[60] M.J. van der Horst, P.H.M. Bovendeerd, R. Happee, J.S.H.W. Wismans, and H. Kingma. Simulation of rear end impact with a full body human model with a detailed neck: role of passive muscle properties and initial seating posture. In *Proceedings of the 17th ESV Conference, Amsterdam, The Netherlands*. NHTSA, USA, 2001. Paper No. 119.

[61] M.J. van der Horst, J.G.M. Thunnissen, R. Happee, R.M.H.P. van Haaster, and J.S.H.M. Wismans. The influence of muscle activity on head-neck response during impact. In *Proceedings of the 41st Stapp Car Crash Conference*, pages 487–507. Society of Automotive Engineers, 1997. SAE Paper No. 973346.

[62] R.L. Huston, J.C. Huston, and M.W. Harlow. Comprehensive, three-dimensional head-neck model for impact and high-acceleration studies. *Aviation, Space, and Environmental Medicine*, 49:205–210, 1978.

[63] M. de Jager, A. Sauren, J. Thunnissen, and J. Wismans. A three-dimensional head-neck model: Validation for frontal and lateral impacts. In *Proceedings of the 38th Stapp Car Crash Conference*, pages 93–109. Society of Automotive Engineers, 1994.

[64] M. de Jager, A. Sauren, J. Thunnissen, and J. Wismans. A global and a detailed mathematical model for head-neck dynamics. In *Proceedings of the 40th Stapp Car Crash Conference*, pages 269–281. Society of Automotive Engineers, 1996. SAE Paper No. 962430.

[65] M.K.J. de Jager. *Mathematical Head-Neck Models for Acceleration Impacts*. PhD thesis, University of Eindhoven, 1996.

[66] L. Jakobsson, H. Norin, C. Jernström, S.-E. Svensson, P. Johnsén, I. Isaksson-Hellman, and M.Y. Svensson. Analysis of different head and neck responses in rear-end car collisions using a new humanlike mathematical model. In *International IRCOBI Conference on the Biomechanics of Impacts*, pages 109–125. IRCOBI, 1994.

[67] G.C. Joyce, R.M.H Rack, and D.R. Westbury. The mechanical properties of cat soleus muscle during controlled lengthening and shortening movement. *Journal of Physiology*, 204:461–474, 1969.

[68] D. Kallieris, A. Rizzeti, R. Mattern, J. Thunnissen, and M. Phillippens. Cervical human spine loads during traumatomechanical investigations. In *International IRCOBI Conference on the Biomechanics of Impacts*, pages 89–105. IRCOBI, 1996.

[69] I.A. Kapandji. *The Physiology of the Joints, Volume 3: The Trunk and the Vertebral Column*. Churchill Livingstone, Edinburg, 2nd edition, 1974.

[70] M. Kleinberger. Application of finite element techniques to the study of cervical spine mechanics. In *Proceedings of the 37th Stapp Car Crash Conference*, pages 261–272. Society of Automotive Engineers, 1993.

[71] A. van der Kroonenberg, M. Philippens, H. Cappon, J. Wismans, W. Hell, and K. Langwieder. Human head-neck response during low-speed rear end impacts. In *Proceedings of the 42nd Stapp Car Crash Conference*, pages 207–221. Society of Automotive Engineers, 1998. SAE no. 983158.

[72] A. van der Kroonenberg, J. Thunnissen, and J. Wismans. A human model for low-severity rear-impacts. In *International IRCOBI Conference on the Biomechanics of Impacts*, pages 117–132. IRCOBI, 1997.

[73] A.M. Krylow and Th.G. Sandercock. Dynamic force responses of muscle involving eccentric contraction. 30(1):27–33, 1997.

[74] S. Kumaresan, N. Yoganandan, and F.A. Pintar. Finite element modeling approaches of human cercial spine facet joint capsule. *Journal of Biomechanics*, 31:371–376, 1998.

[75] E. Lizee, S. Robin, E. Song, N. Bertholon, J.Y. Le Coz, B. Besnault, and F. Lavaste. Development of a 3D finite element model of the human body. In *Proceedings of the 42nd Stapp Car Crash Conference*, pages 115–138. Society of Automotive Engineers, 1998. SAE Paper No. 983152.

[76] C. Lydon, J.J. Crisco, M. Panjabi, and M. Galloway. Effect of elongation rate on the failure properties of the rabbit anterior crutiate ligament. *Clinical Biomechanics*, 10(8):428–433, 1995.

[77] K. Mabuchi, K. Hayatsu, H. Fujie, and M. Yamamoto. Stiffness of canine stifle joint ligaments at relatively high rates of elongation. *Journal of Biomechanical Engineering*, 113:404–409, 1991.

[78] I. Macnab. Acceleration injuries of the cervical spine. *J Bone Joint Surg*, 46, 1964.

[79] A. Magid and D. Law. Myofibrils bear most of the resting tension in frog skeletal muscle. *Science*, 230:1280–1282, 1985.

[80] K.L. Markolf and J.M. Morris. The structural components of the intervertebral disc. A study of their contributions to the ability of the disc to withstand compressive force. *Journal of Bone and Joint Surgery*, 56:675–687, 1974.

[81] H.J. Marotzki. Isometric measurements of the forces at the head-neck system with younger and older people. *Arch. Orthop. Unfall. Chir.*, 74:42–62, 1972.

[82] T. Matsushita, T.B. Sato, K. Hirabayashi, S. Fujimura, T. Asazuma, and T. Takatori. X-ray study of the human neck motion due to head inertia loading. In *Proceedings of the 38th Stapp Car Crash Conference*, pages 55–64. Society of Automotive Engineers, 1994. SAE Paper No. 942208.

[83] M.A. Mayoux-Benhamou, M. Wybier, and M. Revel. Strength and cross-sectional area of the dorsal neck-muscles. *Ergonomics*, 32:513–518, 1989.

[84] W.E. McConnell, R.P. Howard, H.M. Guzman, J.B. Bomar, J.H. Raddin, J.V. Benedict, H.L. Smith, and C.P. Hatsell. Analysis of human test subject kinematic responses to low velocity rear end impacts. In *Vehicle and Occupant Kinematics: Simulation and Modelling*, pages 21–30. Society of Automotive Engineers, 1993. SAE Special Publication SP-975, Paper No. 930889.

[85] W.E. McConnell, R.P. Howard, J. Van Poppel, R. Krause, H.M. Guzman, J.B. Bomar, J.H. Raddin, J.V. Benedict, and C.P. Hatsell. Human head and neck kinematics after low velocity rear-end impacts – Understanding "whiplash". In *Proceedings of the 39th Stapp Car Crash Conference*, pages 215–238. Society of Automotive Engineers, 1995. SAE Paper No. 952724.

[86] J.H. McElhaney, J.G. Paver, H.J. McCrackin, and G.M. Maxwell. Cervical spine compression responses. In *Proceedings of the 27th Stapp Car Crash Conference*, pages 163–177. Society of Automotive Engineers, 1983. SAE Paper No. 831615.

[87] H.J. Mertz. Anthropomorphic test devices. In A.M. Nahum and J.W. Melvin, editors, *Accidental Injury: Biomechanics and Prevention*, chapter 4, pages 66–84. Springer-Verlag, 1993.

[88] H.J. Mertz and Patrick L.M. Investigation of the kinematics and kinetics of whiplash. In *Proceedings of the 11th Stapp Car Crash Conference*, pages 267–317. Society of Automotive Engineers, 1967. SAE Paper No. 670919.

[89] N. Milne. The role of zygapophysial joint orientation and uncinate processes in controlling motion in the cervical spine. *Journal of Anatomy*, 178:189–201, 1991.

[90] S.P. Moroney, A.B. Schultz, J.A.A. Miller, and G.B.J. Andersson. Load-displacement properties of lower cervical spine motion segments. *Journal of Biomechanics*, 21:769–779, 1988.

[91] A.P. Morris and P. Thomas. Neck injuries in the UK co-operative crash injury study. In *Proceedings of the 40th Stapp Car Crash Conference*, pages 317–329. Society of Automotive Engineers, 1996. SAE Paper No. 962433.

[92] M.H. Muser, F.H Walz, and K.U. Schmitt. Injury criteria applied to seat comparison tests. In *Dynamic testing for Whiplash Injury Risk*. International Insurance Whiplash Prevention Group, IRCOBI, 2001.

[93] B.S. Myers. Cervical spine muscle. Final Report F.2c, Duke University, Durham, North Carolina, USA, 1998.

[94] J.B. Myklebust, F. Pintar, N. Yoganandan, J.F. Cusick, D. Maiman, T.J. Myers, and A. Sances Jr. Tensile strength of spinal ligaments. *Spine*, 13:526–531, 1988.

[95] R.W. Nightingale, J.H. McElhaney, D.L. Camacho, M. Kleinberger, B.A. Winkelstein, and B.S. Myers. The dynamic responses of the cervical spine: Buckling, end conditions, and tolerance in compressive impacts. In *Proceedings of the 41st Stapp Car Crash Conference*, pages 451–471. Society of Automotive Engineers, 1997. SAE paper No. 973344.

[96] S. Nitsche, G. Krabbel, H. Appel, and E. Haug. Validation of a finite element model of the human neck. In *International IRCOBI Conference on the Biomechanics of Impacts*, pages 107–122. IRCOBI, 1996.

[97] F.R. Noyes, J.L. DeLucas, and P.J. Torvik. Biomechanics of anterior cruciate ligament failure: An analysis of strain-rate sensitivity and mechanisms of failure in primates. *Journal of Bone and Joint Surgery*, 56, 1974.

[98] Å. Nygren. Injuries to car occupants. Some aspects of the interior safety of cars. *Akta Oto-Laryngological*, (Supplement 395), 1984. ISSN 0365-5237.

[99] T. Oda, M.M. Panjabi, J.J. Crisco III, H.U. Bueff, D. Grob, and J. Dvorak. Role of tectorial membrane in the stability of the upper cervical spine. *Clinical Biomechanics*, 7:201–207, 1992.

[100] T. Oda, M.M. Panjabi, and J.J. Crisco III. Three-dimensional translational movements of the upper cervical spine. *Journal of Spinal Disorders*, 4:411–419, 1991.

[101] B. O'Neill, W. Haddon, A.B. Kelly, and W.W. Sorenson. Automobile head restraints: Frequency of neck injury insurance claims in relation to the presence of head restraints. *American Journal of Public Health*, 62(3):399–406, 1972.

[102] K. Ono, S. Inami, K. Kaneoka, T. Gotou, Y. Kisanuki, S. Sakuma, and K. Miki. Relationship between localized spine deformation and cervical vertebral motions for low speed rear impacts using human volunteers. In *International IRCOBI Conference on the Biomechanics of Impacts*, pages 149–164. IRCOBI, 1999.

[103] K. Ono and K. Kaneoka. Motion analysis of human cervical vertebrae during low speed rear impacts by the simulated sled. In *International IRCOBI Conference on the Biomechanics of Impacts*, pages 223–238. IRCOBI, 1997.

[104] K. Ono, K. Kaneoka, and S. Inami. Influence of seat properties on human cervical vertebral motion and head-neck-torso kinematics during rear-end impacts. In *International IRCOBI Conference on the Biomechanics of Impacts*, pages 303–318. IRCOBI, 1998.

[105] K. Ono, K. Kaneoka, A. Wittek, and J. Kajzer. Cervical injury mechanism based on the analysis of human cervical vertebral motion and head-neck torso kinematics during low speed rear impacts. In *Proceedings of the 41th Stapp Car Crash Conference*, pages 339–356. Society of Automotive Engineers, 1997. SAE Paper No 973340.

[106] K. Ono and M. Kanno. Influences of the physical parameters on the risk to neck injuries in low impact speed rear-end collisions. In *International IRCOBI Conference on the Biomechanics of Impacts*, pages 201–212. IRCOBI, 1993.

[107] M. Panjabi, J. Dvorak, J. Duranceau, I. Yamamoto, M. Gerber, W. Rauschning, and H.U. Bueff. Three-dimensional movements of the upper cervical spine. *Spine*, 13:726–730, 1988.

[108] M. Panjabi, J. Dvorak, J.J. Crisco III, T. Oda, P. Wang, and D. Grob. Effects of alar ligament transection on upper cervical spine rotation. *Journal of Orthopaedic Research*, 9:584–593, 1991.

[109] M.M. Panjabi, J. Cholewicki, K. Nibu, J. Grauer, and M. Vahldiek. Capsular ligament stretches during in vitro whiplash simulations. *Journal of Spinal Disorders*, 11(3):227–232, 1998.

[110] M.M. Panjabi, J.J. Crisco, C. Lydon, and J. Dvorak. The mechanical properties of human alar and transverse ligaments at slow and fast extension rates. *Clinical Biomechanics*, 13(2):112–120, 1998.

[111] M.M. Panjabi, J. Duranceau, V. Goel, T. Oxland, and K. Takata. Cervical human vertebrae: Quantitative three-dimensional anatomy of the middle and lower regions. *Spine*, 16:861–869, 1991.

[112] M.M. Panjabi, J. Dvorak, J.J. Crisco III, T. Oda, A. Hilibrand, and D. Grob. Flexion, extension, and lateral bending of the upper cervical spine in response to alar ligament transections. *Journal of Spinal Disorders*, 4:157–167, 1991.

[113] M.M. Panjabi, T. Oxland, K. Takata, V. Goel, J. Duranceau, and M. Krag. Articular facets of the human spine: quantitative three-dimensional anatomy. *Spine*, 18:1298–1310, 1993.

[114] M.M. Panjabi, K. Takata, V. Goel, D. Frederico, T.Oxland, J. Duranceau, and M. Krag. Thoracic human vertebrae: quantitative three-dimensional anatomy. *Spine*, 16:888–901, 1991.

[115] M.M. Panjabi, J. Wang, and N. Delson. Neck injury criterion based on intervertebral motions and its evaluation using an instrumented neck dummy. In *International IRCOBI Conference on the Biomechanics of Impacts*, pages 179–190. IRCOBI, 1999.

[116] S. Parkin, G.M. Mackay, and A. Cooper. How drivers sit in cars. In *37th Annual Proceedings*, pages 375–388. Association for the advancement of automotive medicine, 1993.

[117] L. Penning. Acceleration injury of the cervical spine by hypertranslation of the head. Part I: Effect of normal translation of the head on cervical spine motion: a radiologic study. *European Spine Journal*, 1:7–12, 1992.

[118] L. Penning. Acceleration injury of the cervical spine by hypertranslation of the head. Part II: Effect of normal translation of the head on cervical spine motion: discussion of literature data. *European Spine Journal*, 1:13–19, 1992.

[119] F.A. Pintar. *The Biomechanics of Spinal Elements*. PhD thesis, Marquette University, 1986.

[120] F.A. Pintar, J.B. Myklebust, A. Sances Jr., and N. Yoganandan. Biomechanical properties of the human intervertebral disk in tension. In *1986 Advances in Bioengineering*, pages 38–39. American Society of Mechanical Engineers, 1986.

[121] F.A. Pintar, N. Yoganandan, M. Pesigan, J.M. Reinartz, A. Sances Jr., and J.F. Cusick. Cervical vertebral strain measurements under axial and eccentric loading. *Journal of Biomechanical Engineering*, 117(4):474–478, 1995.

[122] F.A. Pintar, N. Yoganandan, A. Sances Jr., J. Reinartz, G. Harris, and S.J. Larson. Kinematic and anatomical analysis of the human cervical spinal column under axial loading. In *Proceedings of the 33rd Stapp Car Crash Conference*, pages 191–214. Society of Automotive Engineers, 1989. SAE Paper No. 892436.

[123] W. Platzer, editor. *Pernkopf Anatomy. Atlas of Topographic and Applied Human Anatomy*, volume 1: Head and Neck. Urban & Schwarzenberg Baltimore–Munich, 3rd edition, 1989.

[124] D.P. Quiring. *The Head, Neck, and Trunk. Muslces and Motor Points*. Lea & Febiger, Philadelphia, 1947.

[125] P.M.H. Rack and D.R. Westbury. The effects of lenght and stimulus rate on tension in the isometric cat soleus muscle. *J. of Physiology*, 204:443–460, 1969.

[126] M.P. Reed and C.A.C. Flannagan. Anthropometric and psotural variability: Limitations of the boundary manikin approach. In *Digital Human Modelling for Design and Engineering, international conference Michigan*, pages 1–6. Society of Automotive Engineers, 2000. SAE Paper No. 2000-01-2172.

[127] S.E. Reid, G. Raviv, and S.E. Reid, Jr. Neck muscle resistance to head impact. *Aviation, Space, and Environmental Medicine*, pages 78–84, 1981.

[128] R.E. Roberson and R. Schwertassek. *Dynamics of Multibody Systems*. Springer-Verlag, 1988.

[129] K.U. Schmitt, M.H. Muser, and P. Niederer. A new neck injury criterion candidate for rear end collisions taking into account shead forces and bending moments. In *Proceedings of the 17th ESV Conference, Amsterdam, The Netherlands*. NHTSA, USA, 2001. Paper No. 124.

[130] L.W. Schneider, D.R. Foust, B.M. Bowman, R.G. Snyder, D.B. Chaffin, T.A. Abdelnour, and J.K. Baum. Biomechanical properties of the human neck in lateral flexion. In *Proceedings of the 19th Stapp Car Crash Conference*, pages 455–485. Society of Automotive Engineers, 1975. SAE Paper No. 751156.

[131] M.R. Seemann, W.H. Muzzy, and L.S. Lustick. Comparison of human and Hybrid III head and neck dynamic response. In *Proceedings of the 30th Stapp Car Crash Conference*. Society of Automotive Engineers, 1986. SAE Paper No. 861892.

[132] A. Seireg and R.J. Arvikar. *Biomechanical Analysis of the Muscoloskeletal Structure for Medicine and Sports*. Hemisphere Publishing Corporation, New York, NY, 1989.

[133] D.M. Severy, J.H. Mathewson, and C.O. Bechtol. Controlled automobile rear end collisions - an investigation of related engineering and medical phenomena. *Canadian Services Medical Journal*, pages 727–759, 1955.

[134] G.P. Siegmund and J.R. Brault. Role of cervical muscles during whiplash. In N. Yoganandan and F.A. Pintar, editors, *Frontiers in Whiplash Trauma, Clinical and Biomechanical*, pages 295–320. IOS Press, Amsterdam, 2000. ISSN 0929-6743, ISBN 1-58603012-4.

[135] G.P. Siegmund, D.J. King, J.M. Lawrence, J.B. Wheeler, J.R. Brault, and T.A Smith. Head/neck kinematic response of human subjects in low-speed rear-end collisions. In *Proceedings of the 41th Stapp Car Crash Conference*, pages 357–385. Society of Automotive Engineers, 1997. SAE Paper No. 973341.

[136] R.G. Snyder, D.B. Chaffin, and D.R. Foust. Bioengineering study of basic physical measurements related to susceptibility to cervical hyperextension-hyperflexion injury. Report UM-HSRI-BI-75-6, Highway Safety Research Institute, University of Michigan, Ann Arbor, Michigan, 1975.

[137] W.O. Spitzer, M.L. Skovron, L.R. Salmi, J.D. Cassidy, J. Duranceau, S. Suissa, and E. Zeiss. Scientific monograph of the Quebec task force on whiplash-associated disorders: redefining 'whiplash' and its management. *Spine*, 20(8S):S2–S73, 1995.

[138] M. Sturzenegger, G. DiStefano, B.P. Radanov, and A. Schnidrig. Presenting symptoms and signs after whiplash injury: the influence of accident mechanisms. *Neurology*, 44:688–693, 1994.

[139] M.Y. Svensson, B. Aldman, H.A. Hansson, P. Lövsund, T. Seeman, A. Suneson, and T. Örtengren. Pressure effects in the spinal canal during whiplash motion - a possible cause of injury to the cervical spinal ganglia. In *International IRCOBI Conference on the Biomechanics of Impacts*, pages 189–200. IRCOBI, 1993.

[140] T.J. Szabo. Influence of seat properties on occupant kinematics. In N. Yoganandan and F.A. Pintar, editors, *Frontiers in Whiplash Trauma, Clinical and Biomechanical*, pages 348–371. IOS Press, Amsterdam, 2000. ISSN 0929-6743, ISBN 1-58603012-4.

[141] T.J. Szabo and J.B. Welcher. Human subject kinematics and electromyographic activity during low speed rear-end impacts. In *Proceedings of the 40th Stapp Car Crash Conference*, pages 295–315. Society of Automotive Engineers, 1996. SAE Paper No. 962432.

[142] T.J. Szabo, J.B. Welcher, R.D. Anderson, M.M. Rice, J.A. Ward, L.R. Paulo, and N.J. Carpenter. Human occupant kinematic response to low speed rear-end impacts. In *Occupant Containment and Methods of Assessing Occupant Protection in the Crash Environment*. Society of Automotive Engineers, 1994. SAE Special Publication SP-1045, Paper No. 940532.

[143] S.A. Tennyson, N.K. Mital, and A.I. King. Electromyographic signals of the spinal musculature during +Gz impact acceleration. *Orthopedic Clinics of North America*, 8:97–119, 1977.

[144] J.G.M. Thunnissen. Analysis of human head-neck response during low severity rear-end impacts. Report 96.OR.BV.041.1/JTH, TNO Crash Safety Centre, Delft, The Netherlands, 1996.

[145] J.G.M. Thunnissen. Human response in extension: A literature review. Report 97.BV.OR.021.1/JTH, TNO Crash Safety Centre, Delft, The Netherlands, 1997.

[146] J.G.M. Thunnissen, J.S.H.M. Wismans, C.L. Ewing, and D.J. Thomas. Human volunteer head-neck response in frontal flexion: a new analysis. In *Proceedings of the 39th Stapp Car Crash Conference*, pages 439–460. Society of Automotive Engineers, 1995. SAE Paper No. 952721.

[147] C.S. Tien and R.L. Huston. Numerical advances in gross-motion simulations of head/neck dynamics. *Journal of Biomechanical Engineering*, 109:163–168, 1987.

[148] C. Tingvall. Personal communication between J. Thunnissen and C. Tingvall. Department of Injury Prevention S-412 96, Chalmers University of Technology, Göteborg, Sweden, 1993.

[149] TNO Crash Safety Centre, Delft, The Netherlands. *MADYMO Application Manual, Version 5.4*, 1999.

[150] TNO Crash Safety Centre, Delft, The Netherlands. *MADYMO Theory Manual, Version 5.4*, 1999.

[151] TNO Crash Safety Centre, Delft, The Netherlands. *MADYMO User's Manual, Version 5.4*, 1999.

[152] J. Tonetti, M. Peoc'h, P. Merloz, B. Pasquier, and J.P. Chirossel. Elastic reinforcement and thickness of the joint capsules of the lower cervical spine. *Surg. Radiol. Anat.*, 21:35–39, 1999.

[153] VdS. Fahrzeugsicherheit 90, Ein Betrag zur Analyse des Unfallgeschehens. Report, VdS, Munich, Germany, 1994. (in German).

[154] D.C. Viano. Biomechanics of bone and tissue: A review of material properties and failure characteristics. In *Biomechanics and Medical Aspects of Lower Limb Injuries*, pages 33–64. Society of Automotive Engineers, 1986.

[155] D.C. Viano and J. Davidsson. Neck displacements of volunteers, BIORID P3 and HYBRID III in rear impacts: implication to whiplash assessment by a neck displacement criterion NDC. In *Dynamic testing for Whiplash Injury Risk*. International Insurance Whiplash Prevention Group, IRCOBI, 2001.

[156] B. Walmsley and U. Proske. Comparison of stiffness of soleus and medial gastrocnemius muscles in cats. *J. Neurophysiol.*, 46:250–259, 1981.

[157] J.B. Wheeler, T.A. Smith, G.P Siegmund, J.B. Brault, and D.J. King. Validation of the neck injury criterion (NIC) using kinematic and clinical results from human subjects in rear-end collisions. In *International IRCOBI Conference on the Biomechanics of Impacts*, pages 335–348. IRCOBI, 1998.

[158] A.A. White III and M.M. Panjabi. *Clinical Biomechanics of the Spine*. J.B. Lippincott Company, 2nd edition, 1990.

[159] J.L. Williams and T.B. Belytschko. A three-dimensional model of the human cervical spine for impact simulation. *Journal of Biomechanical Engineering*, 105:321–331, 1983.

[160] B.A. Winkelstein and B.S. Myers. Cervical motion segment, combined loading, muscle forces, and facet joint: A mechanical hypothesis for whiplash injury. In N. Yoganandan and F.A. Pintar, editors, *Frontiers in Whiplash Trauma, Clinical and Biomechanical*, pages 248–262. IOS Press, Amsterdam, 2000. ISSN 0929-6743, ISBN 1-58603012-4.

[161] J. M. Winters and L. Stark. Analysis of fundamental human movement patterns through the use of in-depth antagonistic muscle models. *IEEE Transactions on Biomedical Engineering*, BME-32:826–839, 1985.

[162] J.M. Winters. Hill-based muscle models: A systems engineering perspective. In J.M. Winters and S.L-Y. Woo, editors, *Multiple Muscle Systems: Biomechanics and Movement Organization*, pages 69–93. Springer-Verlag, 1990.

[163] J.M. Winters and J.D. Peles. Neck muscle activity and 3-D head kinematics during quasi-static and dynamic tracking movements. In J.M. Winters and S.L-Y. Woo, editors, *Multiple Muscle Systems: Biomechanics and Movement Organization*, pages 461–480. Springer-Verlag, 1990.

[164] J.M. Winters and L. Stark. Estimated mechanical properties of synergistic muscles involved in movements of a variety of human joints. *Journal of Biomechanics*, 21:1027–1041, 1988.

[165] J. Wismans, M. Philippens, E. van Oorschot, D. Kallieris, and R. Mattern. Comparison of human volunteer and cadaver head-neck response in frontal flexion. In *Proceedings of the 31st Stapp Car Crash Conference*. Society of Automotive Engineers, 1987. SAE Paper No. 872194.

[166] J. Wismans, E. van Oorschot, and H.J. Woltring. Omni-directional human head-neck response. In *Proceedings of the 30th Stapp Car Crash Conference*. Society of Automotive Engineers, 1986. SAE Paper No. 861893.

[167] J.S.H.M Wismans. Reduction of neck injuries and their societal costs in rear end collisions. In *First European Vehicle Passive Safety Network Conference*, 2000.

[168] J.S.H.M. Wismans and C.G. Huijskens. Incidentie & preventie van het "whiplash" trauma (Incidence and prevention of the 'whiplash' trauma). report 94.OR.BV.041.1/JW, TNO Crash Safety Centre, Delft, The Netherlands, 1994. (in Dutch).

[169] J.S.H.M. Wismans, E.G. Janssen, M. Beusenberg, W.P. Koppens, R. Happee, and P.H.M. Bovendeerd. *Injury Biomechanics*. Course Notes (4J610). Eindhoven University of Technology, Eindhoven, The Netherlands, 2000.

[170] J. Wittenburg. *Dynamics of Systems of Rigid Bodies*. Teubner, Stuttgart, 1977.

[171] S. L-Y. Woo, R.H. Peterson, K.J. Ohland, T.J. Sites, and M.I Danton. The effects of strain rate on the properties of the medial collateral ligament in skeletally immature and mature rabbits: a biomechanical and histological study. *Journal of Orthopaedic Research*, 8(5):712–721, 1990.

[172] H. Yamada. *Strength of Biological Materials*. Williams and Wilkins, Baltimore, 1970. Editor: F.G. Evans.

[173] K.Y. Yang, P.C. Begeman, M. Muser, P. Niederer, and F. Wa lz. On the role of cervical facet joints in rear end impact neck inju ry mechanisms. In *Motor Vehicle Safety Design Innovations*, pages 127–129. Society of Automotive Engineers, 1997. SAE Paper No. 970497.

[174] K.Y. Yang, F. Zhu, F. Luan, L. Zhoa, and P.C. Begeman. Development of a finite element model of the human neck. In *Proceedings of the 42nd Stapp Car Crash Conference*, pages 195–205. Society of Automotive Engineers, 1998. SAE Paper No. 983157.

[175] N. Yoganandan, F. Pintar, J. Butler, J. Reinartz, A. Sances Jr., and S.J. Larson. Dynamic response of human cervical spine ligaments. *Spine*, 14:1102–1110, 1989.

[176] N. Yoganandan and F.A. Pintar. *Frontiers in Whiplash Trauma, Clinical and Biomechanical*. IOS Press, Amsterdam, 2000. ISBN 1586030124.

[177] N. Yoganandan, F.A. Pintar, and M. Klienberger. Cervical spine vertebral and facet joint kinematics under whiplash. *Journal of Biomechanical Engineering*, 120:305–307, 1998.

[178] N. Yoganandan, F.A. Pintar, S. Kumaresan, and A. Elhagediab. Biomechanical assessment of human cervical spine ligaments. In *Proceedings of the 42nd Stapp Car Crash Conference*, pages 223–236. Society of Automotive Engineers, 1998. SAE Paper No. 983159.

[179] N. Yoganandan, F.A. Pintar, and B.D. Stemper. Single rear impact produces lower cervical spine soft tissue injuries. In *International IRCOBI Conference on the Biomechanics of Impacts*, pages 201–211. IRCOBI, 2001.

[180] N. Yoganandan, F.A. Pintar, B.D. Stemper, M.B. Schlick, M. Philippens, and J. Wismans. Biomechanics of human occupants in simulated rear crashes: Documentation of injuries, determinations of forces and moments at the occipital condyles, and comparison of injury metrics with proposed injury criteria. In *STAPP Car Crash journal 44*, pages 189–204, 2000.

[181] F.E. Zajac. Muscle and tendon: properties, models, scaling, and application to biomechanics and motor control. *CRC Critical Reviews in Biomedical Engineering*, 17:359–411, 1989.

Appendix A

Muscle geometry

In Tables A.1, A.2 and A.3 the muscle geometry used in the neck model is presented. The muscles in the new neck model are shown in Figures A.1, A.2 and A.3.

Table A.1: *Flexor muscles in the neck model (see Figure A.1).*

No.	Flexor muscle	Origin	Insertion	PCSA in model cm^2	PCSA Myers [93] cm^2	s_{rest} Myers [93] μm
1	Longus colli	T1	C6	0.3914		
2	Longus colli	T1	C5	0.3914		
3	Longus colli	T1	C4	0.3914		
4	Longus colli	T1	C3	0.3914		
5	Longus colli	T1	C2	0.3914		
6	Longus colli	T1	C1	0.3914		
7	Longus colli	T1	Skull	0.3914		
	TOTAL longus colli[o]			2.74[b]	[a]	2.66[d]
8	Longus capitis	C3	Skull	0.3425		
9	Longus capitis	C4	Skull	0.3425		
10	Longus capitis	C5	Skull	0.3425		
11	Longus capitis	C6	Skull	0.3425		
	TOTAL longus capitis [o]			1.37	1.37	2.9
12	Scalenus anterior [o]	T1	C4	1.88	1.88	3.1
13	Scalenus medius [o]	T1	C3	1.36	1.36	2.8
14	Scalenus posterior [o]	T1	C5	1.05	1.05	2.6
15	Lumped hyoids [c,*]	T1	Skull	2.35	2.35	2.66[d]

[*] new compared to De Jager model
[o] modified compared to De Jager model
[a] no data available
[b] arbitrarily chosen as two times the PCSA longus capitis
[c] the sum of the PCSAs of omohyoid, sternohyoid, sternothryhoid and thryhoid
[d] average of s_{rest} because no data available
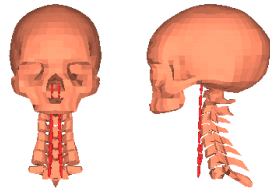
(a) Longus colli
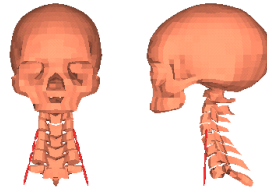
(b) Scalenus anterior
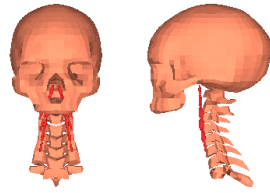
(c) Longus capitis
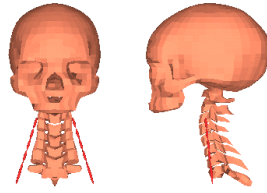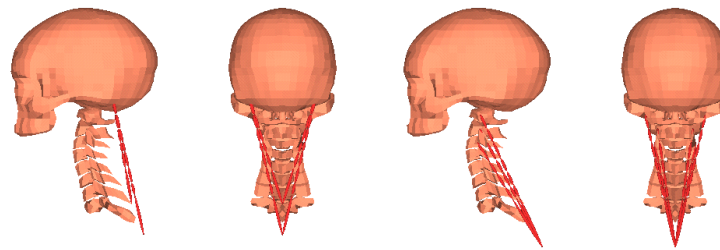
(d) Scalenus medius
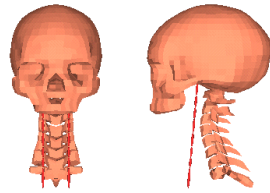
(e) Lumped hyoid
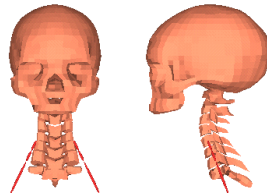
(f) Scalenus posterior

Figure A.1: *Flexor muscles in the neck model (see Table A.1), frontal and lateral view.*
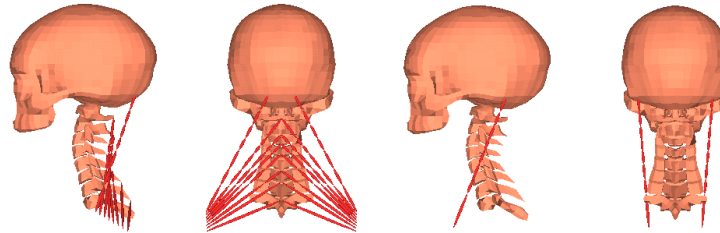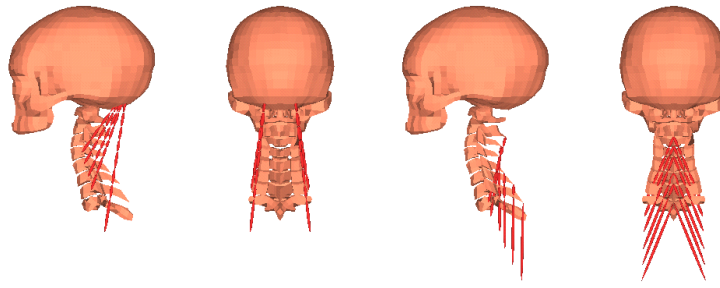
(a) Trapezius

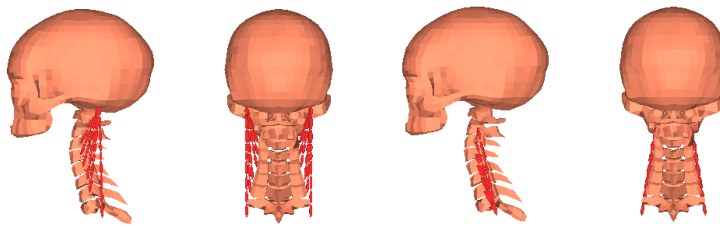(b) Sternocleidomastoid

(c) Splenius capitis

(d) Splenius cervicis

Figure A.2: *Extensor muscles in the neck model (part 1, see Table A.2); lateral and rear view.*
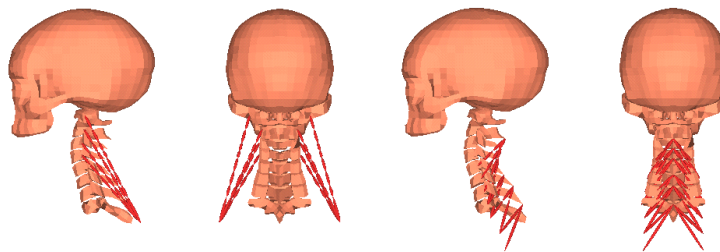
(a) Semispinalis capitis

(b) Semispinalis cervicis

(c) Longissimus capitis

(d) Longissimus cervicis

(e) Levator scapulae

(f) Multifidus cervicis

Figure A.3: *Extensor muscles in the neck model (part 2, see Table A.3); lateral and rear view.*

Table A.2: *Extensor muscles in the neck model (part 1, see Figure A.2).*

No.	Extensor muscle	Origin	Insertion	PCSA in model cm^2	PCSA Myers [93] cm^2	s_{rest} Myers [93] μm
16	Trapezius	T1	Skull	0.4713		
17	Trapezius	T1	C1	0.4713		
18	Trapezius	T1	C2	0.4713		
19	Trapezius	T1	C3	0.4713		
20	Trapezius	T1	C4	0.4713		
21	Trapezius	T1	C5	0.4713		
22	Trapezius	T1	C6	0.4713		
23	Trapezius	T1	C7	0.4713		
	TOTAL Trapezius [a],[o]			3.77	3.77	2.8
24	Sternocleidomastoid [o]	T1	Skull	4.92	4.92	2.9
25	Splenius capitis	C7	Skull	1.545		
26	Splenius capitis	T2	Skull	1.545		
	TOTAL Splenius capitis [o]			3.09	3.09	2.7
27	Splenius cervicis	T3	C3	0.833		
28	Splenius cervicis	T3	C2	0.833		
29	Splenius cervicis	T3	C1	0.833		
	TOTAL Splenius cervicis [o]			2.5	1.43	2.6

[*] new compared to De Jager model

[o] modified compared to De Jager model

[a] only that part of trapezius that originates from the base of the skull
and inserts on the scapula; 25 % of total PCSA [93]

Table A.3: *Extensor muscles in the neck model (part 2, see Figure A.2).*

No.	Extensor muscle	Origin	Insertion	PCSA in model cm^2	PCSA Myers [93] cm^2	s_{rest} Myers [93] μm
30	Semispinalis capitis	C4	Skull	0.9		
31	Semispinalis capitis	C5	Skull	0.9		
32	Semispinalis capitis	C6	Skull	0.9		
33	Semispinalis capitis	C7	Skull	0.9		
34	Semispinalis capitis	T3	Skull	0.9		
	TOTAL Semispinalis capitis [o]			4.5	5.52	2.5
35	Semispinalis cervicis	T1	C2	0.1275		
36	Semispinalis cervicis	T2	C3	0.255		
37	Semispinalis cervicis	T3	C4	0.3825		
38	Semispinalis cervicis	T4	C5	0.8		
39	Semispinalis cervicis	T5	C6	1.0		
40	Semispinalis cervicis	T6	C7	1.1		
	TOTAL Semispinalis cervicis [o]			3.665	3.06	2.4
41	Longissimus capitis	C3	Skull	0.1633		
42	Longissimus capitis	C4	Skull	0.1633		
43	Longissimus capitis	C5	Skull	0.1633		
44	Longissimus capitis	C6	Skull	0.1633		
45	Longissimus capitis	C7	Skull	0.1633		
46	Longissimus capitis	T2	Skull	0.1633		
	TOTAL Longissimus capitis [o]			0.98	0.98	2.4
47	Longissimus cervicis	T2	C2	0.2483		
48	Longissimus cervicis	T2	C3	0.2483		
49	Longissimus cervicis	T2	C4	0.2483		
50	Longissimus cervicis	T2	C5	0.2483		
51	Longissimus cervicis	T2	C6	0.2483		
52	Longissimus cervicis	T2	C7	0.2483		
	TOTAL Longissimus cervicis [o]			1.49	1.49	2.6
53	Levator scapulae	Scapula	C1	0.78		
54	Levator scapulae	Scapula	C2	0.78		
55	Levator scapulae	Scapula	C3	0.78		
56	Levator scapulae	Scapula	C4	0.78		
	TOTAL Levator scapulae [o]			3.12	3.12	2.5
57	Multifidus cervicis	C5	C2	0.15		
58	Multifidus cervicis	C6	C2	0.15		
59	Multifidus cervicis	C6	C3	0.15		
60	Multifidus cervicis	C7	C3	0.15		
61	Multifidus cervicis	C7	C4	0.15		
62	Multifidus cervicis	T1	C4	0.15		
63	Multifidus cervicis	T1	C5	0.20		
64	Multifidus cervicis	T2	C5	0.20		
65	Multifidus cervicis	T2	C6	0.40		
66	Multifidus cervicis	T3	C6	0.40		
67	Multifidus cervicis	T3	C7	1.10		
68	Multifidus cervicis	T4	C7	1.30		
	TOTAL Multifidus cervicis [*]			4.5[c]	[b]	2.66[a]

[*] new compared to De Jager model
[o] modified compared to De Jager model
[a] average of s_{rest} because no data available
[b] no data available
[c] based on MRI scans and discussions with anatomists

Appendix B

Results of frontal and lateral impact simulations compared to results of the De Jager model

In this appendix the dynamic reponse of the De Jager neck model and the Van der Horst model (this thesis) are compared. Model simulations with passive and active muscle behaviour are performed for 15g frontal and 7g lateral impact (see also Chapter 4). The setup of the simulation is presented in Section 4.1.2. It should be noted that the De Jager model has a fixed T1, therefore no T1 rotation is prescribed for the De Jager model. An overview of the figures presented in this Appendix is listed below.

- Frontal impact with passive muscle behaviour: see Figures B.1 and B.2.

- Frontal impact with active muscle behaviour: see Figures B.3 and B.4.

- Lateral impact with passive muscle behaviour: see Figures B.5 and B.6.

- Lateral impact with active muscle behaviour: see Figures B.7 and B.8.
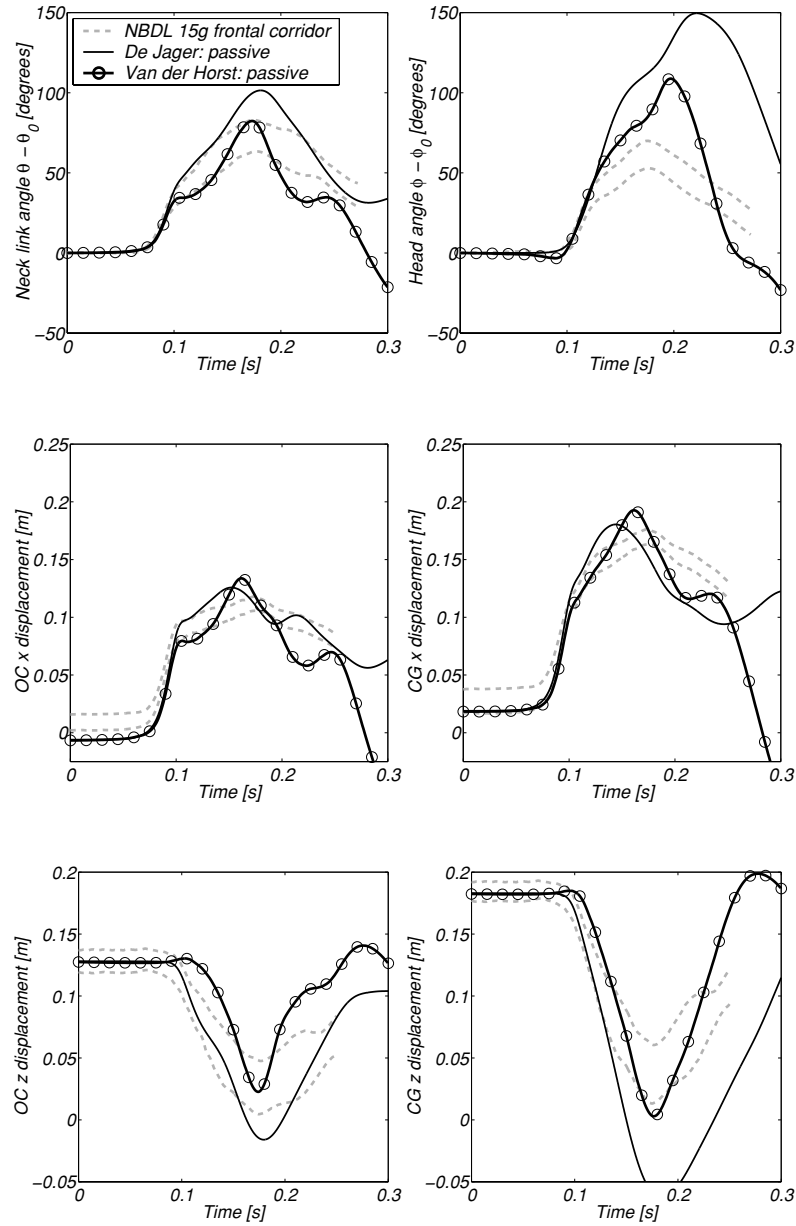
Figure B.1: *Head-neck rotation and displacement with respect to T1 versus time. Response to 15g frontal impact of the De Jager neck model and the Van der Horst neck model both with passive muscle behaviour compared with human volunteer response corridors.*
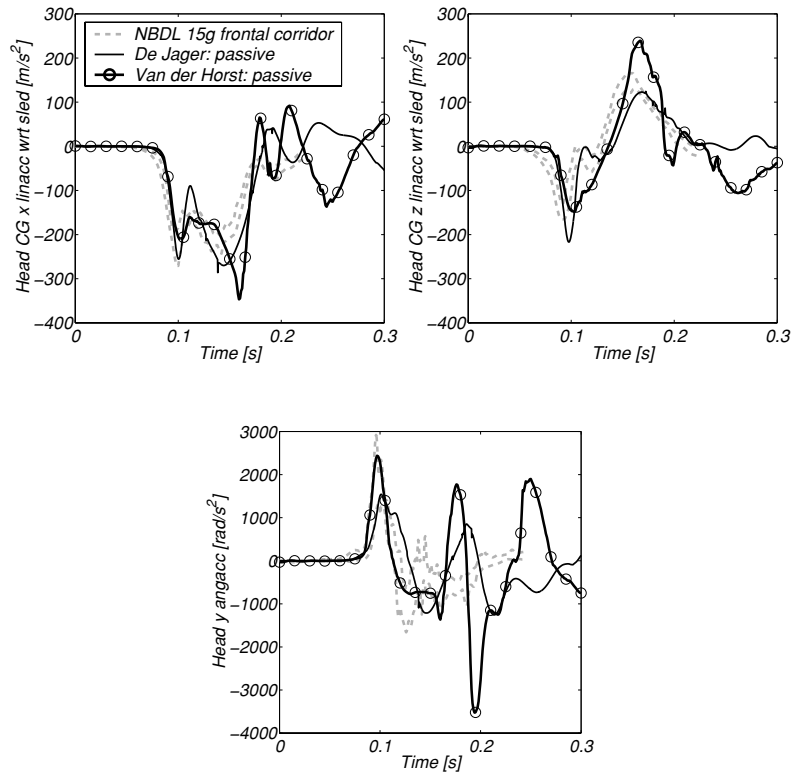
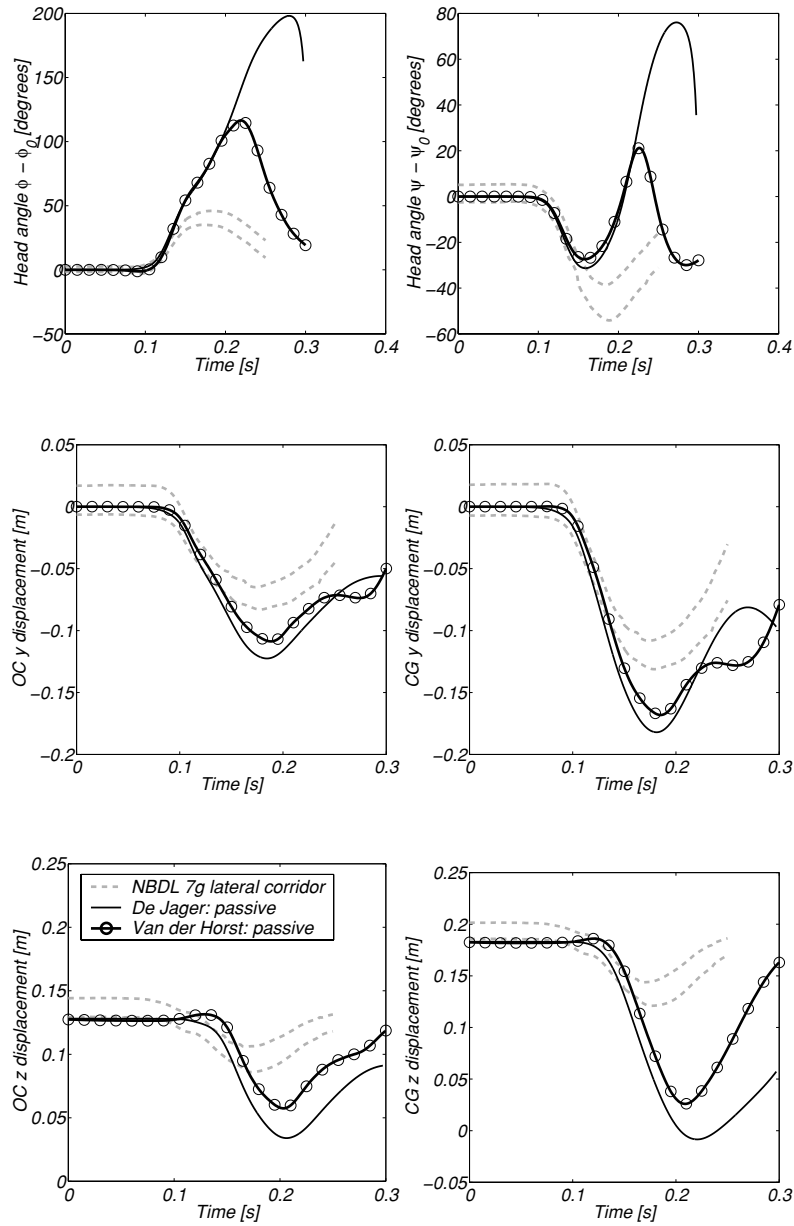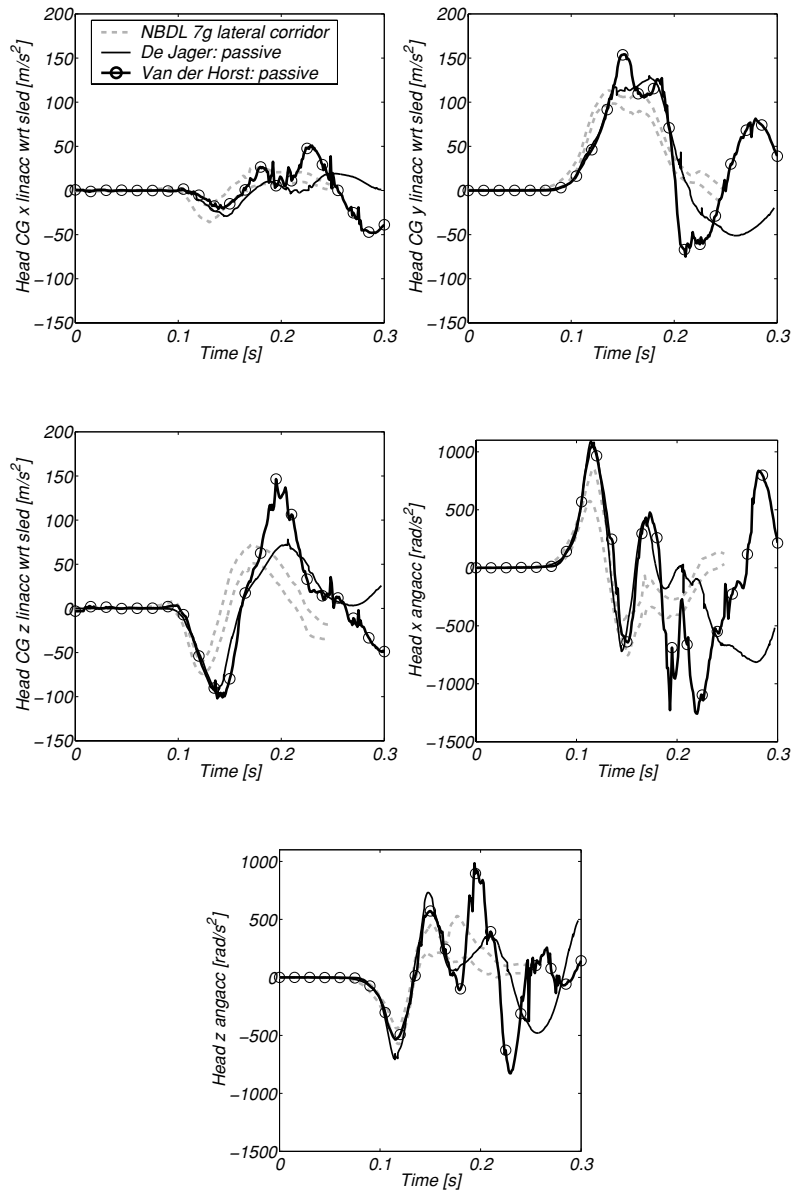**Figure B.2:** *Head acceleration versus time. Response to 15g frontal impact of the De Jager neck model and the Van der Horst neck model both with passive muscle behaviour compared with human volunteer response corridors.*
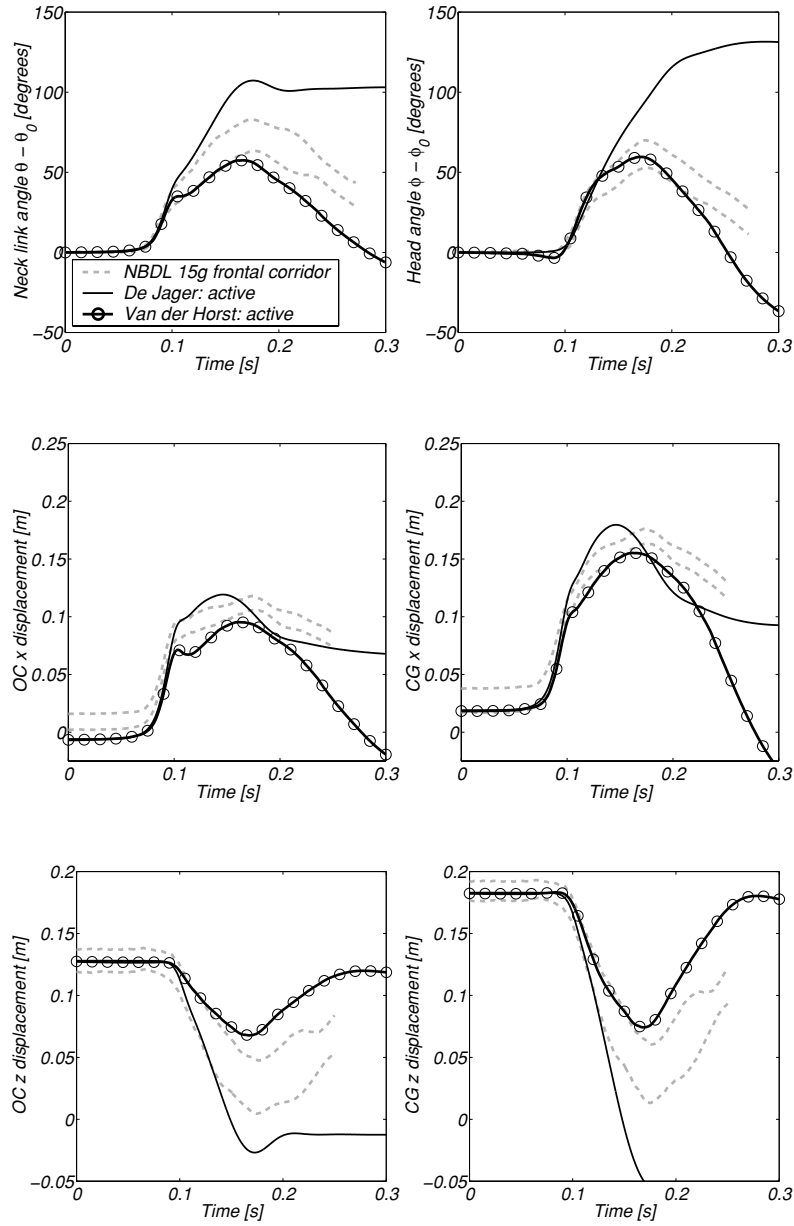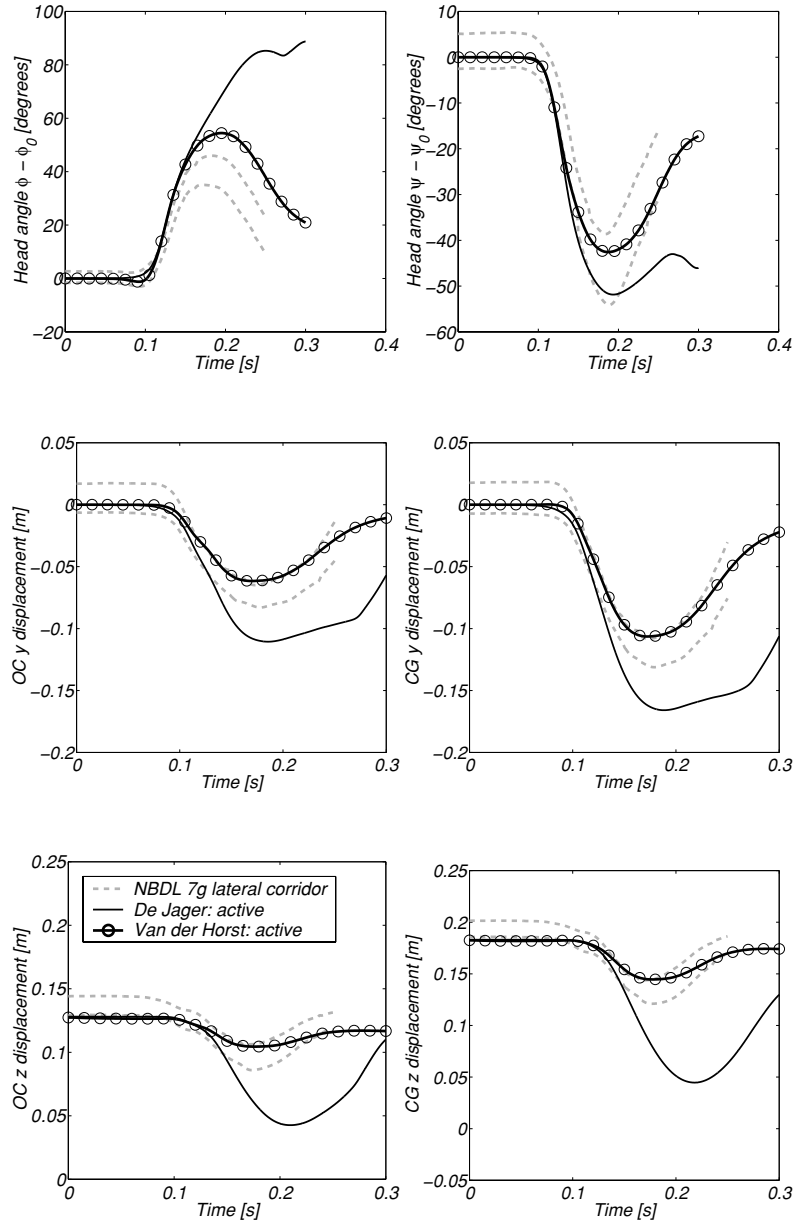
Figure B.3: *Head-neck rotation and displacement with respect to T1 versus time. Response to 15g frontal impact of the De Jager neck model and the Van der Horst neck model both with active (t_{act} = 74 ms) muscle behaviour compared with human volunteer response corridors.*
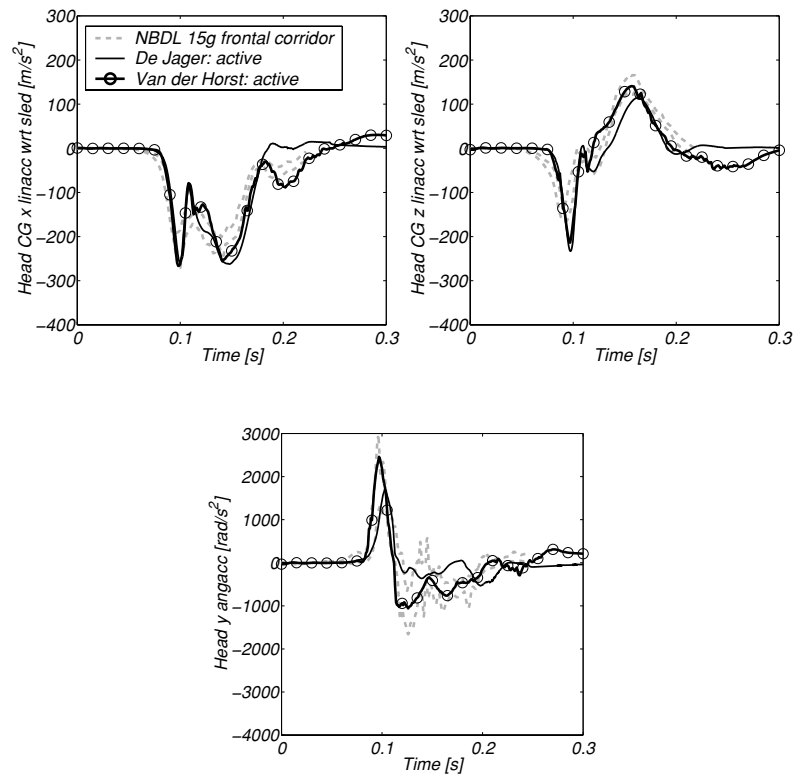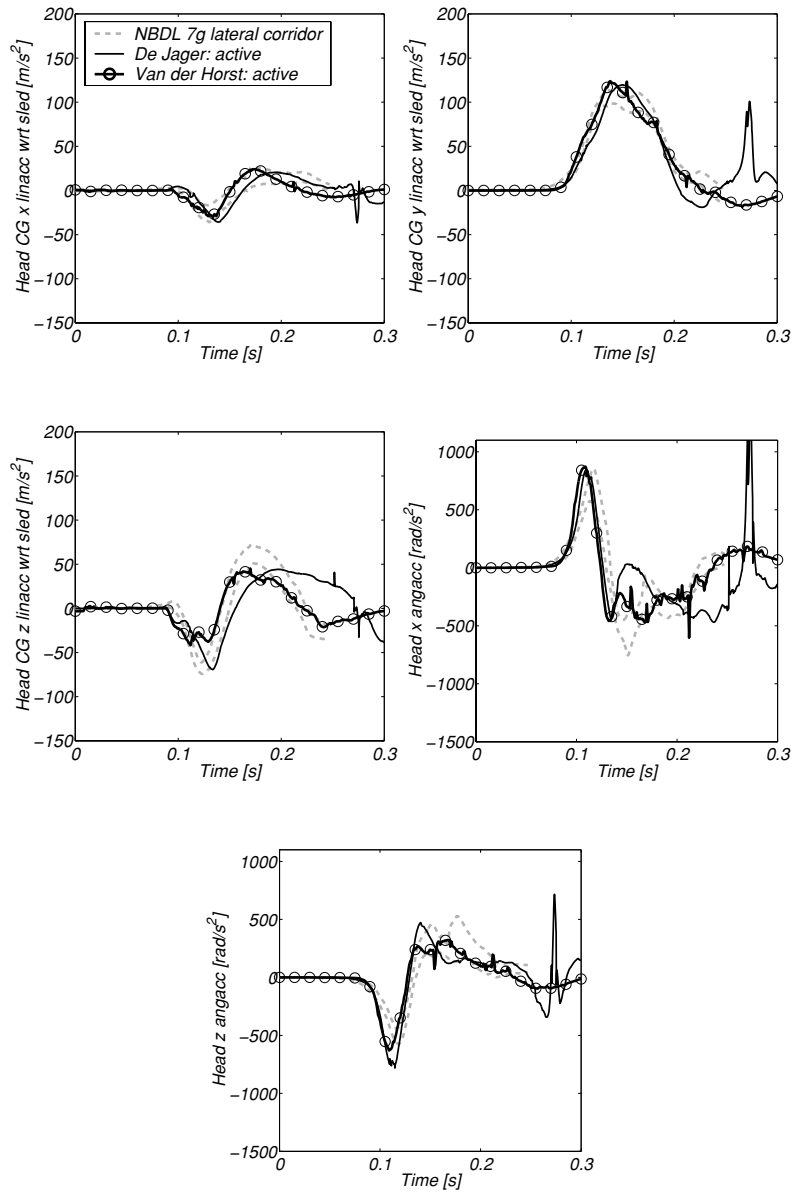
Figure B.4: *Head acceleration versus time. Response to 15g frontal impact of the De Jager neck model and the Van der Horst neck model both with active (t_{act} = 74 ms) muscle behaviour compared with human volunteer response corridors.*

Figure B.5: *Head angles and displacement of Occipital Condyles (OC) and Centre of Gravity of Head (CG) with respect to T1 versus time. Response to 7g lateral impact of the De Jager neck model and the Van der Horst neck model both with passive muscle behaviour compared with human volunteer response corridors. +x is forward, +z is upward.*

Figure B.6: *Head acceleration versus time. Response to 7g lateral impact of the De Jager neck model and the Van der Horst neck model both with passive muscle behaviour compared with human volunteer response corridors.*

Figure B.7: *Head angles and displacement of Occipital Condyles (OC) and Centre of Gravity of Head (CG) with respect to T1 versus time. Response to 7g lateral impact of the De Jager neck model and the Van der Horst neck model both with active (t_{act} = 87 ms) muscle behaviour compared with human volunteer response corridors. +x is forward, +z is upward.*

Figure B.8: *Head acceleration versus time. Response to 7g lateral impact of the De Jager neck model and the Van der Horst neck model both with active (t_{act} = 87 ms) muscle behaviour compared with human volunteer response corridors.*

Appendix C

Results of additional rear end impact simulations

In this Appendix additional results of the rear end impact simulations as discussed in Chapter 5 are shown. The AZT simulation results (5g rear end impact, standard seat with head restraint) for the passive model response (U1) and the active model response (U4) are presented in Figure C.1 - C.3. In Figure C.4 results of varying initial muscle activations are presented for 5g rear end impact simulation (standard seat without head restraint).
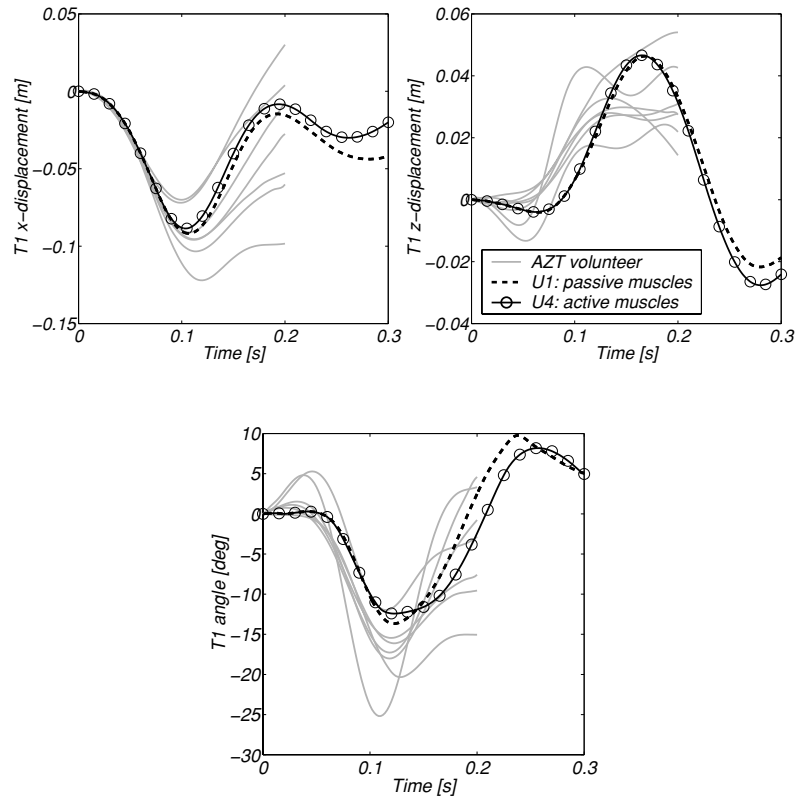
Figure C.1: *T1 kinematics with respect to sled versus time. Simulated response to 5g rear end impact of the neck model with passive and active muscle behaviour compared to AZT volunteer response.*
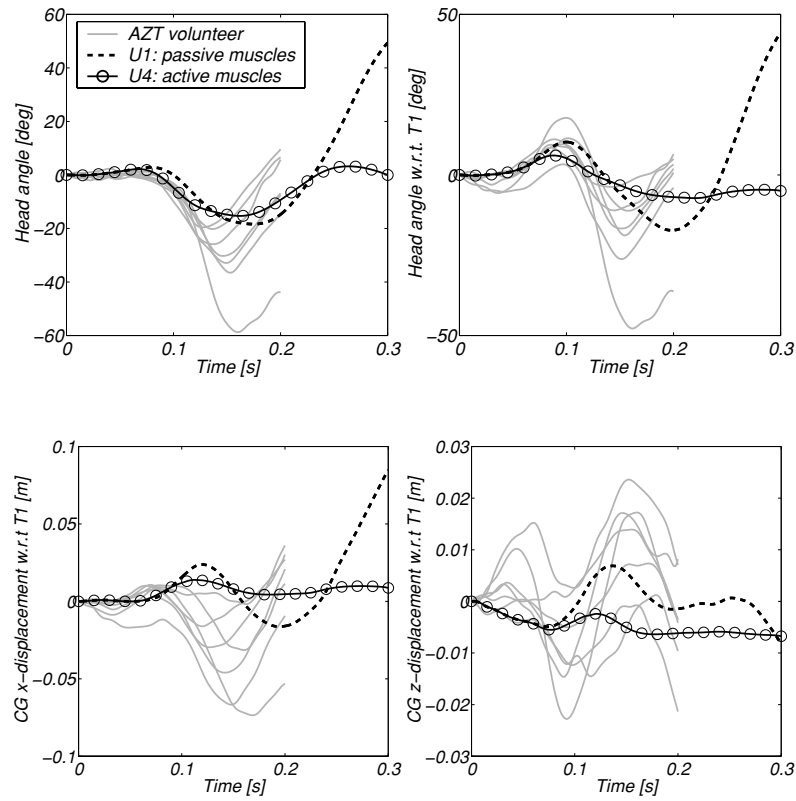
Figure C.2: *Head kinematics versus time. Simulated response to 5g rear end impact of the neck model with passive and active muscle behaviour compared to AZT volunteer response.*
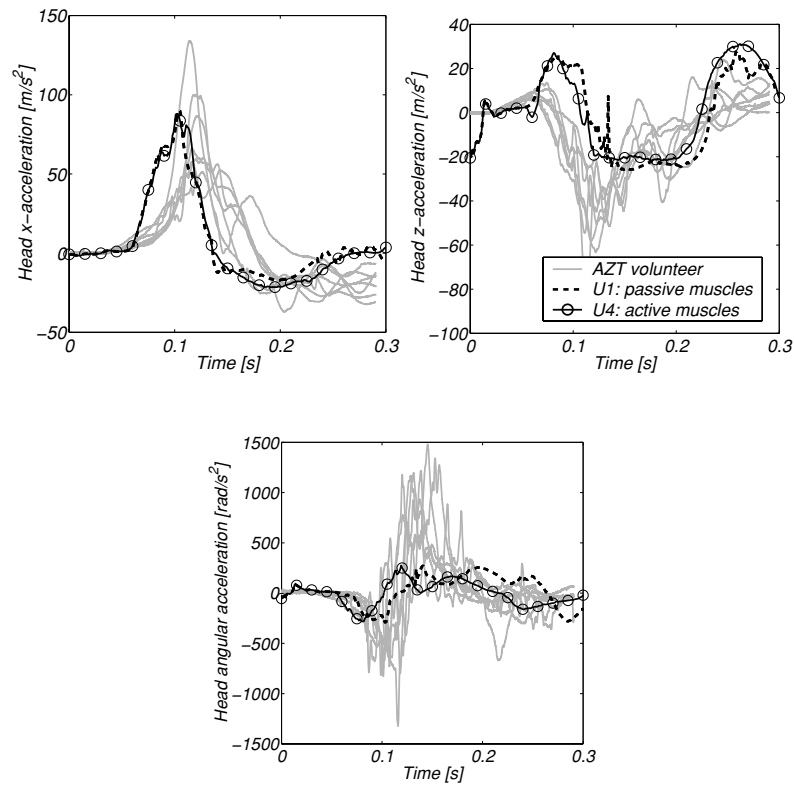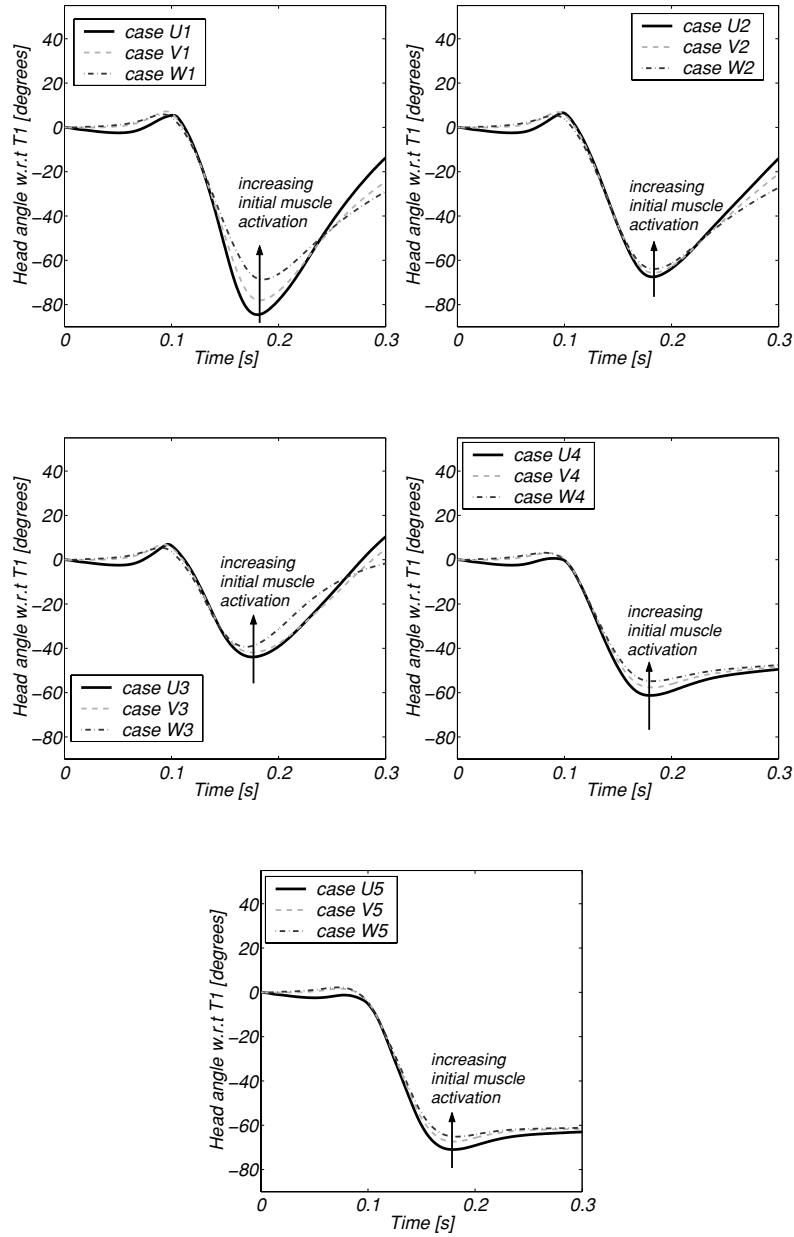
Figure C.3: *Head acceleration versus time. Simulated response to 5g rear end impact of the neck model with passive and active muscle behaviour compared to AZT volunteer response.*

Figure C.4: *Head angle at varying initial muscle activation conditions (increasing initial muscle activation from U to W, increasing maximum muscle activation from case 1 to 5) for a 5g rear end impact simulation (standard seat without head restraint, see Table 5.3).*

Appendix D

Global injury criteria of rear end impact simulations

In this Appendix additional global injury criteria of the rear end impact simulations as discussed in Chapter 5 and 6 are presented.
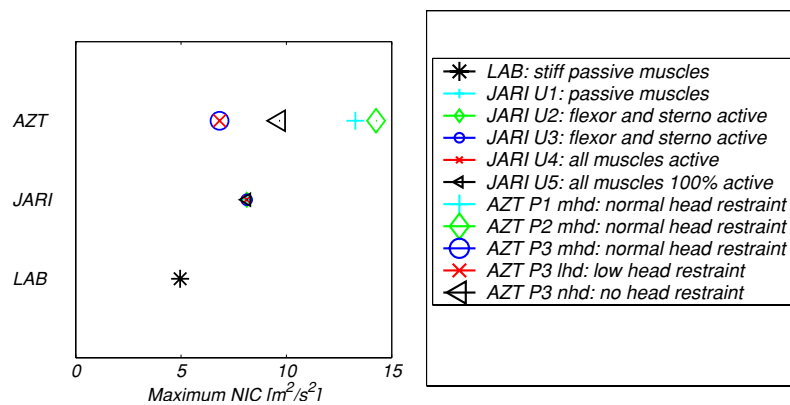

Figure D.1: *NIC for LAB, JARI and AZT rear end impact simulations (see Table 6.1).*
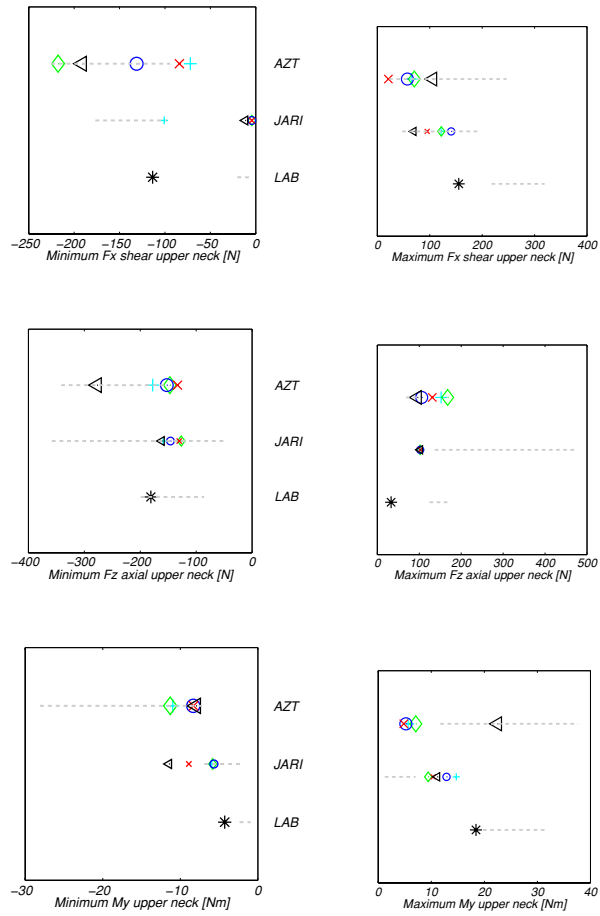
Figure D.2: *Peak neck loads for LAB, JARI and AZT rear end impact simulations (see Table 6.1). The dotted lines represent the range of peak values of the corresponding experimental data, while the explanation of the symbols can be found in the legend of Figure D.1.*

Appendix E

Impact of muscle contraction upon head stabilisation during sudden forward acceleration

This Appendix presents a copy of the article on low severity rear end impact experiments performed at Maastricht University. The article is written by Herman Kingma.

Impact of muscle contraction upon head stabilisation during sudden forward acceleration.

H.Kingma[1], J.Patijn[1], I.de Jong[1], H.W.Gosens[1], J.Stevens[1], A. Dekker[1], M. Lansbergen[1], M.v.d.Horst[2], J.Wismans[2], H.van Mameren[3]

[1]ENT-Department, University Maastricht
[2]Technical University Eindhoven
[3]Department of Anatomy, University Maastricht

Abstract

The impact of muscle contraction upon head movements induced by a forward acceleration as a model for low impact car-accidents was studied. The purpose of our research is to examine 1. whether and by which mechanism neck muscle contraction is induced after onset of the movement and 2. if voluntary neck muscle contraction prior to the movement affects head motion. Eight healthy volunteers (±21,4 yrs) were included in this study. Volunteers were sitting on a standard car seat mounted on a sled. The computer controlled motor driven sled was forward accelerated with 0,6 g. In test series 1, head and body movement were detected with a standard video camera (20 ms per frame) and accelerometers mounted on the head without interference with muscle activity. Muscle activation was detected by simultaneous measurement of surface EMG of m. splenius capitis, m. trapezius (descending part), m. scalenis medius, m. sterno-cleido mastoideus, m. digastricus (venter anterior), m. mylohyoideus, m. pectoralis major, m. quadriceps, tibialis anterior and triceps surae. The subject's movements and muscle activity were examined during forward sled acceleration when 1. the subjects were relaxed and could not anticipate on the precise start of sled acceleration and 2. when they contracted all body muscles about 4 seconds prior to and during the sled acceleration and 3. when head and trunk were fixed to the chair. The same subjects were accelerated in test series 2, but now head and trunk movements were measured with a better time resolution by use of a high-speed video camera (500 Hz) and accelerometers mounted to the head (bite board), body and sled. Head and body movements were measured under conditions 1 and 2 as described above. Reproducibility was tested by repeating each test condition once, including repositioning of the subjects, the accelerometers and body fixed sell spot markers.
Results and Conclusion. The current experimental set-up allows a low cost evaluation of head and body movements induced by low impact velocity impulses. We observed that sudden whole body acceleration induces head accelerations that exceed the acceleration of the impact by a factor of 2-3. After the impact, the head

first remains stationary in space while the sled and trunk move forward (relative head and upper trunk translation). Subsequently head and trunk rotate backwards, ultimately followed by an additional retro flexion of the head alone. Pre-contraction and anticipation to the impact leads to a faster and increase of general muscle tone. It does not affect the initial translation but leads to a reduction of about 30-35% of head rotations and head angular velocities. The muscle contraction is most like a generalised alerting response. It should be noted that the current results were obtained at a loading level of 0,7 g, which is far below the 5-12 g levels observed in rear end collisions. Since the current study shows only small influences of the muscle contraction it is assumed that the contraction will not be strong enough to limit the larger head and trunk motion in the higher impacts.

Introduction

Rear end car collisions can cause substantial forces in different anatomical structures of the neck resulting in neck pain, headache, and restriction of neck mobility. Together with other complaints like dizziness and cognitive deficits, the syndrome is generally known as "whiplash trauma". Research might help us to understand the whiplash mechanism and the associated complaints and function loss. During a rear end impact, the car is subjected to a forward acceleration during which the body of a subject is pushed forward by the seatback. At moderate to severe impacts (>5g), the head lags behind forcing the neck into extension. This motion continues until the head and neck hit the head restraint, reaches its maximum range of motion, or is counteracted by the muscles. The head than reacts by moving forward into a flexed neck posture.[1] Hyper translation of the head might explain the genesis of craniovertebral disruptions (like occipitoatlantal and atlantoaxial dislocation) better than hyper flexion or hyperextention.[2] Hyper translation produces horizontal shear between the vertebrae, resulting in compression of the facet joints and stretching annular fibres at the anterior part of the disc.[3]

It is questioned if muscles play a significant role in the restriction of passive motion of the head induced by acceleration.[4] It has been argued that muscles do not respond fast enough to manifest any changes in occupant motions during such an impact. However, to our knowledge this claim has been made largely without actual experimental validation. Only a few studies have been published concerning EMG activity of cervical spine extension- flexion, induced by low speed rear end impacts but they show no consistent results.[5][6] Information about EMG activity can provide information whether and to which extent cervical muscles effect head motion, under conditions where volunteers could and could not anticipate at the onset of sled acceleration. Latency times can create insight about the moment of on set of muscle activity in the characteristic motion of the head induced by

acceleration. Magnusson et al (1999) studied muscle activity of cervical flexors and extensors using wire and surface EMG. They found that for both anticipated and unanticipated sled accelerations, trunk movement occurred after 18,8 ms, head movement after 53,3 ms and neck muscle activity after 112 ms measured from the onset of sled acceleration. Szabo and Welcher studied the muscle activity of cervical flexors and extensors and the lumbar paraspinal musculature, using surface EMG. Muscle reaction times of 100-125 ms after the moment of bumper contact were found. They reported latency times as low as 20-30 ms from head acceleration for the neck flexors and tensors in some tests, significantly lower than the reflex times of 77 and 66 ms reported in other studies.[7] [8]

It can be questioned what should be defined as the reaction time (latency) in case of an rear end impact. Either the time lag between seat acceleration and the first noticeable burst of EMG activity, or the time lag between start head or trunk acceleration and first noticeable burst of EMG activity might be used. This is especially relevant, as there is still no unequivocal answer of what the trigger mechanism is for possible neck muscle activity induced by acceleration. Szabo en Welcher infer that the stimulus for the generated response mechanism occurred prior to the on set of response head acceleration. Other studies indicate such a response might come from at least the following three sources: the somato-sensory system, the vestibular system and vision.[9]

The aim of this study is to examine whether and to which extent the cervical muscles affect head motion induced by whole body acceleration. We formulated the following hypotheses:

1. Whole body low acceleration evokes involuntary head motion and neck muscle activity.
2. Muscle reaction times are affected by precontraction and/or anticipation to the on set of sled motion.
3. Pre-contraction of neck muscles limits head motion.

Materials and Methods

Subjects

The Medical Ethics Committee of the Maastricht University Hospital approved the test protocol. After being informed, all subjects signed an informed consent form before participating. Eight healthy Dutch male subjects (mean age of 21,4 yrs, range 19-23) participated in the study.

Subject's history revealed no indications for a neurological or otological disorder. General physical examination was normal in all subjects. No neurological function loss, motion restriction or abnormalities of the cervical spine were found on physical examination. MRI excluded congenital abnormalities of the cervical spine.

Sled specifications

The 4 meter long sled (linear accelerator) was developed and build by the Instrumental Service of Maastricht University. Safety aspects were evaluated and optimised in close co-operation with the Instrumental Service of the Maastricht University Hospital. The seat was propelled forward by a spindle motor, which could generate a maximum acceleration of 1,2 g and a maximum velocity of 3,5 m/s that simulates a rear end impact. For safety reasons maximum acceleration and velocity were limited at 0,7 g and 3,0 m/s respectively. A PC controlled the sled movement profile. A regular car seat provided with a 4- point seatbelt and head restraint was mounted on the sled. The head restraint bar stood in a 14- degree angle relative to the sled. The sled reached maximum acceleration after 70 ms and started decelerating after 680 ms. ΔV (sled velocity change from t=0 s until acceleration is back to 0 g) averaged over all tests was 9,8 km/hr.

Two test series were performed.
Test series 1. This series of measurements were performed to study impact of acceleration upon the contraction state of muscles. Electromyography activity (EMG) was measured with Meditrace surface ECG electrodes. Electrodes were placed bilateral on the m. splenius capitis (Spl. Cap), m. trapezius (descending part), m. scalenis medius, m. sterno-cleido mastoideus (St.cleido), m. digastricus (venter anterior, Digast.), m. mylohyoideus, m. pectoralis major, m. quadriceps, tibialis anterior (Tib.ant) and triceps surae (Tric.surae).

Signals were filtered with 2-200 Hz band filters. First muscle contraction amplitude was measured when subjects were asked to contract the specific muscle as much as possible (100%). Muscle contraction amplitudes were measured during the test series and given as a proportion of maximum amplitude found in the pre-test.

Head-, trunk- and sled accelerations were detected by piezo-resistive accelerometers (Analogue Devices ADXL05, 5 g maximum, accuracy 0,005 g). The sensors were provided with low pass 200 Hz filters. One sensor was mounted on the sled to detect sled acceleration (x-axis). The two sensors used on the head and trunk measured accelerations in the sagittal plane (horizontal or x-axis and vertical or z-axis). The 2D sensor placed on the head was fixed on the top of the scull by a swimming cap; a second 2D sensor was placed on the chest at the sternum in a tightly fitted neoprene smock assuming a fixed distance to T1. Measurements in one subject (subject 4) had to be repeated because of initial problems with fixation of the accelerometers relative to T1.In a pilot study, the reliability of the fixation of the 2D sensor in the swimming cap was tested in two subjects by comparison of the 2D accelerometer and video data of the swimming cap sensor and the 2 swimming cap sell spots with those of the 4 sensors and 2 sell spots mounted on a simultaneously worn bite board. The correlation coefficient between the outputs of the aligned accelerometers was better than 0,94. The

correlation between the position data calculated from the video frames was better than 0,96.

In the test series 1 the impact of muscle contraction upon body movement was studied. As a consequence no bite boards were applied to fix the accelerometers or video markers to avoid muscle contraction in the head and neck region. Accelerometers were mounted such that the x output (g-load) was close to zero at the on set of the experiments (x in the horizontal plane).

Video documentation of test runs was accomplished by a DBS (type DMM 8003) camera, positioned at a distance of 250 cm from the sagittal plane of the body. See figure 1. The sensor used in this camera was a Sony ICX 059 AC with a resolution of 768 x 494 and a shutter-time of 1 ms. Even and odd frames of the interlaced images were analysed separately. This procedure resulted in a temporal resolution of 20 ms and a spatial resolution of 768 x 247 pixels. The lens used in this experiment was a 8mm lens set at a diaphragm f 8,0.
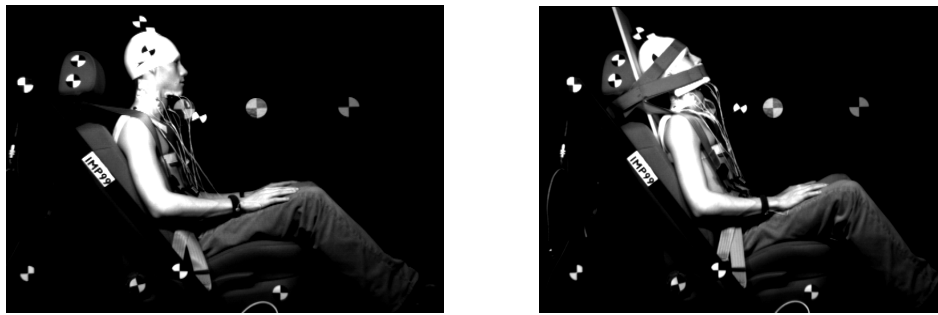

Fig. 1. Experimental set-up test series 1, prior to the impact. Selspot markers and accelerometers were located on the sled, trunk (neoprene smock) and head (in the swimming cap). Left video-frame: condition 1 or 2. Right video-frame: condition 3.
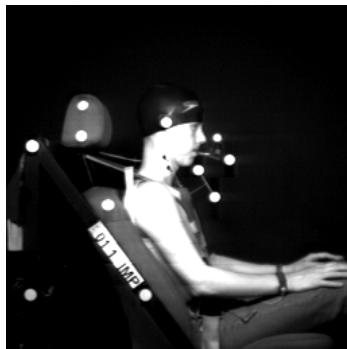

Fig. 2. Experimental set-up test series 2, prior to the impact. Markers and accelerometers were located on sled, trunk and head
on the sled, trunk (neoprene smock) and head (bite board).

The video camera was time-synchronised with the onset of sled acceleration (jitter less than 2 ms). Sell spot markers were placed on the head, trunk, sled and wall to allow detection of displacement of head and trunk relative to each other, relative to the sled and relative in space.

Test series 2. This series of measurements were performed a few months after test series 1 were completed. This series was performed to study *the impact* of muscle contraction upon passive head and body movement in detail. Sell spot markers were placed on the head, trunk, sled and wall to allow video detection of displacement of head and trunk absolute, relative to each other, relative to the sled and relative to space. During these test series a high-speed video system was used (500 Hz). See figure 2. Trunk- and sled accelerations were detected by piezo-resistive accelerometers as described above. One sensor was mounted on the sled to detect sled acceleration (Cxac). The sensors used on the head and trunk measured accelerations in the sagittal plane (horizontal or x-axis and vertical or z-axis). Four accelerometers were mounted on a bite board (x-axes: Bxac1, Bxac2, z-axes: Bzac1, Bzac2) and the bite board was supplied with three sell spot markers to detect the spatial orientation of the sensors by video. See figure 3a. A 3D sensor was placed on the trunk and was fixed by a neoprene smock at a fixed distance of T1 (Txac, Tyac, Tzac). This sensor was also supplied with sell spot markers. Figure 3b shows an example of the signal output of the accelerometers.
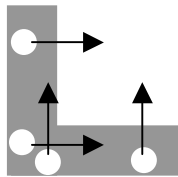

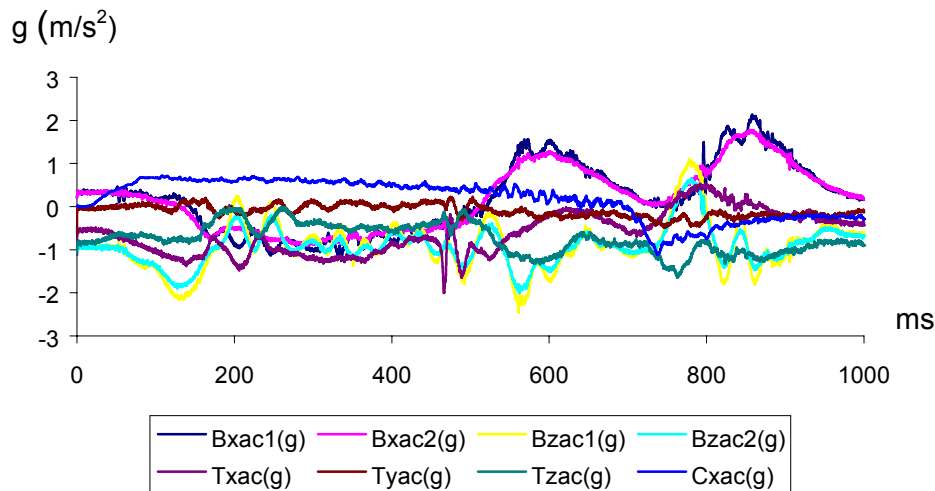Fig. 3a. Orientation and direction sensitivity of the 4 accelerometers on the bite board

Fig. 3b. Typical output of accelerometers as a function of time

Test Procedure.

Subjects were seated on the car seat mounted on a sled. They were told to sit in upright position with the Frankfort Plane oriented horizontally (horizontal position of the head where an imaginary line is passing through the external ear canal and across the top of the lower bone of the eye socket, immediately under the eye). Both hands were resting in the lap. Legs and feet were positioned as in a normal driving position. The soft car seat was fitted with a 4- point seatbelt and a head restrain. Depending on the anatomy of the subjects, the horizontal distance between occiput and head restrain varied from 8 to 14 cm.

Prior to and after the simulated rear-end impacts, the subjects – in seated position- were asked to contract all tested muscles maximally against the resistance of the opposing operators hand (isometric). This allowed normalisation of the responses per subject by comparison of these maximum values with those observed during impact.

The volunteers were exposed to three different test conditions.

1. Condition 1: the relaxed "relaxed" condition, where volunteers could not anticipate at the on set of sled acceleration. Volunteers were asked to relax prior to the impact while they counted down from fifty in English, to distract the test subjects from the onset of sled acceleration.

2. Condition 2: the expected "precontraction" condition, where the test subjects were asked to anticipate on the on set of sled acceleration by contracting all muscles to avoid head motion while they kept their head horizontal in the Frankfort Plane. The volunteers were notified 4 seconds prior to the impact to allow anticipation.
3. Condition 3: In the test series 1 a third test condition was studied: here head and body were mechanically fixed to the seat and head restraint by belts; to optimise fixation a plate was placed between the back seat and the subject; condition 3 was implemented to verify whether any muscles were activated by passive whole body translational acceleration, when no head to trunk movements were possible. Conditions 1 and 2 were repeated once in test series 2 to study reproducibility. A pause of 5 minutes was allowed between subsequent tests.

Test series 2 were performed 4-5 months after test series 1.

Signal processing and analysis
Test Series 1. EMG and acceleration signals were fed into a 40-channel electrophysiological measurement system provided with Poly-5 software (REFA-40, Twente Medical Systems). Latencies of muscle activity and maximum amplitudes were determined for all muscles tested. The low speed video camera was time synchronised with the on set of sled acceleration. On set of sled-, trunk- and head acceleration were defined at the time when the absolute acceleration signal had increased by more than 2 standard deviations (SD) compared to the acceleration signal during an interval of 100 ms before the start of the sled. Similar, the on set of EMG activity was defined at the time when the rectified and filtered EMG-activity had increased by more than 2 standard deviations (SD) of the EMG-activity during an interval of 100 ms before the start of the sled acceleration EMG latencies were calculated relative to the on set of sled-, trunk- and head acceleration. Muscle activity and accelerations were measured in the relaxed and the pre-contraction condition. Head and trunk rotations were detected by manual analysis of the displacement of the sell spot markers in the video-images.
Test series 2. Head, trunk and head to trunk rotations were calculated from the high-speed video frames based upon the position of the sell spot markers. Head translation was calculated from the accelerometer output corrected for the rotation of the sensor, which was calculated from the video data.

Statistic analysis
Variables were described in terms of means with standard deviation (SD) unless otherwise indicated. Data were statistical analysed with Excel (Microsoft Corp., Redmond, Washington) and SPSS (SPSS Inc. Chicago, version 9.2). Significance

was defined with a non-parametric test for 2/ K related samples (Wilcoxon Signed Rank test) at P< 0,05.

Results

General description and typical examples.
The upper two graphs of figure 4 illustrate the typical sled acceleration profile, which was the same for all tests performed thanks to the computer controlled feed back of sled position, velocity and acceleration. The lower two graphs of figure 4 illustrate a typical EMG as detected during the test series 1. The upper part of figure 5 shows the video graphs in 2 subjects at the start of sled acceleration and 300 ms later in test series 1. The lower part of figure 5 shows the video graphs of 1 subject in test condition 1 and 2, including the result of the manual analysis of the movement of the sell spots relative to space or to the sled. Figure 6 shows the head and trunk rotation as a function of time in both conditions as calculated by detection of the sell spots in the low speed video graphs in subject 1. Figure 7 shows an example of the rectified EMG detected in the three different conditions.
Figure 8 shows the high-speed video graphs obtained in 4 different subjects, with automatic detection of the sell spots (resampled in the graphs by a factor of 10 for clarity), either relative in space (first two columns) or related to the sled position (third column). The first two columns illustrate the intra-individual variability (reproducibility), which was only poor in subject 3.
Figures 9abcd show head to sled, trunk to sled and head to trunk rotations in all 8 subjects in condition 1 and 2 based on high-speed video data (time resolution 2 ms). Figures 10ab show the head and trunk angular movements. In each graph the 8 curves of all subjects are displayed for condition 1 (figure 10a) and condition 2 (figure 10b). Figure 11 shows a typical example of the linear accelerations along the x-axis of sled (relative to space, accelerometer output of the sensor fixed to the sled) and head (relative to the sled) in two subjects measured in condition 1 and 2, test series 2. Head linear translation is derived from the accelerometers on the bite board, corrected for the head rotation as detected by the high-speed video recordings. In the upper graph of figure 11, sled acceleration is displayed twofold. The gray curve is calculated by two-fold differentiation of the high-speed video-position data (sell spot on the sled); 8 points moving average smoothing preceded each differentiation. The dark curve is the direct output of the accelerometer on the sled. The relatively poor video-based signal compared to the better accelerometer output gives an indication about the reliability of acceleration data that are derived indirectly like the head-linear acceleration data.
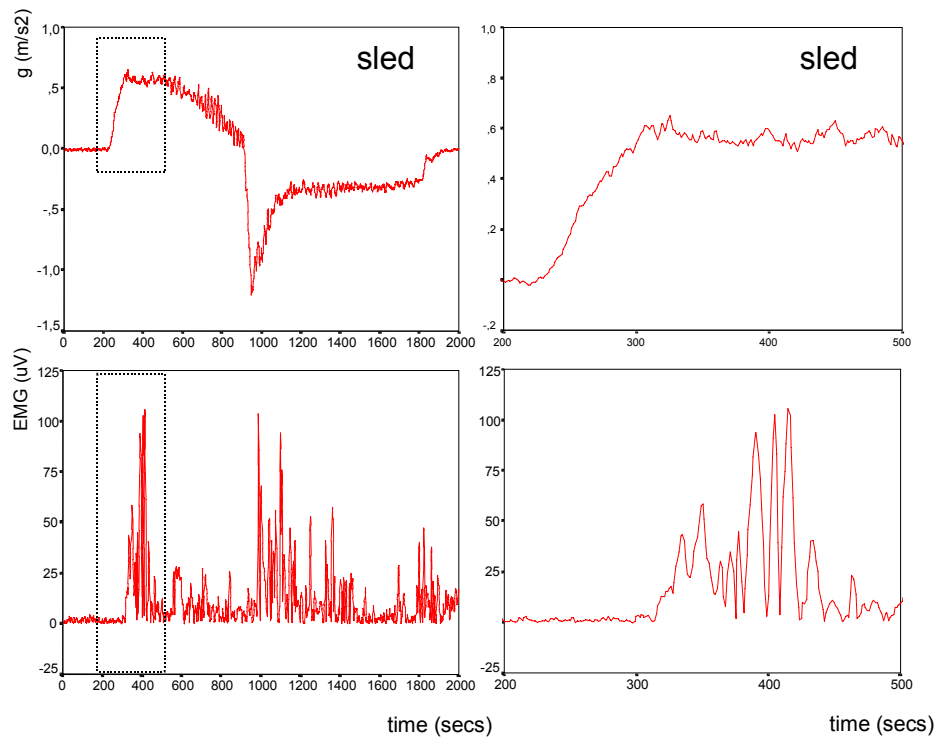
Figure 4. Experiment series I:
Typical stimulus and EMG activity

Figure 5. Experiment series I:
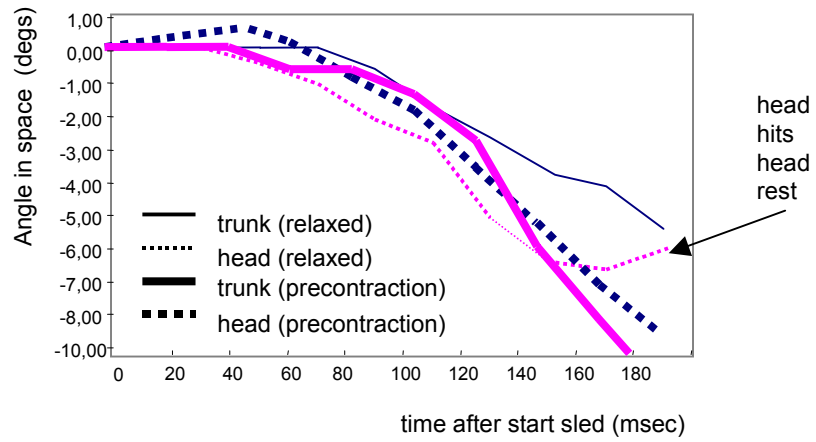Impact contraction upon head and body movement

Fig. 6: experiment series I: Subject 1
impact pre-contraction on movement
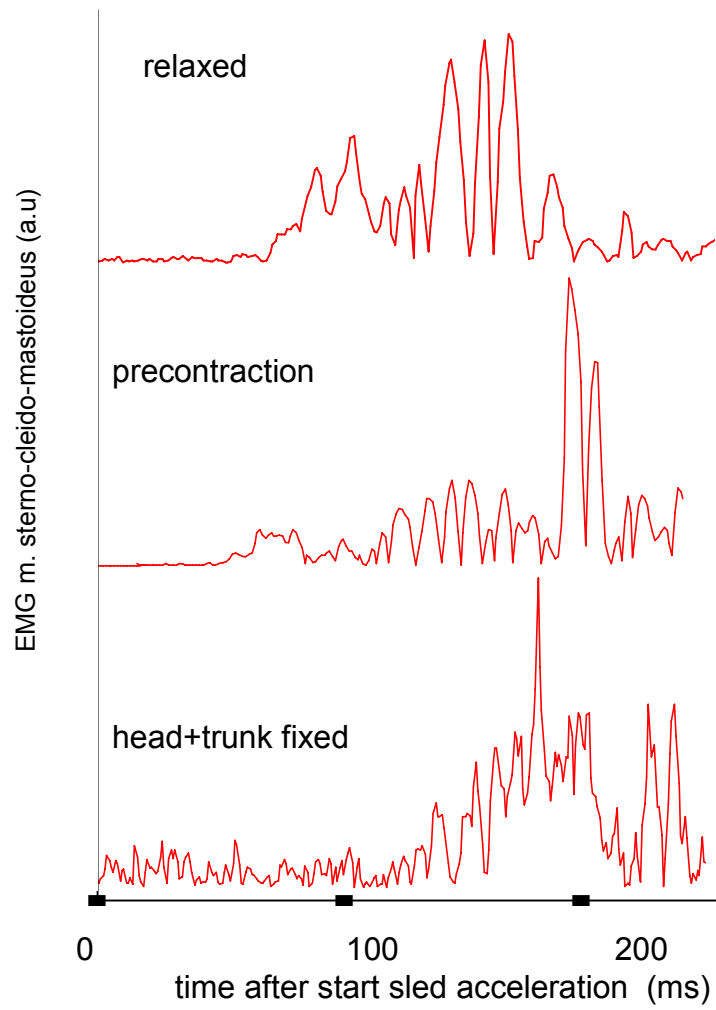manual analysis low speed video

Figure 7. Experiment series I:
impact precontraction and body fixation on muscle activity
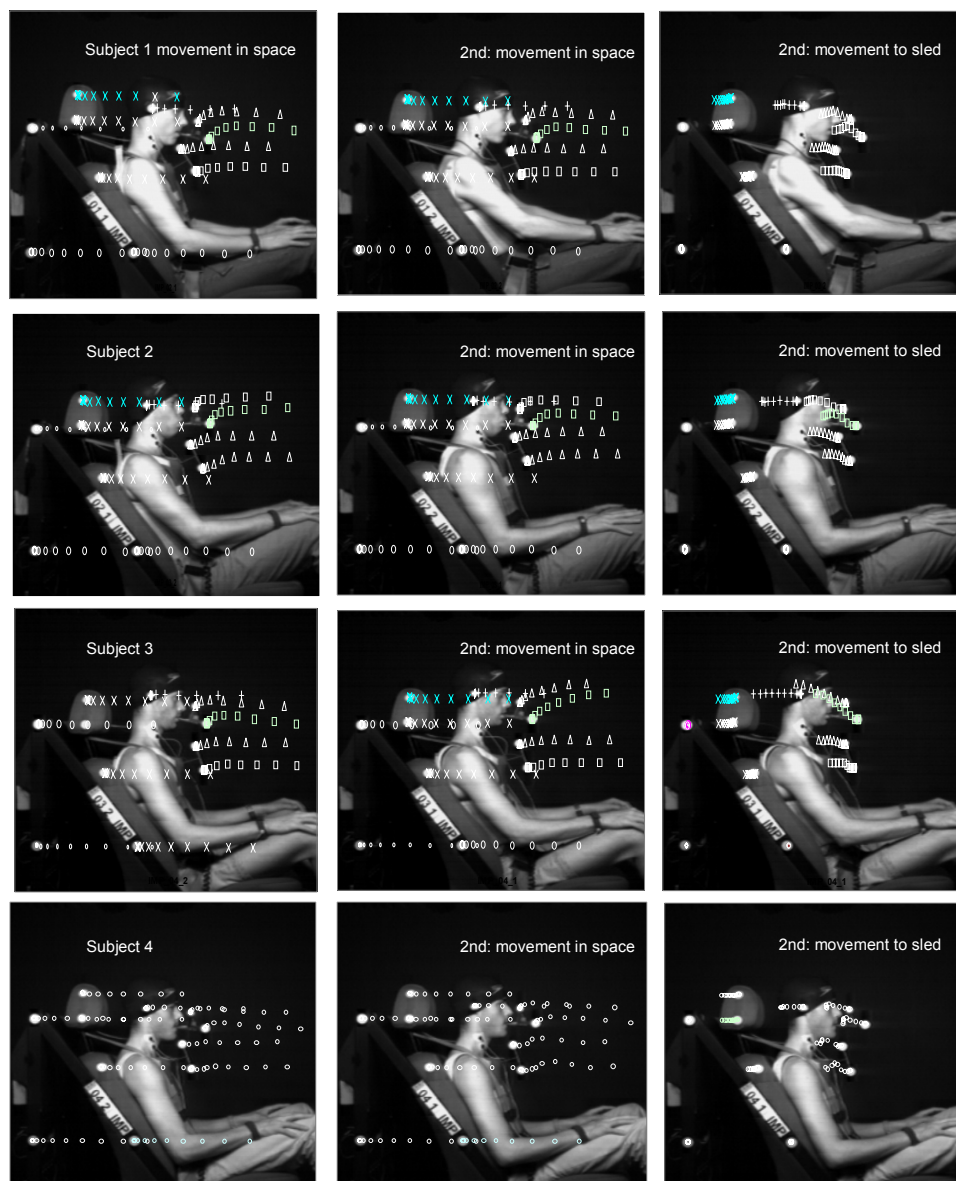
Figure 8. Experiment series II:
resampled high speed video: intra- and intervariability in 4 subjects

subject 1, relaxed

10

start sled

subject 1, precontraction

10

subject 2, relaxed

10

subject 2, precontraction
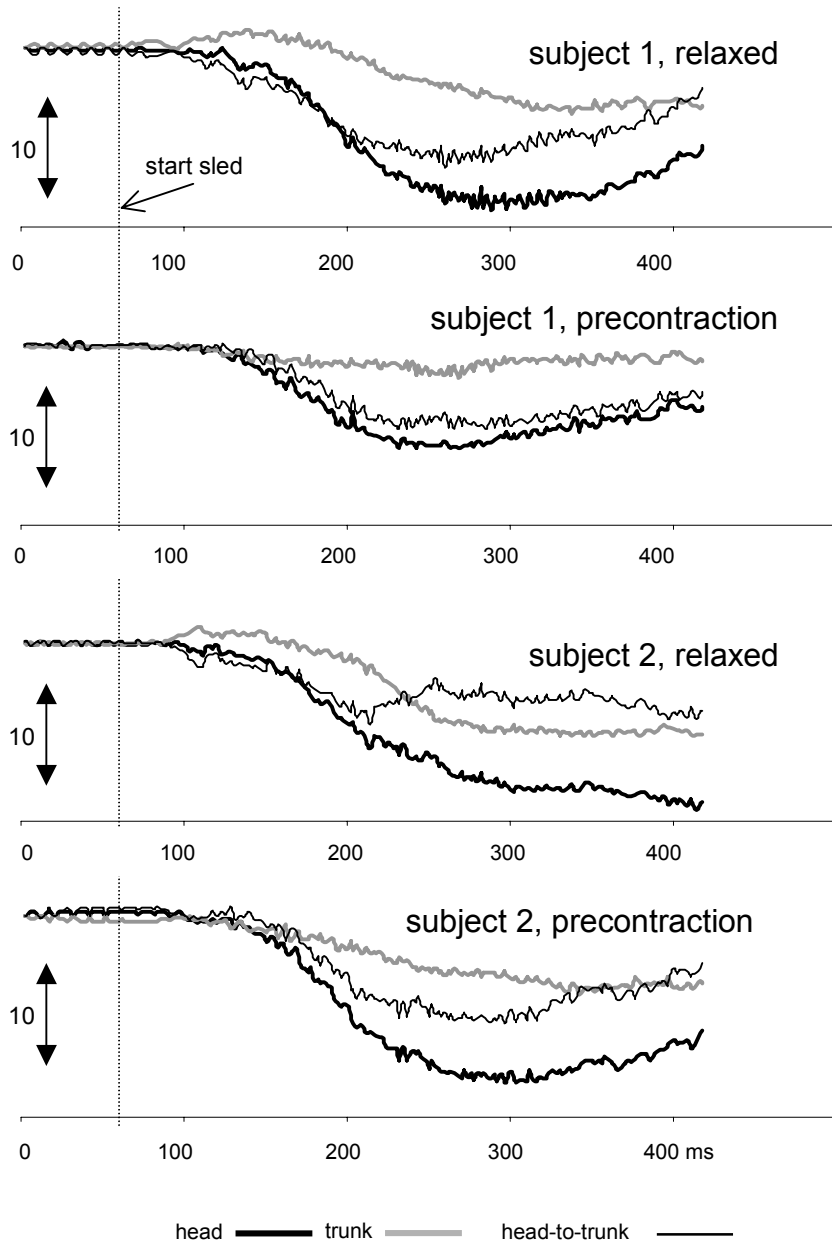
10

head ▬▬▬ trunk ▬▬▬ head-to-trunk ▬▬▬
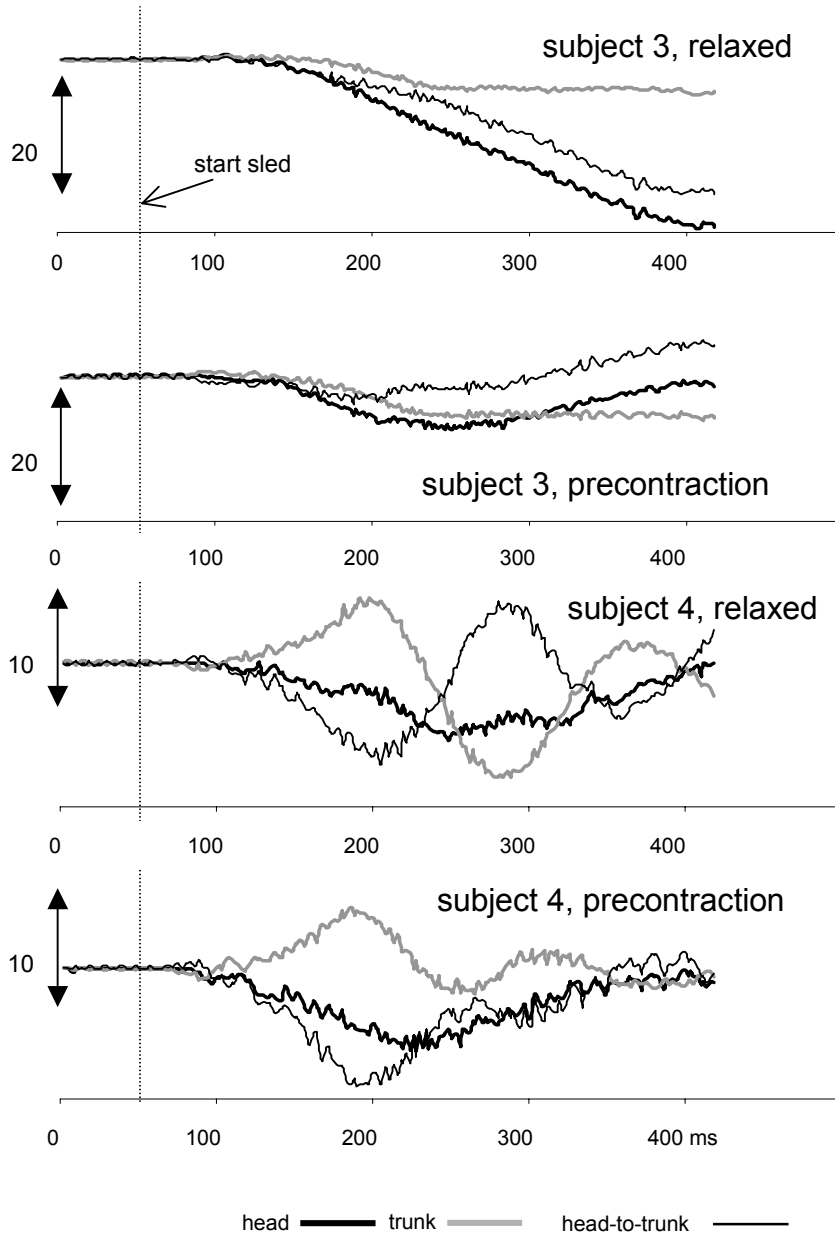
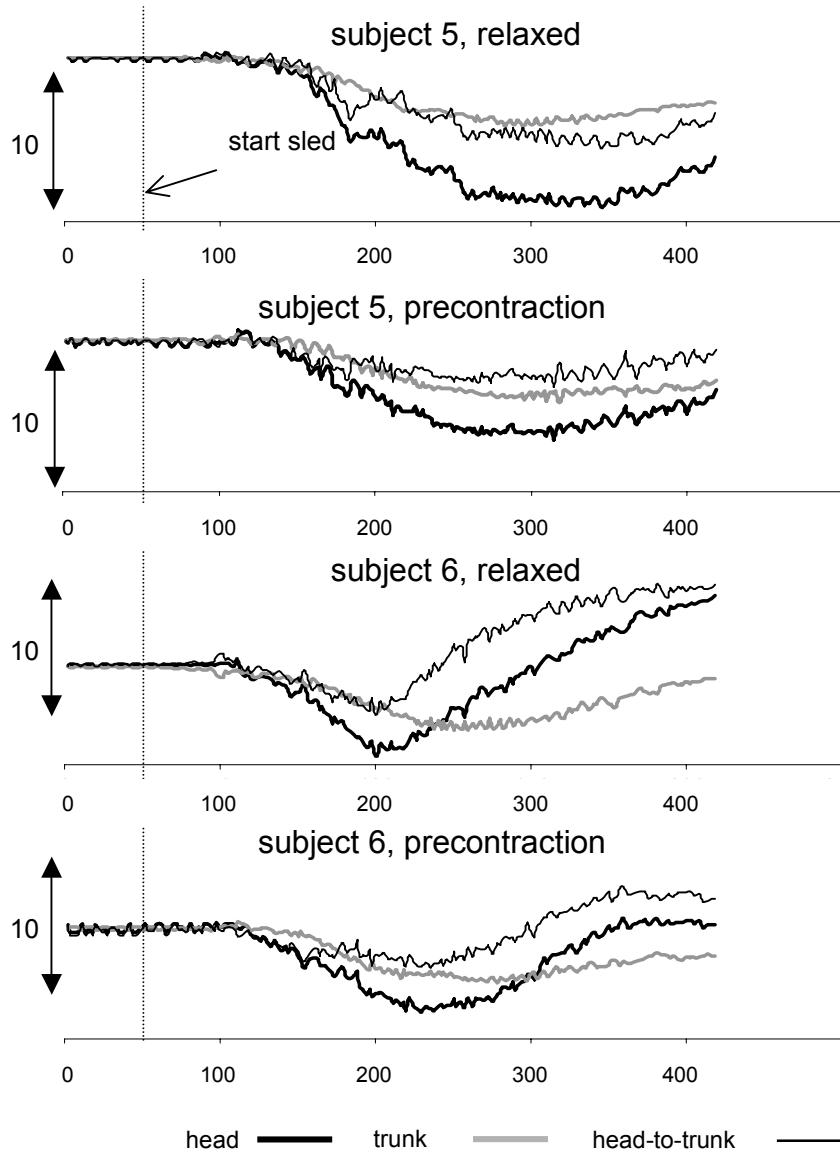Figure 9a   high speed video

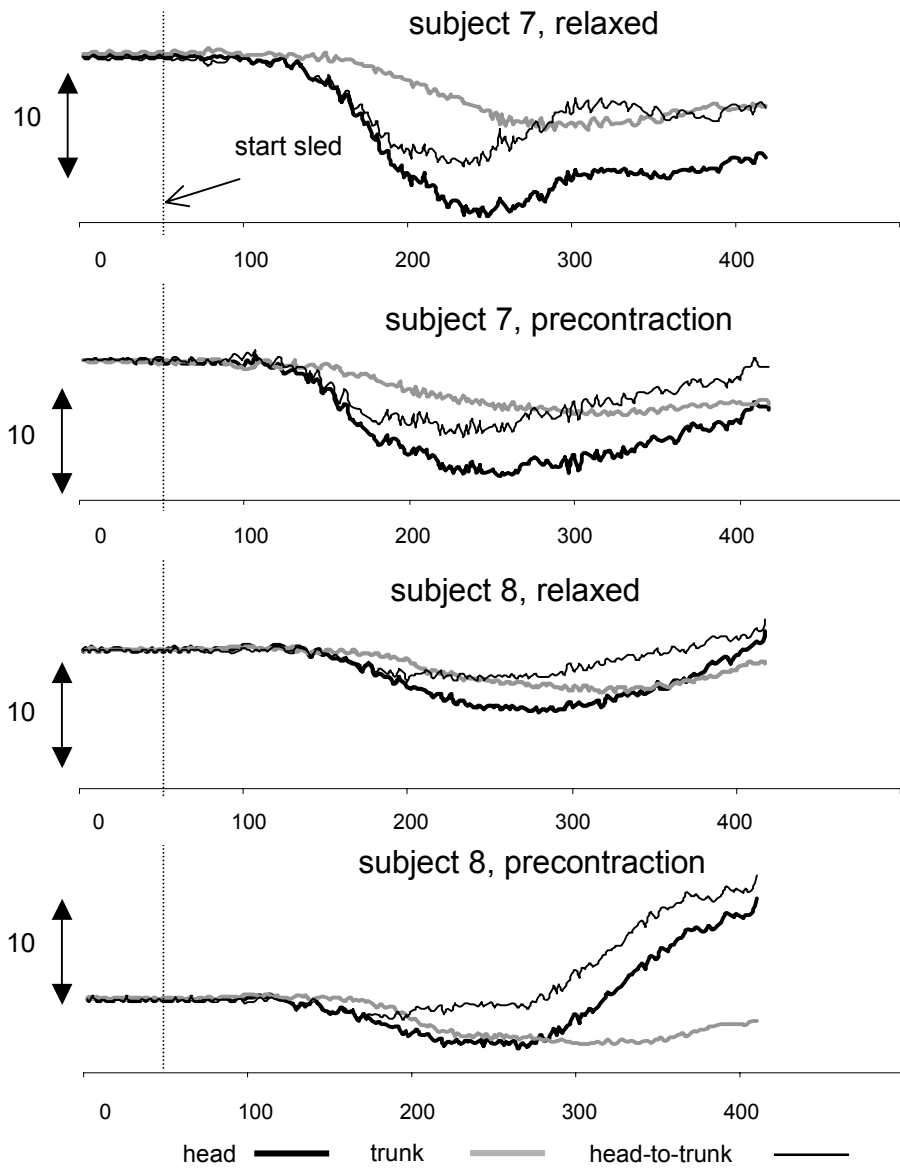Figure 9b   high speed video

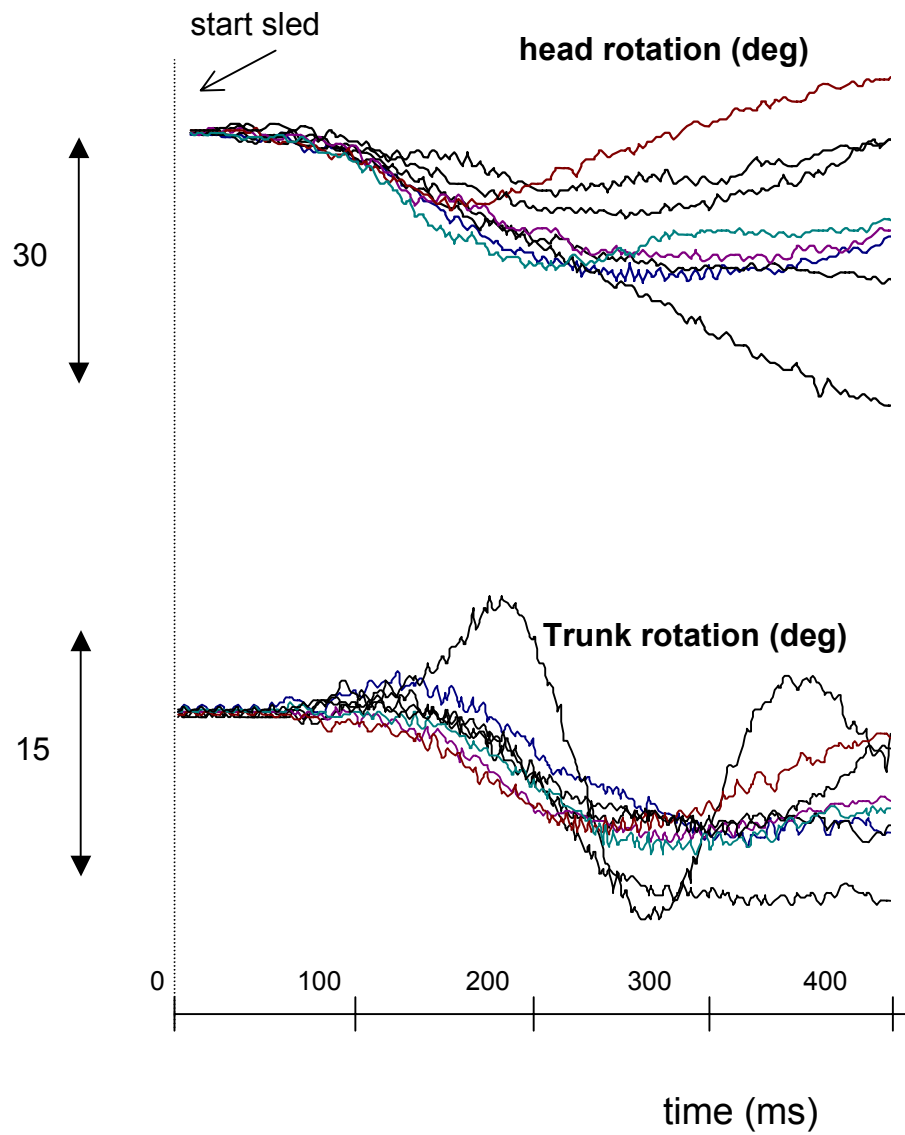Figure 9c high speed video

Figure 9d high speed video

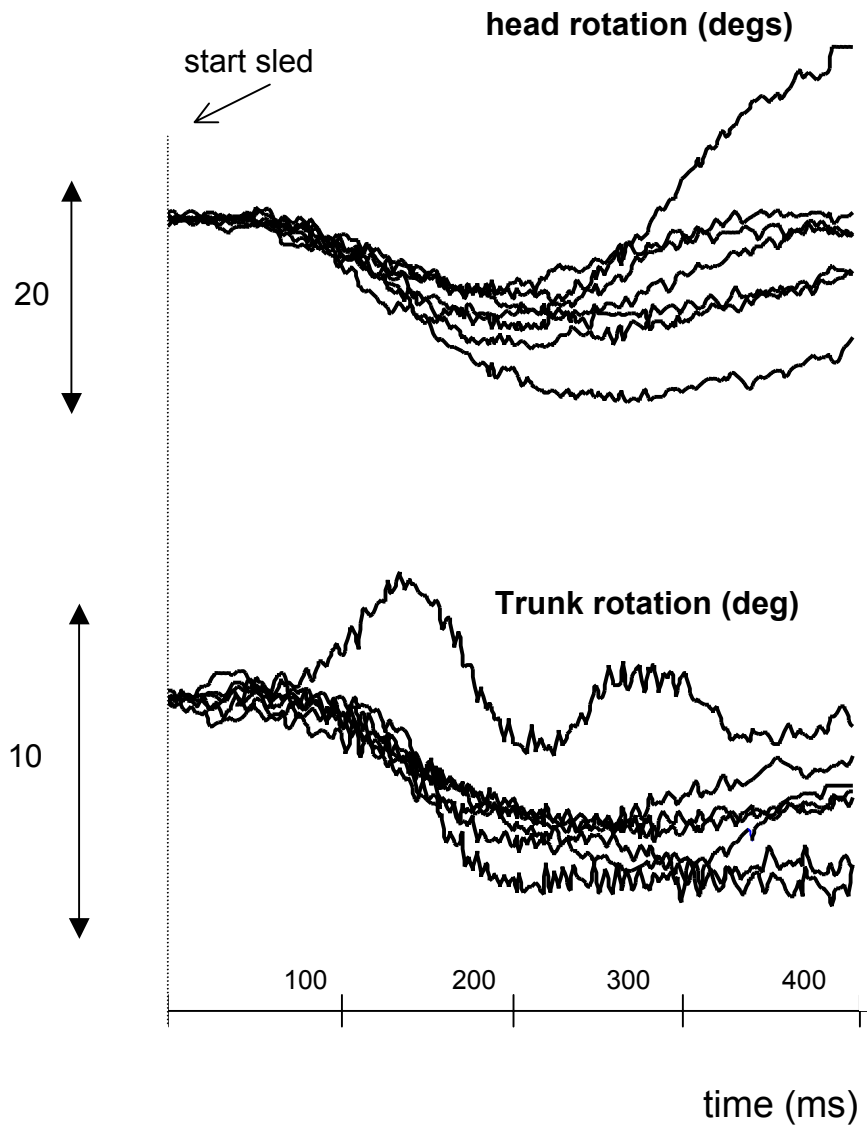Figure 10a. Experiment series II:
head and trunk movement: (relaxed)

Figure 10b. Experiment series II:
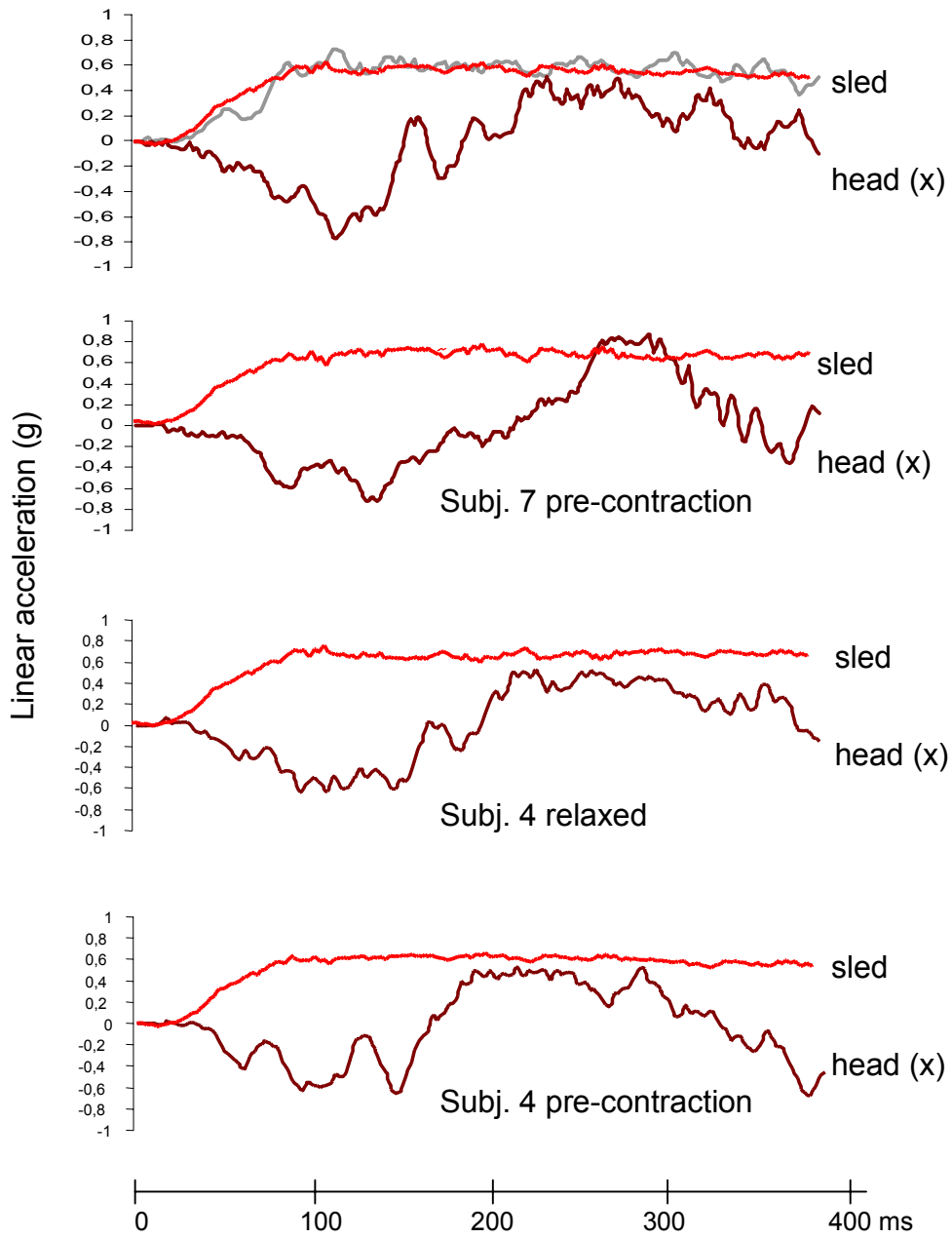head and trunk movement: (precontraction)

Figure 11. Experiment series II:
Sled and Head (relative to sled) linear acceleration

Numerical analysis

1. Latency of head and body movement

In the relaxed condition, the upper part of body of the subjects appeared motionless in space due to compression of the car seat during the first 44,6 ms after impact (Table 1). Only the lower back and the lower limbs translate forward with the sled. Significant translation of upper trunk and head relative to the sled occurs, but no consistent ramping up of the upper trunk or head is observed. Figure 11 indicates that –relative to the sled- the head accelerates backwards, both in condition 1 and 2. In condition 1, trunk-head translation relative to the sled is on average 2,6 cm with a standard deviation of 0,9 cm.

Meanwhile, the sled and seat back frame move forward. After on average 44,6 ms, head and trunk rotate slightly backwards simultaneously. About 84,4 ms after the start of the sled acceleration, the head rotates further more backwards (retro-flexion).

On set times of accelerations of trunk and head relative to the on set of sled acceleration are shown in table 1.

	Latency trunk and head rotation (ms)	latency head to trunk rotation (ms)
Relaxed Mean (SD)	44,6 (14,2)	84,4 (14,9)
Pre-contraction Mean (SD)	49,0 (15,6)	88,8 (16,4)

Table 1. Mean (SD) latency (ms) of head and trunk from start of sled acceleration. There was no significant difference in latency of trunk and head referred to the on set of sled acceleration between the relaxed condition and pre-contraction condition (Wilcoxon Signed Rank Test, p>0,05).

In the pre-contraction condition too, the upper part of body of the subjects appeared motionless relative to the test site background due to compression of the car seat during the first 49,0 ms after impact. Again only the lower back and the lower limbs translate forward with the sled. Again, the head –relative to the sled- accelerates linearly backwards (figure 11), but no rotation occurs initially (figures 9abcd). The translation of upper trunk and head relative to space is on average 1,9 cm with a standard deviation of 0,7 cm. This is not significantly different from the translation (2,6 cm) in the relaxed condition 1 (Wilcoxon Signed Rank Test, p>0,05). Although the general movement pattern seems to be the same for the first 40-50 ms to that described in the relaxed condition, a major difference can be observed next. After this first 44 ms, most subjects indeed limit the body and head motion by the muscle contraction. Some of them allow only the trunk to move and fix the head to the trunk predominantly; others try to prevent any body movement relative to the sled chair. Two subjects made more or less additional voluntary head

movements during the impact: after an initial backwards rotation of the head and trunk they moved the head forward (in flexion) despite the ongoing forward acceleration.

There was no significant difference between the relaxed condition and the pre-contraction condition for maximum acceleration of the head. The mean linear acceleration of the head relative to the sled was 1,3 g (with a minimum of 0,8 g and a maximum of 1,7 g). This is maximally about 3 times the magnitude of the sled (0,621g) during the relaxed condition. During the pre-contraction condition the mean acceleration of the head relative to the sled was 1,2 g (with a minimum of 0,7 g and a maximum of 1,3 g). This is maximally about 2 times the peak sled acceleration. Maximum head translational acceleration was not significantly different between condition 1 and 2 (Wilcoxon Signed Rank Test, p>0,05)
No head or body movement was detected in condition 3 (test series 1) when the head and body were fixed to the chair (fig. 1).

2. Amplitude, velocity and acceleration of head and body motion
Table 2 shows the time to reach the maximum head, trunk and head-to trunk rotation amplitudes and velocities, and shows the maximum rotation amplitudes and velocities reached.
No significant differences regarding the times needed to reach the peak values was observed, when we compared condition 1 and 2 (Wilcoxon-Signed Rank Test (p<0,05).
As mentioned above already, an initial significant *translation* of upper trunk and head occurs, but no ramping up of the upper trunk or head is observed. In the pre-contraction condition 2, head and trunk *translation* is not affected by the muscle contraction (fig 11), but *rotations* are significant reduced in all but one subjects (figure 9abcd). Only subject 2 does not show a significant decrease. In the total group, maximum head rotation amplitude and velocity, in space and relative to the trunk are significantly reduced (Wilcoxon-Signed Rank Test (p<0,05). Trunk rotation amplitude and velocity are not significantly affected (p>0,05, see table 2, test series 2). Head in space rotation decreases by about 29,3% (SD 21,1), head in space rotation velocity by 30,1 % (SD 27,9 %), head to trunk rotation decreases by about 36,0 % (SD 33,3 %), head to trunk rotation velocity by 31,0 % (SD 28,9 %). See table 2.

	Time after start sled acceleration		Mean		SD
RELAXED	Max Head rotation	253 (67) ms	28,3	°	14,1
	Max Trunk rotation	213 (27) ms	14,0	°	3,2
	Max Head to Trunk rotation	234 (47) ms	20,5	°	11,5
	Max Head velocity	128 (16) ms	273,3	°/s	66,6
	Max Trunk velocity	116 (15) ms	192,8	°/s	131,5
	Max Head to Trunk velocity	158 (25) ms	253,8	°/s	100,9
PRE-CON-TRACTION	Max Head rotation	234 (47) ms	17,8	°	5,4
	Max Trunk rotation	229 (65) ms	10,5	°	2,8
	Max Head to Trunk rotation	229 (65) ms	12,3	°	5,8
	Max Head velocity	144 (27) ms	190,3	°/s	81,8
	Max Trunk velocity	141 (38) ms	113,4	°/s	61,7
	Max Head to Trunk velocity	128 (13) ms	169,1	°/s	67,1

Table 2. Mean and SD of maximum rotation amplitude (°) and angular velocity
(°/s) and time (mean, SD) at which the maximum values are reached; test series 2.

3. Muscle activity
Muscle contraction amplitude
In table 3 the peak amplitudes measured during the test series 1 are shown as a
proportion of the maximum amplitude (100%) found in the pre-test to give insight
in the amount of activity during for all 3 conditions.

	Spl. Cap.	Trapezius	St. cleido	Digast.	Tib. ant	Tric. Surae
Relaxed	36 %	41 %	87 %	65 %	40 %	52 %
Precontraction	72 %	65 %	93 %	85 %	71 %	91 %
Fixed	40 %	45 %	80 %	60 %	44 %	48 %

Table. 3. Relative contraction amplitude (%) during the test, compared to
maximum contraction amplitude, test series 1.

No significant differences between the contraction amplitudes of left and right
muscles were found in any condition (Wilcoxon-Signed Pair test, p>0,05). No
significant difference was observed in contraction amplitudes between condition 1
and 3, (Wilcoxon-Signed Pair test, p>0,05)). Substantial more muscle activity was
present in condition 2, both before as well as during sled movement (Wilcoxon-

Signed Pair test, p<0,05). Muscle contraction reaction times are displayed in table 4.

In condition 1, muscle activity occurred on average 95 ms after the start of sled acceleration, 50 ms after on set of trunk movement, 11 ms after on set of head to trunk rotation (see table 3). Muscle reaction times of all individual muscles were measured from on set of sled, trunk and head acceleration. In condition 2, muscle activity occurred on average 82 ms after the start of sled acceleration, 33 ms after on set of trunk movement, 7 ms *before* on set of head to trunk rotation (see table 4). Substantial muscle activity was also present prior to the sled acceleration but showed a marked increase about 82 ms after the start of sled acceleration. The muscle reaction time in condition 2 was significantly shorter than in conditions 1 and 3 (table 4, Wilcoxon-Signed Pair test, p<0,05).

Muscle reaction times of all individual muscles were measured from on set of sled, trunk and head acceleration. In condition 3, muscle activity showed the same intensity and reaction times as in condition 1 (Wilcoxon-Signed Pair test, p>0,05).

	Spl. Cap.	Trapezius	St. cleido	Digast.	Tib. ant	Tric. Surae
Relaxed	99,5 (18,6)	96,8 (15,3)	92,4 (15,1)	97,5 (15,5)	94,6 (14,3)	93,7 (16,4)
Precontraction	84,3 (17,0)	78,8 (17,6)	77,8 (10,1)	85,9 (9,8)	86,4 (12,1)	83,5 (11,6)
Fixed	96,5 (12,6)	94,2 (15,6)	95,5 (12,3)	93,6 (13,4)	97,7 (16,8)	92,5 (13,4)

Table 4. Mean (SD) reaction time (ms) measured from start sled acceleration.

Discussion

Methodological limitations.

Several problems complicated the experimental set-up of this study.

Measuring motion at the level of T1 is a basic problem in living humans. The obvious place of a motion sensor would be on the back close to T1. However this is troublesome because of the direct contact between the back of the seat and the sensor, which easily induces motion artefacts. The curvature of the back does not allow an accurate fixation either. The sensor is also visually hidden in this position whereas the spatial orientation of the sensor needs be measured by a video system to allow knowing the relation of the 2D sensory output and spatial coordinates.

For this study, we developed a special tightly fitting neoprene smock that held the accelerometer on the chest and was supplied with easy to observe sell spot visual

markers. The position of the sensor relative to T1 was estimated by measuring the geometrical data when the sensor was brought into position. Our data did not indicate any slippage of the sensor relative to the trunk during the measurements: we verified this by adding natural markers on the trunk to the video frames and measuring the position of the sell spots relative to these markers.

The best way to measure acceleration of the head in living human subjects is for sure the use of a bite board that holds the accelerometers. The major draw back in this study is that substantial muscle activity in the cranio-cervical region is needed to hold the bite board in position. This may affect the head motion per se. We therefore measured all 8 subjects in two ways: series 1 without bite board, but using a tightly fitted swimming cap and series 2 with a bite board. In a pilot study we compared the accelerometer output in subjects that were equipped with accelerometers mounted in the tightly fitted swimming cap as well as on the bite board. The correlation coefficient between the outputs of the aligned accelerometers was better than 0,94. We concluded that –at these low impacts- application of the tightly fitting swimming cap is a good alternative for the bite board and does not lead to different results.

The video data provided position data with a limited spatial resolution (2 mm with standard video technique, 4 mm with the high speed technique). Given, the position of the sell spot markers, the resolution of the detection of the various rotation angles is between 1 and 2 degrees with the low speed video system and between 2 and 4 degrees with the high-speed video system.
The limited resolution in rotation detection by the video techniques also limits the accuracy to which extend the accelerometer data can be interpreted in spatial coordinates (e.g. figure 11 shows the relatively noisy signals of the head acceleration due to the mathematical various operations required). Another more fundamental limitation of the accelerometer data is that head and trunk motion relative to the sled can only be derived by subtracting the output of the sled mounted sensor from the output of the body fixed sensors and by subtracting the gravity component. This procedure reduces the signal to noise ration further by a factor 1,4 to 2. These inaccuracies introduce errors in absolute values of head and trunk velocities when derived by integration of the accelerometer data. Head and trunk velocities can also be derived by differentiation of the high-speed video position data. Here the limited accuracy in position induces substantial noise in the velocity signals.
We optimised the calculation of head and trunk velocities (table 2) by cross reference through maximizing the correlation coefficient between the velocity data from the accelerometer and video-data. Figure 11 allows a good comparison between directly obtained acceleration data ((upper graph, dark line) accelerometer

on the sled) and indirect obtained acceleration data ((upper curve, gray line), sell spot markers on the sled)).
To avoid errors, the consistency of all calculations was verified qualitatively by careful observation of the original video recordings.

Careful analysis of translation and rotation components, first by using the video data to calculate the translational components in the accelerometer data, and later by frame to frame visual inspection of the high speed video images, showed that the initial head and trunk movement is composed of both a translational and a rotational component, variable in relative amplitudes over the subjects.
The induced head and trunk motion profiles vary widely from subject to subject (figs. 9 and 10). In some subjects head and trunk motions relative to the sled were observed in the direction of sled acceleration, suggesting a voluntary and active component (fig 9, subjects 4,6 and 8). The general impression is that the current low impact induces substantial passive head and trunk movement.
A summary of the generally observed motion patterns and impact of muscle contraction is summarized for clarity and easy comparison in table 5 (see below).

Condition 1, when anticipation to the impact was prevented

Phase 1: Translation phase
Initial **45 ms**: upper trunk and head are stationary in space, while the sled moves forward. Only the lower trunk and lower limbs are translated forward. Without a clear detectable latency, upper trunk and head translate on average **2,6 cm** backwards relative to the sled, with a peak head to the sled acceleration of about **1,3 g** on average.

Phase 2. Upper body rotation phase
After **45 ms**, head and trunk rotate slightly backwards simultaneously.

Phase 3. Additional Head rotation phase
After **84 ms**, the head rotates further more backwards (retro-flexion).

Phase 4. Muscle contraction phase
After **95 ms**, all muscles investigated contract simultaneously

Phase 5. Maximum velocity phase
Maximal angular velocities (head, trunk, head- trunk) are **192-274 º/s** after **125-160 ms**.

Phase 6. Maximum amplitude phase
Maximum rotation amplitudes (head, trunk) are **14-28 º** and reached between **210-250 ms**.

Condition 2, when anticipation to the impact was promoted and all body muscles were pre-contracted

Phase 1: Translation phase
Initial **49 ms**: all muscles are partly contracted. Upper trunk and head are stationary in space, while the sled moves forward. Only the lower trunk and lower limbs are translated forward. Upper trunk and head therefore translate on average **1,9 cm** backwards relative to the sled without any considerable latency. Peak head to the sled acceleration mounts about **1,2 g** on average (NS different).

Phase 2. Upper body rotation phase
After **49 ms**, head and trunk rotate slightly backwards simultaneously (NS different).

Phase 3. Additional Head rotation phase
After **89 ms**, the head rotates further more backwards (NS different).

Phase 4. Muscle contraction phase
After **82 ms**, all muscles contract simultaneously significantly faster and stronger than in conditions 1 and 3.

Phase 5. Maximum velocity phase
Maximal angular velocities are reduced **113-190 º/s** and reached between **128-141 ms** (NS).

Phase 6. Maximum amplitude phase
Maximum rotation amplitudes (head, trunk) are **12-18 º** and reached between **229-234 ms.**

Condition 3, when head and trunk are immobilised by fixation to the sled chair
Without head or trunk movement, all muscles nevertheless contract simultaneously after 95 ms, and to the same extend as in condition 1.

In many popular publications and in the daily clinical practice it is often suggested that anticipation on a rear-end collision may lead to contraction of the neck muscle and through that might reduce head motion and reduce the probability to acquire a whiplash injury. In this study we specifically addressed this question. From table 5 it is clear that precontraction and anticipation does not affect the initial translation or the subsequent rotation phases. Although pre-contraction and anticipation does not affect trunk rotation amplitude or trunk velocity, head to trunk and head in space rotations and angular velocities are significantly reduced: head in space rotation decreases by about 29,3% and head in space angular velocity by 30,1 %, head to trunk rotation decreases by about 36,0 % and head to trunk rotation velocity by 31,0 %. The relatively small impact of pre-contraction and anticipation can be expected to be even less in case of bigger impacts. We conclude that it is unlikely that anticipation might prevent or limit the severity of whiplash injuries in case of larger impacts that occur in the regular rear-end collisions.

To summarise, three observations related to the muscle activity measured might help us to understand the mechanism behind it. First, muscle contraction occurs roughly at the same moment where the head to trunk rotation starts, which might suggest that muscle contraction occurs due to the head motion. However, this is clearly not the case because the same time course of muscle activity is observed when the head and trunk are immobilised by fixation to the chair (condition 3). Apparently not the head motion itself, but possible the multi-sensory perception of the sled movement might form the trigger, the stimulus, to increase muscle tone, may be as a simple alerting response.
Second, the increase of muscle tone observed concerns all muscles evaluated, and not only those that control head stabilisation and regards agonist and antagonists. The detected muscle activity occurred at approximately the same time and was not dependent on acceleration or movement of the area of the body, as seen in other studies.[13] Muscles that are situated at the dorsal part of the neck cannot reduce the backward movement of the head caused by sled acceleration. So there is no logical explanation for them contracting if these muscles want to prevent the head from going backwards. These findings suggest a centrally generated response. This is consistent with the literature in which also a general central mechanism is hypothesized to account for the muscle response to low level anterior-posterior perturbations of a seated subject [14]: it is suggested that the central nervous system shifts the equilibrium point of the limbs, resulting in a increased level of muscle

activity in both the agonist and antagonist group. This again suggests that the muscle activity is not a specific reflex (vestibulo-collic- vestibulo-spinal, cervico-collic etc) but indeed a more generalised alerting response. The trigger mechanism for the centrally generated response (muscle activity) might be arising from stimulation of the somato-sensory (almost instantaneously when the sled pushed the lower trunk), the auditory (subjects could hear the start of spindle motor). Detection of motion by vestibular input is relatively late because the head is stationary in space for the first 45-50 ms. Detection by the visual system (volunteers could see they were forward accelerated[9][15]) is also late: the latencies of motion perception by vision generally exceeds 40-70 ms. Third, muscle tone increase is slightly faster and substantially bigger in case of pre-contraction and anticipation. To this respect our results do not agree with those of Magnusson et al. who found no effect of anticipation upon the muscle reaction times. Our results support the hypothesis that the muscle contraction is an alerting response per se, that is easier generated and stronger when the subjects anticipate on the impact.

Conclusion
Pre-contraction and anticipation to the impact leads to a faster and increase of general muscle tone. It also leads to a reduction of about 30-35% of head rotations and head angular velocities. The muscle contraction is most like a generalised alerting response. It should be noted that the current results were obtained at a loading level of 0,7 g, which is far below the 5-12 g levels observed in rear end collisions. Since the current study shows only small influences of the muscle contraction it is assumed that the contraction will not be strong enough to limit the larger head and trunk motion in the higher impacts.

References

1. McConnell WE, Howard RP, Guzman HM, Bomar JB, Raddin JH, Benedict JV, Smith LH, Hatsell CP. Analysis of human test subject responses to low velocity rear end impacts. SP 975, SAE no. 930889 1993; 21-30.

2. Penning L. Acceleration injury of the cervical spine by hypertranslation of the head. 2. Effect of hypertranslation of the head on cervical spine motion: discussion of literature data. Eur Spine 1992; J1:13-19.

3. Barnsley L, Lord S, Bogduk N. Whiplash injury: clinical review Pain 1994;58:283-307.

4. Tennyson SA, Mital NK, King AI. Electromyographic signals of the spinal musculature during +Gz impact acceleration. Orthop Clin North Am 1977;8:7-119.

5. Matsushita T, Sato TB, Hirabayashi K, Fujimora S, Asazuma T, Takatori T. X-ray study of the human neck motion due to head inertia loading. Proceedings of the 38th Stapp car Crash Conference SAE no. 942208 1994;55-64.

6. Ono K, Kanno M. Influences of the physical parameters on the risk to neck injuries during low impact speed rear end collisions. Proceeding of the international IRCOBI Conference on the Biomechanics of Impacts 1993;201-212.

7. Reid SE, Raviv G, Reid SE. Neck muscle activity resistance to head impact. Aviat Space Environ Med 1981; 52:78-84.

8. Snyder RC, Chaffin DB, Foust DR. Bioengineering study of basic physical measurements related to susceptibility to cervical hyperextension- hyperflexion injury. Highway Safety Research Institute 1975; UM-HSRI-BI-75-6.

9. Horak FB, Nashner LM, Diener HC. Postural strategies associated with somato-sensory and vestibular loss. Experimental Brain Research 1990;82(1):167-177.

10. Magnusson ML, Pope MH, Wilder DG. Cervical electromyographic activity during low-speed rear impact. Eur Spine J 1999; 8:118-125.

11. Navin FPD, Macnabb MJ, Romilly DP, Thompson RW. An investigation into vehicle and occupant response subjected to low-speed rear impacts. Proceeding of the Multidisciplinary Road Safety Conference VI Fredericton, New Brunswick June 1989:5-7.

12. Lieber R. Skeletal muscle structure and function: Implications for rehabilitation and sport medicin. Wiliams and Wilkins, Baltimore 1992.

13. Szabo TJ, Welcher JB. Human subjects kinematics and electromyographic activity during low speed rear impacts. Proceedings of the 40th Stapp Car Crash Conference Alberquerque 1996:295-314.

14. Forssberg H, Hirchfeld H. Postural adjustments in sitting humans following external perturbations: muscle activity and kinematics. Exp Brain Res 1994;97:515-527.

15. Jones FP, Kennedy JL. An electromyographic technique for reading the startle Pattern. Journal of Psychology 1951;32:63-68.

Acknowledgements

Firstly, I would like to acknowledge:

- the contribution of professor Barry Myers from Duke University in Durham to the neck muscle modelling in particular by supplying muscle geometry parameters.

- the European Whiplash Programme for providing the standard car seat model used in this study.

- the research institutes who gave their permission to use their data for model validation: the Laboratory of Accidentology and Biomechanics in France, the Japanese Automobile Research Institute and the Allianz Zentrum für Technik in Germany.

- the TNO Crash Safety Centre in Delft for providing the human body model in order to include the neck model, for facilitating several extensions to the MADYMO software, and for the use of their research and office facilities.

Ten tweede, wil ik iedereen die een bijdrage geleverd heeft aan mijn onderzoek en het tot stand komen van dit proefschrift bedanken. In het bijzonder:

- de begeleiders van TNO Botsveiligheid: Riender Happee en Jac Wismans. Zonder jullie inhoudelijke inbreng en de vele tijd die jullie in het correctiewerk hebben gestoken was ik nooit zover gekomen. Bedankt!

- de begeleiders van de Technische Universiteit Eindhoven: Peter Bovendeerd, Fons Sauren en Dick van Campen. Jullie kritische kijk op de inhoud van het onderzoek en op de rapportage ervan heb ik zeer gewaardeerd.

- de begeleiders van de Universiteit Maastricht: Herman Kingma, Jaap Patijn en Henk van Mameren. Jullie medische inbreng voor het onderzoek alsmede de grote inspanningen die jullie geleverd hebben omtrent de experimenten was erg belangrijk voor mij. Dank jullie wel.

- de begeleiders tijdens de eerste jaren van het onderzoek: Aya van den Kroonenberg en Jan Thunnissen. Jullie hebben me een goede start gegeven en enthousiast gemaakt voor dit onderzoek.

- de collega's van de biomechanica groep van TNO Botsveiligheid: Hans Cappon, Ronald de Lange, Muriëlle Verver, Jack van Hoof, Riske Meijer, Marian Rekveldt en Mat Phillipens. Zowel inhoudelijk, als ook op het persoonlijke vlak hebben jullie de afgelopen jaren veel voor mij betekend. Ook wil ik Ydo de Vries van de ongevallenanalyse groep bedanken voor zijn hulp bij de statistische berekeningen.

- de studenten die middels een stage of afstudeeropdracht een bijdrage aan het proefschrift hebben geleverd: Muriëlle Verver, Falke Hendriks en Marleen Kroeders.

- de proefpersonen die hebben deelgenomen aan de experimenten in Maastricht maar vooral de studenten en medewerkers van de Universiteit Maastricht: Willem Gosens, Jeroen Stevens, André Dekkers, Michaël Lansbergen, Iwan de Jong en Ron Jongen. Dank jullie wel voor het vele werk dat verzet is met betrekking tot de uitvoering en het analyseren van de experimenten. Ook wil ik Paul Laeven en Paul Verjans, van IDEE van de Universiteit Maastricht bedanken voor de vele technische werkzaamheden rondom de experimenten.

- de collega's van TNO Automotive Crash Safety Centre, de medewerkers van de Technische Universiteit Eindhoven en van het Academisch Ziekenhuis Maastricht en de Universiteit van Maastricht.

- de collega's van het TNO Prins Maurits Laboratorium voor de ruimte die ze me gegeven hebben om naast de gewone werkzaamheden van het afgelopen jaar dit proefschrift af te ronden.

- Andrew Godfrey voor de taalcorrecties en Dave Brands voor de praktische tips omtrent de opmaak van het proefschrift.

Ik wil mijn ouders, Jaap en Geeske, mijn zus en zwager, Lidwine en Dominique, en vrienden en collega's bedanken voor hun steun gedurende de afgelopen jaren van mijn promotie onderzoek. Bedankt voor de aanmoedigingen om dit onderzoek af te ronden en het proefschrift te schrijven. Zonder jullie opbeurende woorden was dit proefschrift nooit tot een goed eind gekomen.

Tot slot wil ik mijn vriendin, Simone, bedanken voor haar vertrouwen in mij en het geduld dat zij vooral het afgelopen jaar heeft op weten te brengen. Lieverd, ik zal nu weer meer tijd hebben voor de huishoudelijke klussen en de rust hebben om samen heerlijk te wandelen, te fietsen en te genieten van het leven.

Curriculum Vitae

Marike van der Horst werd geboren op 24 december 1971 in Sneek. In 1990 behaalde zij haar VWO diploma aan het Ichthus College te Enschede. Aansluitend studeerde zij werktuigbouwkunde aan de Universiteit Twente. Haar afstudeerproject betrof het modelleren van de zwaaifase voor een bovenbeenprothese met een vierassig kniemechanisme met behulp van inverse en directe dynamica. Het doel van deze opdracht was constructieve ontwerprichtlijnen op te stellen voor een zwaai-faseregelaar voor deze prothese. In augustus 1996 studeerde zij af. Omdat de biomechanica haar interesse had, solliciteerde zij naar de functie als assistent in opleiding binnen het onderzoeksgebied letselbiomechancia. Dit proefschrift is het resultaat van haar promotie-onderzoek, dat binnen het samenwerkingsverband viel van de Technische Universiteit Eindhoven, de Universiteit Maastricht en de afdeling Botsveiligheid van TNO Automotive te Delft. Sinds 1 mei 2001 is zij werkzaam als wetenschappelijk medewerker bij het TNO Prins Maurits Laboratorium waar zij onderzoek doet naar de personele kwetsbaarheid in situaties die kunnen ontstaan tijdens orde handhavende acties, vredes-operaties alsmede tijdens oorlogstaken.